Summer 2009

Reactivity and Chemical Characterization of Dissolved Organic Matter in an Estuary

Hussain A. Abdulla
Old Dominion University

REACTIVITY AND CHEMICAL CHARACTERIZATION OF DISSOLVED ORGANIC MATTER IN AN ESTUARY

by

Hussain A. Abdulla
B.S. February 1998, University of Bahrain
M.S. August 2005, Old Dominion University

A Dissertation Submitted to the Faculty of
Old Dominion University in Partial Fulfillment of the
Requirement for the Degree of

DOCTOR OF PHILOSOPHY

OCEANOGRAPHY

OLD DOMINION UNIVERSITY
August 2009

Approved by:

David J. Burdige (Co-Director)

Elizabeth C. Minor (Co-Director)

Robert F. Dias (Co-Director)

Patrick G. Hatcher (Member)

Margaret R. Mulholland (Member)

Desmond C. Cook (Member)

ABSTRACT

REACTIVITY AND CHEMICAL CHARACTERIZATION OF DISSOLVED ORGANIC MATTER IN AN ESTUARY

Hussain A. Abdulla
Old Dominion University, 2009
Co-Director:Dr. David J. Burdige
Dr. Elizabeth C. Minor
Dr. Robert F. Dias

This dissertation used Fourier transform infrared spectroscopy (FTIR) and nuclear magnetic resonance spectroscopy (^{13}C-NMR) data to quantify the changes of major chemical compound classes in high molecular weight (HMW, >1kDa) DOM isolated along a transect from Great Dismal Swamp through the Elizabeth River /Chesapeake Bay system to the coastal Atlantic Ocean off Virginia, USA. Results show that both carboxylic acids and aromatic compounds are lost along the transect, while amide, and carbohydrate moieties could have a mid–transect source.

Addressing the seasonal and spatial changes in the chemical composition of high molecular weight DOM using C/N ratio and δ^{13}C signatures indicates a dramatic shift in the relative importance of the processes affecting the HMW-DOM as it moves from fresh water to the marine end member. Sorption and flocculation and reworking by heterotrophic bacteria seem to be the major players in the lower salinity region, but at the higher salinity regions the introduction of new carbon sources by primary production seems to be the major process.

Applying principal component analysis (PCA) and two dimensional correlation spectroscopy to the ^{13}C-NMR spectra of the HMW-DOM shows that HMW-DOM consists of three major components that have different biogeochemical reactivity. The first component appears to be composed of a heteropolysaccharide (HPS) component and it increases as I move to the marine end member, while the second component appears to be composed of carboxyl-rich compounds (CRC) and its carbon percentage decreases as we move away from the fresh water end member. The third component contains the major functional group of amide/amino sugar (AMS) and its carbon percentage stays almost constant regardless of the seasonal and spatial changes along the salinity transect.

It seems that the HPS and CRC components are present in many aquatic environments at different relative ratios. Across aquatic environments the components contain compounds that share similar backbone structures although there is significant variation in some of their functional groups as a function of aquatic system.

The ^{13}C-label method presented here for determining the enhanced aqueous solubility of organic compounds by natural aqueous DOM is a promising new tool for investigating the reactivity of DOM. Applying the method to Dismal Swamp DOM shows that the reactivity differences between high molecular weight, low molecular weight, and total DOM samples are consistent with potential variations in their higher order structures. However, coupling the method with FTIR analysis indicates that ultrafiltration is not merely a pure physical separation but involves a chemical separation as well.

This dissertation is dedicated to my wife and my two kids (Ali and Fatima)

ACKNOWLEDGMENTS

Honestly, one would imagine that having a Ph.D. degree is an effort of an individual, but it is a reflection of huge efforts done by many people who were willing to support and help to make it happen. Starting from my advisors, I really feel fortunate to have more than one with diverse field expertise which plays a great role in enriching my knowledge in the field, David Burdige was a great mentor during all my studies years, David, I really have deep respect for all the valuable time and effort you spent with me through all these years, your advice had a great impact in shaping my thesis, especially the three golden rules. I would like to present my deepest appreciation to Liz Minor. Liz, your belief in me, optimism, fast responses, support and help in navigating the challenges during all these years is really what leads me to this stage, your advice always made me think outside the box and generate the best of me. I would like to give my greatest thanks to Bob Dias "master of obvious" for introducing me to the stable isotope world, Bob I have learnt a lot from interacting with you over the years especially the way you look at a situation " the obvious way", Bob, our science discussions while we were eating burritos at Moe's is my best moments during the last years. I give my greatest gratitude to Pat Hatcher for counting me as one of his students, for giving me access to all his instruments and for the financial support during the last year without which I would not have been able to achieve this dissertation, Pat, your encouragement and belief were the fuel for me to get this done. Also I would like to thank my committee member Margie Mulholland for allowing me use her lab equipments especially the ultrafiltration system, without

which I would not have been able to collect these samples. And I would like to thank Desmond Cook for his valuable comments.

I would like to give my great thank to Richard Zimmerman (chair of OEAS department), Greg Cutter , George Wong, John Donat, Fred Dobbs, Ken Mopper, Dennis Darby and all the faculty and staff at the department of ocean, earth and atmospheric sciences and chemistry department for their supports during these years. I acknowledge Susan Hatcher, Junyan Zhong, and Mahasilu Amunugama at the College of Science Major Instrumentation Cluster (COSMIC) for their help in running the samples by ^{13}C-NMR and FT-ICR-MS.

I would like to thank Pete Morton and Gonzalo Carrasco (Consolvo) for being great friends during these years, for the "lunching" times and for their help in settling with my family. Gonzalo I will miss eating Chinese food with you. Pete, coffee times are always refreshing and reenergizing. Also, I would like to express my thanks to John Helms, for all the valuable science discussions and help during these years. I also would like to thank Dr. Hatcher group's especially Rachel Sleighter, Aron Stubbins, Zhanfei Liu, Elodie Salmon for all their help and fun time we had. I would like to express my merit to graduate students at OEAS and Chemistry for all the good and entertaining times. My special thanks to Tammy Subotich and Alicia Herr for their help, patience and hard work during the last years. Also, I would like to thank Dana Oblak for making sure that this thesis is following the college of science guidelines.

If I have the choice, I will give half of the degree to my soul mate, the most wonderful and patient woman I have ever known to Hoor "my wife" for all her support, patience, love, encouragement, and for giving me the best gifts in my life Ali and Fatima,

their smiles, kisses, hugs whenever I come home is what keeps me going on. This guides me to my biggest supporters, my family in Bahrain. DAD and MOM, your sacrifices for all of us (4 brothers and 9 sisters) was the driving force for all our success. You really did a miracle for providing the best life and the highest education for all 13 of us, which makes my main goal in life, is striving to make you proud of me. To my oldest brother ALI, I still remember my first day at the first grade, as an excited kid accompanied by his oldest brother running toward school, from that day you always been there for me as my best friend and the wise man I return to ask for advice. To my brother Mohammed, for all the back-up and fun time we had. To my brother/friend Ahmed "the computer geek" simply, without you I couldn't have done it. For my beloved sisters, I'm speechless when I get to you. Your frequent calls, messages, e-mails, supports, encouragements (I could not count it all) are what help me to get where I'm. To all my nieces and nephews, your support and calls are highly appreciated; I miss the weekly lunch with you all. To my parents- in-law I'm proud to have a second family like you, I always feel like a son to you. To you and my brothers and sisters in law, I can't thank you enough for raising my kids and taking care of my kids and wife while I'm away from them.

To my undergraduate advisor, my chemistry godfather Ahmed Yousif (AYAM) - Bahrain University, You are the one who implanted the love of chemistry and research on me. I owe it all to you. My best friends: Sameer Iksail and Issa Al-Hawi , you always pushed me to go in this direction, and your messages and e-mails kept me entertained during all these years. I couldn't wait to have dinner again at "Al-Naaim Grills". My brother/friend Mohammed Darwish "Abu Walaa" for being a friend and brother I depend on him for vital decision in my life. For my friends: Ahmed Al-Abadi, Ahmed Saeed,

Jameel Iksail, Hussain Saeed, S. Hamza, S. Mahdi, Luai Al-Arayed, Yasser Ali, Jawad Khamees, Hani Darwish, Jaffar Ahmed, Mirza Khalaf, and all the staff in the at Environmental affair- Bahrain for encouraging and especial thanks to Afaf Al-Shoola and Hassan Juma for continuous support during these years.

Finally I would like to thank Fulbright foreign program, Dorothy Brown Smith scholarship, teaching assistantships and research assistantship for providing the financial support during these years.

TABLE OF CONTENTS

Page

TABLE OF CONTENTS (continued)

Chapter Page

TABLE OF CONTENTS (continued)

Chapter Page

LIST OF TABLES

LIST OF TABLES (continued)

LIST OF FIGURES

LIST OF FIGURES (continued)

Figure Page

LIST OF FIGURES (continued)

LIST OF FIGURES (continued)

CHAPTER I

INTRODUCTION

1. BACKGROUND

Dissolved organic matter (DOM) plays an important ecological and environmental role in natural waters. Studies of DOM reactivity have focused on several topics including: photochemical (Latch and McNeill, 2006; Mopper and Kieber, 2002) and biological degradation (Amon and Benner, 1994; Azam, 1998); chlorination (Kitis et al., 2002); examining the contribution of DOM remineralization to CO_2 fluxes (Hansell and Carlson, 2001); determining the general fate and transport of organic matter (Benner and Opsahl, 2001; McCarthy et al., 1996); examining the interaction of DOM with mineral surfaces (Arnarson and Keil, 2001); metal chelation by DOM (Karlsson et al., 2007; Santschi et al., 1997); and reactions with man-made pollutants (Chiou et al., 1987; Chiou et al., 1986).

The relative importance of the various roles of DOM in an aquatic system depends mainly on its chemical composition. Although a large portion of natural dissolved organic matter is located in marine and estuarine environments, little is known about its chemical composition due to the low concentration of DOM and the high concentration of co-dissolved inorganic species (such as Na^+ and Cl^-) in these waters. Partially because of this salt complication, the direct analyses of specific subsets of compounds in seawater accounts for the characterization of less than 11% of the bulk DOM (Benner, 2002).

This dissertation follows the journal style of Organic Geochemistry.

1.1. Dissolved organic matter in estuaries

Estuaries and the continental shelf regions act as a biogeochemical reactor for dissolved organic matter (DOM), where most of the terrestrial dissolved organic matter (T-DOM) is lost and a small portion of the T-DOM reaches the open ocean (Benner et al., 2005; Hedges et al., 1997). On the other hand, new sources of DOM are introduced into estuaries and continental shelf water through primary production; these regions account for 30% of the net oceanic productivity (Holligan, 1992) even though they represent only 7% of the total oceanic surface areas (Gattuso et al., 1998).

Despite the fact that the global annual discharge of riverine dissolved organic carbon (DOC) could sustain the amount of DOC in the marine pool (Williams and Druffel, 1987), evidence from carbon isotopes, elemental analysis and molecular biomarkers shows that only a small portion of identifiable terrestrial DOM reaches the open ocean (Meyers-Schulte and Hedges, 1986; Opsahl and Benner, 1997; Williams and Druffel, 1987). This indicates that there are significant changes in the sources and chemical composition of the DOM as it moves from continents to the open ocean, which could influence the ecological and environmental roles of DOM.

The distribution of dissolved organic mater (DOM) in estuaries is affected by changes in physical parameters such as river discharge, water residence time, tidal exchange, and resuspension events. DOM is also exposed to large changes in pH and salinity as it moves downstream in a typical estuary. The sources and sinks of DOM in estuaries are caused by many different biogeochemical processes. For example, as the ionic strength increases in low salinity regions, some DOM flocculates and aggregates (Sholkovitz, 1976; Sholkovitz et al., 1978) into larger particles (Stumm, 1990) perhaps

through interactions with cations such as Ca^{2+} (Hunter and Liss, 1982) removing the DOM from the water column. Additional estuarine processes include the increase of light penetration due to a decline in turbidity, which can lead to increased photodegradation of chromophoric DOM, and, in conjunction with the availability of nutrients, can also provide the ideal conditions for a primary production maximum in the middle of estuarine ecosystem (Cloern et al., 1983; Filardo and Dunstan, 1985; Fisher et al., 1988; Harvey and Mannino, 2001; Pennock and Sharp, 1986).

While flocculation and primary production maxima are more likely to be limited to specific regions of estuaries, photooxidation and bacterial utilization of DOM more likely occur throughout the estuary, though their degree and chemical selectivity may vary with location (Waidner and Kirchman, 2008). On one side, heterotrophic bacteria could be a sink for DOM by converting it to CO_2 (Azam et al., 1983). On the other side, they could contribute to the DOM pool directly by converting carbon into refractory DOM (Ogawa et al., 2001) or indirectly by the regeneration of inorganic nutrients from DOM, thus enhancing primary productivity (Gardner et al., 1994; Pakulski et al., 1995; Pakulski et al., 2000). Photooxidation could be a biogeochemical sink for DOM by converting it into CO_2 or CO either directly (Miller and Zepp, 1995) or indirectly by making DOM more bioavailable for heterotrophic bacteria to respire (Moran and Zepp, 1997). In addition to spatial variations, the relative importance of these processes are highly varied between different seasons; for example, the summer season provides the perfect conditions for intense phytoplankton blooms to occur in the middle of the estuary as compared to other seasons (Harvey and Mannino, 2001; Pennock and Sharp, 1986).

1.2. Characterization of dissolved organic matter in estuaries

Because estuaries represent the interface between land-derived DOM and open ocean DOM, they have been under intense study with many different approaches used to estimate and understand the alteration in the chemical composition of DOM along estuarine transects. The majority of these studies have tried to quantify the amount of terrestrial organic matter that could reach the open ocean by constructing mixing models using bulk properties such as the C/N ratio, single or dual $\delta^{13}C$ and $\Delta^{14}C$ isotope signatures of bulk DOM, and UV-visible absorption. Biomarker approaches have involved studies of long-chain odd-number n-alkanes, lignin compounds, or branched and isoprenoid tetraether lipids (Eglinton and Hamilton, 1963; Hopmans et al., 2004; McCallister et al., 2006; Mitra et al., 2000; Opsahl et al., 1999; Raymond and Bauer, 2001; Rochelle-Newall and Fisher, 2002). Other have also used a combination of proxies (e.g., lignin, N/C and $\delta^{13}C$, Gordon and Goňi, 2003). Other approaches have focused on molecular biomarkers as indicators of both the alteration of organic matter and the organic matter source (e.g. Mannino and Harvey, 2000; Wakeham et al., 1997; Zuo and Wang, 2004). These approaches have been considerably enhanced recently through the use of compound specific analysis of ^{13}C, ^{14}C and D isotopes (e.g. Eglinton et al., 1997; Hayes et al., 1990; Sessions et al., 1999). Recent advances in mass spectroscopy techniques have also led to investigations of the molecular-level composition of DOM isolated from estuarine water (Dalzell et al., 2009; Minor et al., 2001; Minor et al., 2002; Sleighter and Hatcher, 2008).

Although using molecular biomarkers (including compound-specific isotopic information) is an elegant approach for identifying the chemical and biological processes

and carbon sources in estuaries, biomarkers comprise only a small subset of the DOM chemical composition (Benner, 2002), which can yield misleading conclusions when extrapolating biomarker data to the entire DOM pool (Hedges, 2002). Mass spectrometry provides a somewhat wider window into DOM composition and processes but is only semi-quantitative and limited in many cases by matrix effects and differences in ionization efficiency among different compound types. Therefore there remains a need for additional approaches to quantify the relative changes in the chemical compound classes of DOM as I move from land to the open ocean, especially as changes in the chemical structure of estuarine DOM could reflect changes in their ecological role,. e.g. bioavailability and transportation of both hydrophobic organic contaminants (Chefetz et al., 2000; Chin et al., 1997; Chiou et al., 1987), and trace metals (Shiller et al., 2006).

1.3. Interaction between anthropogenic and natural organic matter

The increased identification of organic pollutants in natural waters has made it even more critical that we understand the interactions between natural DOM and anthropogenic organic compounds and the environmental fate of these compounds. The ability of DOM to interact with different types of organic compounds is primarily a function of its structural heterogeneity and hydrophobic and hydrophilic properties (Hassett, 2006). Variations in composition, chemical structure, polarity and size of DOM isolated from different locations, have been related to variations in partition coefficient K_{iDOM} (or K_{iDOC}) value (Chin et al., 1997; Chiou et al., 1987; Gauthier et al., 1987; Rutherford et al., 1992; Salloum et al., 2002). For example, an inverse correlation was observed between the polar group content in humic substances (measured by elemental

analysis) and the solubility enhancement of such hydrophobic organic compounds as p,p'-DDT, 2,4,5,2',5'-PCB, benzene and carbon tetrachloride (Chiou et al., 1987; Rutherford et al., 1992). Gauthier and co-workers (1987) show that the aromaticity (as measured by three independent methods) of fourteen different humic substances is directly related to their pyrene K_{iDOC} values. Chin et al. (1997), using pyrene as probe molecule and several humic and fulvic acids as DOM co-solutes, found that pyrene binding increased with increasing molecular weight and the degree of aromaticity within the DOM co-solute and decreased with aliphatic I character as determined by ^{13}C-NMR. However, Salloum et al. (2002) observed a positive correlation between the aliphatic content of natural organic matter and K_{OC} values when phenanthrene was used as the probe molecule.

Because the largest fraction of DOM is as of yet uncharacterizable (Benner, 2002), studying the reaction and interaction of DOM with other organic species is at best an analytical compromise between understanding chemical functionality and specific chemical structure within DOM. The major drawback of using the current solubility enhancement approaches as a probe to investigate DOM reactivity is their inability to detect small changes in partitioning of organic compounds by DOM. To date, current methods have had limited applicability for: 1) low-DOM-concentration samples such as those found in estuarine and marine DOM (Rutherford et al., 1992), or 2) across spatial (e.g. down-estuary) and temporal (e.g. seasonal) scales as the natural DOM pool shifts in composition in response to mobility, source and sink variations. In addition, current studies have generally been limited to highly hydrophobic compounds that are expected to exhibit high solubility enhancement values. To use solubility enhancement as an

effective probe of the reactivity of aquatic DOM, a more precise quantification method is required that can detect both very small partition values and small changes in incorporation values, and be capable of estimating the interactions of different probes with the same DOM.

In this dissertation, I coupled two non-destructive techniques 1) Nuclear magnetic resonance spectroscopy (^{13}C-NMR) and 2) Fourier transform infrared spectroscopy (FTIR) (including resolution enhancement in the FTIR approach) to study the spatial and seasonal changes (during two years) in the chemical composition of high molecular weight (>1000 Da) estuarine DOM isolated along transect from the Dismal Swamp (Virginia, USA) to the coastal Atlantic Ocean passing through the Elizabeth River and the mouth of the Chesapeake Bay. In order to detect significant changes in the FTIR and ^{13}C-NMR, I used two chemometric data analysis techniques: 1) Principal component analysis (PCA) and 2) Two dimensional correlation spectroscopy (2D-Spectroscopy).

Because I was only able to characterize the isolated salt free fraction-high molecular weight (>1000 Da) DOM, which accounts only for 15-71% of the entire DOM pool, I developed a method based on the use of the solubility enhancement of model organic compounds as a tracer for the chemical reactivity of unfractionated DOM. I will present a new high-precision technique to measure the solubility enhancement of model organic compounds in natural waters by utilizing isotopic mass balance (^{13}C). To test the method, I applied it to a study of seasonal changes in the reactivity of DOM in sterile-filtered Dismal Swamp water (VA, USA) and its high and low molecular weight fractions (isolated by ultrafiltration), using ^{13}C-labeled styrene as a probe.

2. SAMPLING SITIES

Samples were collected from five sites along a transect from Great Dismal Swamp through the Elizabeth River /Chesapeake Bay system to the coastal Atlantic Ocean (see Fig. 1.1). Site DS (Portsmouth Ditch in Great Dismal Swamp, Virginia, USA) is representative of the swampy headwaters of the Elizabeth River system, has very high DOC loadings, and contains a large proportion of terrestrially-derived DOM. Site GB in Great Bridge, Virginia is forested with marshes along the shoreline. The TP site (Town Point Park, Norfolk, Virginia) represents mid-river and contains natural autochthonous and allochthonous organic matter from the three branches of the Elizabeth River and the lower Chesapeake Bay. The down-river CBB (Chesapeake Bay Bridge-Tunnel) is at the mouth of the Chesapeake Bay; its organic matter sources include salt marshes and sediments of the lower Chesapeake Bay and its sub-estuaries as well as imported coastal marine material and autochthonous algal production. The Offshore coastal ocean site (OSC, 37° 10.132' N, 75° 37.891' W) could be impacted by water flowing out of the Chesapeake Bay, but should also contain significant proportions of autochthonous marine organic matter.

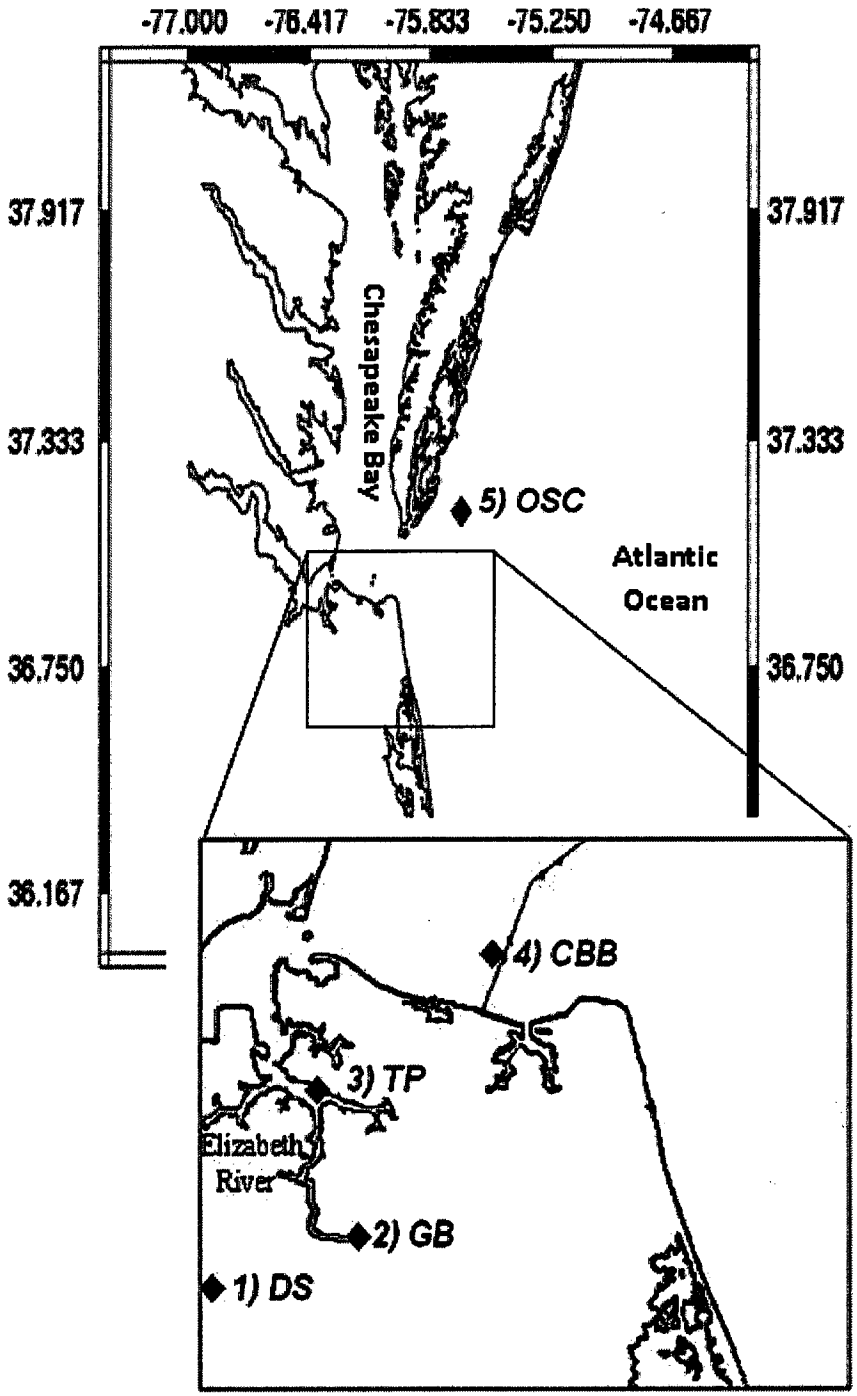

Fig. 1.1. The map of the lower Chesapeake Bay area, showing the five sampling locations. 1) Great Dismal Swamp-DS. 2) Great Bridge-GB. 3) Town Point-TP. 4) Chesapeake Bay Bridge-CBB. 5) Offshore site-OSC.

3. ULTRAFILTRATION

One of the most common techniques to isolate DOM is ultrafiltration, which is based on the use of a membrane made of cellulosic, polysulfone or acrylic polymer with a typical pore size of 1 nm, equating to a nominal molecular weight cut-off of 1 KDa. Briefly, the separation works by passing the aqueous solution through the membrane under pressure; the low molecular weight fraction (filtrate) will pass through the membrane while the high molecular weight fraction (rententate) remains.

The major advantages of using ultrafiltration are: the separation is theoretically based on size rather than the chemistry of the DOM, providing a less chemically-biased view of the DOM fractions; moreover, the water is not artificially acidified, allowing the isolated compounds to retain their natural chemical speciation and conformation. The potential contamination from the ultrafiltration is low. Ultrafiltration can accommodate very large sample volumes, in the range of hundreds to thousands of liters, allowing for the isolation of DOM from marine environments. It can retain from 90% in terrestrial system to 20% of the total DOC in the open ocean.

The major disadvantages are: although fairly reproducible, the actual separation depends on the membrane (e.g. constriction material, manufactory), sample type (e.g. rivers, coastal, open ocean), total DOC concentration, concentration factor and operating conditions (Buesseler, 1996; Buesseler et al., 1996; Guo and Santschi, 1996). Losses to the ultrafiltration membrane can also be significant (Guo et al., 2000). Assemi et al. (2004) proposed that ultrafiltration could also separate the DOM based on their chemical characterization in addition to the size fractionation, which can complicate the interpretation of results based upon the retained material.

4. CHEMICAL CHARACTARIZATION OF DOM

4.1 Carbon-13 nuclear magnetic resonance spectroscopy

Nuclear magnetic resonance spectroscopy (NMR) provides a useful analytical window into DOM composition with the additional benefit of being non-destructive, thus preserving painfully obtained samples for additional characterization. It has the ability to spread out specific nuclei in DOM along a wide chemical shift spectrum based on their different electronic environments, giving it the ability to look into the distribution of DOM functional groups. The direct relationship between the number of nuclei at a specific chemical shift and the intensity at the same chemical shift makes NMR quantifiable, allowing the assessment of the relative contribution of DOM functional groups containing specific types of nuclei e.g. ^{13}C , ^{1}H , ^{15}N, ^{31}P (Wilson, 1987).

^{13}C-NMR has been widely applied to study the chemical distribution of different carbon structures of DOM isolated from swamp water (Finmen et al., 2007; Lu et al., 2000), rivers and lakes (Bianchi et al., 2004; Hedges et al., 1992; Repeta et al., 2002), and coastal, surface and deep open ocean waters (Benner et al., 1992; Hedges et al., 1992; Repeta et al., 2002). From these studies, it appears that autochthonously derived DOM (e.g. that prevalent in ocean samples) has a higher aliphatic, lower aromatic, and higher carbohydrate content than terrestrially derived DOM (e.g. swamp water). However, to my knowledge no ^{13}C-NMR study has followed the changes in the chemical composition of DOM as it moves through an estuary from terrestrially-impacted to marine waters.

4.2. Fourier transform infrared spectroscopy

Fourier transform infrared spectroscopy (FTIR), which like NMR is a non-destructive technique, can be used to provide an additional view of the functional groups in organic compounds, and can help to resolve the carboxyl, amide and aliphatic ester contributions to DOM. Fundamentally, infrared spectroscopy is based on the vibration of molecules when they are exposed to infrared radiation; each bond in the molecule is involved in different vibration modes, e.g., stretching and bending (Mayo et al., 2004; Smith, 1996). The frequency of each vibration mode is a function of the bond force constant (k) and the reduced mass of the atoms involved in the vibration, so any changes in the force constant of the bond due to changes in the bond angle or the electronic environment around it, could shift the band position to higher or lower frequency. On the other hand, the intensity of each band is directly related to the square of the change in the electrical dipole moment $(\partial\mu)^2$ of the bond during the vibration, so bonds with higher changes in the dipole moment (e.g. O-H, N-H, C=O, C-O) will have higher intensity bands relative to the other bonds (Günzler and Gremlich, 2002; Mayo et al., 2004; Steele, 2002). Another factor that affects the intensity of a band is the concentration of the functional group or its abundance in the molecule or mixture of compounds, which allows FTIR to be used quantitatively, assuming that the dipole-moment-related "response factor" is taken into account (Mayo et al., 2004; Smith, 1996).

FTIR is used widely in the characterization of humic substances given its ability to provide quantitative as well as qualitative analyses of major functional groups such as carboxylic acid, phenol, amide, ester and saturated and unsaturated hydrocarbons (Stevenson, 1994). For example, a strong relationship with a slope of one has been found

between the carboxylic content of humic acids determined by both wet chemical analysis and FTIR methods (Celi et al., 1997), and a strong inverse relationship has also been found between the intensity ratio of 1415 to 1590 cm^{-1} and O/C ratio determined by elemental analysis (Johnston et al., 1994). Mecozzi and Pietrantonio (2006) have used FTIR to study the distribution of carbohydrates, proteins and lipids within different molecular weight fractions of fulvic and humic acids in sediments.

5. MULTIVARIATE DATA ANALYSIS

5.1 Principal component analysis (PCA)

One of the traditional multivariate data analysis techniques is the principal component analysis (PCA); it is used to treat the spectra as a whole entity and represents it as a linear combination of a set of factors. The major advantage of PCA is its ability to reduce the dimensionality of the data set by eliminating redundant dimensions, i.e., those containing low information content, and identifying new meaningful underlying variables that represent the differences and similarities within a specific data set. Mathematically it starts with a matrix of H (s x n) where (s) is the number of spectra (samples) and (n) is number of wavenumbers / chemical shift in each spectra, from that dimension based on calculating the covariant among the original spectra according to this Eq. 1.1

$$\mathrm{cov}(X, Y) = \frac{\sum_{i=1}^{s} (Xi - \overline{X})(Yi - \overline{Y})}{(s - 1)} \qquad \text{Eq. 1.1}$$

Where X and Y are wavenumbers or chemical shift in the spectra, and s is number of spectra (number of samples).

This will produce a square matrix called the coefficient matrix (n x n)

$$M = \begin{bmatrix} \mathrm{cov}(1,1) & - & - & \mathrm{cov}(1,n) \\ - & - & - & - \\ - & - & - & - \\ \mathrm{cov}(n,1) & - & - & \mathrm{cov}(n,n) \end{bmatrix}$$

From that, I need to find the eigenvectors χ (principal component PC) and their eigenvalues λ by solving this matrix equation

$$M\chi = \lambda\chi \qquad \text{Eq. 1.2}$$

This equation could be solved by finding a vector that when you multiply it by M (n x n) matrix it will produce itself multiplied by constant value (λ). The result of that should produce N orthogonal vectors and their eigenvalues. The first principal component – eigenvector- is the one with the highest eigenvalues.

5.2. Two dimensional correlation spectroscopy

Noda (1993) developed a new concept of generalized perturbation based on two dimensional correlation spectroscopy (2D-Spectroscopy), by spreading the changes in spectra intensity within a data set collected across a perturbation (e.g. time, temperature, pressure, chemical reaction) as a function of the perturbation over a second dimension. This reduces the complexity of overlapped peaks (as many of them do not co-evolve throughout the data set), provides relations between different peaks, and gives us the sequential order of the changes in these bands. The application of 2D-spectroscopy results in two orthogonal correlation spectra (synchronous and asynchronous). The synchronous spectrum indicates coincidental or in-phase changes of two separate peaks, while the asynchronous spectrum will exhibit cross peaks if changes in the original data peaks are out of phase, which will be an indication of the order of the functional group

changes. The use of 2D-spectroscopy in this fashion resolves many ambiguities especially in a complex mixture of compounds with many overlapping peaks (Noda and Ozaki, 2004; Wang and Palmer, 1999). The practical computation of two-dimensional correlation spectroscopy were generated according to Noda and Ozaki (2004). In brief, the reference spectrum $\bar{y}(v)$ is calculated first, by taking the average values of all the data points at each specific wavenumber or chemical shift (v). The second step involves calculating the dynamic spectra $\tilde{y}$ (υ) for all spectra by subtracting the reference spectrum $\bar{y}(v)$ from each normalized spectrum y (υ) at each perturbation (t).

The synchronous 2D spectrum $\Phi(\upsilon_1,\upsilon_2)$ is calculated according to Eq.1.3

$$\Phi(v_1, v_2) = \frac{1}{2(t_m - t_1)} \sum_{j=1}^{m} \tilde{y}_j(v_1).\tilde{y}_j(v_2).(t_{j+1} - t_{j-1}) \qquad \text{Eq.1.3}$$

where m the total number of spectra, equal to 24 in my case. I also define two additional points in the perturbation, t_0 and t_{m+1}, located outside the observation period as $t_o = 2t_1 - t_2$ and $t_{m+1} = 2t_m - t_{m-1}$.

Repeating the above calculations to the entire range of the wavenumber/chemical shifts will produce a square matrix that could be represented by a two dimensional contour map or what is called a synchronous spectrum. An example of a schematic synchronous spectrum is shown in Figure 1.2. As the figure shows, the synchronous spectrum is a symmetric spectrum with respect to the a diagonal line, where each auto peak along the diagonal line represents a correlation between the specific wavenumber/chemical shift and itself ($v_1 = v_2$). The auto peak appears only if the band shows changes in the intensity during the perturbation period. On the other hand, the peaks located at the off-diagonal positions of Fig. 1.2 represent the correlations between

the different spectral variables (ν_1 and ν_2) which are called cross peaks. Cross peaks could have either a positive correlation (white shaded) or a negative correlation (gray shaded); when the cross peaks of two bands have the same sign, they indicate that these two bands are changing in the same direction (they are increasing or decreasing together). When they have different signs that means one of them is increasing while the other is decreasing.

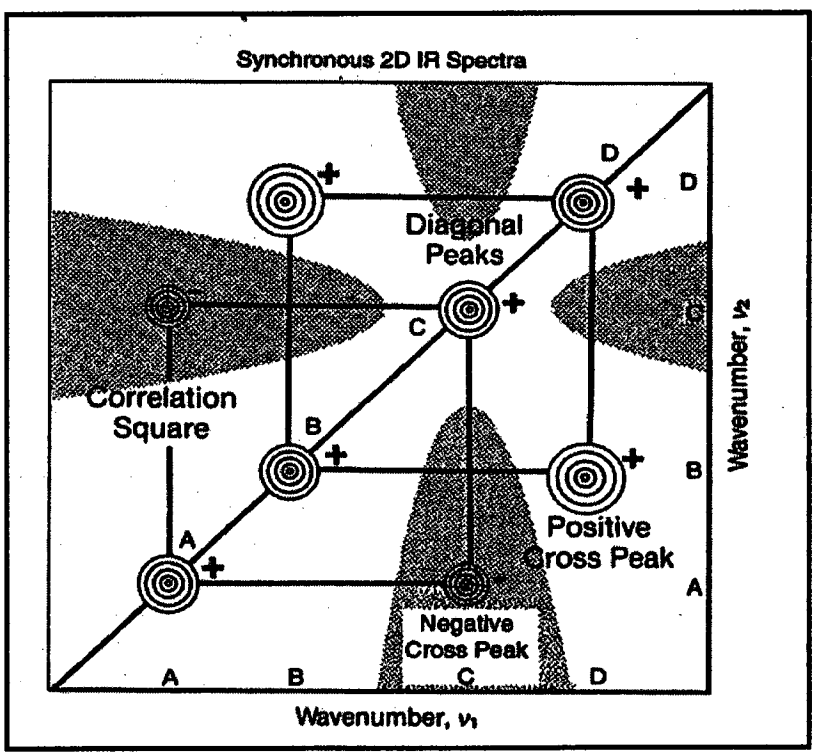

Fig. 1.2. Schematic contour map of a synchronous 2D correlation spectrum. Shaded areas indicate negative correlation intensity (Adapted from Noda and Ozaki, 2004).

The asynchronous 2D spectrum $\Psi(\upsilon_1,\upsilon_2)$ is calculated according to the following equation

$$\Psi(\nu_1,\nu_2) = \frac{1}{2(t_m - t_1)} \sum_{j=1}^{m} \tilde{y}_j(\nu_1).\tilde{z}_j(\nu_2).(t_{j+1} - t_{j-1}) \qquad \text{Eq.1.4}$$

where the $\tilde{z}_j(\nu_2)$ is the Hilbert transformation of $\tilde{y}_j(\nu_2)$ that is calculated by numerical integration according to Eq. 1.5

$$\tilde{z}_j(\nu_2) = \sum_{k=1}^{m} N_{jk} \cdot \tilde{y}_k(\nu_2) \qquad \text{Eq.1.5}$$

The term N_{jk} is the element of Hilbert-Noda transformation matrix. See Noda and Ozaki (2004).

Applying the above calculations to the entire range of the wavenumbers/chemical shifts will produce a square matrix that could be represented by a two dimensional contour map or what is called an asynchronous spectrum, similar to the schematic asynchronous spectrum shown in Fig. 1.3. Unlike the synchronous spectrum, the asynchronous spectrum is a non symmetric spectrum and has no autopeaks. The signs of the cross peaks on the asynchronous spectrum could be used to provide valuable information on the sequential order of the changes of the bands with respect to the perturbation variables. For more details see Noda and Ozaki (2004).

In the last two decades, two-dimensional correlation spectroscopy of the kind described above has been applied to many different spectroscopic techniques such as infrared (Buffeteau and Pezolet, 1998; Ekgasit and Ishida, 1995; Sasic et al., 2000; Sasic and Ozaki, 2001), Raman (Ebihara et al., 1993; Matsushita et al., 2000), near infrared (Awichi et al., 2002; Liu et al., 1996), UV-visible (Liu et al., 2000; Zhao et al., 2002), and fluorescence (He et al., 2001; Nakashima et al., 2000) spectroscopy.

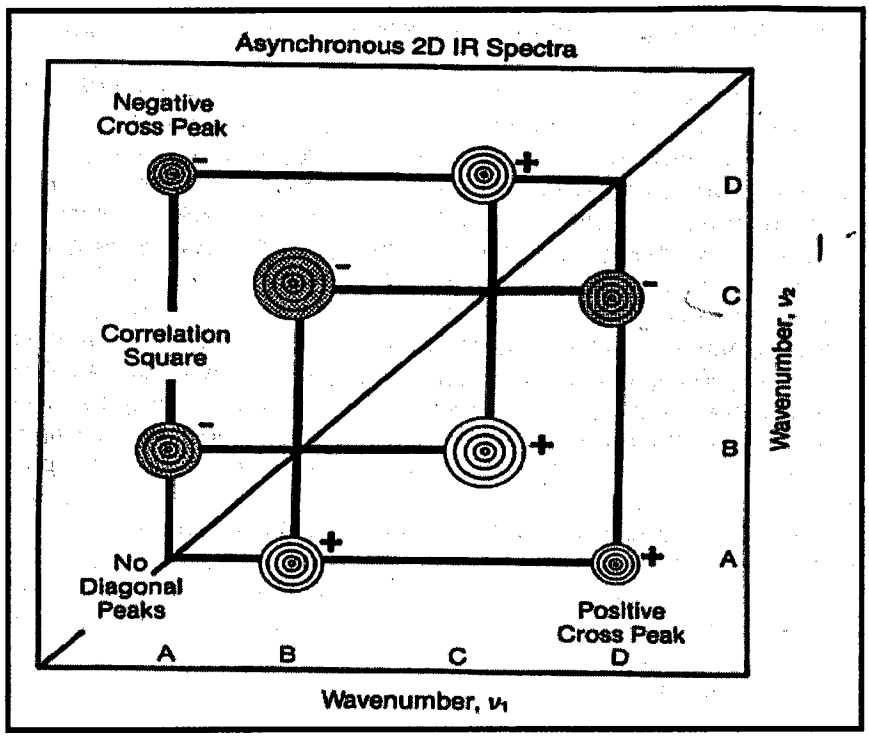

Fig. 1.3. Schematic contour map of asynchronous 2D correlation spectrum. Shaded areas indicate negative correlation intensity (Adapted from Noda and Ozaki, 2004).

It also has been applied to time-resolved gel permeation chromatography (Izawa et al., 2002a; Izawa et al., 2002b). Two dimensional correlation spectroscopy has been applied widely and successfully to understand the changes within polymer materials and proteins, to follow chemical reactions and to investigate other questions in biological and biomedical sciences (see the reviews by Noda and Ozaki, 2004; Ozaki, 2002).

Unlike principal component analysis, which investigates variations in the spectra viewed as a single data set to investigate how samples are different from each other, two dimensional correlation spectroscopy looks into the intensity changes of the individual

chemical bands or peaks throughout all of the spectra in order to identify correlations between different bands based on in-phase and out-of-phase changes in their intensity across the data set. Combining both PCA and 2D-correlation can help to confirm trends seen in each analysis of the data set, and will also provide additional complementary data about sample composition.

6. DISSERTATION OUTLINE

This dissertation is a result of two years of seasonal sampling along the salinity transect from the Dismal Swamp (Virginia, USA) to the coastal Atlantic Ocean passing through the Elizabeth River and the mouth of the Chesapeake Bay. I used the advantage of ^{13}C-NMR and FTIR as non-destructive techniques and their complementarily in providing information on the distribution of DOM functional groups, which could help to construct a better comprehensive picture of the change in the DOM as it moves from land to ocean through an estuary.

In chapter II, I coupled the two non-destructive techniques (^{13}C-NMR and FTIR) including resolution enhancement in the FTIR approach, to quantify the change in DOM compound classes (with emphasis on the carboxyl, amide and ester compound classes) within high molecular weight DOM (HMW DOM, > 1000 Da) during an intensive red tide bloom (*Cochlodinium polykrikoides*).

In chapter III, I look into the spatial and seasonal changes (during two years) in the chemical composition of HMW estuarine DOM isolated along the transect by using PCA and two dimensional correlation spectroscopy of ^{13}C-NMR and FTIR of the HMW-DOM.

Most of my chemical characterization was based on the analysis of the high molecular weight fraction, and there are some concerns as to if it is representative of the entire DOM pool. In chapter IV, I used the solubility enhancement of model organic compounds as a tracer for the chemical reactivity of DOM in its ambient environment. I present a new high-precision technique to measure the solubility enhancement of model organic compounds in natural waters by utilizing isotopic mass balance (^{13}C). To test the method, I applied it to examine seasonal changes in the reactivity of DOM in sterile-filtered Dismal Swamp water (VA, USA) and its high and low molecular weight fractions (isolated by ultrafiltration), using ^{13}C-labeled styrene as a probe.

Chapter V highlights the major finding and conclusions of this dissertation, and discusses further studies that could help us to have a better understanding of the chemical characterization of dissolved organic matter.

CHAPTER II

CHANGES IN THE COMPOUND CLASSES OF DISSOLVED ORGANIC MATTER ALONG AN ESTUARINE TRANSECT: A STUDY USING FTIR AND ^{13}C-NMR

1. INTRODUCTION:

Despite the fact that the global annual discharge of riverine dissolved organic carbon (DOC) could sustain the amount of DOC in the marine pool (Williams and Druffel, 1987), evidence from carbon isotopes, elemental analysis and molecular biomarkers shows that only a small portion of identifiable terrestrial DOM reaches the open ocean (Meyers-Schulte and Hedges, 1986; Opsahl and Benner, 1997; Williams and Druffel, 1987). This indicates that there are significant changes in the sources and chemical composition of the DOM as it moves from continents to the open ocean, which could influence the role of DOM as a short-term sink of atmospheric CO_2 (Hedges, 1992), a bacterial food source (Amon and Benner, 1996; Azam et al., 1983), and as a reactant and absorbant of man-made pollutants (Chiou et al., 1986).

Because estuaries represent the interface between land derived DOM and open ocean DOM, they have been under intense study with many different approaches used to estimate and understand the alteration in the chemical composition of DOM along estuarine transects. The majority of these studies have tried to quantify the amount of terrestrial organic matter that could reach the open ocean by constructing mixing models using bulk properties such as the C/N ratio, single or dual $\delta^{13}C$ and $\Delta^{14}C$ isotope

signatures of bulk DOM, and UV-visible absorption. Biomarker approaches have involved studies of long-chain odd-number n-alkanes, lignin compounds, or branched and isoprenoid tetraether lipids (Eglinton and Hamilton, 1963; Hopmans et al., 2004; McCallister et al., 2006; Mitra et al., 2000; Opsahl et al., 1999; Raymond and Bauer, 2001; Rochelle-Newall and Fisher, 2002). Other have also used a combination of proxies (e.g., lignin, N/C and $\delta^{13}C$, Gordon and Goňi, 2003). Other approaches have focused on molecular biomarkers as indicators of both the alteration of organic matter and the organic matter source (e.g. Mannino and Harvey, 2000; Wakeham et al., 1997; Zuo and Wang, 2004). These approaches have been considerably enhanced recently through the use of compound specific analysis of ^{13}C, ^{14}C and D isotopes (e.g. Eglinton et al., 1997; Hayes et al., 1990; Sessions et al., 1999). Recent advances in mass spectroscopy techniques have also led to investigations of the molecular-level composition of DOM isolated from estuarine water (Dalzell et al., 2009; Minor et al., 2001; Minor et al., 2002; Sleighter and Hatcher, 2008).

Although using molecular biomarkers (including compound-specific isotopic information) is an elegant approach for identifying the chemical and biological processes and carbon sources in estuaries, biomarkers comprise only a small subset of the DOM chemical composition (Benner, 2002), which can yield misleading conclusions when extrapolating biomarker data to the entire DOM pool (Hedges, 2002). Mass spectrometry provides a somewhat wider window into DOM composition and processes but is only semi-quantitative and limited in many cases by matrix effects and differences in ionization efficiency among different compound types. Therefore there remains a need for additional approaches to quantify the relative changes in the chemical compound

classes of DOM as I move from land to the open ocean, especially as changes in the chemical structure of estuarine DOM could reflect changes in their ecological role,. e.g. bioavailability and transportation of both hydrophobic organic contaminants (Chefetz et al., 2000; Chin et al., 1997; Chiou et al., 1987), and trace metals (Shiller et al., 2006).

Nuclear magnetic resonance spectroscopy (NMR) provides a useful analytical window into DOM composition with the additional benefit of being non-destructive, thus preserving painfully obtained samples for additional characterization. It has the ability to spread out specific nuclei in DOM along a wide chemical shift spectrum based on their different electronic environments, giving it the ability to look into the distribution of DOM functional groups. The direct relationship between the number of nuclei at a specific chemical shift and the intensity at the same chemical shift makes NMR quantifiable, allowing the assessment of the relative contribution of DOM functional groups containing specific types of nuclei e.g. ^{13}C , ^{1}H , ^{15}N, ^{31}P (Wilson, 1987).

^{13}C-NMR has been widely applied to study the chemical distribution of different carbon structures of DOM isolated from swamp water (Finmen et al., 2007; Lu et al., 2000), rivers and lakes (Bianchi et al., 2004; Hedges et al., 1992; Repeta et al., 2002), and coastal, surface and deep open ocean waters (Benner et al., 1992; Hedges et al., 1992; Repeta et al., 2002). From these studies, it appears that autochthonously derived DOM (e.g. that prevalent in ocean samples) has a higher aliphatic, lower aromatic, and higher carbohydrate content than terrestrially derived DOM (e.g. swamp water). However, to my knowledge no ^{13}C-NMR study has followed the changes in the chemical composition of DOM as it moves through an estuary from terrestrially-impacted to marine waters.

While ^{13}C-NMR is a useful, non-destructive approach to investigating functional groups variations, it (like all analytical techniques) suffers from some ambiguities in the structural information it provides. For example, the carbonyl band (C=O) of carboxyl, amide and aliphatic esters in DOM all appear at the same position around 175 ppm, (Dria et al., 2002; Knicker and Lüdemann, 1995; Wilson, 1987 and many others), which considerably complicates the resolution and quantification of these functional groups using NMR.

The distinction of these groups is important due to their independent roles in aquatic ecosystems. The carboxyl group is the dominant oxygen functional group in terrestrial DOM (Cabaniss, 1991; Leenheer et al., 1995), and it can play an important role in determining both DOM and natural water acidity (especially in freshwaters with little buffering capacity, (e.g., Wellington and Driscoll, 2004), in chelating metals (Byler et al., 1987; Stevenson, 1994; Strathmann and Myneni, 2004), in photooxidation processes (Faust and Zepp, 1993; Xie et al., 2004), and in the adsorption of DOM to particulate phases (Huang et al., 2003; Stevenson, 1994), However, little is known about transport of carboxyl groups through estuaries to the open ocean. With the recent identification of refractory carboxyl-rich alicyclic molecules (CRAM) in both ocean (Hertkorn et al., 2006) and fresh waters (Lam et al., 2007), it is important to estimate the carboxyl content that could transferred from land to the open ocean through estuaries.

A better understanding of amide group distributions is important in understanding the role of amide-containing compounds as nitrogen as well as a carbon sources for biota. Although dissolved organic nitrogen (DON) can be used as a nitrogen source by both heterotrophic and autotrophic organisms (Bronk, 2002; Mulholland et al., 2002); and

references within), the nitrogen content in DOM increases as I go through estuaries (Benner, 2002; Bronk, 2002; Hedges et al., 1997) and organic nitrogen has been shown to persist in aquatic ecosystems, despite nutrient demand. Analysis by ^{15}N-NMR has shown that most marine DON is in the amide form (McCarthy et al., 1997), and many preservation mechanisms have been proposed to explain why intrinsically reactive amide N might persist; one explanation is the encapsulation hypothesis, where protein is protected by aliphatic macromolecules (Knicker and Hatcher, 1997; Nguyen et al., 2003). Recent results show that, in addition to its presence in protein, amide could also be found in significant amounts in an amide acetate form (N-acetyl amino polysaccharides), which could also help to explain the preservation of DON (Aluwihare et al., 2005). All these results show the importance of understanding the association of amide functional groups with other functional groups (e.g. esters, aliphatic and carbohydrate moieties).

Fourier transform infrared spectroscopy (FTIR), which like NMR is a non-destructive technique, can be used to provide an additional view of the functional groups in organic compounds, and can help to resolve the carboxyl, amide and aliphatic ester contributions to DOM. Fundamentally, infrared spectroscopy is based on the vibration of molecules when they are exposed to infrared radiation; each bond in the molecule is involved in different vibration modes, e.g., stretching and bending (Mayo et al., 2004; Smith, 1996). The frequency of each vibration mode is a function of the bond force constant (k) and the reduced mass of the atoms involved in the vibration, so any changes in the force constant of the bond due to changes in the bond angle or the electronic environment around it, could shift the band position to higher or lower frequency. On the other hand, the intensity of each band is directly related to the square of the change in the

electrical dipole moment $(\partial\mu)^2$ of the bond during the vibration, so bonds with higher changes in the dipole moment (e.g. O-H, N-H, C=O, C-O) will have higher intensity bands relative to the other bonds (Günzler and Gremlich, 2002; Mayo et al., 2004; Steele, 2002). Another factor that affects the intensity of a band is the concentration of the functional group or its abundance in the molecule or mixture of compounds, which allows FTIR to be used quantitatively, assuming that the dipole-moment-related "response factor" is taken into account (Mayo et al., 2004; Smith, 1996).

FTIR is used widely in the characterization of humic substances given its ability to provide quantitative as well as qualitative analyses of major functional groups such as carboxylic acid, phenol, amide, ester and saturated and unsaturated hydrocarbons (Stevenson, 1994). For example, a strong relationship with a slope of one has been found between the carboxylic content of humic acids determined by both wet chemical analysis and FTIR methods (Celi et al., 1997), and a strong inverse relationship has also been found between the intensity ratio of 1415 to 1590 cm^{-1} and O/C ratio determined by elemental analysis (Johnston et al., 1994). Mecozzi and Pietrantonio (2006) have used FTIR to study the distribution of carbohydrates, proteins and lipids within different molecular weight fractions of fulvic and humic acids in sediments.

Due to the nature of DOM, as a mixture of organic compounds, there will be an overlap among bands that are close in frequencies. In addition, bands that are more common among compounds will be above the background, while less common bands will disappear under the background. This will make the DOM spectra appear simpler than those from any known single constituent compound (Mayo et al., 2004; Smith,

1996). Thus one could expect that identifiable changes in the DOM FTIR spectra would imply profound changes in DOM structure.

The high signal to noise ratio of an FTIR spectrum gives researchers the capability to enhance the resolution of bands broader than the instrumental resolution. One of the most often applied resolution enhancement methods is taking the second derivative of an FTIR spectrum, an approach widely used in peak identification and library search software (Denoyer and Dodd, 2002; Griffiths and De Haseth, 2007; Smith, 1996). Another resolution enhancement method is Fourier self-deconvolution, which can resolve the position of the peaks, albeit with distortion of the band width and its intensity (Griffiths and De Haseth, 2007; Smith, 1996).

The power of ^{13}C-NMR and FTIR as non-destructive and complementary techniques in providing information on the distribution of DOM functional groups could help to construct a better comprehensive picture of the change in the DOM as it moves from land to the ocean through an estuary. In this work, I will couple the two techniques (including resolution enhancement in the FTIR approach) to quantify the change in DOM compound classes (with emphasis on the carboxyl, amide and ester compound classes) on a transect from the Dismal Swamp (Virginia, USA) to the coastal Atlantic Ocean passing through the Elizabeth River and the mouth of the Chesapeake Bay.

2 METHODS

2.1. Sampling sites

Samples were collected from late August to early September 2007 at five sites along a transect from the Great Dismal Swamp through the Elizabeth River /Chesapeake

Bay system to the coastal ocean (see Fig. 1.1). Site DS (Portsmouth Ditch in Great Dismal Swamp, Virginia, USA) is representative of the swampy headwaters of the Elizabeth River system, has very high DOC loadings, and contains a large proportion of terrestrially-derived DOM. Site GB in Great Bridge, Virginia is forested with marshes along the shoreline. The TP site (Town Point Park, Norfolk, Virginia) is mid-river and contains natural autochthonous and allochthonous organic matter from the three branches of the Elizabeth River and the lower Chesapeake Bay. The down-river CBB site (Chesapeake Bay Bridge-Tunnel) is at the mouth of the Chesapeake Bay; its organic matter sources include salt marshes and sediments of the lower Chesapeake Bay and its sub-estuaries as well as imported coastal marine material and autochthonous algal production. The Offshore coastal ocean site (OSC, 37° 10.132' N, 75° 37.891' W) could be impacted by water flowing out of the Chesapeake Bay, but should also contain significant proportions of autochthonous marine organic matter.

My sampling was concurrent with an intensive harmful red tide bloom (over 15,000 cell ml^{-1} and chlorophyll *a* levels of up to 367 ug/L) caused by the dinoflagellate *Cochlodinium polykrikoides.* This bloom started in the James River and progressed throughout the lower Chesapeake Bay area and into the coastal Atlantic Ocean, starting in August 2007 and continuing for over a month (Bernhardt et al., 2008).

2.2. Sampling

Surface water samples were collected using an acid-cleaned and pre-conditioned polypropylene bucket from late August to beginning of September 2007; water temperature was measured concurrently at the sampling sites. The GB, TP, and CBB

samples were collected within half an hour of low tide using the shoreline (GB) or pier structures (TP and CBB) for access to the water. The Offshore sample (OSC) was collected onboard the R/V Fay Slover. The samples were transported to the laboratory in 20 L fluorinated polypropylene jerricans. Prior to filling the jerrican with sample, it was soaked overnight in an alconox solution, rinsed with deionized water, then soaked overnight (or longer) in 10% hydrochloric acid, rinsed with deionized water again and preconditioned with sample (3x) before being filed with sample. Upon arriving in the laboratory, salinity and pH were measured with a refractometer and a calibrated pH meter respectively. Sub-samples of the whole water were taken for TOC measurements. Then, samples were sterile-filtered using 0.1μm Whatman Polycap cartridge filters which had been previously soaked in methanol and back flushed with Milli-Q for at least one hour, then conditioned with 1-2 liter of the sample. A representative aliquot (10% volume) of sterile-filtered sample from each jerrican was taken and these aliquots were mixed in a cleaned jerrican to represent the average composition from all the jerricans. A sub-sample for DOC measurement was taken from this mix. DOC samples were collected in acid cleaned and pre-combusted (450 C^{o}) TOC vials (I-Chem*), then acidified immediately to pH 2 with 5 M phosphoric acid.

2.3. Ultrafiltration

An ultrafiltration system equipped with a polysulfone 1KDa cartridge that has 25 sq. ft active surface area (Separation Engineering, Inc.) was used to separate both high and low molecular weight fractions (hereafter HMW and LMW, respectively). The filtration system was cleaned and conditioned after Guo and Santschi (1996). In brief the

system was cleaned before each sample with 8 L of each of the following solutions: Alconox detergent (1-2%), sodium hydroxide (0.05M) and hydrochloric acid (0.02M). Between each cleaning solution the system was rinsed with 40 L of de-ionized water (2 x 20 L). After the total cleaning protocol was completed, 20 L of de-ionized water was run as a blank and a sub-sample of retentate (concentration factor of 8) was taken to measure the DOC blank. The system was then conditioned with 4-5 L of actual, sterile-filtered (<0.1μm) natural-water sample, after which 40-160 L of sterile-filtered sample was concentrated through the system to approximately 2.3 L at pressures of approximately 30 psi. Subsamples were taken from both HMW and LMW fractions for DOC mass balance; the salt-containing retentate (HMW) solution was then diafiltered with 15-20 L de-ionized water until the filtrate reached a salinity of zero (measured by refractrometer). The freshwater Dismal Swamp sample (DS) was also diafiltered, but with only 5 L de-ionized water. In all cases, the system was rinsed twice with 5 L de-ionized water to recover HMW left in the "dead volume" of the system. These retentate rinses were added to the diafiltrated retentate, and the mixed retentate was stored frozen until further processing. During each step subsamples were taken from both retentate and filtrate for DOC measurements to allow recovery and mass balance calculations.

The retentate fractions (HMW) from Great Bridge (GB), Town Point park (TP), Chesapeake Bay Bridge (CBB) and the Offshore site (OSC), were further concentrated to around 50 ml and further diafiltered with 3 L de-ionized water using stirred cells (Amicon 8400) pressurized with nitrogen gas, equipped with 1kDa regenerated cellulose membrane (Millipore). Subsamples from the final retentate were taken for DOC measurements, and subsequent recovery and mass balance calculations. The resulting

retentates were frozen and, along with the Dismal Swamp retentate from the large-volume cross-flow system were then freeze dried.

Due to the differences in processing the Dismal Swamp sample relative to the other (salt-containing) samples, there may be some difference in sample recovery/fractionation. However, ionic strength and pH also affect recoveries by ultrafiltration (e.g., Dalzell et al., 2007), and the variation due to adding a stirred cell step for the salt samples is most likely a second-order effect relative to these, especially as the majority of the concentration and desalting for all samples occurred on the larger-volume cross-flow system.

2.4. DOC measurements

DOC concentrations were measured (with triplicate injections) using a standard dissolved organic carbon analyzer (Aurora 1030W TOC analyzer, College Station, TX) with 20% sodium persulfate (98%, Fisher Scientific) as the oxidizer. To correct for any incomplete combustion of DOC due to the competition between chloride and DOC for persulfate, calibration standards were dissolved in artificial seawater, prepared according to Kester et al., (1967). To insure removal of any organic traces contaminants in the artificial seawater, it was UV photooxidized (24 h; 1.2 kW Hg-arc lamp; Ace Glass) prior to use. The calibration standards were prepared in the same salinity range as the samples with sucrose used as the DOC standard.

2.5. $\delta^{13}C$ and elemental analysis

The $\delta^{13}C$, carbon and nitrogen percentages of freeze dried HMW DOM were measured (in duplicate) by a Europa elemental analysis (EA) system coupled to a Europa Geo 20-20 IRMS (SerCon Limited, Crewe, UK). Ascorbic acid ($\delta^{13}C$ value = - 24.45‰) was used for the calibration standards and sucrose ($\delta^{13}C$ value = -10.67‰) was introduced as a check standard. Data are reported as $\delta^{13}C$ values where $\delta^{13}C$= $(R_{sample}/R_{standard} -1) *1000$ and $R_{standard}$ is the Pee Dee Belemnite (PDB) standard.

2.6. Solid state ^{13}C-NMR

Cross polarization/magic angle spinning solid NMR (CP/MAS ^{13}C NMR) spectra were collected using a Bruker Avance II 400 spectrometer operating at 100 MHz for ^{13}C, spun at 14 KHz for 4569 scans. Note that due to high levels of iron, a paramagnetic ion, in the Dismal Swamp sample, DS DOM was analyzed for longer (65536 scans) in order to improve the signal-to-noise ratio. For all samples, the recycle delay (D1) and contact time were 1 sec and 1.5 ms respectively. All the experiments were conducted using a 4-mm triple resonance probe and the samples were packed into 4-mm NMR tubes with Kel-F caps.

The spectra were integrated in segments according to Dria et al. (2002), with the region from 0-45 ppm assigned to paraffin carbon (CH_x), the 45-60 ppm to the methoxy group (CH_3O-), 60-90 ppm to carbohydrate or O-alkyl (HCOH) groups, 90-120 ppm to anomeric carbon in carbohydrate (O-C-O), 120-140 ppm to substituted aromatic carbon or double bond carbon (C=C/Ar-C), 140-160 ppm to oxygen substituted aromatic C, 160-

190 ppm to carboxyl, aliphatic ester and amide (COO/CON) carbon and the 190-220 ppm region was assigned to aldehyde and ketone carbon (C=O).

A mixing curve of the chemical composition of each of the compound classes (e.g. carbohydrate, aromatic etc.) was constructed by calculating the conservative carbon percentage of each compound class at a specific salinity ($\%C_M$) according to the modified mass balance equation(Eq. 2.1)

$$\%C_M = \frac{(f.DOC_{DS}.\%C_{DS} + (1-f).DOC_{OSC}.\%C_{OSC})}{DOC_M} \quad \text{Eq. (2.1)}$$

Where f is the riverine fraction calculated from the salinity, DOC_M is the expected DOC concentration (HMW fraction) due to a conservative mixing between the riverine and open ocean end members, $\%C_{DS}$ and $\%C_{OSC}$ is the carbon percentage of the compound class calculated (e.g. carbohydrate, aromatic.etc.) of the Dismal Swamp and Offshore sites respectively. The DOC_{DS} and DOC_{OSC} are the DOC concentration of the high molecular weight (HMW) fraction (after desalting via stirred cells) of Dismal Swamp and Offshore sites respectively. This conservative mixing curve is used for comparison with the actual composition of the HMW DOM at each sampling point in the transect.

2.7. FTIR analysis

Samples were introduced as KBr discs where exactly 1.0 mg sample is diluted with 100.0 mg KBr (which had been previously heated in a lab oven for two hours at 105° to remove any moisture). To reduce light scatter during the analyses, the mixture was then crushed and homogenized (Smith, 1996) using a Wig-L-Bug grinding mill. A

subsample was then compressed between two clean, polished iron anvils in a hydrolic press at 20,000 psi to form a KBr window. To minimize wedging effects (Hirschfeld, 1979), the discs were pressed for a second time after they had been rotated 90° before removal from the hydrolic press. FTIR spectra were obtained by collecting 200 scans with a Nicolet 370 FTIR spectrometer (DTGS detector and KBr beam splitter) equipped with purge gas generator unit. Spectra were collected using a resolution of 4 cm^{-1} and Happ-Genzel apodization. To guard against CO_2 contamination from lab air, a 4-min lag-time between closing the analytical chamber and starting the analysis was implemented. A pure KBr disc was analyzed before each sample analysis as a background blank. The FTIR spectra were converted into absorbance units, normalized by summed absorbance from 4000-500 cm^{-1}, and multiplied by 1000.

Using Grams/Al 8.0 spectroscopy software (Thermo Electron Corporation), the normalized absorbance spectra were processed with the 2nd order Savitzky-Golay method with 11 convolution points used to generate the second derivative of the spectra. For comparison, another second derivative was also calculated using the Gap method with an 11 cm^{-1} Gap value (note that the instrument resolution is 1.9 cm^{-1}). For an additional comparison, the spectral region from 1850-1450 cm^{-1} was also processed by Fourier self-deconvolution with a gamma factor of 20, and the deconvoluted spectrum was 60% smoothed using a Bessel function.

For an additional test of peak overlaps and quantification of these peaks, the FTIR area from 1900-900 cm^{-1} was peak fitted using Grams/Al 8.0 software with Voigt line shape, which is a convolution between Gaussian and Lorentzian line shapes, The reason behind using the Voigt line shape is that it can correct for the broadening features due to

molecular collisions and the Doppler effect during infrared measurements (Griffiths and De Haseth, 2007). The numbers and the exact frequencies of the peaks in the region were obtained from the 2nd derivative of the corresponding spectrum, while the peak width was optimized to within ± 15 cm^{-1} of the peak width obtained from the 2nd derivative.

3. RESULTS AND DISCUSSION

3.1. DOC and pH along the transect

As the salinity along the transect increases from 0 at the Dismal Swamp (DS) to 35 at the Offshore site (OSC), the DOC concentration decreases from 7722 to 98 μM-C (see Table 2.1). Although it is tempting to view this transect as a traditional freshwater to Offshore transect, there is a lock between the Dismal Swamp and Great Bridge sites and the hydrological connection is complex. Plotting the DOC values against the salinity of the sites from Great Bridge to Offshore (sites sharing a clear hydrological connection) shows a concave up curve (Fig. 2.1), which indicates either that there was a net sink of DOC in the middle of the estuary, that there was dilution from the confluence of the Elizabeth River branches and the James River, or that variations in the DOC values in the two end members are shorter than the residence time of the water between GB and OSC. As the DOC decreased there was a concurrent loss of acidity as observed from the pH values (Table 2.1)

Table 2.1. Water temperature, salinity, pH and DOC concentration of the water samples from the five sites.

Site	Water Temp. (C^0)	Salinity	pH	DOC (s.d.) µM-C
DS	25.0	0	3.15	7722 (98)
GB	29.0	18	7.58	620 (11)
TP	29.0	24	7.65	278 (7)
CBB	28.4	30	7.93	179 (7)
OSC	25.5	35	8.07	98 (3)

(s.d.) standard deviation based on three runs.

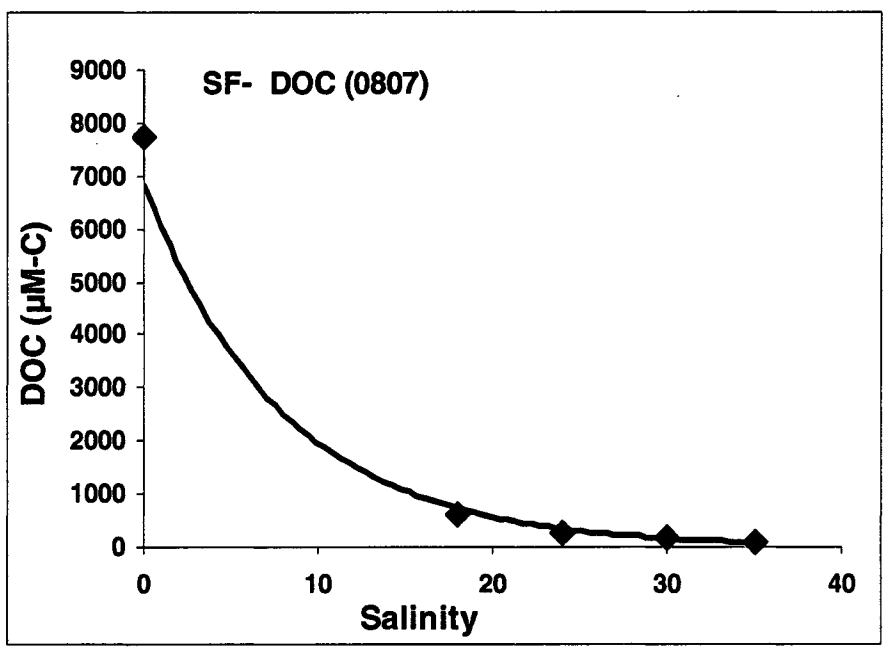

Fig. 2.1. Plot of dissolved organic carbon (DOC) concentration of the sterile-filter (SF) versus the corresponding water-column salinity along the transect. The solid line represents the exponential fit.

3.2. $\delta^{13}C$ and elemental analysis of HMW

From cross-flow ultrafiltration, the DOC recovery in the HMW fraction ranged from 71– 27% (Table 2.2) with the recovery decreasing in the more saline samples; similar recovery trends relative to salinity have been made in other studies (Benner et al., 1997; Repeta et al., 2002; Wang et al., 2004). The percent recovery was further decreased for the GB, TP, CBB and OSC samples by an extra 4-7% (Table 2.2) due to the second diafiltration step (using the stirred cell). Plotting the DOC concentration of the HMW DOM versus salinity (Fig. 2.2) shows a similar behavior (concave up) as the DOC of sterile-filtered (SF) bulk DOM (Fig. 2.1).

Elemental analysis of the freeze-dried retentates showed that the carbon content within the HMW fraction (after desalting via stirred cells) was higher than most of the reported values for estuarine/marine HMW isolates (Benner et al., 1997; Benner et al., 1992; Guo and Santschi, 1997), indicating that I was successful in removing most of the inorganic salts during the two diafiltration steps. The high carbon content (45.77 wt%) in the DS sample compared to other sites may indicate that DS HMW DOM has more unsaturated carbon and less nitrogen and oxygen relative to HMW DOM from the other sites. The nitrogen content of the DOM increases as I move to the ocean; an indication of the effects of autochthonous sources and microbial reworking on the DOM along the transect. This is reflected in the decrease of the C/N atomic ratio from 55.12, typical for vascular-plant DOM sources, to 11.18, which is within the range of marine microalgae and microbial C/N values (Bianchi, 2007).

Table. 2.2. The DOC recovery, elemental analysis and stable carbon isotope values for the high molecular weight (HMW) DOM from the five sites.

Site	% HMW(s.d.) Recovery*	%Mass-balance (s.d.) †	% C (s.d.) mass	% N (s.d.) mass	C/N (s.d.) mole	$\delta^{13}C$ (s.d.) PDB
DS	71 (1)	103 (2)	45.77 (0.42)	0.83 (0.01)	55.12 (0.37)	-27.35 (0.01)
GB	48 (3)	97 (6)	34.48 (1.76)	2.76 (0.15)	14.58 (0.07)	-25.34 (0.01)
TP	41 (4)	95 (6)	30.79 (0.97)	2.98 (0.06)	12.08 (0.60)	-21.76 (0.93)
CBB	31 (4)	90 (8)	33.04 (0.70)	3.17 (0.09)	12.17 (0.09)	-21.87 (0.16)
OSC	27 (5)	95 (9)	32.62 (n.d.)	3.40 (n.d.)	11.18 (n.d.)	-20.37 (n.d.)

* HMW recovery is based on DOC measurements of the retentate recovered from the ultrafiltration system after the first diafiltration step and the initial sterile filter sample, as well as the concentration factor.

† The mass-balance percentages were calculated from DOC measurements of the retentate recovered after the first diafiltration, the filtrate (LMW) and the initial sterile filter samples.

§ The HMW-DOC concentration after the second diafiltration step (stirred cell), taking into account the concentration factor.

HMW recovery after the second diafiltration step (stirred cell), calculated based on DOC measurements, taking into account the concentration factor

n.d. one of the EA-IRMS runs was lost so we could not calculate the standard deviation.

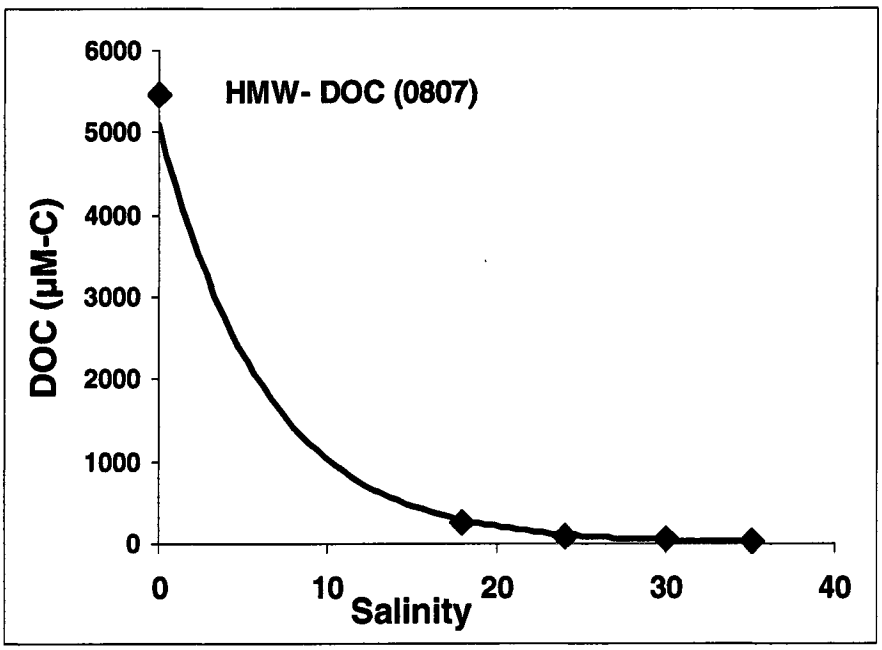

Fig. 2.2. Plot of dissolved organic carbon (DOC) concentrations of the high molecular weight fraction (HMW-DOC) after the second diafiltration step versus their corresponding water-column salinity along the transect. The solid line represents the exponential fit.

The hypothesized change in carbon sources is also strongly supported by the enrichment of $\delta^{13}C$ values from -27.35 at DS to -20.37‰ at OSC corresponding to typical values for organic matter from C3 vascular plants and marine autochthonous sources, respectively. The contribution from C4 plants (e.g. from salt marshes) into DOM looks insignificant in this transect; because the compound-specific ^{13}C values of lignin components in C_{18} DOM extracts from the same transect indicate that the lignin is mainly coming from C3 plants (Sleighter et al., 2008).

Both the C/N and $\delta^{13}C$ data show that there are gradient changes in the bulk chemical characterization of the HMW-DOM as I move along the estuary. The percentage of terrestrial organic matter ($\%OC_{Terr}$) contribution at each site could be calculated by constructing a simple two end member mixing model using the isotope values of DS and OSC as the terrestrial and marine end members respectively, represented in the following mass balance equation:

$$\delta^{13}C_{Site} = \delta^{13}C_{Terr} * \%OC_{Terr} + (100 - \%OC_{Terr}) * \delta^{13}C_{Marine} \qquad \text{Eq. (2.2)}$$

The mixing model shows that 71% of the carbon in the HMW-DOM at Great Bridge is coming from terrestrial sources while only 20 and 21% coming from terrestrial sources at Town Point and Chesapeake Bay Bridges sites respectively. This dramatic change in the contribution of terrestrial sources in the lower estuary has also seen in other studies of HMW-DOM isolated along Galveston Bay and Chesapeake Bay (Guo and Santschi, 1997).

3.3. Solid state- CP/MAS ^{13}C NMR analysis

The ^{13}C-NMR spectra of HMW DOM from the Dismal Swamp (Fig. 2.3) covers the entire range of the chemical shift (0–230 ppm) and indicates the complexity of Dismal Swamp DOM and its wide varieties of chemical functional groups. A strong band at 175 ppm, coupled with knowledge of the low nitrogen content and high C/N ratio (Table 2.2) of this sample, can be attributed mainly to carboxylic acid and aliphatic ester groups. The DS spectrum looks very similar to previously reported ^{13}C-NMR spectra of aquatic humic substances and fulvic acid isolated from the Neranie swamp region in Australia and the Dismal Swamp respectively (Finmen et al., 2007; Lu et al., 2000). The quantification of

the Dismal Swamp functional groups (Table 2.3) in the NMR-spectrum shows that 20% of the carbon appears as paraffinic carbon (CH_x); most likely a high concentration of CH_3 and CH_2 carbon comes from lipids and biopolymers (Dria et al., 2002) The carboxyl/ester (COO) and carbohydrate or O-alkyl (HCOH) functional groups are somewhat less prevalent, 17.67% and 17.55%, respectively.

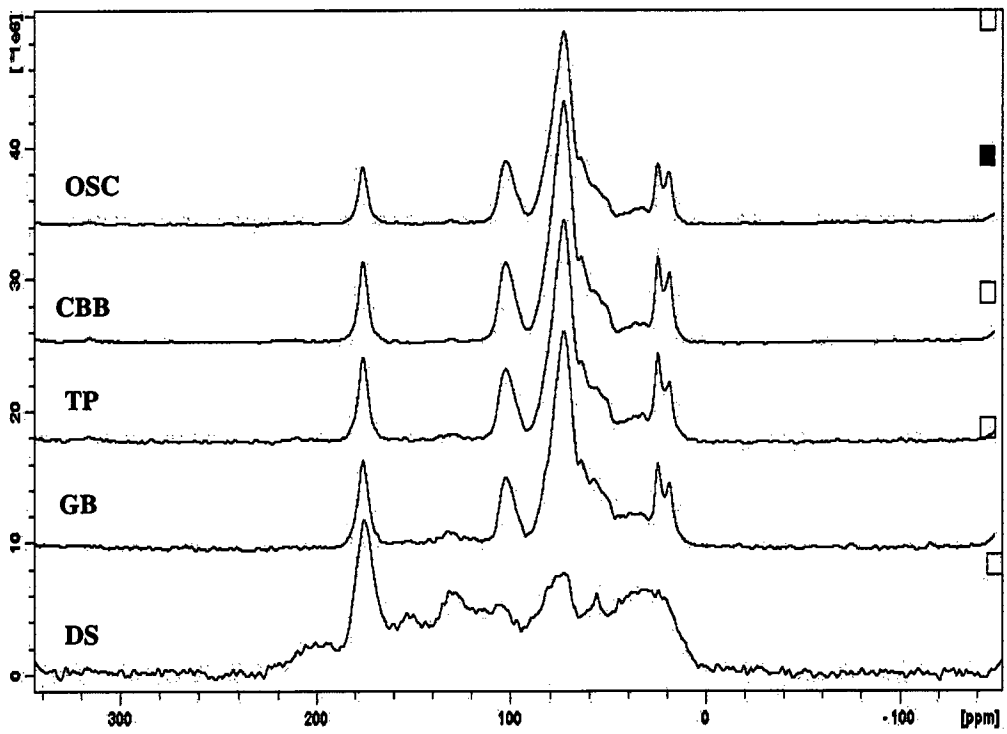

Fig. 2.3. CP/MAS solid ^{13}C-NMR spectra of HMW-DOM isolated from the five sites.

Table.2.3. The relative carbon percentage of HMW-DOM functional groups and compound classes (total aliphatic, total carbohydrate and total aromatic) obtained from ^{13}C-NMR spectra.

Site	CH_x (0-45) ppm	CH_3-O (45-60) ppm	Total aliphatic	HCOH (60-90) ppm	O-C-O (90-120) ppm	Total Carbohydrate	C=C/ Ar-C (120-140) ppm	Ar-O (140-160) ppm	Total Aromatic	COO/CON (160-190) ppm	C=O (190-220) ppm
DS	20.01	7.49	27.5	17.55	13.54	31.09	10.82	7.89	18.71	17.67	5.04
GB	18.54	10.41	28.95	43.66	11.47	55.13	3.33	1.93	5.26	9.99	0.68
TP	17.39	8.95	26.34	47.44	12.48	59.92	1.79	0.93	2.72	9.72	1.3
CBB	15.6	7.93	23.53	52.35	13.43	65.78	0.68	0.21	0.89	8.73	0.07
OSC	15.19	7.58	22.77	53.73	13.62	67.35	0.74	0.44	1.18	7.94	0.77

Many studies (Benner et al., 1992; Bianchi et al., 2004; Finmen et al., 2007; Lu et al., 2000) have combined the integrated functional group areas from ^{13}C-NMR into compound classes (carbohydrate, aromatic and aliphatic). Following this lead I combined the integrated area of CH_x (0-45 ppm) and methoxy groups (45-60) to represent the total aliphatic pool (0-60 ppm); the total carbohydrate pool (60-120 ppm) is considered the sum of the integrated area between the HCOH group (60-90 ppm) and anomeric carbon O-C-O (90-120); and the total aromatic contribution (120-160 ppm) is equal to the combination of the C=C/Ar groups (120-140 ppm) and oxygen substituted aromatic groups (140-160 ppm). Applying this approach I found that total carbohydrate (most likely cellulose) accounts for 31% of the Dismal swamp HMW-DOM, the aliphatic carbons account for 27.5%, and the aromatic carbons (120-160 ppm) account for only 18.7%. The higher percentage of aliphatic carbon and carbohydrate compared to aromatic carbon could be a sign of the low degree of humification of the Dismal Swamp DOM. This is in agreement with previous results showing that swamp water has a lower humification degree than swamp soil, peat and brown coal humic substances (Lu et al., 2000; Stevenson, 1994).

As I move from the Dismal Swamp to the Great Bridge site, the ^{13}C-NMR spectra display more resolved peaks (Fig. 2.3) and the total carbohydrate (60-120 ppm) increased from 31% to 55% (Table 2.3), while the total aromaticity (120-160 ppm) drops to 5.2% from 18.7%, the carboxyl/amide functional groups drop from 17.67% to almost 10%, aldehyde/ketone decreases from 5% to 0.68% and the paraffinic carbon drops slightly from 20% to 18.54%; the total aliphatic contribution (0-60 ppm), however, increases slightly to 28.94% from 27.49%. The same trends were observed with a smaller change

as I move to the most saline site (OSC) through sites TP and CBB. The total carbohydrate contributes more than 67% of the total carbon at OSC; at the same time total aromaticity and carboxyl/amide represent 1.17% and 7.94% respectively (see Fig. 2.3 and Table 2.3). In my HMW data set, there were strong inverse relationships between total carbohydrates and total aromaticity (r^2=0.985) and between total carbohydrates and carboxyl/amide (r^2= 0.976).

Plotting total carbohydrates, total aromaticity and total aliphatic carbon against salinity (Fig. 2.4a-c) shows that total carbohydrate-C percentage is higher than the expected mixing curve while the total aromaticity is lower than mixing curve. This could indicate that the periodic variation in delivering these compound classes from the two end members are shorter than the residence time of the water along the transect, that the river confluence is acting as a source for carbohydrate material and dilutes the aromatic component, or that there is net production of carbohydrate compounds along with net loss of aromaticity of DOM in the middle of the transect. Unfortunately, I couldn't calculate the residence time or delivery of the water along the transect due to the complexity of the area and absence of fresh water flow-rate records. However, there is evidence supporting the third explanation. For example, the work conducted by Minor et al. (2007) on three of my sampling sites (GB, TP and CBB) shows that photobleaching of DOM could be responsible for decreasing the aromatic moieties, while the increase of carbohydrate groups could be related to autochthonous production (Bianchi et al., 2004).

On the other hand, the total aliphatic-C percentage (Fig. 2.4c) shows a scatter behavior around the mixing curve, with the GB site appearing slightly above the mixing curve while the TP and CBB appear slightly below the mixing curve. A likely

explanation of this behavior is that the ^{13}C-NMR integrated region between (0-60 ppm) consists of different aliphatic components that have different biogeochemical reactivities where some components increase toward the marine end member while the others decrease; the addition of such components would exhibit such behavior. This needs further investigation.

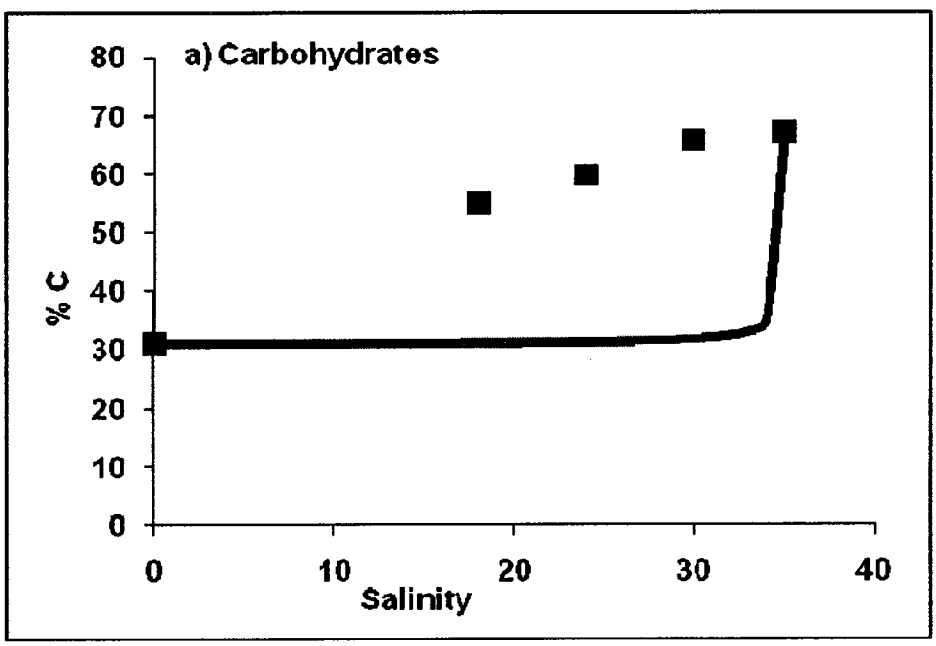

Fig. 2.4. The plot of relative carbon percentage (from ^{13}C-NMR) of a) Total carbohydrates, b) Total aliphatic material and c) Total aromatic material within the HMW-DOM isolated from the five sites vs. the corresponding water-column salinity at these sites. The solid line represents the expected line if DOM changes were due only to the mixing of two end-members, as calculated from Eq.(2.1).

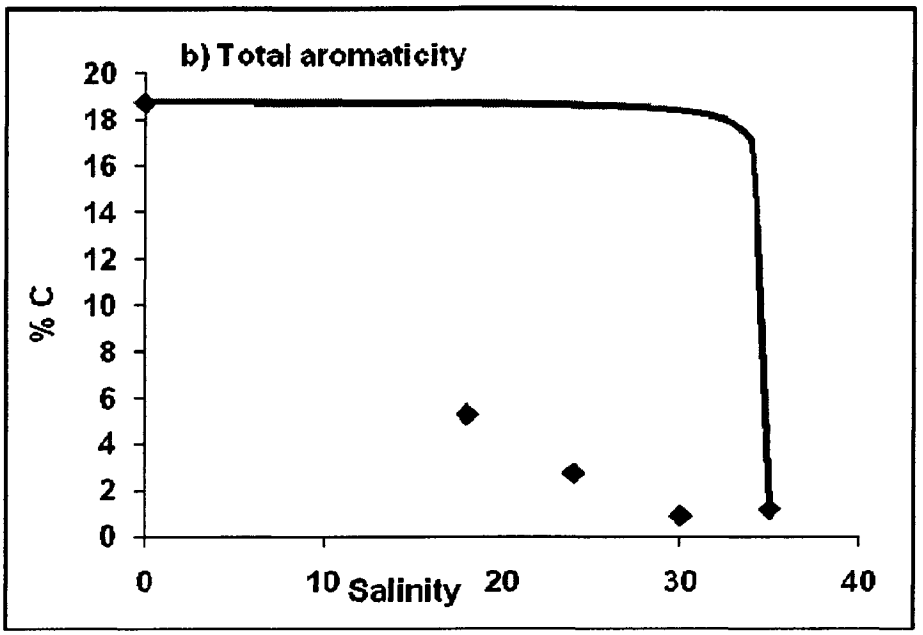

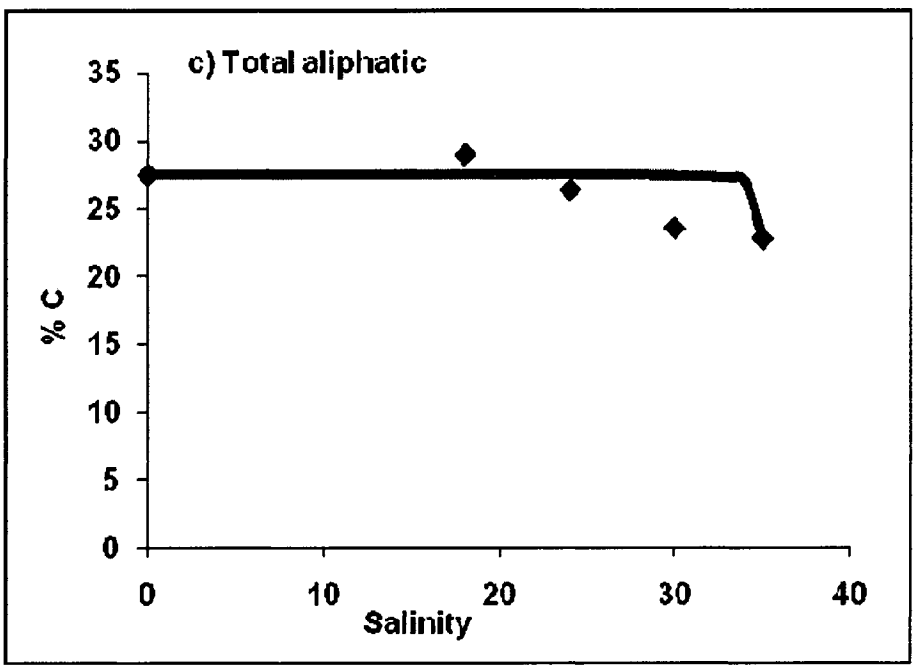

Fig. 2.4. Continued.

The coupling of the loss in aromaticity and the increase in carbohydrate contents (r^2=0.985) could indicate that they were affected by the same process, as photooxidation is the major process in removing lignin compounds (one group of terrestrial aromatic compounds) in aquatic systems (Hernes and Benner, 2003) and photooxidation could make terrestrial DOM more bioavailable (Bertilsson et al., 1999; Mopper and Kieber, 2000) which will increase the carbohydrate contents both as residual, less photoreactive, material and due to microbial inputs (Benner and Opsahl, 2001; Bianchi et al., 2004; Repeta et al., 2002).

The increase of %C of total carbohydrates in the middle of the transect is also in agreement with the observed red tide during my sampling window (Bernhardt et al., 2008) and evidence of the gradual increase in polysaccharides within the culture media of the same red tide organism (*Cochlodinium polykrikoides*, Kim et al., 2002). In field studies in the Mississippi plume, Benner and Opsahl, (2001) also report a higher concentration of combined carbohydrates at the middle salinity relative to adjacent salinities. These authors interpret this as indicating autotrophic production at the middle salinity of the plume.

3.4. FTIR analysis

The FTIR spectrum of the HMW DOM from the Dismal Swamp (Fig. 2.5) is very similar to published FTIR spectra for humic substances isolated from terrestrial soil (MacCarthy and Rice, 1985; Stevenson, 1994; Stevenson and Goh, 1971). A very broad band around 3400 cm^{-1} can be attributed to the overlap of O-H stretching of phenol, carbohydrate and carboxylic acid compounds, the broadness of this peak resulting mainly

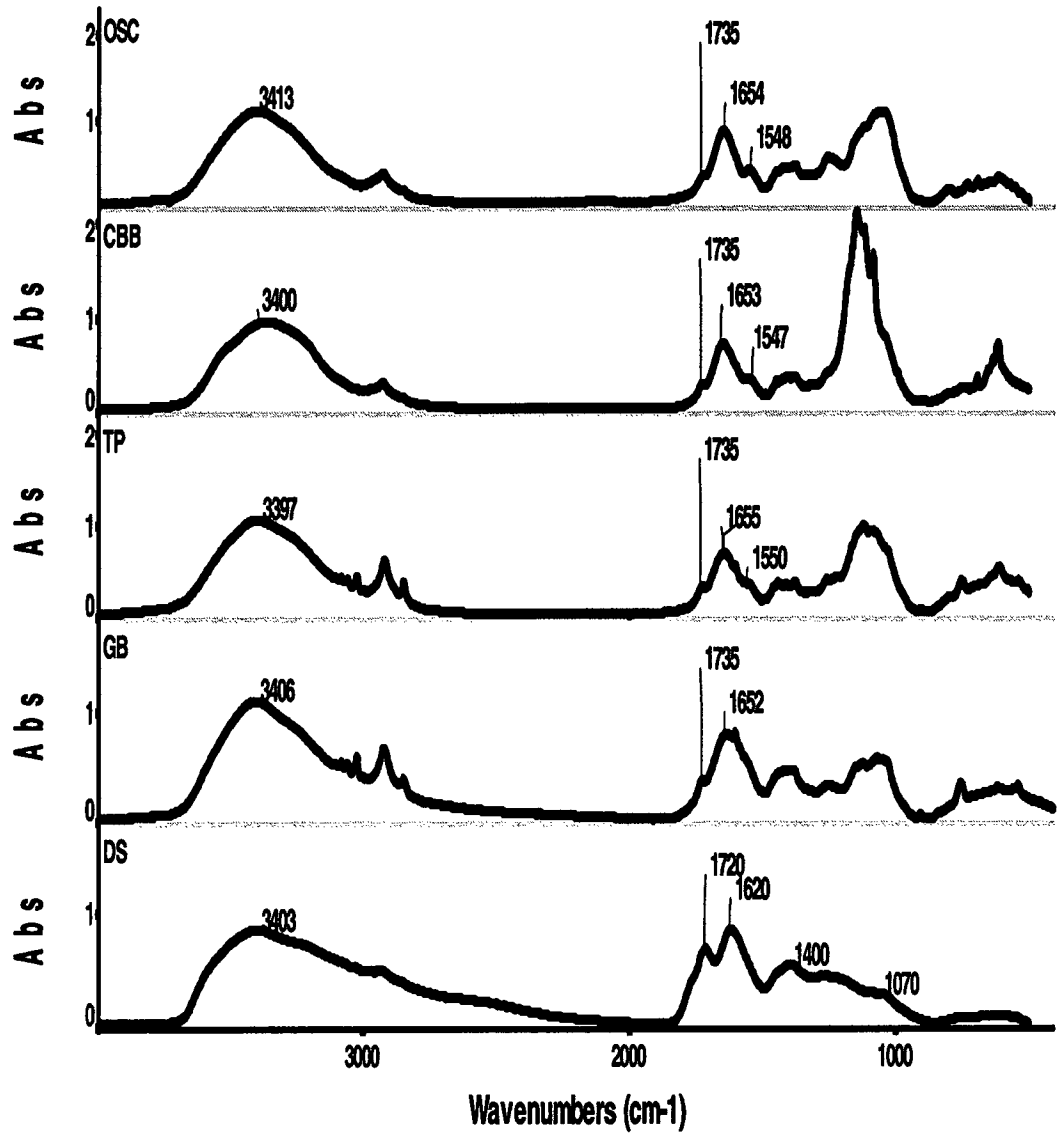

Fig. 2.5. The FTIR spectra of the high molecular weight (HMW) DOM for the five sites.

from the intra-molecular and inter-molecular hydrogen bond interactions of carboxylic acids (Pavia et al., 1996). The area just below 3000 cm^{-1} shows stretching bands for aliphatic C-H bonds. The band at 1720 cm^{-1} is a result of carbonyl stretching of the protonated carboxylic acid functional group (MacCarthy and Rice, 1985; Stevenson, 1994) and the band near 1620 cm^{-1} can be attributed to the de-protonated asymmetric carboxyl stretching, while the symmetric stretching of the de-protonated carboxyl group appears as a broad band around 1400 cm^{-1} (MacCarthy and Rice, 1985; Mayo et al., 2004). The bands around 1070 cm^{-1} could come from overlap of the vibrational coupling of C-O stretching of carbohydrate, ether and ester compounds (Mayo et al., 2004; Stevenson and Goh, 1971).

As I move to the Great Bridge site, the FTIR spectrum (Fig.2.5), still shows a band around 3400 cm^{-1}, however the band is less broad compared to the DS spectrum, probably due to a loss in hydrogen bonding at higher pH. The intense bands above and below 3000 cm^{-1} are attributed to C-H stretching of aromatic and aliphatic compounds respectively. The band at 1720 cm^{-1} is missing and a new band appears at 1735 cm^{-1}, which can be attributed to aliphatic ester (Mayo et al, 2004, Pivia et al., 1996 and many other references). The band around 1620 cm^{-1} has been replaced by a higher energy band (1652 cm^{-1}), which is a typical amide I band, resulting from stretching of the carbonyl bond (C=O) in the amide functional group (Mayo et al., 2004; Shurell, 2002) As the salinity gradient increase along TP, CBB and OSC, FTIR spectra continue to exhibit the aliphatic ester and amide I bands around 1735 cm^{-1} and 1650 cm^{-1}, respectively, however a shoulder starts to resolve around 1550 cm^{-1}, consistent with an amide II band and a

strong indication of a secondary amide (Mayo et al., 2004; Pavia et al., 1996; Shurell, 2002). The bands around 1070 cm^{-1} become more intense and are shifted to lower frequency in the more marine samples.

The FTIR bands in the area from 1900-900 cm^{-1} in all the spectra are very broad and exhibit many shoulders (see Fig. 2.5), indicating the presence of overlapping bands close in frequency; detailed structural information could be hidden under these broad bands. One of the ways that has been applied widely in the spectroscopy, biochemistry and food science communities to enhance infrared spectral resolution in complex mixtures is employing the 2^{nd} derivative of the FTIR spectrum (Brandenburg and Seydel, 1996; Denoyer and Dodd, 2002; Naumann et al., 1996). This derivative can identify the number of overlapping bands and the exact frequencies of peak response, based on its ability to clarify changes in the slope within the original spectrum (Griffiths and De Haseth, 2007; Smith, 1996). Applying the 2^{nd} order Savitzky-Golay method to generate the second derivative of the FTIR spectra from all the sites results in the resolution of each broad band into sharper downward pointing bands. Comparing the 2^{nd} derivative spectra with the original spectra form DS, GB and OSC as examples (Fig. 2.6a-c) shows that 2^{nd} derivative spectrum points downward for all the major bands in the original spectrum, and also resolves the shoulders of the original spectra.

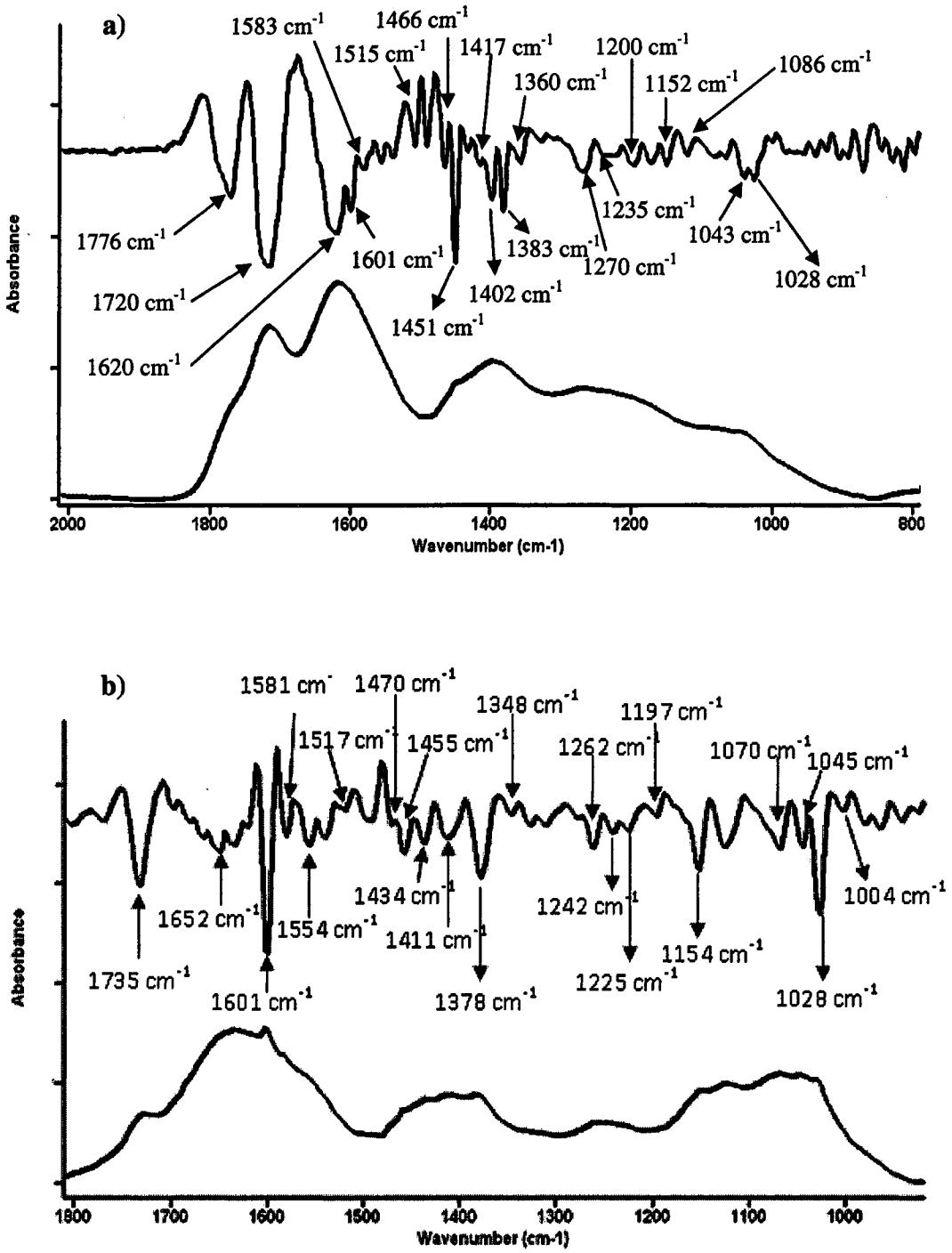

Fig. 2.6. The region between 1800-800 $cm^{-1}$of the FTIR spectra (bottom spectrum) and its 2nd derivative (upper spectrum) of high molecular weight (HMW) DOM of a) Dismal Swamp, b) Great Bridge and c) Offshore site.

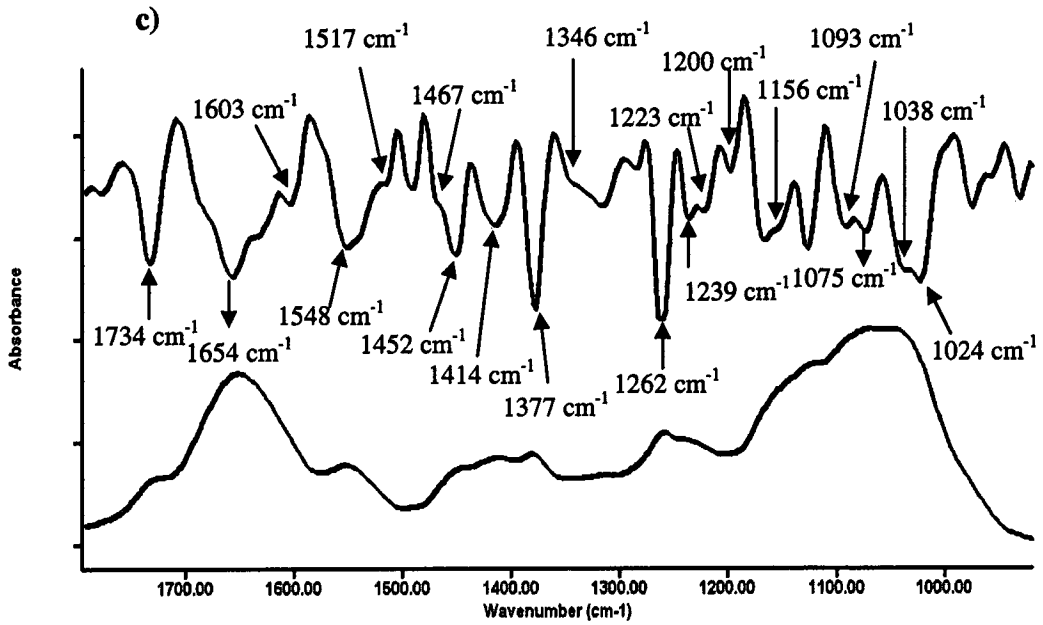

Fig. 2.6. Continued.

Keeping in mind that these spectra are representative of mixtures of biologically and chemically derived compounds called DOM, I have identified the major/common functional group bands of compound classes, e.g. carboxyl, ester, amide, carbohydrate, and phenol (see Table 2.4). In order to verify the presence of each functional group, I use several criteria. First, the band frequency should be within the published range of the specific vibration mode and the other vibration modes of the tentatively identified band should also be present. Second, the absorbance ratio of counterpart vibration modes should match with their change in electrical dipole moment. For example, to verify the

Table 2.4. The frequency of the major FTIR vibration modes for the functional groups identified from the 2nd derivative FTIR spectra of the HMW DOM isolated from the five sites.

Compound class	Type[Reference]	FTIR band (band range)	Band position in (cm^{-1})				
			DS	GB	TP	CBB	OSC
Carboxylic acid	-COOH[a-q]	C=O stretching (1710 ± 15 cm^{-1})	1720	N.P	N.P	N.P	N.P
		C-O stretching (1265 ± 55 cm^{-1})	1270	N.P	N.P	N.P	N.P
		O-H bend in-plane (1418 ± 22 cm^{-1})	1417	N.P	N.P	N.P	N.P
		O-H out- off plane bend (930 ± 30 cm^{-1})	940	N.P	N.P	N.P	N.P
	-COO^-[a-q]	Asymm. stretching (1600 ± 40 cm^{-1})	1620, 1601 & 1583	1601 & 1581	1602 & 1582	1601 & 1582	1603
		Symmetric stretching (1405 ± 45 cm^{-1})	1402	1411	1410	1413	1414
Ester	Aliphatic[f-q]	C=O stretching (1740 ± 10 cm^{-1})	N.P	1735	1735	1735	1734
		C-C-O stretching (1185 ± 25 cm^{-1})	1200	1197	1184	1184	1200
		O-C-C stretching (1065 ± 35 cm^{-1})	1043	1045	1046	1040	1038
	Acetyl[m-o]	C-C-O stretching (1240 ± 5 cm^{-1})	N.P	1242	1243	1243	1239
	γ-lactones[b,r]	C=O stretching (1770 ± 10 cm^{-1})	1775	N.P	N.P	N.P	N.P
Amid[f-q]		Amide I (C=O) (~ 1650 cm-1)	N.P	1652	1655	1653	1654
		Amide II (~ 1550 cm^{-1})	N.P	1554	1549	1547	1548
		Amide III (1260 ± 40 cm^{-1})	N.P	1262	1262	1262	1262
Carbohydrate[m-v]		O-H in plane bending (1350 ± 50 cm^{-1})	1360	1348	1347	1348	1346
		O-H out-of-plane bending (~ 650 cm^{-1})	647	654	647	658	650
		C-O asymm. stretching (1100 ± 100 cm^{-1})	1151 1086, 1069 & 1028	1151 1070 1028& 1004	1152 1092, 1071, 1028 & 1003	1151 1084, 1064 & 997	1152 1093, 1075 & 1024
Lignin (Phenol)	Ar-OH[f-q]	C-O asymm. stretching (1230 ± 30 cm^{-1})	1235	1225	1223	1210	1223
	Ar- (lignin)[u-y]	Vibration of aromatic ring (1515 ± 5 cm^{-1})	1515	1517	1515	1511	1517
paraffin	Aliphatic[f-q]	CH_2 scissoring (1450 ± 10 cm^{-1})	1451	1455	1446	1452	1452
		CH_3 asymm. deformation (1460 ± 10 cm^{-1})	1466	1470	1465	1468	1467
		CH_3 umbrella mode (1375 ± 10 cm^{-1})	1383	1378	1378	1379	1377
	Acetyl[m-o]	CH_3 symmetric bend (1430 ± 5 cm^{-1})	N.P	1434	1430	1430	1430

a) Stevenson, 1994. b) Byler et al., 1987. c) Cabaniss, 1991. d) Johnston et al., 1994. e) Celi et al., 1997. f) MacCarthy et al., 1985. g) Piccolo and Stevenson 1994. h) Schnitzer and Ghosh 1982. i) Schnitzer and Skinner 1963. j) Stevenson and Goh 1971. k) Hay and Myneni 2007. l) Smith 1996. m) Smith 1999. n) Mayo et al. 2004. o) Günzler and Gremlich 2002. p) Pavia et al., 1996. q) Shurell 2002. r) Madyastha et al., 1977. s) Brandenburg and Seydel 1996. t) Brandenburg and Seydel 2002. u) Michalska et al., 1984. v) Vonach et al., 1997. w) Mascarenhas et al., 2000. x) Hergert, 1960. y) Pandey 1999.

presence of a de-protonated carboxylic group, the symmetric and asymmetric stretching of this group should be both present and the asymmetric stretch should have higher absorbance than symmetric stretching. Third, when two bands show up in the same published range I use the band shape (e.g. wide, sharp) from the 2nd derivative that matches the published FTIR database of that band. For example the bands at 1348 and 1378 cm^{-1} from the 2nd derivative GB spectrum are in the range of in-plane bending of O-H (1350± 50 cm^{-1}) and the C-H symmetric bending/umbrella mode (1375± 10 cm^{-1}); the band at 1348 cm^{-1} is assigned to O-H bending because it is much wider than 1378 cm^{-1}, which agrees with databases of these bands (Mayo et al., 2004; Shurell, 2002; Smith, 1996). A final criterion used in the band assignment is that the band with a higher change in the electrical dipole moment ($\delta\mu$), e.g. C=O, will dominant over the band with lower $\delta\mu$, e.g. C=C, keeping in mind that the bands representing moieties with high concentration/availability – such as C-H bending in aliphatic compounds- will show above the absorbance background.

Based on the above criteria I have tried to identify the common functional groups of the compound classes (carboxylic acid, ester, amide, carbohydrate, phenol/lignin, and paraffin) in the 2nd derivative spectra within the range from 1900-900 cm^{-1} and determine how the distribution of these functional groups changes as I move along the salinity gradient (See Table 2.4).

3.4.1 Carboxylic acid functional groups

The 2nd derivative spectrum of the Dismal Swamp sample identified all major vibrational modes of both protonated (COOH) and de-protonated (COO^-) carboxyl

groups (see Table 2.4). In addition, the Savitzky-Golay 2nd derivative spectrum shows the presence of three types of de-protonated carboxyl groups at 1620, 1601 and 1583 cm^{-1}, which also appeared in the Gap 2nd derivative and the Fourier self-deconvolution (data not shown). Reviewing the published FTIR spectra of isolated terrestrial humic substances from different sources shows that all spectra share the same band around 1720 cm^{-1}, attributed to the protonated carboxyl group (COOH), however the major de-protonated band (COO^-) could appear either at 1600 or 1580 cm^{-1} and some spectra showed it at 1620 cm^{-1} instead (Byler et al., 1987; Celi et al., 1997; Hay and Myneni, 2007; Stevenson, 1994; Stevenson and Goh, 1971). Adding base or sodium salt to the humic substances decreases the absorbance around 1720 cm^{-1} and 1270 cm^{-1} and increases the absorbance around 1580 cm^{-1} and 1400 cm^{-1}, which is a strong indication of de-protonation of the COOH group (Hay and Myneni, 2007; Stevenson, 1994). However, adding iron salts to humic substances shifts the band at 1720 cm^{-1} to around 1620 cm^{-1} instead of 1580 cm^{-1} (Byler et al., 1987; Schnitzer and Skinner, 1963). This is a strong indication that iron (Fe) could be complexed by the carboxyl groups with the resulting band shifted to higher frequency than the un-complexed carboxyl groups. This suggested iron effect is supported further by the work of Schnitzer and Ghosh (1982) showing that iron makes a strong complex with carboxylic acid of the fulvic acid. Dismal Swamp (DS) is known for its high iron content, for example, Finmen and co-workers (2007) report that iron could account for 0.33% of the elemental composition of humic substances isolated from Dismal Swamp; additionally the iron concentration measured on sterile-filtered water collected from the same sampling site as my DS water (Portsmouth Ditch) was 29.0 $\mu mole\ L^{-1}$ (Minor et al., 2006). All these observations guide me to believe that a

major fraction of the de-protonated carboxyl bands (at 1620 cm^{-1}) in my DS HMW-DOM is complexed to iron while other minor fractions (at 1601 and 1583 cm^{-1}) could present free or complexed with other metals.

The carboxyl group composition changed significantly from the DS to the GB sample. In GB the bands at 1720 and 1620 cm^{-1} are missing and the only bands left are 1601 and 1581 cm^{-1}. The loss of the band at 1720 cm^{-1} along with its associated vibration bands is expected due to the change in salinity and pH between the two sites, as the protonated carboxyl group (COOH) will be converted to the de-protonated carboxyl group (COO^-), appearing either around 1600 or 1580 cm^{-1}. Conversely, disappearance of the 1620 cm^{-1} band with its accompanied symmetric stretching at 1402 cm^{-1} is unexpected; one possible explanation is that iron had been removed from the water column due to ionic strength effects (e.g., Sholkovitz, 1976). The iron-carboxyl signal could be lost due to actual sorption or precipitation of the material containing the complex (Sholkovitz, 1976; Sholkovitz et al., 1978) or the carboxyl group could lose its iron (this shifting the FTIR band to a lower frequency) while remaining present in the HMW DOM. The two bands around 1600 and 1580 cm^{-1} are present in both TP and CBB samples but the 2nd derivative spectrum of OSC HMW-DOM was only able to detect the band around 1600 cm^{-1} while the band around 1580 cm^{-1} had disappeared (see Table 2.4).

3.4.2. Ester functional groups

The 2nd derivative spectrum of Dismal Swamp HMW-DOM reveals a clear broad band at 1775 cm^{-1} which was a shoulder on the original 1720 cm^{-1} band (Fig. 2.4). I have seen the same band in the 2nd derivative FTIR spectra for both sterile-filtered and LMW

Dismal Swamp DOM fractions (unpublished data). The band has also appeared in one of the few reported 2nd derivative spectra of humic substances, a fulvic acid taken from the Armadale Bh horizon (Byler et al., 1987). I assign this band to C=O stretching of a five member ring ester (γ-lactone) based upon the following evidence: gamma-butyrolactone (γ-lactone) is one of very few compounds that has vibration at this frequency (Günzler and Gremlich, 2002; Mayo et al., 2004; Pavia et al., 1996; Shurell, 2002); there is no evident peak from the C=O stretching of aliphatic esters, which normally appears around 1735 cm^{-1}, yet two vibration modes of an ester (C-C-O and O-C-C stretching, Mayo et al., 2004; Pavia et al., 1996; Shurell, 2002) are present. When Piccolo and Stevenson (1994) tried to de-carboxylate humic substances by heating, they found the amount of CO_2 produced was not analogous to the decrease in 1720 cm^{-1} intensity, and one of their explanations for this observation is masking of the 1720 cm^{-1} band by nearby C=O stretching from γ-lactones. The possible sources of γ-lactones could be biodegradation of linalool (terpene alcohol) by soil bacteria, e.g. *Pseudomonas* (Madyastha et al., 1977), or release as a major intermediate compound during the biodegradation of the alicyclic ring of terpenoids (Leenheer et al., 2003); another possible source is production from inter-molecular esterification between carboxylic and alcohol functional groups.

The C=O stretching of γ-lactones is missing in the 2nd derivative GB spectrum (Fig. 2.6 and Table 2.4). The γ-lactones have probably been hydrolyzed as the pH became more basic. However, an aliphatic C=O stretching appears at 1735 cm^{-1}, which is confirmed by the presence of the corresponding two vibration modes and C-C-O and O-C-C stretching (see Table 2.4). Although acetate has the same C=O stretching band as other aliphatic esters, its C-C-O stretching appears at higher frequency than other

aliphatic esters (Günzler and Gremlich, 2002; Smith, 1999). So, in addition to the long chain aliphatic esters, I could also detect the signal of the acetyl functional group (CH_3COO-) from the existing of C-C-O stretching band at 1242 cm^{-1} (Table 2.4). This identification is further supported by the presence of distinct CH_3 symmetric bending from acetyl groups at 1434 cm^{-1} (Günzler and Gremlich, 2002; Mayo et al., 2004, and Table 2.4). As I move to the other sites (TP, CBB and OSC), I can still identify both aliphatic ester and acetyl vibration bands. The absence of the aliphatic and acetyl esters in the Dismal Swamp sample and their presence at the other sites is a strong indication that they are aquatically rather than terrestrially derived compound classes. The presence of the acetyl functional group in all the estuarine/marine HMW-DOM samples agrees with work done by Repeta and co-workers, in which they estimate that acetyl groups could account for a significant portion of the carbon (~10%) within marine HMW-DOM (Aluwihare et al., 1997; Repeta et al., 2002).

3.4.3. Amide functional group

The large change in the electrical dipole moment during the C=O bond stretch gives FTIR the ability to detect small concentrations of amide functional groups (CON-), However, I was unable to detect the band at ~1650 cm^{-1} in the 2nd derivative spectrum of Dismal Swamp HMW DOM. By comparison, a very clear broad band at 1652 cm^{-1} is seen in the 2nd derivative FTIR spectra of Great Bridge HMW DOM, and the 2nd derivative also reveals bands around 1554 cm^{-1} and 1262 cm^{-1}, typical Amide II and Amide III bands (Günzler and Gremlich, 2002; Mayo et al., 2004; Shurell, 2002). These amide bands are also present at the other saline sites (TP, CBB and OSC, Table 2.4). The

existence of these three amide bands confirmed that the majority of the amide functional group in the HMW DOM of GB, TP, CBB and OSC is a secondary amide, where the amide nitrogen is attached on one side to a carbonyl carbon and on the other side to another carbon leaving only one position for a hydrogen atom (-CONH-). The absence of amide functional groups in the Dismal Swamp sample and their occurrence at the other sites is in agreement with the low nitrogen content (0.83%) and high C/N ratio (55.12 atomic ratio) in Dismal Swamp HMW DOM and the higher nitrogen content and lower C/N ratio at the other sites (see Table 2.2). While the identification of secondary amide groups is consistent with a protein source, secondary amides are also found in other structures such as N-acetyl aminopolysaccharides. Such aminopolysaccharides have been detected in significant amounts in the HMW-DOM isolated from marine water (Aluwihare et al., 2005; Boon et al., 1998).

3.4.4. Carbohydrate functional groups

The O-H and C-O bands are the two most common functional groups in any carbohydrate; their vibration modes are normally present below 1500 cm^{-1} (with the exception of O-H stretching around 3300 cm^{-1}). Looking at their vibration in the 2nd derivative spectra, I could assign three different vibration modes: two of these vibration modes are due to O-H vibration, they are the in-plane bending at 1360 cm^{-1} for Dismal Swamp (or around 1348 cm^{-1} for the rest of the sites) and the out-of-plane bending that shows around 650 cm^{-1} for all of the sites (Table 2.4).

In the area between 1200 and 1000 cm^{-1}, I could assign multi C-O bands at each site. In DS, there are three C-O stretching bands at 1088, 1069 and 1029 cm^{-1}, while in

GB, the band at 1088 cm^{-1} is missing and replaced by a new band at 1004 cm^{-1}. Compared with GB, TP has an additional band at 1092 cm^{-1}. Although CBB exhibits three bands, their positions are slightly lower than the upstream sites (see Table 2.4). The Offshore site (OSC) shows three bands at 1093, 1075 and 1024 cm^{-1}.

Carbohydrates can exist in many isomers of hexose or pentose compounds which are each further classified into either ketone or aldehyde form. Even though carbohydrates often occur as polysaccharides, they also appear as mono- or oligosaccharides conjugated with proteins or lipids in glycoconjugate compounds (Brandenburg and Seydel, 2002). These different forms and isomers have only a minimum effect on the O-H vibration due to its terminal position. However, they can strongly affect the C-O bond force constant (k) mainly because of the changes in the bond angle or the electronic environment around the carbon in that bond, which ultimately distributes C-O bands along a wide range of frequencies based on their force constant (k). Many studies in food science, biochemical and microbiology fields have used the C-O bands in FTIR spectra as a way to differentiate and quantify different isomers and forms of carbohydrate (see the reviews by Brandenburg and Seydel, 1996; Brandenburg and Seydel, 2002; Naumann et al., 1996). For example, Vonach et al. (1997) used the C-O stretching bands at 1065, 1058 and 1035 cm^{-1} from an online HPLC-FTIR system to distinguish, respectively, the fructose, sucrose and glucose composition within non-alcoholic beverages. The C-O stretching bands have also been used to differentiate between anomeric lyxose where the band at 1030 cm^{-1} is attributed to the α-anomer while the β anomer band appeared at 1070 cm^{-1} (Michalska et al., 1984) .

From the differences in the position and frequency of occurrence of C-O bands at my different sites and within literature studies, it appears promising to use FTIR to examine the change in the carbohydrate composition within aquatic DOM isolates. However, further investigation is needed to assign specific C-O bands to specific isomers and more work is needed to correlate FTIR data to wet chemical analyses of carbohydrates.

3.4.5. Lignin functional groups

In order to identify the lignin compounds in the 2nd derivative FTIR spectra I used two bands that are shared between different lignin structures. The first one is the C-O band of phenol compounds, as phenol is the most common functional group in different lignin chemical structures. Due to conjugation of phenol oxygen with the aromatic ring, the C-O stretching band of phenol compounds appears ~ 100 cm^{-1} higher in wavenumber than normal aliphatic C-O bands, (Günzler and Gremlich, 2002; Mayo et al., 2004; Smith, 1999, see also Table 2.4). The second band is the aromatic ring vibration at 1515 ± 5 cm^{-1}. Many FTIR analyses of different types of lignin and wood materials assign this band as a major common band of lignin (Hergert, 1960; Mascarenhas et al., 2000; Pandey, 1999).

Both of the bands have been easily identified in the 2nd derivative of the DS FTIR spectrum at 1235 and 1515 cm^{-1}, and as I move to the other sites, I'm still able to identify them, but the band around 1515 cm^{-1} becomes a small tip on the side of 1550 cm^{-1} band (see Table 2.4 and Fig. 2.6). Seeing a lignin signal that persists through the estuary and into the ocean is not a surprise; it is consistent with my ^{13}C-NMR data which shows that

some aromatic material reaches the Offshore site. Lignin has been used previously as a biomarker to estimate the amount of terrestrial DOM reaching the ocean and detectible amounts have been seen in open-ocean samples (Benner et al., 2005; Benner and Opsahl, 2001). Furthermore, FT-ICR-MS analysis of C_{18}-isolated DOM from my five sites shows that the lignin region of the resulting Van Krevelen plot is present at all sites from DS to OSC (Sleighter and Hatcher, 2008).

3.4.6. Paraffin functional groups

Due to the small difference in electronegativity, the change in the electrical dipole moment ($\delta\mu$) during the deformation vibration of C-H is small. However, the high availability of C-H bonds in biopolymeric compounds gives it a sufficiently strong intensity to appear above background in my samples. Normaly the region around 3000 cm^{-1} is used to study the C-H stretching, However, both methyl (CH_3-) and methylene (-CH_2-) groups have their specific deformation vibrations that appear in the region 1500-1300 cm^{-1}. Looking for their vibration in the 2nd derivative FTIR spectra from all the sites, I could assign the band around 1450 cm^{-1} to the symmetric deformation (scissor) of CH_2 groups (see Table 2.4). The methyl group that attaches to another carbon (CH_3-C) generates two vibration modes around 1465 cm^{-1} and 1375 cm^{-1} for asymmetric and symmetric(umbrella) deformations, respectively. As I mentioned earlier, I can also identify CH_3 attached to the acetate functional group, as this bonding lowers the normal asymmetric deformation frequency by 30 cm^{-1}, to ~1430 cm^{-1}. The ability to identify paraffin vibration bands in HMW DOM from all the sites shows that aliphatic compounds (or portions of compounds) are a significant component of DOM regardless

of its sources, which agrees with my ^{13}C-NMR results. The presence of CH_3 vibration modes in the HMW-DOM spectra shows that the DOM contains highly branched aliphatic moieties, such as branched lipids or certain carbohydrate structures (e.g. fucose and rhamnose).

3.5. Quantification coupling between FTIR and ^{13}C-NMR

As I showed previously, ^{13}C-NMR is a powerful quantitative technique that estimates the relative distribution of carbon within functional groups in DOM, However, one of its drawbacks is that ^{13}C-NMR can't easily differentiate between ester, amide and carboxylic acid contributions to the C=O signal. It is crucial to quantify the changes of these compound classes to have better understanding of the biogeochemical cycle of DOM in estuaries, especially, as is seen from my FTIR analyses, since each of these compound classes appears to have different source-sink relationships within my estuarine study area. FTIR is complementary to NMR techniques, allowing differentiation between the three functional groups. Coupling the functional group information from FTIR with ^{13}C-NMR data, which provides information on the percent carbon attributable to C=O, and allows us to calculate the percent carbon attributable to ester, amide, and carboxylic acid.

3.5.1. Peak fitting of the FTIR spectra

The coefficients of determination (r^2) of the peak fitting for the region 1900-900 cm^{-1} in all spectra were between 0.999-0.993, while the standard of error was in range of 0.0136-0.0053. The peak fitting areas for the carbonyl groups (C=O) of carboxylic acid,

ester and amide in Fig. 2.6, show that the peak of de-protonated carboxylic acid of Dismal Swamp (DS) -in Fig. 2.7a- at 1620 cm^{-1} has the largest area, followed by the protonated carboxylic acid at 1720 cm^{-1}, then the carbonyl of five member ring ester (γ-lactones). The other two de-protonated carboxylic acids at 1603 and 1583 cm^{-1} have very small peak areas in DS but larger areas in the GB spectrum, where they are the only carboxyl bands present. The differences in the carboxyl bands may be due, as I discussed earlier, to de-protonation of the peak at 1720 cm^{-1} as the pH and salinity increase. The new peak of the amide I band at 1650 cm^{-1} was the largest peak in that region, followed by the amide II band and the de-protonated carboxylic acid at 1683 cm^{-1}, the area of asymmetric stretching of aliphatic carbonyl ester band at 1735 cm^{-1} comes next.

As I move further toward the marine end member sample, the area of the de-protonated carboxylic group around 1580 cm^{-1} decreases and it has disappeared at the Offshore site (OSC, see Fig. 2.7e). Conversely, the other de-protonated band around 1600 cm^{-1}, despite its low intensity, remains relatively constant in peak area through out the salinity gradient. These results demonstrate that there are two pools of carboxylic compounds: one of them appears to be biogeochemically reactive as it moves through the estuary; the other is refractory and could be transported from land to open ocean. These refractory carboxylic compounds could be the carboxyl-rich alicyclic molecules (CRAM) that have been identified in both open ocean (Hertkorn et al., 2006) and fresh water (Lam et al., 2007) DOM.

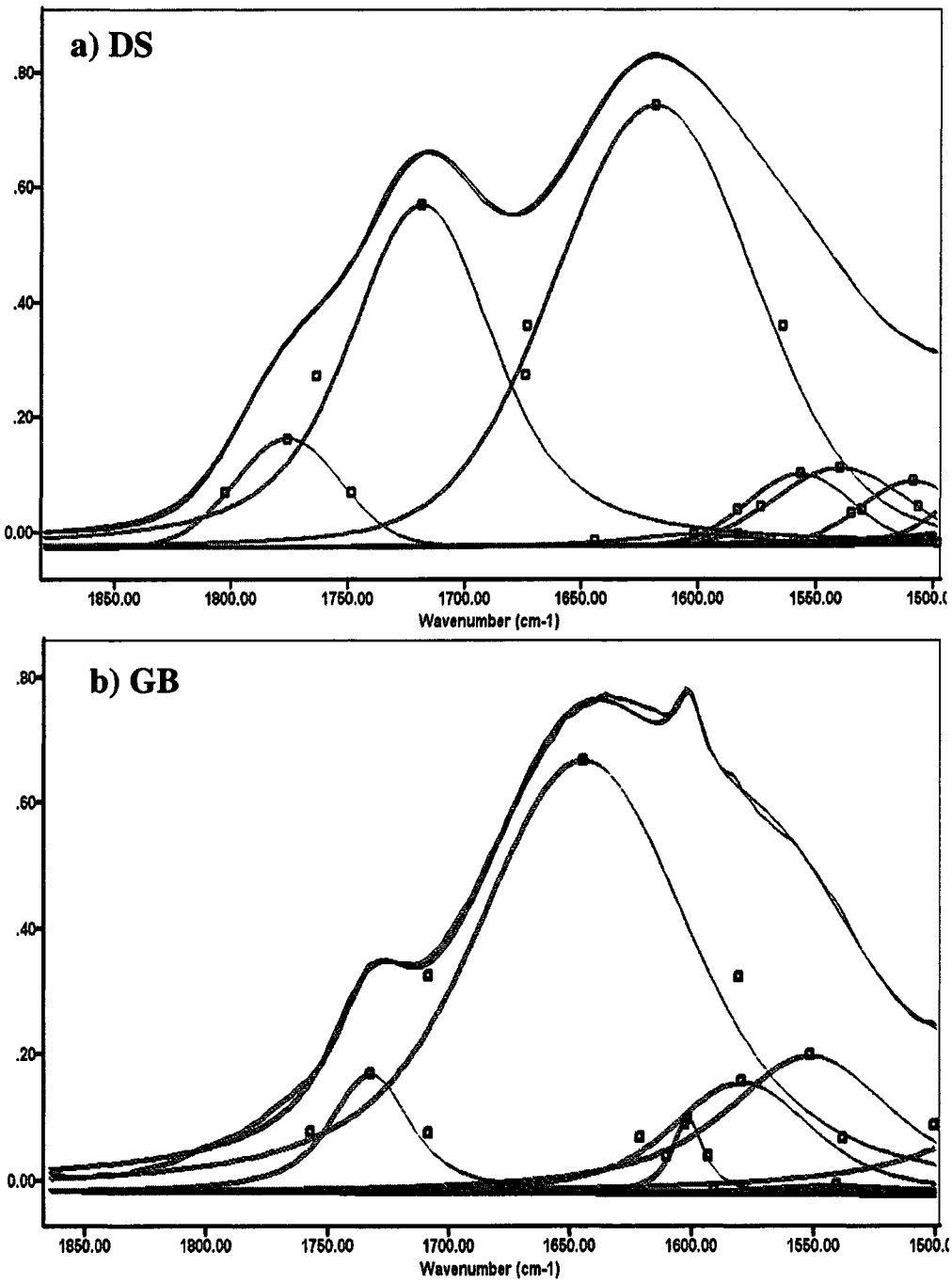

Fig. 2.7. Peak fitting results for the carbonyl area of the FTIR of a) DS, b) GB, c) TP, d) CBB, e) OSC. The red line is the original spectrum, blue line the fitted spectrum, and green line the individual peaks.

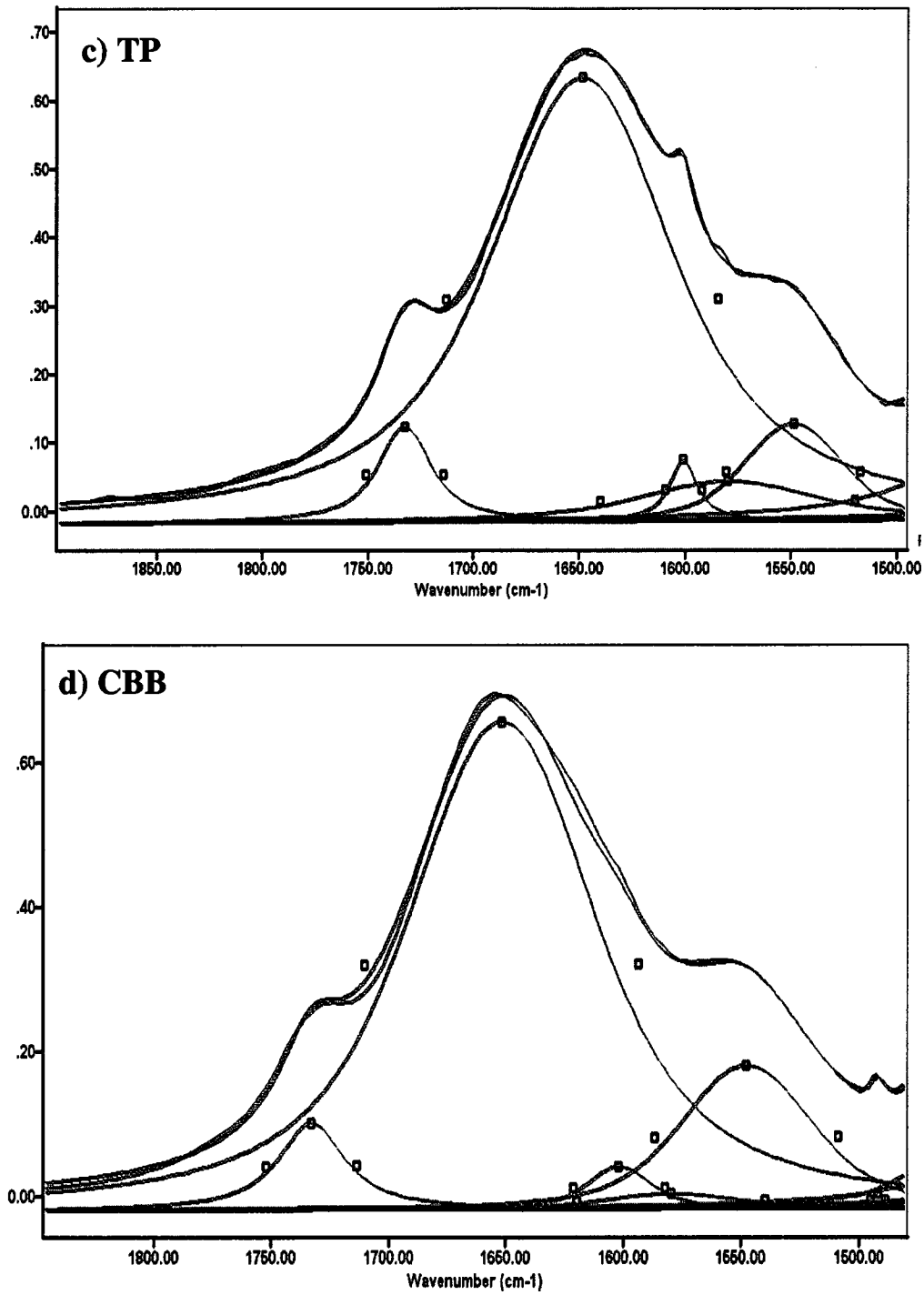

Fig. 2.7. Continued.

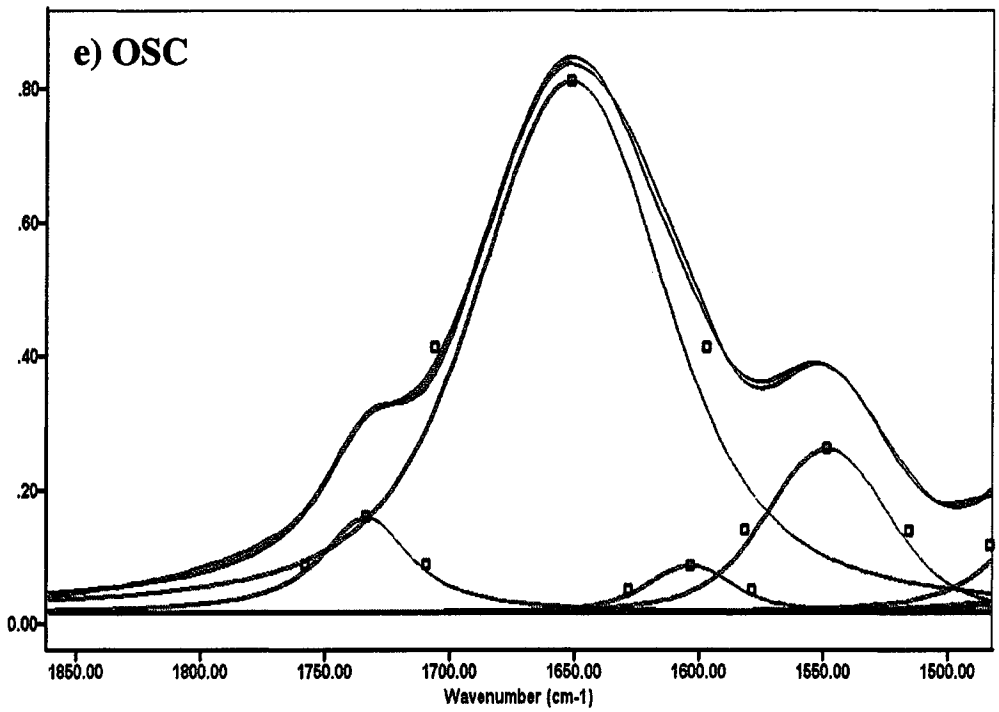

Fig. 2.7. Continued.

3.5.2. Quantification of carboxylic acid, ester and amide by FTIR coupled with ^{13}C-NMR.

As the asymmetric stretching of carbonyl groups are the most intense bands of carboxylic acid, ester and amide, the FTIR area of these bands could be used to quantify the relative amount of each of these functional groups. Using the peak fitting area, the total carboxylic-group contribution was calculated by the addition of individual peak areas for the bands at 1720, 1620, 1583 and 1603 cm^{-1} for DS; the bands around 1580 and 1600 cm^{-1} for GB, TP and CBB; and the band area at 1603 cm^{-1} for OSC. The total

amide of sites GB, TP, CBB and OSC is related to the area of the band around 1650 cm^{-1}; note that there is no amide contribution in DS (see previous discussion). The area of ester is equal to the area of the γ-lactones carbonyl band at 1775 cm^{-1} in DS, while it is equal to the carbonyl band of the aliphatic and acetyl esters at 1735 cm^{-1} in the other samples. The total carbonyl area is considered the addition of the total area of carboxylic acid, amide and ester areas (Table 2.5). There is a strong positive correlation (r^2=0.93) between the total carbonyl area from FTIR analysis (Table 2.5) and the COO/CON area from ^{13}C-NMR (Table 2.3).

Table 2.5. The total area of carboxylic acid, amide and ester estimated from peak fitting the FTIR spectra and the relative carbon percentage obtained by coupling FTIR with ^{13}C-NMR.

Functional	DS		GB		TP		CBB		OSC	
group	area	%C	area	%C	area	%C	area	%C	area	%C
Carboxylic acid	146.5	16.5	18.8	1.6	10.0	0.9	4.3	0.4	2.3	0.2
Amide	0.0	0.0	91.6	7.6	91.8	8.3	83.5	7.8	79.7	7.0
Ester	10.7	1.2	10.2	0.9	6.1	0.6	6.0	0.6	8.5	0.8
Total carbonyl	157.2		120.6		107.9		93.8		90.5	

Although FTIR has the ability to quantify the relative distribution of functional groups (Griffiths and De Haseth, 2007; Günzler and Gremlich, 2002; Smith, 1996); in my case the carbonyl band in carboxylic acid, amide and ester, it cannot be used to calculate relative carbon percentages. But coupling FTIR data on functional group distributions with the ^{13}C-NMR carbonyl signal along with the ^{13}C-NMR estimate of the percentage of carbon within that carbonyl signal, I can estimate the carbon percentages within the sample that are attributable to carboxylic acid, amide, and ester groups. Note that I cannot account for the additional C that may be attached within an actual compound; e.g. for palmitic acid, 15 of the carbons will appear aliphatic (with signal in the C-H regions), while only one will appear as a carboxylic carbon. With this caveat, I can determine the %C within functional groups by multiplying the ratio of the area of functional group (as determined by FTIR) by the COO/CON relative area from the ^{13}C-NMR according to the following equation:

$$\%C_{individual} = (A_{individual} / A_{total.}) * \%C_{COO/CON} \qquad \text{Eq. (2.3)}$$

Where $A_{individual}$ is the FTIR total area of either carboxylic acid, amide or ester (Table 2.5), A_{total} is the FTIR total carbonyl area (Table 2.5) and $\%C_{COO/CON}$ is the relative %C of carboxyl groups from ^{13}C-NMR (Table 2.3).

From the results in Table 2.5 and Fig. 2.8a, the carboxylic acid carbon percentage drops dramatically from 16.5% at Dismal Swamp to 1.6% at the Great Bridge site. It continues to drop as I move toward the Offshore site but with a lower change until it reaches only 0.2% carbon. And it is showing net loss relative to the mixing line (Fig. 2.8a). I hypothesize that carboxylic acid is lost due to sorption processes (as DS is not always linked by overland flow to the GB site) as well as flocculation processes

occurring at low salinity in the river/estuary water column (Boyle et al., 1977; Sholkovitz, 1976; Sholkovitz et al., 1978). The carboxylic acid complexed with iron (the band at 1620 cm^{-1}) that accounts for 60% of carboxylic acid at Dismal Swamp (based on the relative area from FTIR analysis) may be sorbed, may precipitate out of the water column, or may be stripped of iron downstream. Another process that could cause carboxylic acid losses in the DOM is photooxidation (Xie et al., 2004). The strong correlation between the relative percentage of carboxylic acid and the pH value from (Table 2.1) (r^2= 0.999) indicates that the carboxylic acid plays a major role in the pH values of water column, especially in the fresher water portions where carbonate buffering is not very strong. Keeping in mind that I only quantify the functional groups not the entire molecules, the 0.2% carbon as carboxylic acid could be a larger contribution toward total carbon if I take into account the number of carbons present in entire carboxylic acid molecules. In addition to that, the season in which I collected the samples (Summer 2007) was one of the driest seasons in the last two years which means it had the lowest fresh water flow rates and possibly the highest rate of photooxidation. Thus the amount of transferred carboxylic acid seen here is likely to be low compared to other seasons and other years.

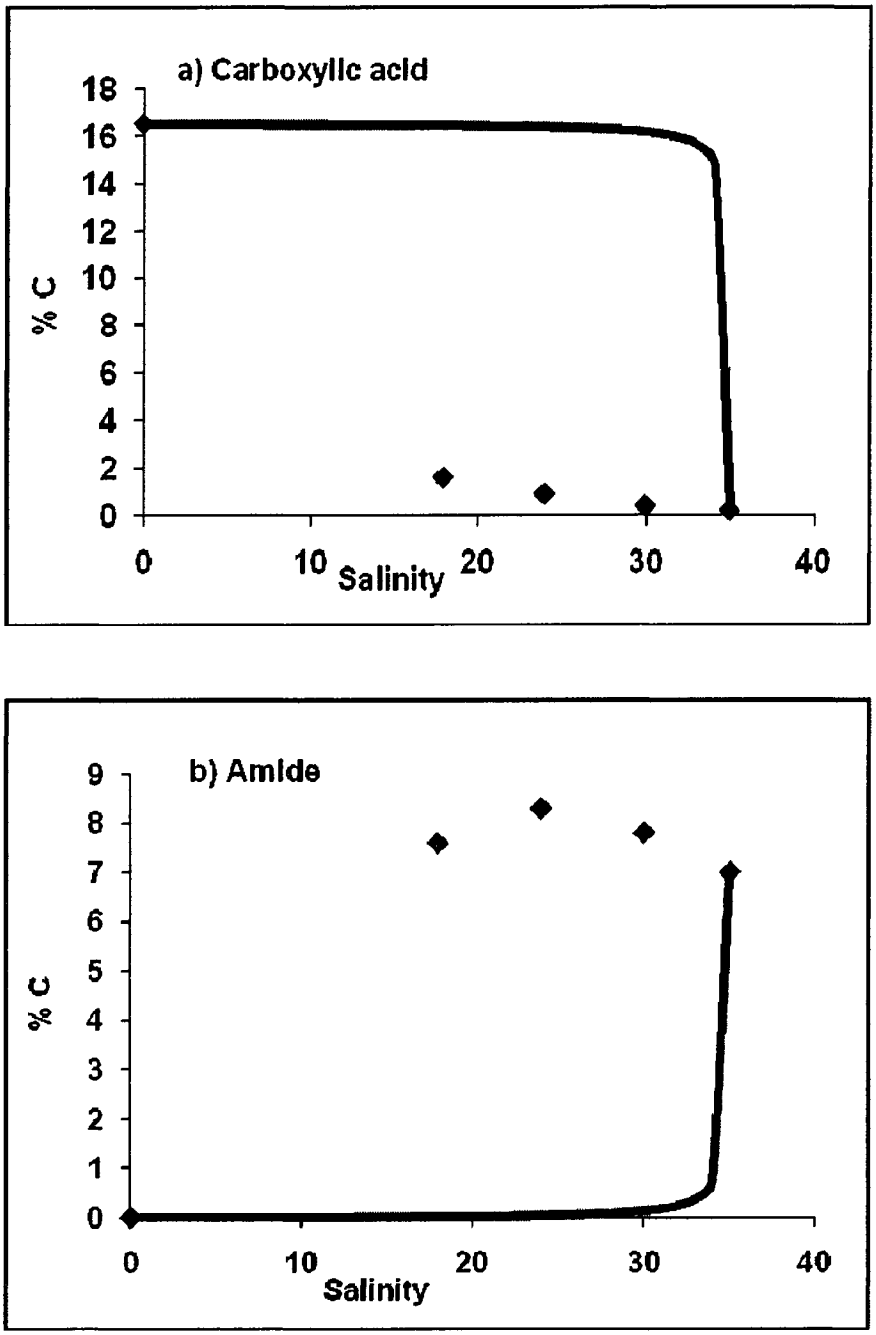

Fig. 2.8. The plot of the relative carbon percentage of a) Total carboxylic acid and b) Amide (from coupling FTIR with ^{13}C-NMR) in the high molecular weight (HMW) DOM isolated from the five sites versus the corresponding water-column salinity. The solid line is the polynomial fit to each of the compound classes; the solid line represents the expected line if distributions are due solely to the mixing of the DS and OSC end-members as calculated from Eq.2.1.

Unlike the carboxylic acid, the amide when plotted against the salinity gradient shows a higher carbon percentage than expected from the mixing line (see Fig. 2.8b). The highest value was at TP, with a carbon percentage of 8.3%. This co-occurs with the ^{13}C-NMR increases for total carbohydrate and total aliphatic material, and thus supports further the hypothesis that autochthonous sources are introduced to the DOM pool in the middle of the transect.

In contrast to both the carboxylic acid and amide contributions, the carbon percentage of ester didn't follow a predicted pattern. It has the highest value at the Dismal Swamp site (1.2%) then drops to 0.9% at Great Bridge and 0.6% at both Town Point and Chesapeake Bay Bridge, and increases to 0.8% at the Offshore site. That the observed ester distribution is more complicated than seen for the other compound classes is probably due to its change in chemical structure with location in the estuary. The esters are dominated by γ-lactones in Dismal Swamp, which seem to be hydrolyzed and replaced by new aliphatic and acetate esters at other sites (see the previous discussion for more details).

3.6 Behavior of the HMW compound class concentrations along the transect

Converting the carbon percentage of each compound classes into DOC concentration and plotting it against the salinity (Fig. 2.9a-e) shows that the total carbohydrate, aromatic, aliphatic and carboxylic acid groups within HMW DOM have a non conservative behavior with a concave shape, while only the amide component has convex behavior which could indicate production along the transect.

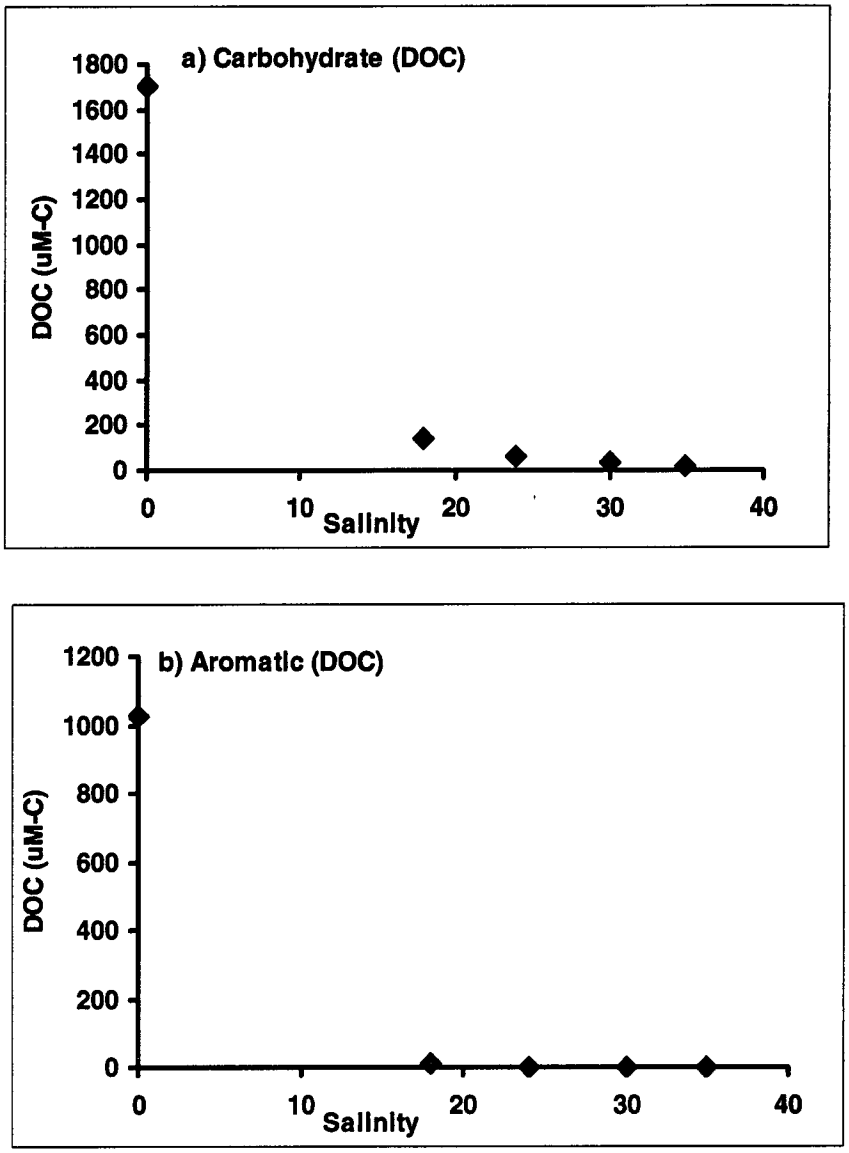

Fig. 2.9. Plot of dissolved organic carbon (DOC) concentrations of compound classes a) Carbohydrate, b) Aromatic, c) Aliphatic d) Carboxylic acid and e) Amide of the high molecular weight fraction (HMW-DOC) after the second diafiltration step versus their corresponding water-column salinity along the transect.

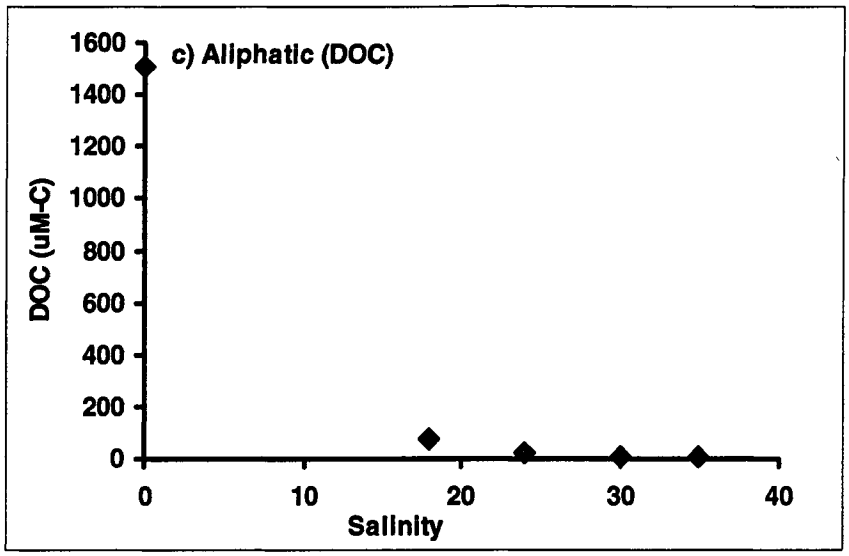

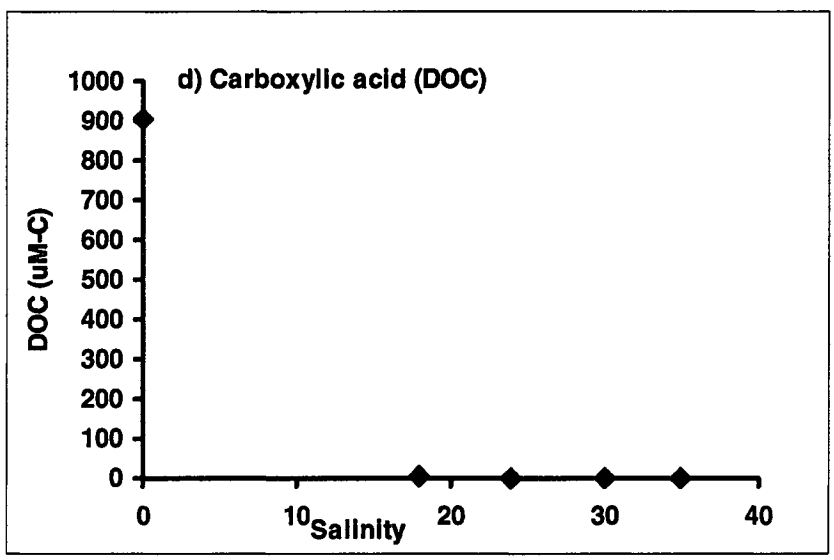

Fig. 2.9. Continued.

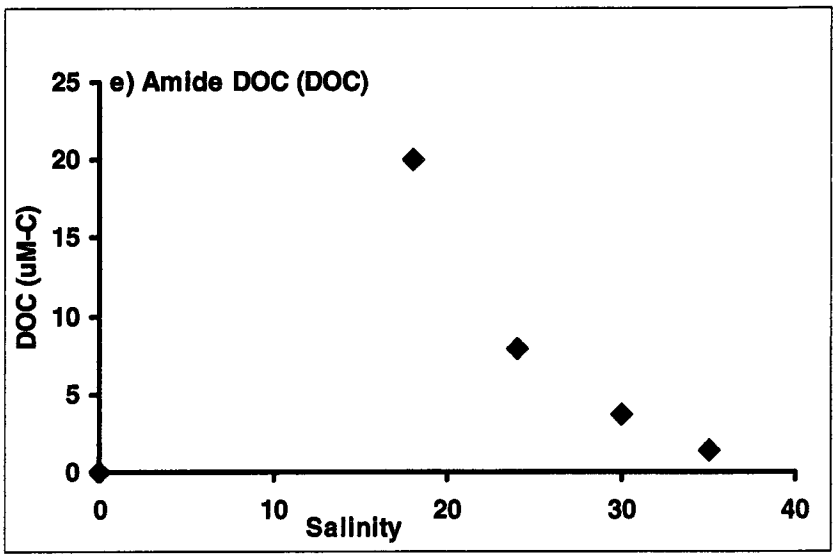

Fig. 2.9. Continued.

The inverse behavior of the carbohydrate concentration (Fig. 2.9a) and the carbohydrate as %C (Fig. 2.4a) along the salinity gradient highlights that, although the amount of total carbohydrate concentration is non-conservative and exhibits loss along the transect, its carbon percentage in the HMW fraction increases relative to the other compound classes (e.g. aromatic) along the transect. One possible explanation is the removal rate of terrestrial carbohydrate is slower than the other compound classes (e.g. aromatic, carboxylic). However, the marine signature of the $\delta^{13}C$ at the Offshore site (OSC), where the carbohydrate is the major component, implies that carbohydrate has rapid recycling/removing rates, and most of terrestrial carbohydrate could be recycled/lost along the transect. This is supported by the significant changes in the

carbohydrate component in the ^{13}C-NMR spectra as DOM moves from Dismal Swamp to the Great Bridge toward the Offshore site (this study) and with the young Δ^{14}C age of the monosaccharide along Mid-Atlantic Bight (MAB) (Aluwihare et al., 2002). Thus it appears that the carbohydrate pool is highly dynamic and while the HMW carbohydrate concentration decreases, the balance of its source vs. sink functions is more positive than those of its co-occurring HMW DOM components (thus leading to its greater percentage within the remaining HMW DOM).

4. CONCLUSIONS

Coupling FTIR and ^{13}C-NMR analyses is a powerful way to investigate the qualitative changes of major compound classes in complex organic matter mixtures such as those seen in estuarine DOM. It appears especially useful in investigating carboxylic acid, amide and ester compositions. Although DOC measurements reveal a net loss in both total and HMW DOC along my transect, the quantitative measurements of individual functional groups within HMW DOC showed a more detailed picture concerning the changes in chemical composition and greater insight into DOM's possible sources and reactivity. For example, carbohydrate and amide functional groups all showed a net source in the middle of the transect which could indicate autochthonous DOM inputs, either directly or from the confluence of the Elizabeth River branches and the James River. Conversely, carboxylic acids and aromatic compounds showed a net loss through the estuary most likely due to a combination of flocculation and photoxidation processes. Interestingly, iron complexed to carboxylic acids appears to be lost from the HMW fraction between the Dismal Swamp and the low-salinity GB site.

Stable carbon isotopes indicate that over 70% of Great Bridge HMW-DOM came from terrestrial DOM; however, both FTIR and ^{13}C-NMR show that there were major changes in the functional groups between Great Bridge and Dismal Swamp. This could be explained by soil processes, water-column microbial and photochemical alteration of major portions of the terrestrial DOM, or flocculation.

Applying the 2nd derivative to FTIR spectra resolved many overlapped peaks and gave greater detail concerning the chemical structure of the HMW DOM. One of the interesting points that results is the availability of three different pools of de-protonated carboxylic acids in Dismal Swamp: one of them is complexed with iron and disappears between the DS and GB sites; the second pool appears biogeochemically reactive and its signal decreases down-estuary, while the third pool seems to be refractory and has the potential to be exported to and accumulate within the open ocean. The ester compounds show different chemical structures between my two transect end members; a five member ring ester (γ-lactone) was the dominant ester in the Dismal Swamp, while the highly aliphatic ester and acetate ester functional groups are the major ester in the other estuary/marine sites.

FTIR and ^{13}C-NMR are complementary techniques with great applicability to characterizing complex organic matter such as water-column, sediment pore-water and soil-derived DOM. Both are non-destructive techniques, they characterize the bulk of the DOM and they provide insight into the major compound classes through their functional groups. Both techniques, as is the case with all analytical approaches, have strengths and weaknesses, but by coupling the two, I can overcome some of the weaknesses and gain greater insight into DOM composition.

CHAPTER III

SEASONAL AND SPATIAL CHANGES IN THE CHEMICAL COMPOSITIONS OF DISSOLVED ORGANIC MATTER ALONG AN ESTUARINE TRANSECT: A STUDY USING ISOTOPE RATIO MASS SPECTROMETRY, FTIR AND ^{13}C-NMR

1. INTRODUCTION

Estuaries and the continental shelf regions act as biogeochemical reactors for dissolved organic matter (DOM), where most of the terrestrial dissolved organic matter (T-DOM) is lost and a small portion of the T-DOM reaches the open ocean (Benner et al., 2005; Hedges et al., 1997). On the other hand, new sources of DOM are introduced into estuaries and continental shelf water through the primary production; these regions account for 30% of the net oceanic productivity (Holligan, 1992) even though they represent only 7% of the total oceanic surface areas (Gattuso et al., 1998).

The distribution of dissolved organic matter (DOM) in estuaries is affected by changes in physical parameters such as river discharge, water residence time, tidal exchange, and re-suspension events. They are also exposed to large changes in pH and salinity as it moves downstream in a typical estuary. The sources and sinks of DOM in estuaries are caused by many different biogeochemical processes. For example, as the ionic strength increases in low salinity regions, some DOM flocculates and aggregates (Sholkovitz, 1976; Sholkovitz et al., 1978) into larger particles (Stumm, 1990) perhaps through interactions with cations such as Ca^{2+} (Hunter and Liss, 1982) removing the

DOM from the water column. Additional estuarine processes include the increase of light penetration due to a decline in turbidity, which can lead to increased photodegradation of chromophoric DOM, and, in conjunction with the availability of nutrients, can also provide the ideal conditions for a primary production maximum in the middle of estuarine ecosystem (Cloern et al., 1983; Filardo and Dunstan, 1985; Fisher et al., 1988; Harvey and Mannino, 2001; Pennock and Sharp, 1986).

While flocculation and primary production maxima are more likely to be limited to specific regions of estuaries, photooxidation and bacterial utilization of DOM more likely occur throughout the estuary, though their degree and chemical selectivity may vary with location (Waidner and Kirchman, 2008). On one side, heterotrophic bacteria could be a sink for DOM by converting it to CO_2 (Azam et al., 1983). On the other side, they could contribute to the DOM pool directly by converting carbon into refractory DOM (Ogawa et al., 2001) or indirectly by the regeneration of inorganic nutrients from DOM, thus enhancing primary productivity (Gardner et al., 1994; Pakulski et al., 1995; Pakulski et al., 2000). Photooxidation could be a biogeochemical sink for DOM by converting it into CO_2 or CO either directly (Miller and Zepp, 1995) or indirectly by making DOM more bioavailable for heterotrophic bacteria to respire (Moran and Zepp, 1997). In addition to spatial variations, the relative importance of these processes are highly varied between different seasons; for example, the summer season provides the perfect conditions for intense phytoplankton blooms to happen in the middle of estuary as compared to other seasons (Harvey and Mannino, 2001; Pennock and Sharp, 1986).

Due to the combination of these processes, the quantity and chemical composition of DOM is significantly altered along an estuarine transect. Many studies have tried to

address estuarine changes in the DOM: by looking into the change in DOC concentrations as conservative or non-conservative behavior (Benoit et al., 1994; Jaffe et al., 2004; Kattner et al., 1999; Miller, 1999), following the photobleaching of color dissolved organic matter (CDOM) (Del Vecchio and Blough, 2004; Rochelle-Newall and Fisher, 2002), or looking at compositional changes in isolated DOM by mass spectroscopy (Minor et al., 2001; Minor et al., 2007; Sleighter and Hatcher, 2008). While these approaches have been informative, they have been unable to provide quantitative insight into compound-class variations within DOM as function of spatial and seasonal changes.

As I have shown in chapter II, coupling ^{13}C-NMR and FTIR can provide a more comprehensive picture of changes in the compound classes of DOM (aliphatic, aromatic, amide, carbohydrate, ester and carboxylic) (Section II , In this Dissertation). However, this picture is complicated by the complex nature of DOM, where the presence of different compounds containing similar functional groups creates overlap between the different bands and reduces the resolution of the spectra of both ^{13}C-NMR and FTIR. It is also complicated by the wide range in the rates of reactivity of DOM compounds (from hours to centuries, (Davis and Benner, 2007) and the addition and removal of different compounds to the DOM pool as DOM moves through the estuary. From all the above, using traditional 1-dimensional approaches will not enable us to detect significant changes in the FTIR and ^{13}C-NMR.

One of the widely used chemometrics data analysis techniques is principal component analysis (PCA); this is applied to all the spectra as a discrete data set and the results are represented as a linear combination of a set of factors. The major advantage of

PCA is its ability to reduce the dimensionality of the data set by eliminating redundant dimensions, i.e., those containing low information content, and identifying some new meaningful underlying variables that better represent the differences and similarities in a specific data set.

Noda (1993) developed a new concept of generalized perturbation-based two dimensional correlation spectroscopy (2D-spectroscopy), by spreading the spectral intensity changes within a data set collected across a perturbation (time, temperature, pressure change, chemical reaction) as a function of the perturbation over a second dimension. This reduces the complexity of overlapped peaks (as many of them do not co-evolve throughout the data set), provides relations between different peaks, and gives us information on the sequential order of the changes in these peaks. The application of 2D-spectroscopy to dynamic spectra results in two orthogonal correlation spectra (synchronous and asynchronous). The synchronous spectrum indicates coincidental or in-phase changes of two separate peaks, while the asynchronous spectrum will exhibit cross peaks if changes in the original data peaks are out of phase, which will be an indication of the order of the functional group changes. The use of 2-D spectroscopy in this fashion can potentially resolve many ambiguities especially in a complex mixture of compounds with many overlapping peaks (Noda and Ozaki, 2004; Wang and Palmer, 1999). In the last two decades, two-dimensional correlation spectroscopy of the kind described above has been applied to many different spectroscopic techniques such as infrared (Buffeteau and Pezolet, 1998; Ekgasit and Ishida, 1995; Sasic et al., 2000; Sasic and Ozaki, 2001), Raman (Ebihara et al., 1993; Matsushita et al., 2000), near infrared (Awichi et al., 2002; Liu et al., 1996), UV-visible (Liu et al., 2000; Zhao et al., 2002), and fluorescence (He et

al., 2001; Nakashima et al., 2000) spectroscopy. It also has been applied to time-resolved gel permeation chromatography (Izawa et al., 2002a; Izawa et al., 2002b). The two dimensional correlation spectroscopy has been applied widely and successfully to understand changes within polymer materials and proteins, to follow chemical reactions, and to investigate several questions in biological and biomedical sciences (see the reviews by Noda and Ozaki, 2004; Ozaki, 2002)

Barton and co-workers (1992) introduced statistical 2D correlation between IR/NIR which was then generalized by Noda and co-workers into two dimensional correlations between any two different electromagnetic probes (e.g. IR and NIR, Raman and IR) obtained from a system under the same perturbation and they called it : 2D hetero-spectral correlation analysis. By correlating between bands generated by different probes I could confirmed the band assignments of one probe (e.g. NIR) by the band from other probe (e.g. IR), In addition, it also could enhance the band resolution (see the review by Noda and Ozaki, 2004). Since its introduction, a large number of studies have used 2D hetero-spectral correlation analysis to correlate between different electromagnetic probes such as NIR/IR, Raman/IR and Raman/NMR applied to same system (Czarnecki et al., 1998; Hu et al., 2006; Kubelka et al., 1999; Watanabe et al., 2008)

Unlike principal component analysis, which investigates variations in the spectra viewed as a single data set to investigate how the samples are different from each other, two dimensional correlation spectroscopy looks into the intensity changes of the individual chemical bands or peaks throughout all the spectra in order to identify correlations between different bands based on in-phase and out-of-phase changes in their

intensities across the data set. Combining both PCA and 2D-correlation can help to confirm trends seen in each analysis of the data set and will also provide additional complementary data about sample composition.

Applying both PCA and two-dimensional correlation spectroscopy to the ^{13}C-NMR and FTIR DOM spectra should therefore give us a more complete picture of the changes in DOM chemical structure along my estuarine transect. Applying 2D hetero-spectral correlation analysis to the NMR and FTIR data will allow us to statistically couple these two data sets, thus strengthening tentative identifications and trends seen individually within the NMR and FTIR results.

In addition, as recent studies show the presence of common components in the HMW-DOM chemical structure isolated from the open ocean and fresh water e.g. heteropolysaccharides (HPS) (Aluwihare et al., 1997; Hertkorn et al., 2006; Repeta et al., 2002) and carboxyl-rich alicyclic molecules (CRAM) (Hertkorn et al., 2006; Lam et al., 2007), an estuary is an ideal location to investigate the distribution and transformation of these two components.

In this work, I will study the spatial and seasonal changes (during two years) in the chemical composition of high molecular weight (>1000 Da) estuarine DOM isolated along a transect from the Dismal Swamp (Virginia, USA) to the coast of the Atlantic Ocean passing through the Elizabeth River and the mouth of the Chesapeake Bay. To the author's best knowledge, this is the first study to investigate the changes in the chemical composition of DOM using PCA and two dimensional correlation spectroscopy upon ^{13}C-NMR and FTIR data.

2. METHODS

2.1. Sampling sites

Samples were collected from five sites along a transect from Great Dismal Swamp through the Elizabeth River /Chesapeake Bay system to the coastal ocean (see Fig. 1.1). Site DS (Portsmouth Ditch in Great Dismal Swamp, Virginia, USA) is representative of the swampy headwaters of the Elizabeth River system, has very high DOC loadings, and contains a large proportion of terrestrially-derived DOM. Site GB in Great Bridge, Virginia is forested with marshes along the shoreline. The TP site (Town Point Park, Norfolk, Virginia) represents mid-river and contains natural autochthonous and allochthonous organic matter from the three branches of the Elizabeth River and the lower Chesapeake Bay. The down-river CBB (Chesapeake Bay Bridge-Tunnel) is at the mouth of the Chesapeake Bay; its organic matter sources include salt marshes and sediments of the lower Chesapeake Bay and its sub-estuaries, as well as imported coastal marine material and autochthonous algal production. The Offshore coastal ocean site (OSC, 37° 10.132' N, 75° 37.891' W) could be impacted by water flowing out of the Chesapeake Bay, but should also contain significant proportions of autochthonous marine organic matter.

2.2. Sampling

Using an acid-cleaned and sample-rinsed polypropylene bucket, surface water samples were collected from seven seasons during a two year period, as follows: 1-from mid October to mid November 2005 (1105) 2-February 2006 (0206) 3-May 2006 (0506) 4-August 2006 (0806) 5-November 2006 6-February 2007 (0207) and 7-May 2007

(0507). Water temperature was measured concurrently at the sampling sites. The GB, TP, and CBB samples were collected within half an hour of low tide using the shoreline (GB) or pier structures (TP and CBB) for access to the water. The Offshore sample (OSC) was collected onboard the R/V Fay Slover, and due to weather instability or unavailability of the research vessel, the samples from Offshore site were collected only in four seasons (1105, 0506, 0806, and 1106). The samples were transported to the laboratory in 20 L fluorinated polypropylene jerricans. Prior to filling with sample, each jerrican was soaked overnight in an alconox solution, rinsed with deionized water, then soaked in 10% hydrochloric acid at least for overnight, rinsed with deionized water again and preconditioned with sample (3x) before being loaded with sample. Upon arriving in the laboratory, salinity and pH were measured with a refractometer and a calibrated pH meter respectively. Sub-samples of the whole water were taken for TOC measurements. Then, samples were sterile-filtered using 0.1μm Whatman Polycap cartridge filters which had been previously soaked in methanol and back flushed with Milli-Q for at least one hour, then conditioned with 1-2 liter of the sample. A representative aliquot (10% volume) of sterile-filtered sample from each jerrican was taken and these aliquots were mixed in a cleaned jerrican to represent the average composition from all the jerricans. A sub-sample for DOC measurement was taken from this mix. DOC samples were collected in acid cleaned and pre-combusted (450 C^{o}) TOC vials (I-Chem*) then acidified immediately to pH 2 with 5 M phosphoric acid.

2.3. Ultrafiltration

An ultrafiltration system equipped with a polysulfone 1KDa cartridge that has 25 sq. ft active surface area (Separation Engineering, Inc.) was used to separate both high and low molecular weight fractions (hereafter HMW and LMW, respectively). The filtration system was cleaned and conditioned after Guo and Santschi (1996). In brief, the system was cleaned before each sample with 8 L of each of the following solutions: Alconox detergent (1-2%), sodium hydroxide (0.05M) and hydrochloric acid (0.02M). Between each cleaning solution the system was rinsed with 40 L de-ionized water (2 x 20 L). After the total cleaning protocol was completed, 20 L de-ionized water was run as a blank and a sub-sample of retentate (concentration factor of 8) was taken to measure the DOC blank. The system was then conditioned with 4-5 L of actual, sterile-filtered (<0.1μm) natural-water sample, after which 40-160 L of sterile-filtered sample was concentrated through the system to approximately 2.3 L at pressures of approximately 30 psi. Subsamples were taken from both HMW and LMW fractions for DOC mass balance; then the salt-containing retentate (HMW) solution was diafiltered with 15-20 L de-ionized water until the filtrate reached a salinity of zero (measured by refractrometer). The freshwater Dismal Swamp sample (DS) was also diafiltered, but with only 5 L de-ionized water. In all cases, the system was rinsed twice with 5 L de-ionized water to recover HMW left in the "dead volume" of the system. These retentate rinses were added to the diafiltrated retentate, and the mixed retentate was stored frozen until further processing. During each step subsamples were taken from both retentate and filtrate for DOC measurements to allow recovery and mass balance calculations.

The retentate fraction (HMW) from Great Bridge (GB), Town Point park (TP), Chesapeake Bay Bridge (CBB) and the Offshore site (OSC), were further concentrated to around 50 ml and further diafiltrated with 3 L de-ionized water using stirred cells (Amicon 8400) pressurized with nitrogen gas and equipped with a 1kDa regenerated cellulose membrane (Millipore). Subsamples from the final retentate were taken for DOC measurements, and subsequent recovery and mass balance calculations. The resulting retentates were frozen and, along with the Dismal Swamp retentate from the large-volume cross-flow system were then freeze dried.

Due to the differences in processing the Dismal Swamp sample relative to the other (salt-containing) samples, there may be some difference in sample recovery/fractionation. However, ionic strength and pH effects also affect recoveries by ultrafiltration (e.g., Dalzell et al., 2007), and the variation due to adding a stirred cell step for the salt samples is most likely a second-order effect relative to these, especially as the majority of the concentration and desalting for all samples occurred on the larger-volume cross-flow system.

2.4. DOC measurements

DOC concentrations were measured (with triplicate injections) using a standard dissolved organic carbon analyzer (Aurora 1030W TOC analyzer, College Station, TX) with 20% sodium persulfate (98%, Fisher Scientific) as oxidizer. To correct for any incomplete combustion of DOC due to the competition between chloride and DOC for the persulfate, calibration standards were dissolved in artificial seawater, prepared according to Kester et al., (1967), to insure removal of any organic traces introduced with

the salts (in other words, the artificial seawater was UV photooxidized, 24 h; 1.2 kW Hg-arc lamp; Ace Glass, prior to use). The calibration standards were prepared in the same salinity range as the samples with sucrose used as the DOC standard.

2.5. $\delta^{13}C$ and Elemental Analysis:

The $\delta^{13}C$, carbon and nitrogen percentages of freeze-dried HMW DOM were measured (in duplicate) using a Europa elemental analysis (EA) system coupled to a Europa Geo 20-20 IRMS (SerCon Limited, Crewe, UK). Ascorbic acid ($\delta^{13}C$ value -24.45‰) was used for the calibration standards and sucrose ($\delta^{13}C$ value -10.67‰) was introduced as a check standard. $\delta^{13}C$ defined as $(R_{sample}/R_{standard} -1) *1000$ where $R_{standard}$ is the Pee Dee Belemnite (PDB) standard .

The isotope mixing curve was constricted according to Raymond and Bauer (2001), where I used the average values of Dismal Swamp (DS) and Offshore (OSC) Sites as the riverine and marine end members respectively. In brief, the conservative $\delta^{13}C$ values at a specific salinity (I_m) were calculated according to the modified mass balance equation Eq. (3.1)

$$I_M = \frac{(f.I_{DS}.DOC_{DS} + (1-f).I_{OSC}.DOC_{OSC})}{DOC_M} \quad \text{Eq. (3.1)}$$

Where f is the riverine fraction calculated from the salinity, DOC_M is the expected DOC concentration (HMW fraction) due to a conservative mixing between the riverine and open ocean end members, I_{DS} and I_{OSC} are the average $\delta^{13}C$ values of the Dismal Swamp and Offshore sites respectively. The DOC_{DS} and DOC_{OSC} are the average

DOC concentration of the high molecular weight (HMW) fraction (after desalting via stirred cells) of Dismal Swamp and Offshore sites respectively.

In similar way, the C/N mixing curve was also constructed using the following equation

$$(C/N)_M = \frac{(f.(C/N)_{DS}.DOC_{DS} + (1-f).(C/N)_{OSC}.DOC_{OSC})}{DOC_M} \quad \text{Eq.3.2}$$

Where $(C/N)_M$ is the conservative C/N value at a specific salinity, $(C/N)_{DS}$ and $(C/N)_{OSC}$ are the average C/N values at Dismal Swamp and Offshore sites respectively.

2.6 Solid state ^{13}C-NMR

All seven seasons of HMW-DOM samples isolated from Great Bridge (GB), Town point (TP), and Chesapeake Bay Bridge (CBB) -with the exception of GB-1105, which was lost before ^{13}C-NMR analysis- and the four seasons of the Offshore site (OSC) were analyzed by cross polarization/ magic angle spinning solid NMR (CP/MAS ^{13}C NMR) using a Bruker Avance II 400 spectrometer operating at 100 MHz for ^{13}C, spun at 14 KHz for 4569 scans. The recycle delay (D1) and contact time were 1 sec and 1.5 ms respectively. All the experiments were conducted using a 4-mm triple resonance probe and the samples were packed into 4-mm NMR rotors with Kel-F caps. ^{13}C-NMR spectra were normalized by their total area from 0-220 ppm and multiplied by 1000 before being used for principal component analysis (PCA) and two-dimensional correlation spectroscopy (2D-correlation ^{13}C-NMR).

The spectra were integrated in segments according to Dria et al. (2002), with the region from 0-45 ppm assigned to paraffin carbon (CH_x), the 45-60 ppm to methoxy (CH_3O-) or amino groups, 60-90 ppm to carbohydrate or O-alkyl (HCOH) groups, 90-120 ppm to anomeric carbon in carbohydrate (O-C-O), 120-140 ppm to substituted aromatic carbon or double bond carbon (C=C/Ar-C), 140-160 ppm to oxygen substituted aromatic C, 160-190 ppm to carboxyl, aliphatic ester and amide (COO/CON) carbon while the 190-220 ppm region is assigned to aldehyde and ketone carbon (C=O). These initial integration segments were slightly modified based upon my results from PCA and 2-D correlation spectroscopy (see the results and discussion section for further details).

2.7. FTIR analysis

Samples were introduced as KBr discs where exactly 1.0 mg sample is diluted with 100.0 mg KBr (which had been previously heated in a lab oven for two hours at 105° to remove any moisture). To reduce light scatter during the analyses, the mixture was then crushed and homogenized (Smith, 1996) using a Wig-L-Bug ginding mill. A subsample was then compressed between two clean, polished iron anvils in a hydraulic press at 20,000 psi to form a KBr window. To minimize wedging effects (Hirschfeld, 1979), the discs were pressed for a second time after they had been rotated 90° before removal from the hydraulic press. FTIR spectra were obtained by collecting 200 scans with a Nicolet 370 FTIR spectrometer (DTGS detector and KBr beam splitter) equipped with purge gas generator unit. Spectra were collected using a resolution of 4 cm^{-1} and Happ-Genzel apodization. To guard against CO_2 contamination from lab air, a 4-min lag-time was implemented between closing the analytical chamber and starting the analysis.

A pure KBr disc was run before each sample analysis as a background blank. The FTIR spectra were converted into absorbance units, normalized by the summed absorbance from 4000-500 cm^{-1}, and multiplied by 1000.

Using Grams/Al 8.0 spectroscopy software (Thermo Electron Corporation), the normalized absorbance spectra were processed with the 2nd order Savitzky-Golay method with 11 convolution points used to generate the second derivative of the spectra. For comparison, another second derivative was also calculated using the Gap method with an 11 cm^{-1} Gap value. For an additional comparison, the spectrum region from 1850- 1450 cm^{-1} was also processed by Fourier self-deconvolution with a gamma factor of 20, and the deconvoluted spectrum was 60% smoothing using a Bessel function.

For an additional test of peak overlap and quantification of these peaks, the FTIR area from 1900-900 cm^{-1} was peak fitted using Grams/Al 8.0 software with a Voigt line shape, which is a convolution between Gaussian and Lorentzian line shapes, and can correct for the broadening features due to molecular collisions and the Doppler effect during infrared measurements (Griffiths and De Haseth, 2007). The numbers and the exact frequencies of the peaks in the region were obtained from the 2nd derivative of the corresponding spectrum, while the peak width was optimized within ± 15 cm^{-1} of the peak width obtained from the 2nd derivative.

2.8. PCA and 2D correlation spectroscopy

The seasonal estuarine/marine HMW-DOM (GB, TP, CBB and OSC) area-normalized spectra of ^{13}C-NMR (24 spectra) were run for principal component analysis (PCA) using an in-house MATLAB code.

Normalized spectra of the ^{13}C-NMR and FTIR (24 spectra each) were analyzed by 2D-correlation spectroscopy using an in-house modified version of 2Dshige software (Kwansei-Gakuin University, Japan). The practical computation of two-dimensional correlation spectroscopy were generated according to Noda and Ozaki (2004). In brief, the reference spectrum $\bar{y}(v)$ is calculated first, by taking the average values of all the data points at each specific wavenumber or chemical shift (v). The second step involves calculating the dynamic spectra $\tilde{y}$ (υ) for all spectra by subtracting the reference spectrum $\bar{y}(v)$ from each normalized spectrum y (υ) at each perturbation (t).

The synchronous 2D spectrum $\Phi(\upsilon_1,\upsilon_2)$ is calculated according to Eq.1.3

$$\Phi(v_1, v_2) = \frac{1}{2(t_m - t_1)} \sum_{j=1}^{m} \tilde{y}_j(v_1).\tilde{y}_j(v_2).(t_{j+1} - t_{j-1}) \qquad \text{Eq.3.3}$$

where m is the total number of spectra, equal to 24 in my case. I also define two additional points in the perturbation, t_0 and t_{m+1}, located outside the observation period as $t_o = 2t_1 - t_2$ and $t_{m+1} = 2t_m - t_{m-1}$.

Applying the above calculations to the entire range of the wavenumber/chemical shift will produce a square matrix that could be represented by a two dimensional contour map or what is called a synchronous spectrum. An example of a schematic synchronous spectrum is shown in Fig. 1.2 As the figure shows, the synchronous spectrum is a symmetric spectrum with respect to the diagonal line, where the auto peak along the diagonal line represents a correlation between the specific wavenumber/chemical shift and itself ($v_1 = v_2$). The auto peak will only appear if the band shows changes in the intensity during the perturbation period. On the other hand, the peaks located at the off-diagonal positions of Fig. 1.2 represent correlations between different spectral variables

(e.g., ν_1 and ν_2) and are called cross peaks. Cross peaks could have either a positive correlation (white shaded) or a negative correlation (gray shaded). When the cross peaks of two bands have the same sign this indicates that the two bands are changing in the same direction (they are increasing or decreasing together); when the cross peaks have different signs, one band is increasing while the other is decreasing.

The asynchronous 2D spectrum $\Psi(\upsilon_1,\upsilon_2)$ is calculated according to the following equation

$$\Psi(\nu_1,\nu_2) = \frac{1}{2(t_m - t_1)} \sum_{j=1}^{m} \tilde{y}_j(\nu_1).\tilde{z}_j(\nu_2).(t_{j+1} - t_{j-1}) \qquad \text{Eq.3.4}$$

where the $\tilde{z}_j(\nu_2)$ is the Hilbert transformation of $\tilde{y}_j(\nu_2)$ that is calculated by numerical integration according to Eq. 3.5

$$\tilde{z}_j(\nu_2) = \sum_{k=1}^{m} N_{jk} . \tilde{y}_k(\nu_2) \qquad \text{Eq.3.5}$$

The term N_{jk} is the element of Hilbert-Noda transformation matrix. See Noda and Ozaki (2004).

Applying the above calculations to the entire range of the wavenumber/chemical shift will produce a square matrix that could be represented by a two-dimensional contour map or what is called an asynchronous spectrum, similar to the schematic asynchronous spectrum shown in Fig. 1.3 Unlike synchronous spectra, the asynchronous spectrum is a non-symmetric spectrum and has no autopeaks. The signs of the cross peaks on the asynchronous spectrum could be used to provide valuable information on the sequential order of the changes of the bands with respect to the perturbation variables. For more details see Noda and Ozaki (2004).

The synchronous map of the two-dimensional hetero-spectral correlation analysis

of FTIR and ^{13}C-NMR was developed according to Noda and Ozaki (2004), simply by replacing one of the dynamic spectra $\tilde{y}$ (υ, t) from ^{13}C-NMR in Eq. (3.1) with the corresponding dynamic spectrum from FTIR. Instead of showing correlations from the same probe (e.g. ^{13}C-NMR), the map correlates between the chemical shift of in ^{13}C-NMR and the wavenumber in FTIR.

Because changes in noise are normally out of phase with each other, noise could cause artifacts and misinterpretation, especially for asynchronous maps (Noda and Ozaki, 2004). To reduce the noise of the ^{13}C-NMR spectra, I applied the noise reduction method proposed by Jung and co-workers (2002), where PCA is used to eliminate noise and reconstruct noise-free spectra.

3. RESULTS AND DISCUSSION

3.1. Salinity, pH and DOC concentration

The DOC concentration of the sterile-filtered Dismal Swamp samples (Table 3.1) shows a wide range of variation between different seasons, with the highest value, 11788± 97 μM-C on August 2006 (0806); this value is over 3x larger than the lowest DOC concentration on February 2007 (3720± 6 μM-C), In general, it seems that the DOC concentration increases as I approach the summer season and starts to decrease after that, which could be explained due to dilution effects in winter-spring where there is higher net precipitation/water flow as compared to the summer season. This agrees with my observation of the water level in the Portsmouth Ditch at Great Dismal Swamp, where the water level was always lower during the summer season and higher during the winter.

Table 3.1. Water temperature, salinity, pH and DOC concentration of the water samples from the five sites during the seven seasons.

Site	Water Temp. (C°)	Salinity	pH	DOC (s.d.) µM-C	Water Temp. (C°)	Salinity	pH	DOC (s.d.) µM-C
	1105				1106			
DS	17.2	0	3.17	8813(382)	11.8	0	3.30	11340(233)
GB	15.0	8	6.76	1015(7)	14.0	12	7.30	856(16)
TP	19.0	18	7.27	519(12)	18.0	20	7.21	438(5)
CBB	16.1	25	7.71	231(25)	15.4	25	7.51	281(14)
OSC	19.1	32	7.92	150(4)	18.5	32	7.81	189(5)
	0206				0207			
DS	8.5	0	3.24	7138(228)	8.9	0	3.26	3720(6)
GB	8.6	10	7.13	940(14)	7.9	11	7.24	754(25)
TP	7.8	20	7.60	581(49)	8.2	19	7.56	578(36)
CBB	6.0	25	7.35	391(19)	3.8	24	7.52	424(22)
OSC	N.S	N.S	N.S	N.S	N.S	N.S	N.S	N.S
	0506				0507			
DS	8.5	0	3.13	5780(237)	13.5	0	3.33	6539(145)
GB	23.0	14	7.27	695(16)	24.4	13	7.26	731(24)
TP	22.0	22	7.41	281(14)	20.9	19	7.53	362(15)
CBB	19.0	24	8.01	185(7)	18.3	23	7.72	190(2)
OSC	21.5	30	8.02	131(5)	N.S	N.S	N.S	N.S
	0806							
DS	20.4	0	3.09	11788(97)				
GB	29.1	16	7.13	648(12)				
TP	29.4	24	7.70	260(12)				
CBB	29.1	25	7.83	168(14)				
OSC	24.4	32	7.94	109(6)				

(s.d.) standard deviation based on three runs.

There were also large variations in the DOC concentration at the Great Bridge site (GB). However, as opposed to Dismal Swamp, the lowest value was on August 2006 (648± 12 μM-C) and the highest value was 1015± 7 μM-C on November 2005. Plotting the DOC concentration from both sites (GB and DS) against each other shows no correlation (r^2= 0.01) (Figure not shown), however because water flow rate data for the Dismal Swamp Channels was unavailable, and missing a clear hydrological connection between the DS and GB (see Fig. 1.1), I could not get a complete picture of how the changes in DOC concentration at Dismal Swamp could effect the transformation of DOM from DS to GB. However, despite the fact that all GB samples were collected during low tide, there was a wide range in the salinity of GB, from 8 to 16 (see Table 3.1). DOC concentration at the GB site also exhibited a strong negative correlation (r^2= 0.85) with salinity (Fig. 3.1), which could indicate high variation in the water flow rates out of DS to GB during different seasons (Loder and Reichard, 1981).

At the other sites (TP, CBB and OSC), I also find that August 2006 has the lowest DOC values of all the seasons (Table 3.1). From Fig. 1.1, there are clear hydrological connection from GB to OSC passing through TP and CBB. When I plot DOC versus salinity at the sites GB to OSC -in the seasons where I was able to sample the OSC (1105, 0506, 0806, 1106)- the plots for each of the four seasons are concave up (Figure not shown), which indicates either that there was a net sink of DOC in middle of estuary or that the variation of the DOC values in the two end members is shorter than the flushing time of the water between GB and OSC (Loder and Reichard, 1981). Based only on the DOC and physical parameters, in addition to unavailability of the fresh water flow

rates and the complex nature of the sampling area, I could not distinguish between these two possible explanations.

There are also seasonal variations in pH values at each site (see Table 3.1); however these variations were more intense at the Great Bridge site as compared to the other sites. In general, pH values at GB, TP, CBB and OSC were positively correlated with salinity (r^2= 0.79, n= 25).

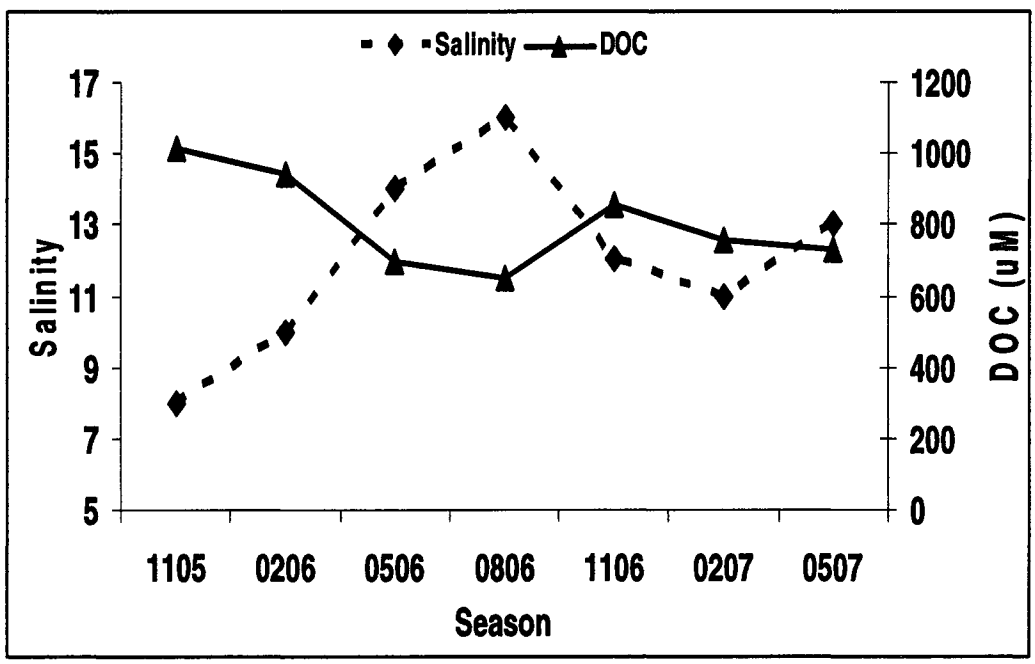

Fig. 3.1. Salinity and DOC concentrations during the seven seasons at Great Bridge Site (GB).

3.2. $\delta^{13}C$ and elemental analysis of HMW

The HMW-DOC recoveries from cross-flow ultrafiltration of water from the five sites during the seven seasons ranged from 69 to 15% (Tables 3.2a and 3.2b). In general, the percentage recovery decreases as I move toward the marine end member, which is in agreement with previous studies (Repeta et al., 2002; Wang et al., 2004). Using the extra step of stirred cell concentration/diafiltration for the estuarine and marine samples (GB, TP, CBB and OSC) seems to be successful in removing most of the inorganic salts as shown in the higher carbon and nitrogen percentages obtained from elemental analyses of the resulting freeze-dried retentates (Tables 3.2a-b). These percentages were 3X higher than previously reported percentages (Benner et al., 1992). Removing most of the salts gives us better interpretation for the $\delta^{13}C$ values and the C/N ratio. It also provides higher-quality spectra in both ^{13}C-NMR and FTIR. One of the drawbacks of using the additional filtration step is a lowering of the percent recovery. However, based on DOC measurements, the decrease in percent recovery from this step never exceeded 5%.

Table 3.2a. The DOC recovery, elemental analysis and stable carbon isotope signatures for the high molecular weight (HMW) DOM from the five sites during the first sampling year.

Site	% HMW(s.d.) Recovery*	%Mass-balance (s.d.) †	HMW DOC (s.d.)#	% C (s.d.) mass	% N (s.d.) mass	C/N (s.d.) mole	$\delta^{13}C$ (s.d.) PDB
				1105			
DS	52(3)	100(5)	4582(105)	44.36(2.08)	0.87(0.02)	51.23(1.55)	-27.42(0.02)
GB	51(3)	106(3)	485(21)	34.50(0.01)	2.03(0.29)	20.13(2.93)	-26.21(0.37)
TP	36(3)	102(6)	171(11)	36.93(3.82)	1.95(0.09)	22.08(1.30)	-26.22(0.10)
CBB	34(4)	92(11)	72(2)	28.38(3.54)	2.88(0.35)	11.53(0.02)	-23.40(0.21)
OSC	33(5)	105(6)	45(4)	25.82(1.51)	3.04(0.12)	9.89(0.21)	-22.46(0.02)
				0206			
DS	54(3)	104(5)	3887(215)	44.34(2.57)	0.86(0.04)	51.81(1.27)	-27.40(0.01)
GB	41(2)	96(4)	363(38)	30.41(3.49)	1.30(0.17)	27.33(0.43)	-26.72(0.01)
TP	33(3)	96(8)	183(9)	31.96(1.78)	1.41(0.06)	22.64(0.43)	-26.52(0.07)
CBB	27(2)	107(10)	93(15)	36.30(4.13)	3.60(0.57)	11.82(0.49)	-23.32(0.01)
OSC	NS	NS	NS	NS	NS	NS	NS
				0506			
DS	53(3)	108(5)	3084(79)	43.05(1.43)	0.84(0.02)	51.16(1.21)	-27.34(0.03)
GB	37(1)	103(3)	485(21)	39.84(0.53)	2.42(0.18)	19.28(1.69)	-25.55(0.23)
TP	24(3)	101(11)	171(11)	36.77(0.18)	2.77(0.04)	15.50(0.32)	-24.59(0.14)
CBB	17(4)	99(5)	72(2)	35.81(0.17)	3.81(0.09)	11.00(0.22)	-23.19(0.02)
OSC	15(4)	97(8)	45(4)	31.65(4.47)	3.34(0.60)	11.07(0.41)	-23.51(0.12)
				0806			
DS	53(2)	98(3)	6248(183)	48.66(3.82)	0.88(0.04)	55.29(2.07)	-27.35(0.03)
GB	38(3)	88(4)	238(28)	37.81(5.66)	2.48(0.05)	17.89(3.00)	-26.06(0.30)
TP	29(6)	96(10)	65(8)	25.91(2.35)	2.14(0.49)	14.41(1.97)	-24.05(0.34)
CBB	28(6)	88(9)	42(6)	27.96(5.03)	2.73(0.40)	11.94(0.38)	-22.52(0.60)
OSC	19(6)	87(9)	19(4)	29.29(5.64)	3.05(0.56)	11.19(0.10)	-22.36(0.31)

* HMW recovery is based on DOC measurements of the retentate recovered from the ultrafiltration system after the first diafiltration step and the initial sterile-filter sample, as well as the concentration factor.

† The mass balance percentages were calculated from DOC measurements of the retentate recovered after the first diafiltration, the filtrate (LMW) and the initial sterile-filter samples.
# The DOC concentration of the HMW-DOM recover after the sterile cell diafiltration take into account the concentration factor.

NS : No samples were collected at the site in that season.

Table 3.2b. The DOC recovery, elemental analysis and stable carbon isotope signatures for the high molecular weight (HMW) DOM from the five sites during the second sampling year.

Site	% HMW(s.d.) Recovery*	%Mass-balance (s.d.) †	HMW DOC (s.d.)#	% C (s.d.) mass	% N (s.d.) mass	C/N (s.d.) mole	$\delta^{13}C$ (s.d.) PDB
				1106			
DS	48(2)	105(3)	5441(158)	38.24(0.94)	0.81(0.03)	47.16(1.26)	-27.52(0.01)
GB	48(4)	98(5)	369(45)	37.45(0.16)	2.04(0.07)	21.44(0.61)	-26.21(0.18)
TP	42(3)	87(5)	166(18)	35.34(1.06)	1.95(0.07)	21.23(0.10)	-26.00(0.02)
CBB	33(3)	92(7)	84(5)	34.99(4.96)	3.24(0.58)	12.71(0.67)	-24.35(0.01)
OSC	32(3)	97(5)	53(9)	30.0(0.60)	3.34(0.13)	10.48(0.21)	-23.46(0.04)
				0207			
DS	52(5)	88(5)	1928(195)	41.56(3.29)	0.79(0.06)	52.70(0.34)	-26.97(0.11)
GB	42(2)	107(5)	302(32)	24.98(n.d)	1.71(n.d)	18.72(n.d.)	-26.75(n.d)
TP	32(3)	94(7)	181(11)	29.90(2.12)	1.45(0.08)	20.59(0.37)	-26.45(0.19)
CBB	25(2)	86(5)	95(15)	31.88(4.26)	3.19(0.49)	11.22(0.27)	-23.30(0.14)
OSC	NS	NS	NS	NS	NS	NS	NS
				0507			
DS	69(3)	87(4)	4489(194)	39.76(4.04)	0.64(0.04)	56.99(1.94)	-26.66(0.38)
GB	35(3)	87(6)	242(39)	34.48(1.76)	1.90(0.08)	21.46(1.01)	-26.30(0.13)
TP	27(2)	103(6)	91(14)	27.81(1.17)	1.61(0.19)	17.37(1.33)	-25.79(0.27)
CBB	24(4)	92(5)	40(4)	39.63(0.30)	4.13(0.13)	11.22(0.27)	-22.48(0.16)
OSC	NS	NS	NS	NS	NS	NS	NS

* HMW recovery is based on DOC measurements of the retentate recovered from the ultrafiltration system after the first diafiltration step and the initial sterile-filter sample, as well as the concentration factor.

† The mass balance percentages were calculated from DOC measurements of the retentate recovered after the first diafiltration, the filtrate (LMW) and the initial sterile-filter samples.
# The DOC concentration of the HMW-DOM recover after the sterile cell diafiltration take into account the concentration factor.

n.d. one of the EA-IRMS runs was lost so we could not calculate the standard deviation.

NS : No samples were collected at the site in that season

Plotting $\delta^{13}C$ values for the HMW-DOM from all the sites versus salinity (Fig. 3.2) shows that the Dismal Swamp (S= 0) has an average seasonal value of -27.24‰ which is a typical $\delta^{13}C$ value for C3 plants (Bianchi, 2007; Raymond and Bauer, 2001). As I move to the brackish region, the $\delta^{13}C$ becomes slightly enriched and stays within a narrow region between -26.72 to -25.55‰ regardless of the season, and they are slightly heavier than the expected mixing curve (derived from Eq. 3.1) However after passing salinity 20, a sudden and significant shift in the $\delta^{13}C$ is observed where the HMW-DOM becomes more carbon-13 enriched and closer to the $\delta^{13}C$ of marine autochthonous sources; at salinities above 20 the $\delta^{13}C$ stays within a range of -24.59 to -22.36‰.

Plotting the C/N atomic ratio against salinity (Fig. 3.3) shows the same features as observed with $\delta^{13}C$, but with a more dramatic drop in the C/N ratio of the HMW-DOM as I move from Dismal Swamp to the estuarine sites (GB). In the estuary region below the salinity of 20, the C/N ratio showed some scatter, however it remained within the range between 27.33 and 17.37. At salinities above 20, the C/N ratio drops to 15.5 (at salinity 22) and continues to drop slightly (to 12.71 to 9.89) at salinity 25 and beyond.

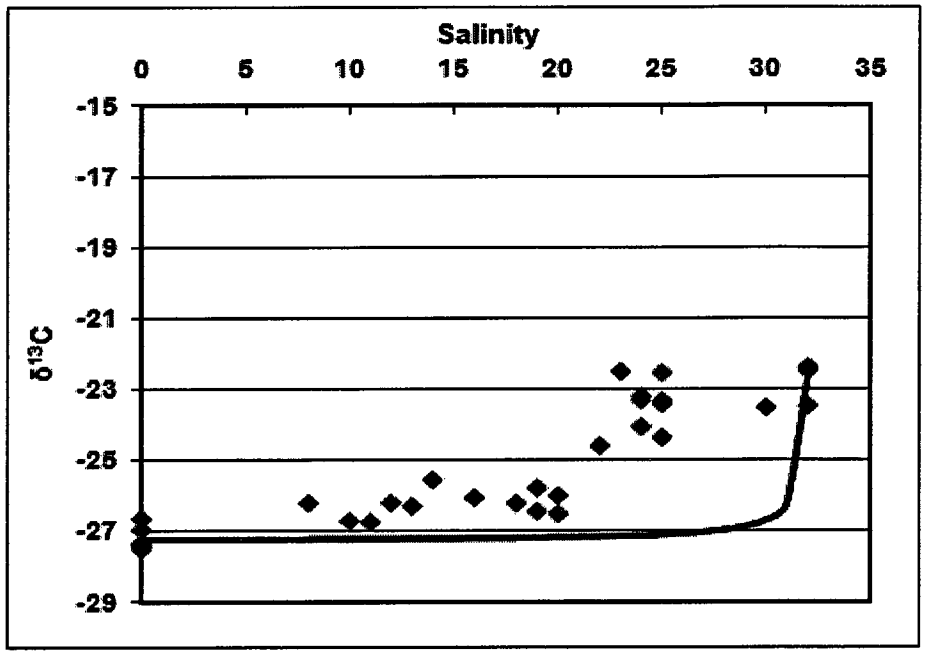

Fig. 3.2. The plot of all the $\delta^{13}C$ of the HMW-DOM against their salinity values from all the five sites during the seven seasons. The solid line represents the expected line if distributions are due solely to the mixing of the DS and OSC end-members as calculated from Eq. 3.1.

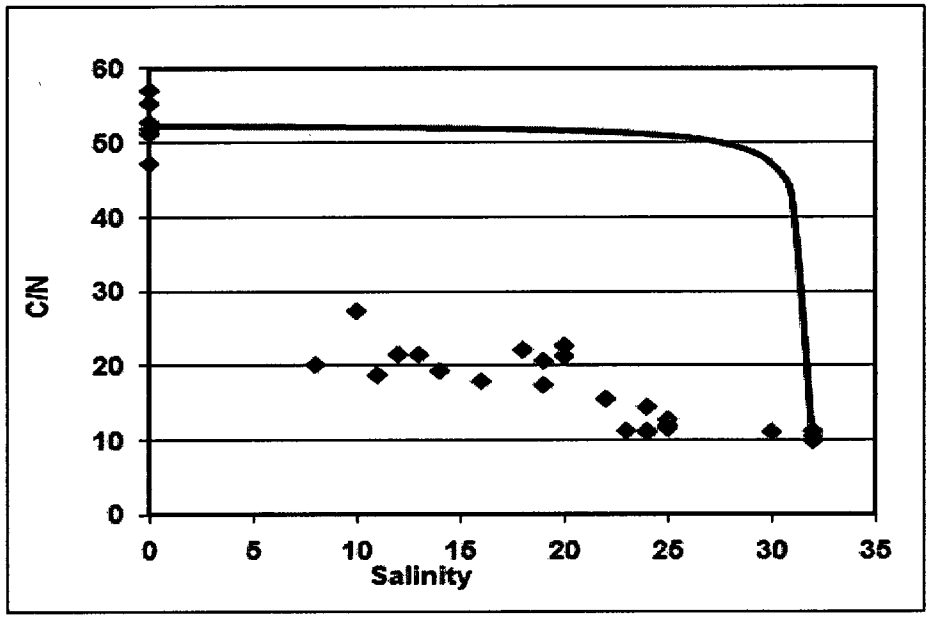

Fig. 3.3. Plot of all the C/N (atomic) values of the HMW-DOM against their salinity values of all the five sites during the seven seasons. The solid line represents the expected line if distributions are due solely to the mixing of the DS and OSC end-members. As calculated from Eq. 3.2.

From both C/N and $\delta^{13}C$ I could divide the transformation of HMW-DOM into three regions based on salinity: First is the Dismal Swamp region at salinity of zero, which has a seasonal average C/N ratio of 52.33 and $\delta^{13}C$ seasonal average value of (-27.24‰); both are typical signals for C3 vascular-plant DOM sources. The second region, from salinity zero to salinity 20, has average values of 20.85 and -26.22‰ for the C/N ratio and $\delta^{13}C$ respectively. The third region, which starts after salinity 20 and continues to salinity 32 is characterized by an average value of 11.84 and -23.31‰ for both C/N atomic ratio and $\delta^{13}C$ respectively.

The dramatic drops in the C/N ratio of HMW-DOM from 52.33 at salinity of zero to an average of 20.85 in region two co-occurs with a $\delta^{13}C$ signal that still indicates the majority of the fixed carbon sources are terrestrial. This could be explained either by preferential removal of carbon relative to nitrogen or by the introduction of new organic nitrogen compounds into the HMW-DOM pool by heterotrophic bacteria. There are many studies that support both explanations. In my previous study on the same transect (Section II in this dissertation), I find significant losses of both aromatic and iron-carboxylic complexes in comparing the DOM from DS and GB, probably due to photooxidation (Xie et al., 2004) and flocculation processes (Sholkovitz, 1976; Sholkovitz et al., 1978). Losing carbon-rich and nitrogen-poor (e.g. aromatic) moieties could be responsible for decreasing the C/N ratio while retaining the $\delta^{13}C$ signal. On the other hand, a study conducted along the Delaware Estuary showed that heterotrophic bacterial production in the upper Delaware Estuary exceeded phytoplankton production by 1.4 fold while exhibiting only a 0.4 fold ratio for the entire estuary (Hoch and Kirchman, 1993). In addition, many studies show that heterotrophic bacteria utilize

allochthonous DOM directly or with the help of photooxidation (Amon and Benner, 1996; Obernosterer and Benner, 2004; Tranvik, 1992). Conversely, as bacteria utilize allochthonous DOM they also release new HMW-DOM (Heissenberger and Herndl, 1994; Kawasaki and Benner, 2006) which could have a similar carbon-13 signature but be richer in nitrogen content. This idea is consistent with the recent estimate that bacteria could account for more than 50% of marine DON (Kaiser and Benner, 2008). It is thus very likely that the combination of photochemical and sorptive/aggregative losses along with microbial reworking plays a major role in lowering the C/N ratio and keeping the carbon-13 signature closer to the allochthonous DOM of the C3 plant as I move from Dismal Swamp to region two.

Continuing down-transect, the $\delta^{13}C$ value and C/N ratio of the HMW-DOM show significant changes as I move from region two to region three, becoming closer to the $\delta^{13}C$ and C/N values of marine microalgal and microbial sources (Bianchi, 2007; Raymond and Bauer, 2001). The significant change in the $\delta^{13}C$ indicates that a new carbon source is introduced either through autochthonous phytoplankton primary production or an increased contribution of C4 plant material (e.g. from salt marshes). Measuring the compound-specific ^{13}C values of lignin components in C_{18} DOM extracts from the same water collected during the November 2006 season (1106) indicates that the lignin is mainly coming from C3 plants (Sleighter et al., 2008), thus discounting an extensive salt marsh contribution. Phytoplankton blooms at higher salinities (20 and above) within estuaries are common (Edmond et al., 1985; Ning et al., 1988), as the high turbidity and possibly the high concentration of colored dissolved organic matter often limits light penetration lower-salinity, upper estuary sites (Dagg et al., 2004; Edmond et

al., 1985; Turner et al., 1990). Unfortunately, due to a lack of chlorophyll-*a* data and the hydrological complexity of my sampling area I can't determine if the phytoplankton source is from in situ productivity mid-transect or if it is from DOM introduced by a third end member (e.g. James River).

Looking into seasonal trends for both $\delta^{13}C$ and C/N along salinity gradients (Fig. 3.4 a-g), I find that all the seasons show similar trends to those seen on the combined Fig. 3.2 and Fig. 3.3 with a dramatic drop between Dismal Swamp and region two in C/N ratio and a drop in C/N ratio and significant enrichment in $\delta^{13}C$ above salinity 20. However, there are some noticeable seasonal differences, for example, both 0206 and 0207 (winter seasons) show almost a straight line in the $\delta^{13}C$ between DS, GB and TP, while $\delta^{13}C$ displays a stronger decrease in slope at other times, especially during both 0506 and 0806 seasons, probably due to the combined effects of higher photooxidation and primary production in spring and summer than winter seasons (Harvey and Mannino, 2001; Pennock and Sharp, 1986).

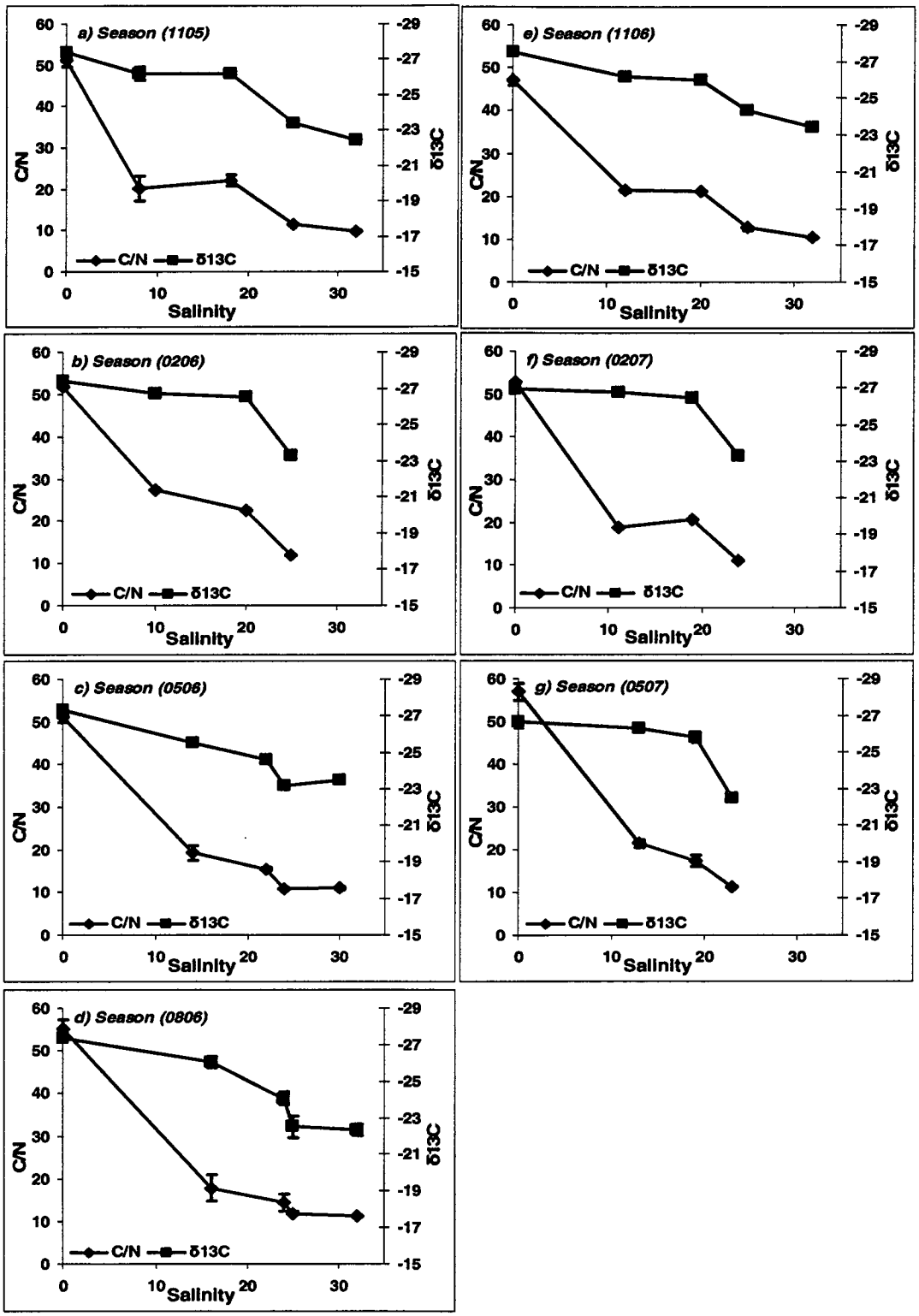

Fig. 3.4a-g. Plots of C/N and $\delta^{13}C$ of the HMW-DOM against their salinity values in each of the seven seasons.

3.3. Solid state-CP/MAS ^{13}C NMR analysis

The average spectrum from my NMR data set of HMW-DOM isolated from the estuarine /marine sites (GB, TP, CBB and OSC) during all the seven seasons (Fig. 3.5) looks similar to previously reported spectra of HMW-DOM isolated from North Pacific surface water (Benner et al., 1992; Eglinton and Repeta, 2003; Sannigrahi et al., 2005). Commonalities include strong signals from the alcohol group (H-C-OH) and anomeric carbon (O-C-O) at 60-90 ppm and 90-120 ppm respectively, which are indications of high carbohydrate content and a resolved band around 178 ppm attributed to carboxyl, ester (COO), and amide (CON); there are also two sharp peaks in the area from 0- 45 ppm which are attributed to a paraffin carbon (CH_x) that could be coming from lipid or biopolymeric material. The C=C/aromatic (120-140 ppm) and oxygen substituted aromatic (140-160 ppm) regions have a wide and low intensity area, and the region between 45- 60 ppm shows a very wide band with many shoulders; this area is normally assigned to methoxy groups and amino groups (CH_3-O/CH_3-N) that are available in lignin and amino compounds (Dria et al., 2002).

3.3.1. PCA of the ^{13}C-NMR spectra

To highlight the variations among the different marine/ estuarine HMW-DOM spectra, I performed principal component analysis (PCA) on the normalized ^{13}C-NMR spectra (n=24). In the PCA results the first two principal components (PC) account for 88% of the variability in the data set (Fig.3.6a-b). From Fig. 3.6a, it is clear that all the seasonal GB samples clustered in the negative side of principal component one (PC-1),

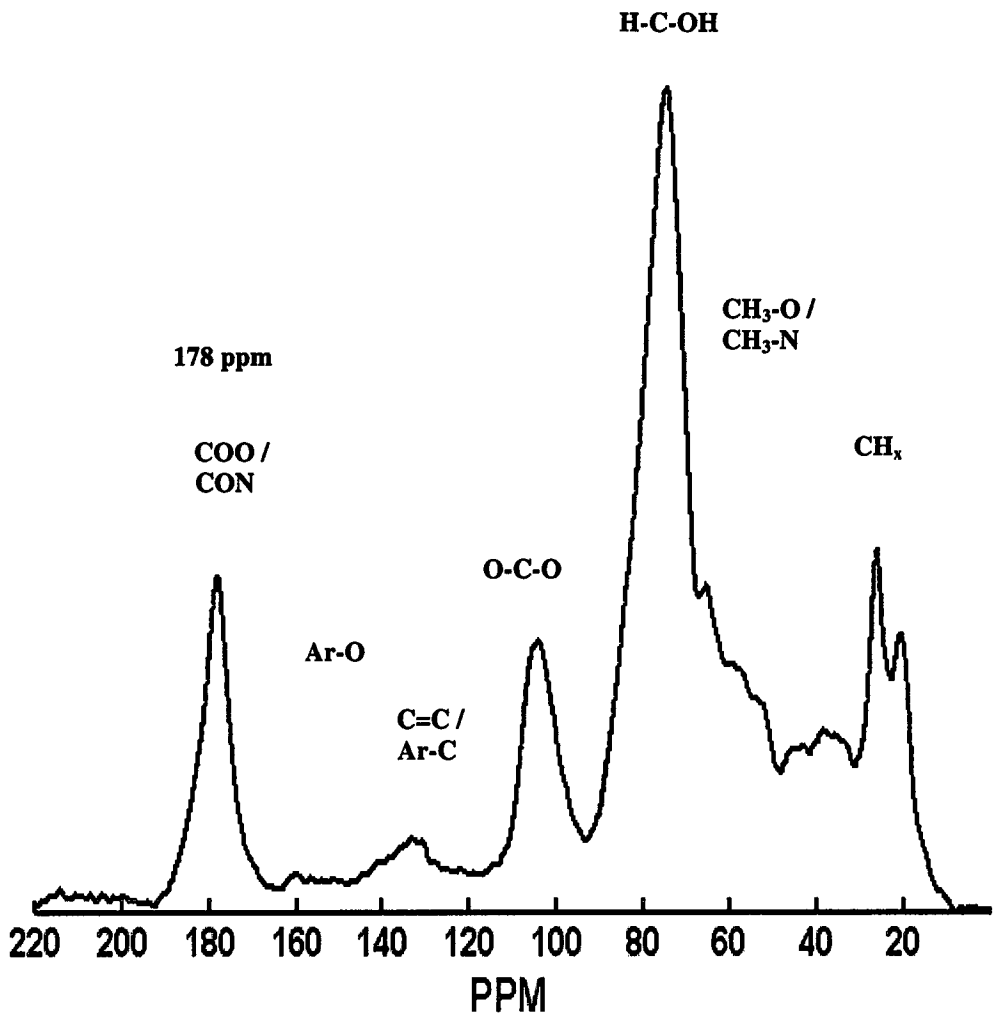

Fig. 3.5. The average ^{13}C-NMR spectrum of the normalized ^{13}C-NMR spectra (n=24) of all the HMW-DOM isolated along the transect during all the seven seasons.

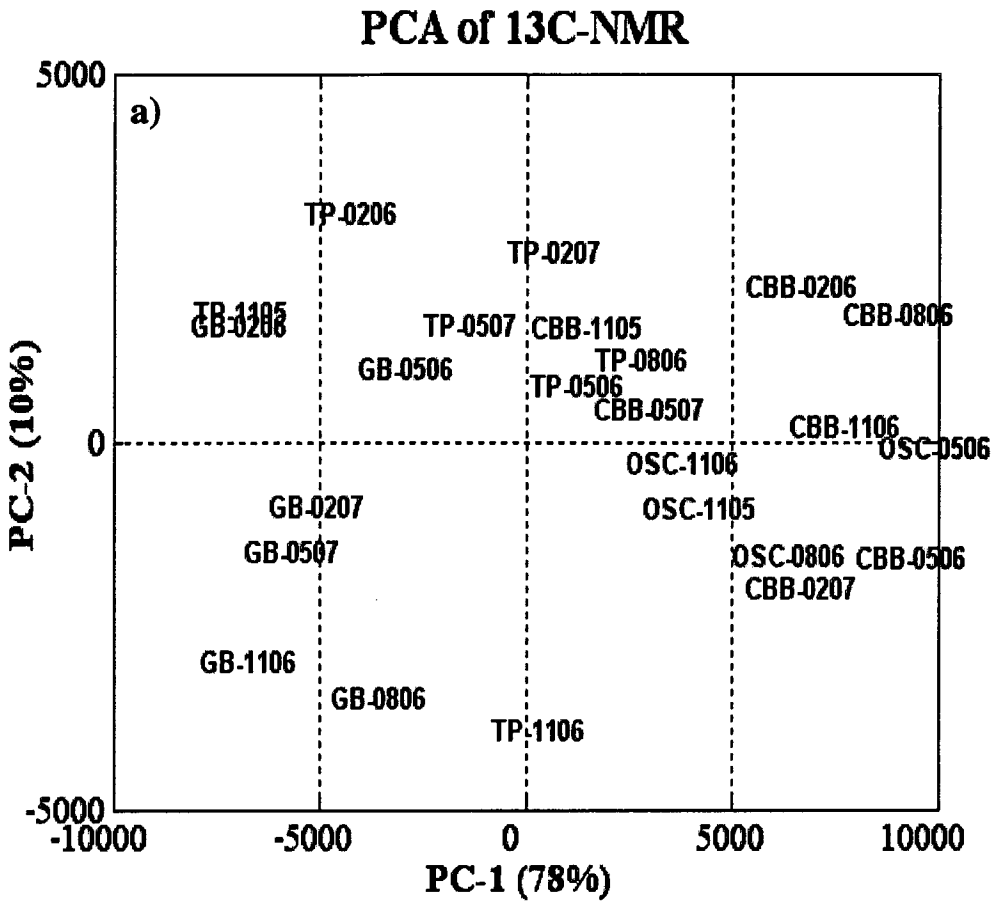

Fig. 3.6. a) Principal component analysis (PCA) score plot of the ^{13}C-NMR (n= 24) spectra of the HMW-DOM isolated from all the five sites: Great Bridge (GB), Town Point (TP), Chesapeake Bay Bridge (CBB) and the Offshore site (OSC) during the seven different seasons (1105, 0206, 0506, 0806, 1106, 0207 and 0507). b) The same as Fig. 3.6a, but with replacing the sites labels with their salinity values.

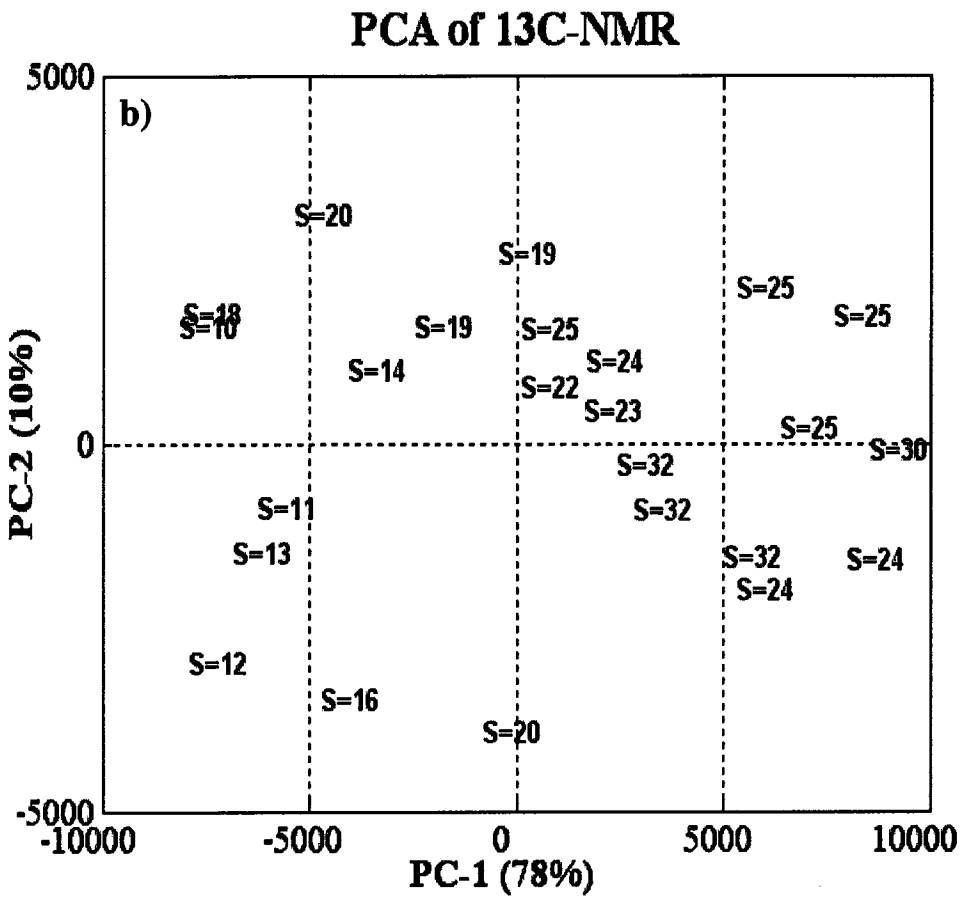

Fig. 3.6. Continued.

while the seasonal ^{13}C-NMR spectra of the TP sites are scattered in both negative and positive space along PC-1. The two sites close to the marine end member (CBB and OSC) appear in positive PC-1. When I replace the site labels with their salinity values (Fig. 3.6b), I see that all the spectra that come from samples with salinity ≤ 20 appear in negative PC-1 space while spectra from samples that have salinity > 20 plot in the positive PC-1 region. This is in good agreement with what I observed from both the δ^{13}C

and C/N results, where a dramatic change in both the $\delta^{13}C$ and C/N occur after salinity of 20.

Plotting the PC-1 loadings spectrum (Fig. 3.7) illustrates that the spectra on the positive side of PC-1 have a higher carbohydrate content as indicated by carbohydrate signature bands: the alcohol group (H-C-OH) at 60-90 ppm and anomeric carbon (O-C-O) at 90-120 ppm, while both of the aromatic signatures (the regions of 120- 140 ppm for C=C/Ar-C and 140- 160 ppm for Ar-O) appeared in negative PC-1. So, in general, the samples at salinity ≤ 20 have higher aromatic and lower carbohydrate contents while the HMW-DOM from salinity > 20 are high in carbohydrate and lower in the aromatic contents. This agrees with what is believed about surface marine DOM, i.e., that it is rich in carbohydrate and very low in aromatic content (Aluwihare et al., 1997; Repeta et al., 2002). Seeing a dramatic change in the chemical structure of DOM at a specific salinity values has been reported before; Hernes and Benner (2003) show a dramatic decrease in lignin compounds at salinity 25 in the Mississippi River plume. They argue that flocculation and microbial degradation are the dominant processes affecting lignin at salinities of less than 25, while photooxidation is the dominant process changing the lignin concentration and composition above salinity 25.

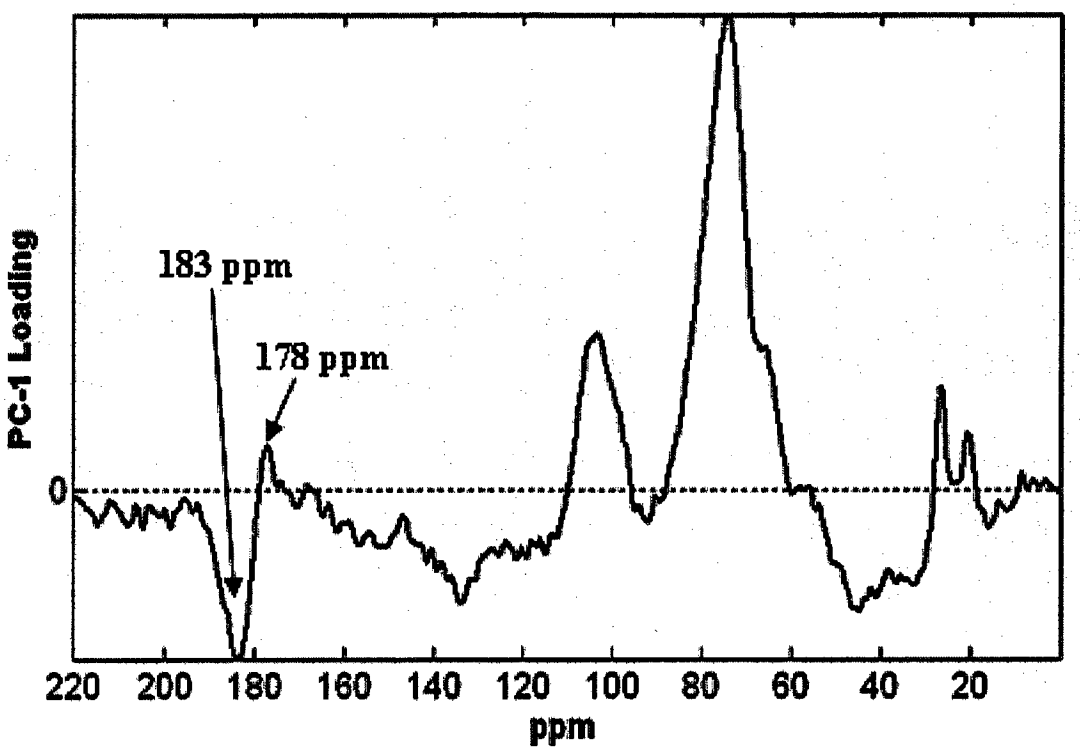

Fig. 3.7. The loading of ^{13}C-NMR spectra along principal component one (PC-1) from the analysis whose score plot is shown in Fig. 3.6.

The loading of the PC-1 revealed interesting biogeochemical changes in the ^{13}C-NMR spectrum of the HMW-DOM as I move through the transect. For instance, the area between 160-190 ppm that is assigned to the carboxylic, ester and amide functional groups (Dria et al., 2002) shows a maximum intensity at 178 ppm in the average ^{13}C-NMR spectrum (Fig. 3.5); however the PC-1 loading revealed a band at 185 ppm on the negative side of the PC-1 while only a small peak at 178 ppm appeared on the positive

side of the PC-1. This indicates that the band at 178 ppm consists of at least two bands having different biogeochemical reactivities. The region between 0-45 ppm is normally assigned to paraffin carbon (CH_x); the PC-1 loading revealed that it is actually a combination of two different biogeochemical paraffin carbon groups, the first one (10-30 ppm) appeared on the positive side of the PC-1 loading while the other region (30-45 ppm) shows in the negative side of the PC-1 loading. This suggests that I should use caution in applying the integrated area between 0-45 ppm as an indication of changes in the aliphatic content of the DOM, as the region actually consists of two paraffin carbon (CH_x) groups that act biogeochemically in opposite directions. Within the PC-1 loading, the region between 45 and 60 ppm, which is assigned to methoxy and amino groups, appears in negative PC-1 space, the same space as the aromatic compounds. This could indicate that mainly methoxy groups are attached to the aromatic compounds, consistent with a typical model structure of lignin-like compounds (Hedges et al., 1988).

3.3.2 Two dimensional correlation ^{13}C-NMR

By overlaying the 24 normalized ^{13}C-NMR spectra of the estuarine/marine HMW-DOM isolates (Fig. 3.8a) I notice major changes in the intensity of most the bands, however, the spectra look somewhat noisy. Since the first two principal components (PC-1 and PC-2) account for a significant amount (88%) of the variation in ^{13}C-NMR spectra, I can use them in the PCA noise reduction method. The resulting reconstructed spectra retain their major peaks and exhibit a reduction in noise (Fig. 3.8b). One of the drawbacks of using only 88% of the variation in the original spectra is that the approach may also remove some information features along with the noise. Therefore I

plotted the spectra of the removed noise (Fig. 3.8c) which exhibits no recognizable features and is clearly background noise. As an additional check I compared synchronous and asynchronous contour maps with and without the noise; the synchronous map shows no noticeable differences, while, the asynchronous contour maps look a little bit noisy with the noisy spectra. All results presented here from the 2D-correlation of the ^{13}C-NMR were generated from the noise free spectra.

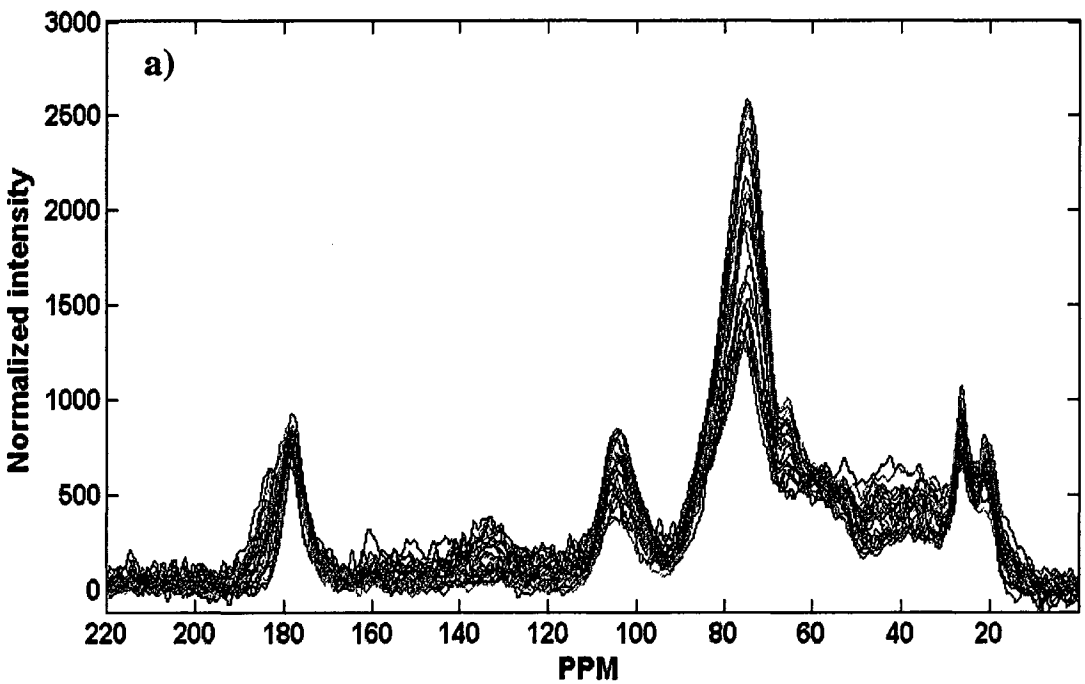

Fig. 3.8. Overlay of the twenty-four area-normalized ^{13}C-NMR spectra of the HMW-DOM isolated from the four sites (GB, TP, CBB and OSC) during the seven seasons. a) Before the removing the noise. b) After removing the noise. c) The spectra of the removed noise.

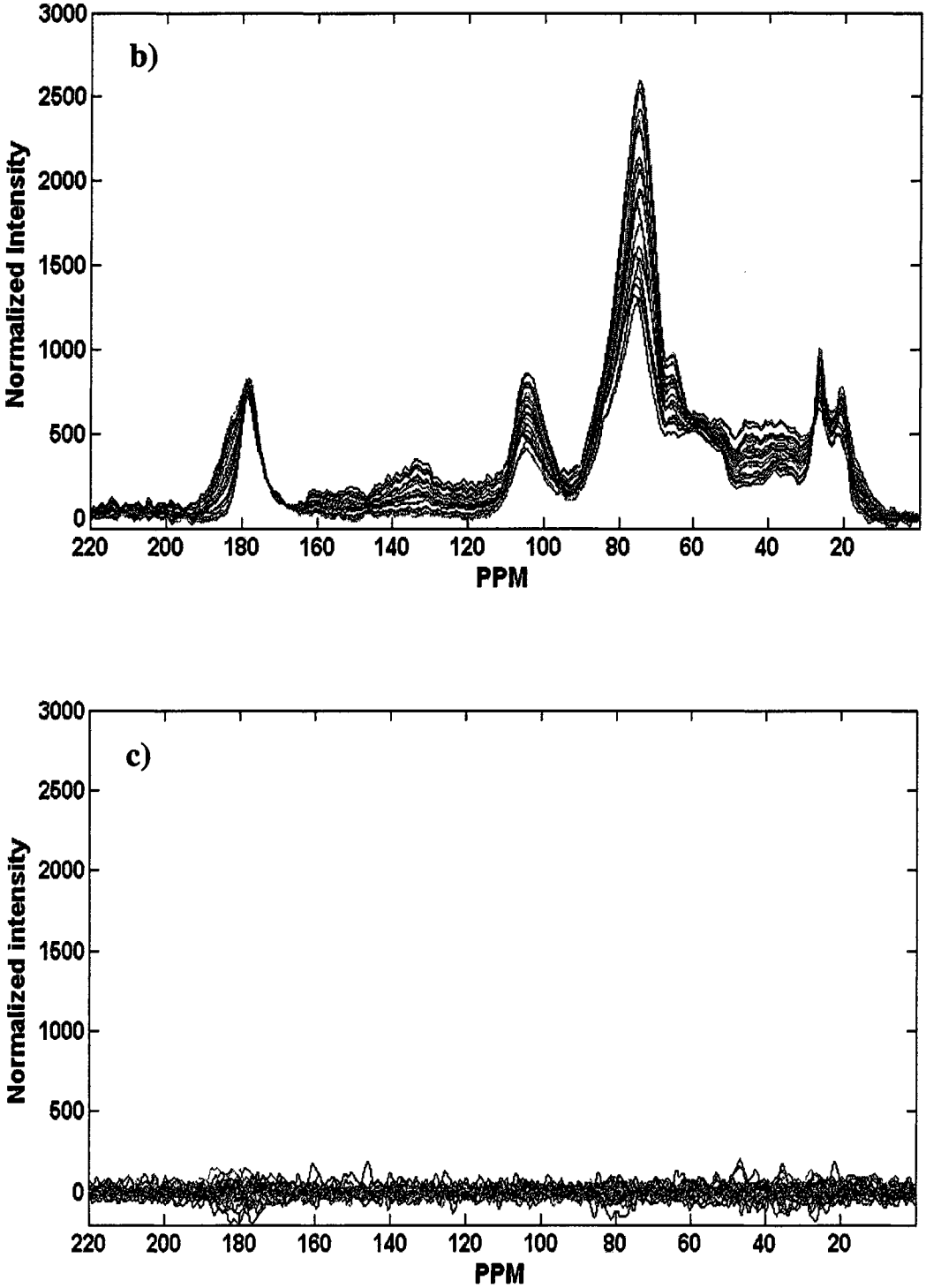

Fig. 3.8. Continued.

3.3.2.1 ^{13}C-NMR synchronous map

The synchronous map shows a symmetric spectrum with respect to the diagonal line (Fig. 3.9a). I could identify nine major autopeaks spread along the diagonal line; the autopeak represents the correlation between a band and itself and only shows up if the intensity of the band changes between different dynamic ^{13}C-NMR spectra. The nine autopeaks in my data set are spread over the entire ^{13}C-NMR spectra: three autopeaks appear in the paraffin carbon region (0-45 ppm) at 20, 26 and 32 ppm; one autopeak is in the methoxy and amino group (45-60 ppm) region at 46 ppm; a major autopeak appears at 74 in the middle of the O-alkyl (HCOH) region; another autopeak at 103 ppm in the region of anomeric carbon (90-120 ppm), while a broad autopeak occurs at 132 ppm in the region of C=C/ aromatic groups. The carboxylic, ester and amide region (160-190 ppm) shows two autopeaks, a very small one at the band maximum (178 ppm) and another larger one at the high chemical shift side of the band (183 ppm). If I look back to the noise free ^{13}C-NMR spectra (Fig. 3.8b) at the region between 160 and 190 ppm, I can see the band maximum intensity (178 ppm) shows very small changes; however, the band width gets much narrower at the higher chemical shift side. From a comparison of the intensities of the identified autopeaks, the band at 74 ppm exhibits the highest spectral variation through the estuarine transect. The band at 178 ppm showed the lowest spectral variation as indicated by the low intensity autopeak.

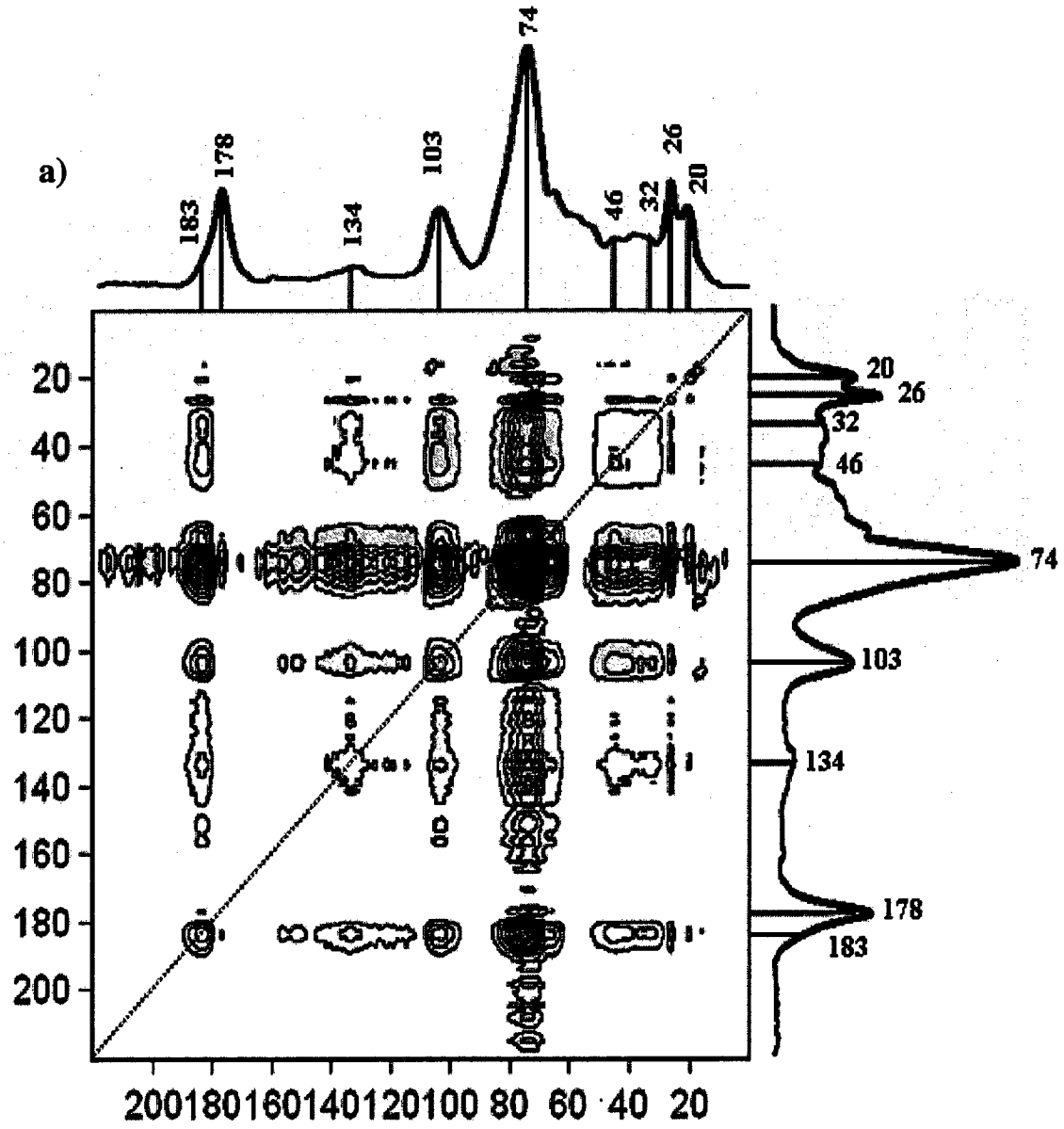

Fig. 3.9. The synchronous contour map generated from all the ^{13}C-NMR (n=24) of the HMW-DOM isolated from the four estuary/marine sites during the seven season where the top and the right side is the average ^{13}C-NMR spectra (included as reference) a) The entire chemical shift region (0-220 ppm) b) From (0-110 ppm) c) From (90-200 ppm)

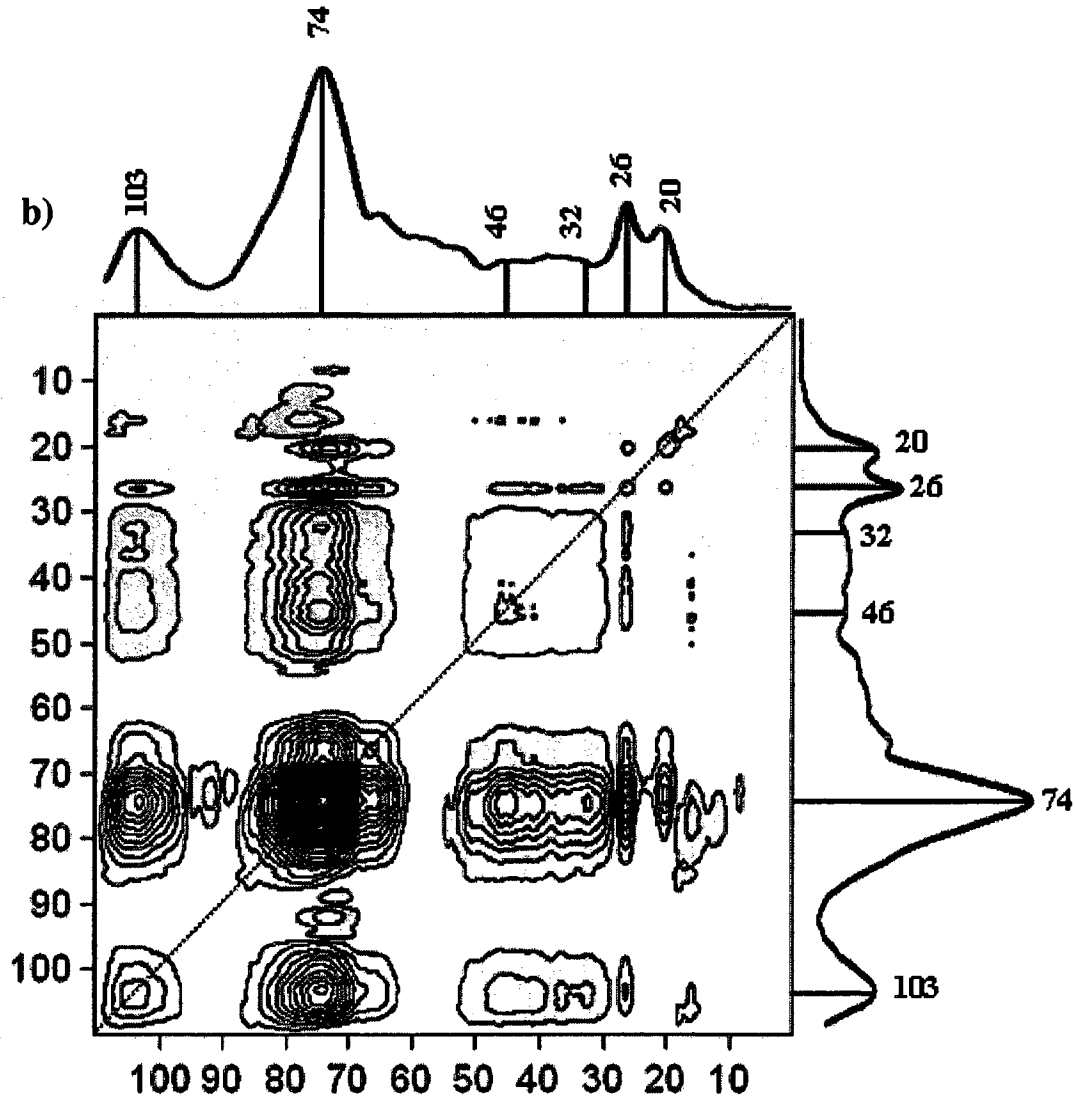

Fig. 3.9. Continued.

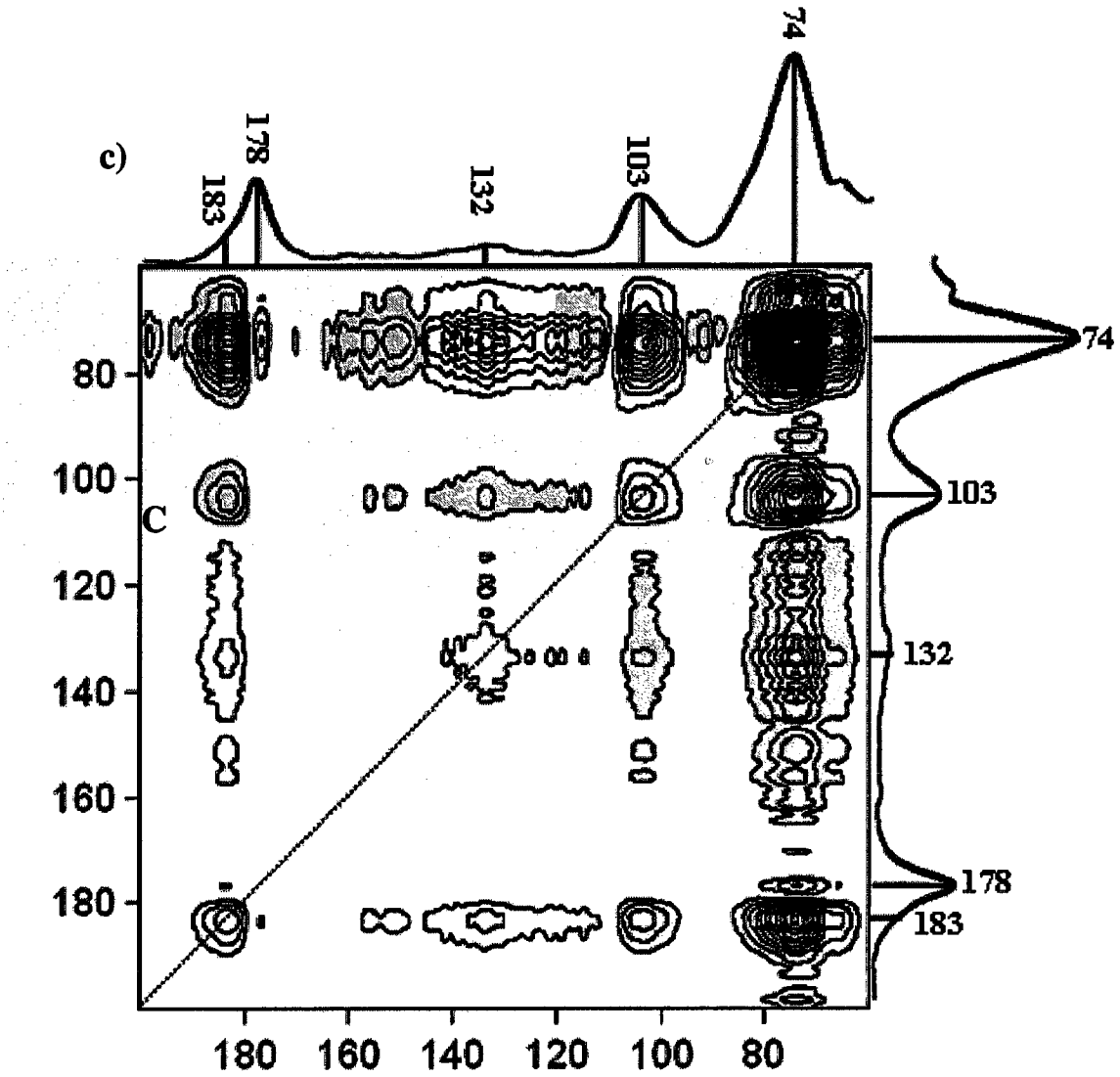

Fig. 3.9. Continued.

In order identify how these nine major bands are correlated with each other, I look to the off-diagonal peaks (cross peaks) in the synchronous map. For a better view I divide the synchronous map into two regions: one from 0-110 ppm (Fig. 3.9b) and the other from 60-200 ppm (Fig. 3.9c), keeping an overlap between these two regions so I can compare the information I get from both figures. The first region of the synchronous map illustrates that the band centered at 74 ppm is negatively correlated with bands at 32 and 46 ppm as indicated by the shaded (gray) crosspeaks between them and positively correlated with the bands at 20, 26, and 103 ppm as it indicated from the clear crosspeaks. The second region of the synchronous map from 60– 200 ppm, illustrates, from the shaded crosspeaks, a negative correlation between the band at 74 ppm and the bands at 132 and 183 ppm while there are positive correlations with the band at 178 ppm. From both of these regions, I could conclude that the bands at 20, 26, 74, 103 and 178 all increase as I move toward the marine end member while the bands at 32, 46, 132 and 183 ppm all decrease as I move toward the marine end member which provides confirmation for what I had seen from the PC-1 loading (Fig. 3.9). However, the 2D-correlation, by spreading the spectra into a second dimension, increases the resolution of the spectra, separating the overlap bands and giving us more detailed information about band positions and changes in band intensity. 2-D correlation also clearly shows the bands that didn't change during the transformation of DOM along the estuary. For example, although most of the chemical shifts within the ^{13}C-NMR spectra show changes either through autopeaks or crosspeaks, the region between 54 and 62 ppm, which is a part of the methoxy/ amino region (45-60 ppm), displays no intensity changes regardless of its high ^{13}C-NMR intensity in all the spectra.

3.3.2.2. ^{13}C-NMR asynchronous map

The asynchronous map can provide information about the sequential order of the changes in spectral bands. However, although salinity is used as the perturbation parameter to generate the asynchronous map, I cannot ascertain if the changes in the bands' order are due only to the ionic strength effects because there are many other factors which correlate with salinity that can play a role in changing the DOM chemical composition. However, the asynchronous map will still be informative, supporting what I observe in the synchronous map and differentiating overlapped band resolution. It is especially useful in investigating whether two bands are totally in-phase with each other.

The asynchronous map (Fig. 3.10), unlike the synchronous map, is antisymmetric with the respect to the diagonal line and exhibits no autopeaks, which is expected as each spectrum becomes out phase with itself after using the Hilbert transform function and will therefore show no correlation at the same chemical shift (Noda and Ozaki, 2004; Wang and Palmer, 1999). The asynchronous map clearly confirms that the band maximum at 178 ppm consists of two biogeochemically different bands at 178 and 183 ppm.

In general, both synchronous and asynchronous maps demonstrate that the DOM in the estuary is a complex mixture of organic compounds that have different biogeochemical reactivity and that the ^{13}C-NMR bands appearing in the original 1-D spectra result from overlapped bands between the common functional groups in the organic compounds of the DOM.

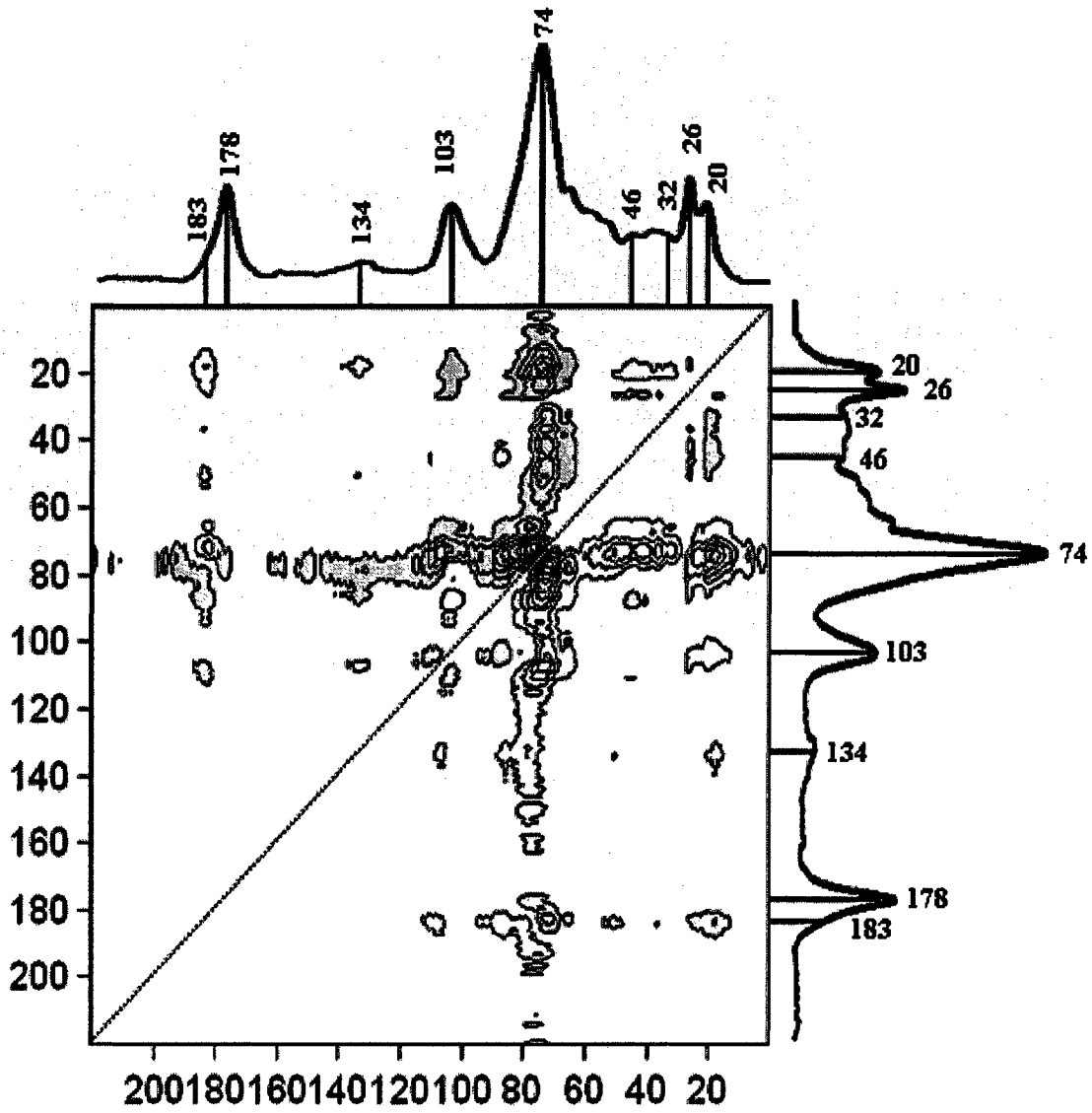

Fig. 3.10. The asynchronous contour map generated from all the ^{13}C-NMR (n=24) of the HMW-DOM isolated from the four estuary/marine sites during the seven season where the top and the right side is the average ^{13}C-NMR spectrum (included as reference).

3.4. FTIR synchronous maps

The synchronous map generated from the 24 FTIR spectra of the HMW-DOM isolated along the transect (Fig. 3.11), displays 8 major autopeaks at 1735, 1660, 1580, 1467, 1402, 1151, 1088 and 1043 cm^{-1}. The highest change in intensity was in the band at 1150 cm^{-1}. The band at 1580 cm^{-1} exhibited the second-highest change in intensity, while the bands at 1735 and 1660 cm^{-1} show the lowest change in intensity within the autopeaks. I previously assigned these bands as followed: the band at 1735 cm^{-1} to the asymmetric stretching of C=O of ester, the band at 1660 cm^{-1} to the asymmetric stretching of the C=O band of amide compounds, the band at 1580 cm^{-1} to the asymmetric stretching of de-protonated carboxylic acid (COO^-), the band at 1402 cm^{-1} to the symmetric stretching of de-protonated carboxylic acid, the band at 1467 cm^{-1} to CH_3 asymmetric deformation, and the band at 1151 cm^{-1} to the carbohydrate ring vibration, the band at 650 cm^{-1} to the O-H out-of-plane bending, and the band at 1088 cm^{-1} to the C-O asymmetric stretching (see Section II, this dissertation). The cross-peaks show a positive correlation between the bands at 1580 and 1402 cm^{-1} and bands at 1151 and 650 cm^{-1}. This correlation helps to confirm my previous assignment of these bands. The cross peaks also indicate that the bands at 1580 and 1402 cm^{-1} change in the opposite direction of the bands at 1151, 1088 and 650 cm^{-1}.

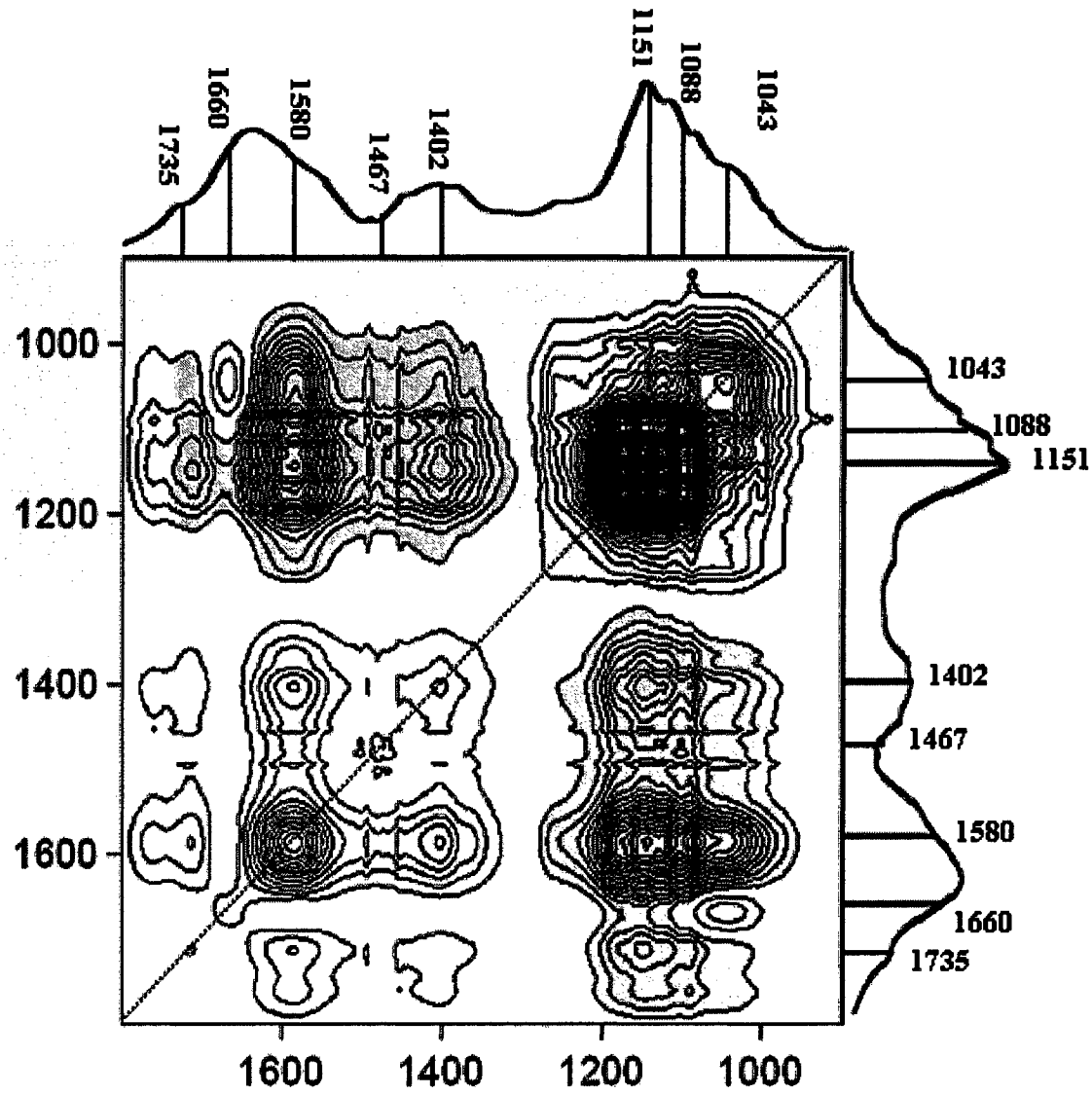

Fig. 3.11. The synchronous contour map generated from all the FTIR region between (between 1800- 800 cm^{-1}) (n=24) of the HMW-DOM isolated from the four estuary/marine sites during the seven seasons where the top and the right side is the average FTIR spectrum (included as reference).

I further suggest that the band around 1580 cm^{-1} is due to asymmetric stretching of highly oxygen substituted aliphatic carboxylic acids. This suggestion is based on the previous extensive study done by Hay and Myneni (2007) where attenuated total reflection Fourier transform infrared (ATR-FTIR) is used on the carboxylic structures in natural organic matter (NOM, humic and fulvic acid and reverse osmosis isolates) isolated from different aquatic and soil environments and the results are compared with those for a large number of model compounds. Hay and Myneni showed that although the location of asymmetric stretching of de-protonated carboxylic acid (COO^-) is very sensitive to changes in chemical structure within the model compounds, in NOM it always appeared at a narrow range centered at 1578 cm^{-1}. This indicates the presence of a limited chemical environment for the carboxyl groups in NOM and matches the band position of model carboxylic compounds that have oxygen substituted (hydroxyl, carboxylic or ester) at the α or β carbon position.

3.5. Two dimension hetero- spectral correlation analysis of FTIR and ^{13}C-NMR

In order to combine the information I get from FTIR and ^{13}C-NMR, I applied 2D hetero-spectral correlation analysis to the FTIR and ^{13}C-NMR spectra. The 2D hetero-correlation map (Fig. 3.12) shows a positive correlation between the FTIR band at 1580 cm^{-1} and the ^{13}C-NMR band at 183 ppm. A positive correlation is also observed between the FTIR band at 1151 cm^{-1} and the ^{13}C-NMR band at 74 ppm.

The similarity in the correlation of each of the FTIR band at 1151 cm^{-1} (Fig. 3.12) and the ^{13}C-NMR band at 74 ppm (Fig. 3.9a) with the entire ^{13}C-NMR spectra, confirm my assignment that the FTIR band at 1151 cm^{-1} to the alkyl-O bond of the carbohydrate ,

which highlights the possibility of using the FTIR band at 1151 cm^{-1} as indication of change in the carbohydrate content between different DOM samples. Similar correlation is also observed between the FTIR band at 1580 cm^{-1} and the ^{13}C-NMR band at 183 ppm, indicating that both of the bands are result from the same chemical bond (the carboxylic group in the highly oxygen substituted aliphatic carboxylic-acid). These band positions match very well previously identified peak positions for carboxylic and carbohydrate bands in both FTIR and ^{13}C-NMR (Mayo et al., 2004; Pavia et al., 1996; Wilson, 1987).

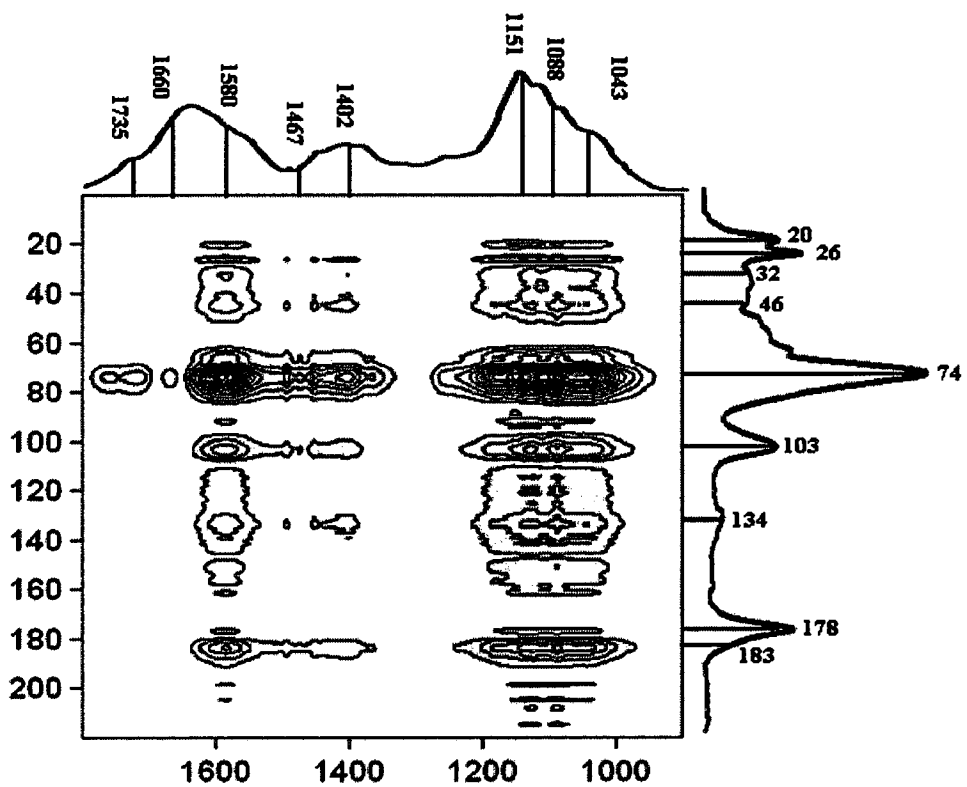

Fig. 3.12. The synchronous contour map of the two dimension hetero- spectral correlation analysis of FTIR and ^{13}C-NMR

3.6. Heteropolysaccharides (HPS)

As the band at 74 ppm represents carbohydrate ring structure (HC-OH) and is the most intense band in the ^{13}C-NMR, it may be a prefect tracer to investigate chemical structures correlated with it. By using a slice of the synchronous map where I keep the entire ^{13}C-NMR spectra on one side and use only the region around the band at 74 ppm on the other side (see Fig. 3.13), I see that the band at 74 ppm has positive correlations with bands at 20, 26, 103 and 178 ppm, which are also the same bands I saw in the top part (positive side) of the PC-1 loading (Fig. 3.7). The 74 ppm band shows negative correlations with the bands at 32, 46, 132 and 183 ppm.

Comparing the upper part of the spectrum from the PC-1 loading in Fig. 3.7 with the previously proposed ^{13}C-NMR spectrum of the heteropolysaccharides (HPS) compounds (Hertkorn et al., 2006), shows the same features. My observation that the HPS component builds up toward the marine end member is not unexpected, especially as it appears to be the major component in the surface open ocean (Aluwihare et al., 1997; Aluwihare et al., 2002; Repeta et al., 2002). However, the difference in the correlation intensity of the HPS major bands (20, 26, 103 and 178 ppm) in synchronous and asynchronous maps indicates that HPS is not a single compound, but a mixture of compounds that have the same basic backbone structures but slightly different geochemical reactivities. This is consistent with what I know about heteropolysaccharides in general, which may be found in many different compound groups (e.g.lipopolysaccharide, peptidoglycan etc.). I will discuss this further in the next section.

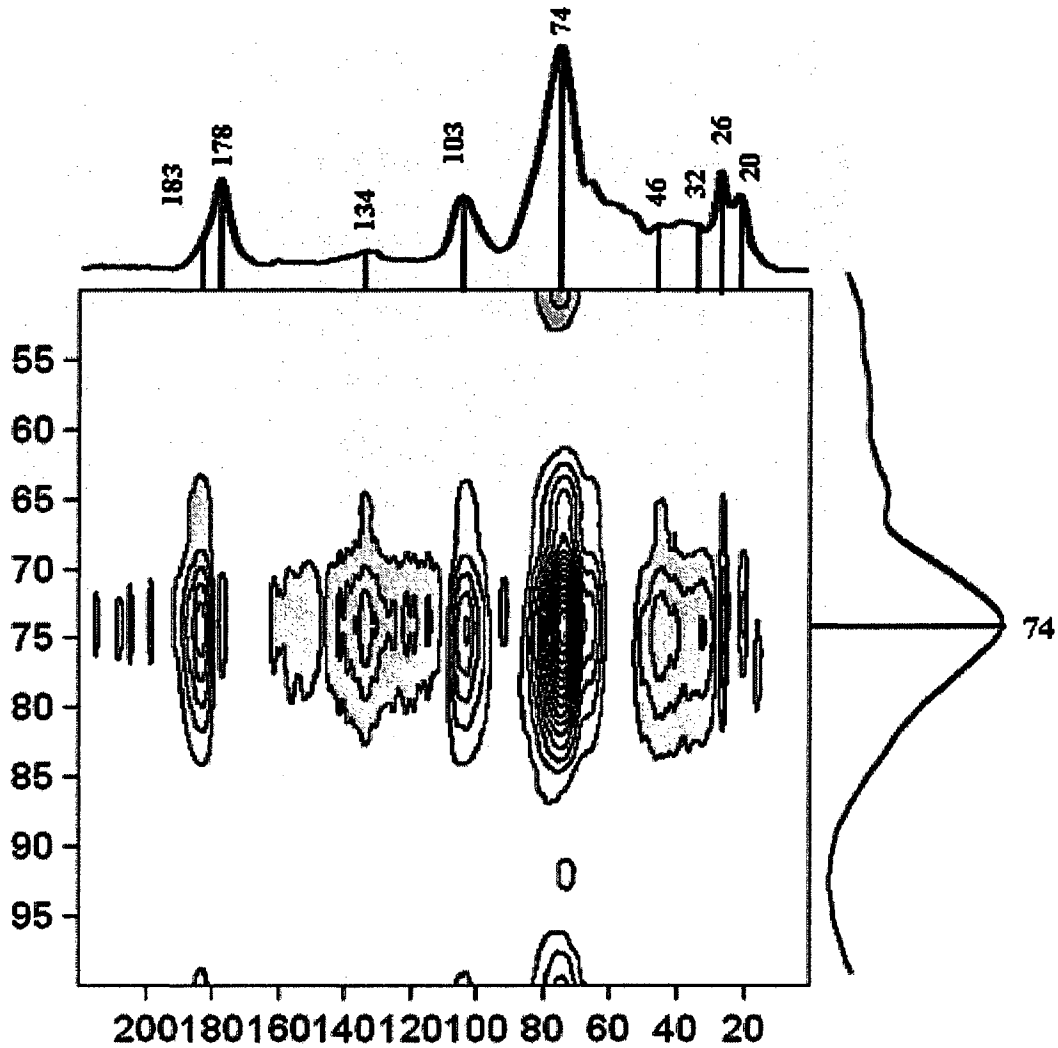

Fig. 3.13. A slice of the synchronous contour map generated from all the ^{13}C-NMR (n=24) shows the synchronous correlation between the band centered at 74 ppm (on the side) and the entire ^{13}C-NMR chemical shift (0-220 ppm) on the top.

3.7. Carboxylic-rich compounds (CRC)

To investigate the chemical structure of the carboxylic rich compounds (CRC), I focused upon the correlations between the band at 183 ppm, indicating the carboxylic functional group, and the other ^{13}C-NMR bands by taking a slice of both synchronous and asynchronous maps where the entire ^{13}C-NMR spectrum is in one side and the bands bracketing and including 183 ppm are on the other side. The synchronous slice map (Fig. 3.14a) shows a positive correlation between the band at 183 ppm and bands at 32, 46 and 132 ppm. However, the asynchronous slice map (Fig. 3.14b) shows no correlation (no cross peak) between the band at 183 ppm and the band at 32 ppm which indicates that both of these bands are originally in phase with each other. The band at 32 ppm is where it expected to see the signal of an α-carbon in carboxylic compounds (Jacobsen, 2007). That there is an in-phase correlation between 183 ppm and 32 ppm makes sense because whatever happens to the carboxylic group during the transformation in the estuary should be reflected in the 32 ppm band. For example, if the carboxylic group has been decarboxylated, the band originally at 32 ppm will exhibit a lower chemical shift. If the carboxylic group has become adsorbed to a particle; the 32 ppm band will disappear.

Based on the above 2D correlation and the negative PC-1 loading spectrum (Fig. 3.7), the chemical structures of the carboxylic rich compounds (CRC) looks very similar to the proposed ^{13}C-NMR spectrum carboxylic-rich alicyclic molecules (CRAM) (Hertkorn et al., 2006). However, there is not enough evidence to determine the alicyclic nature of these compounds, so I only identify them as carboxylic rich compounds.

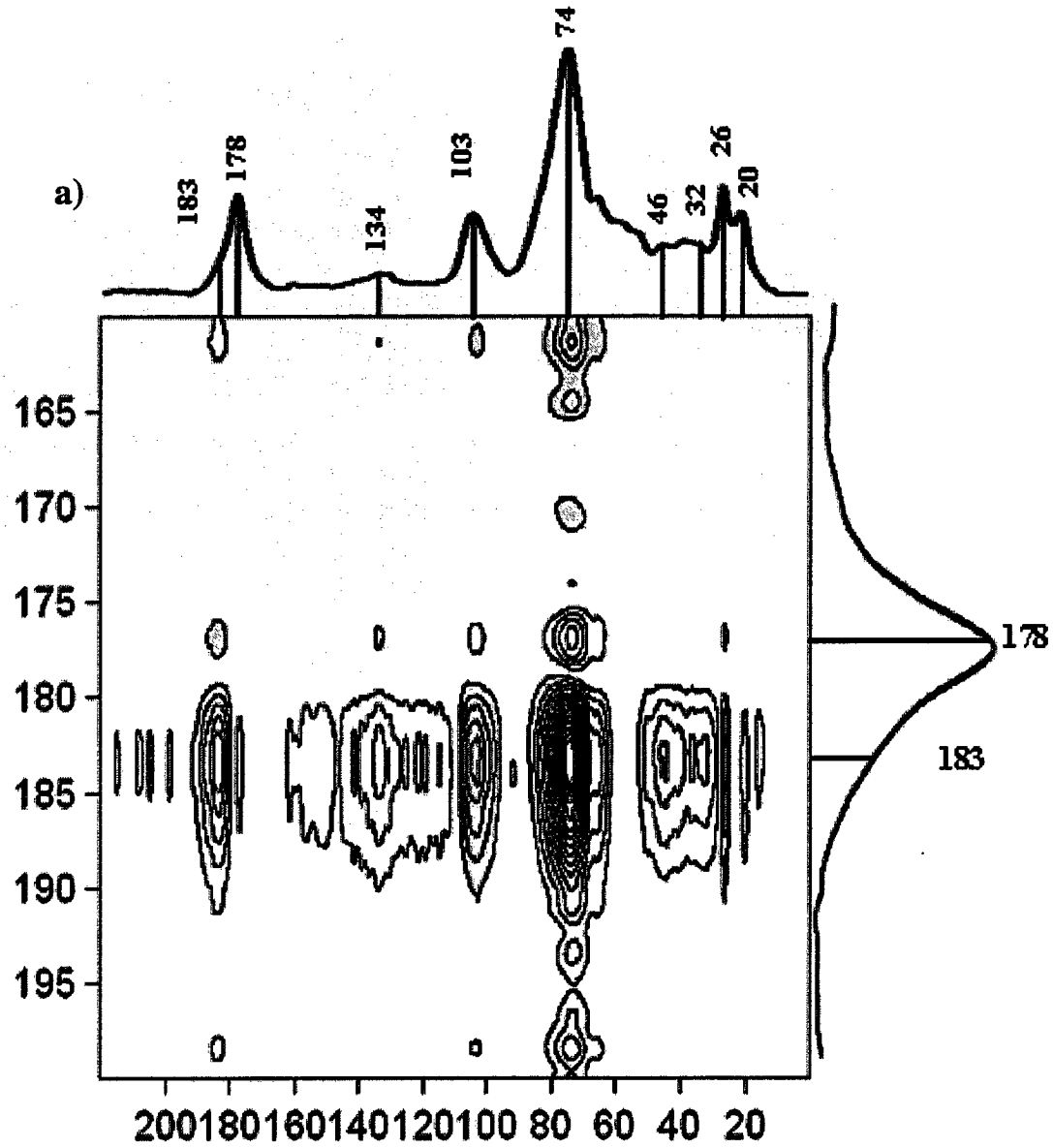

Fig. 3.14. a) Slice of the synchronous contour map showing the synchronous correlation between the band centered at 178 ppm (on the side) and the entire ^{13}C-NMR chemical shift (0-220 ppm) on the top. b) The asynchronous contour map showing the asynchronous correlation between the band centered at 178 ppm (on the side) and the entire ^{13}C-NMR chemical shift (0-220 ppm) on the top.

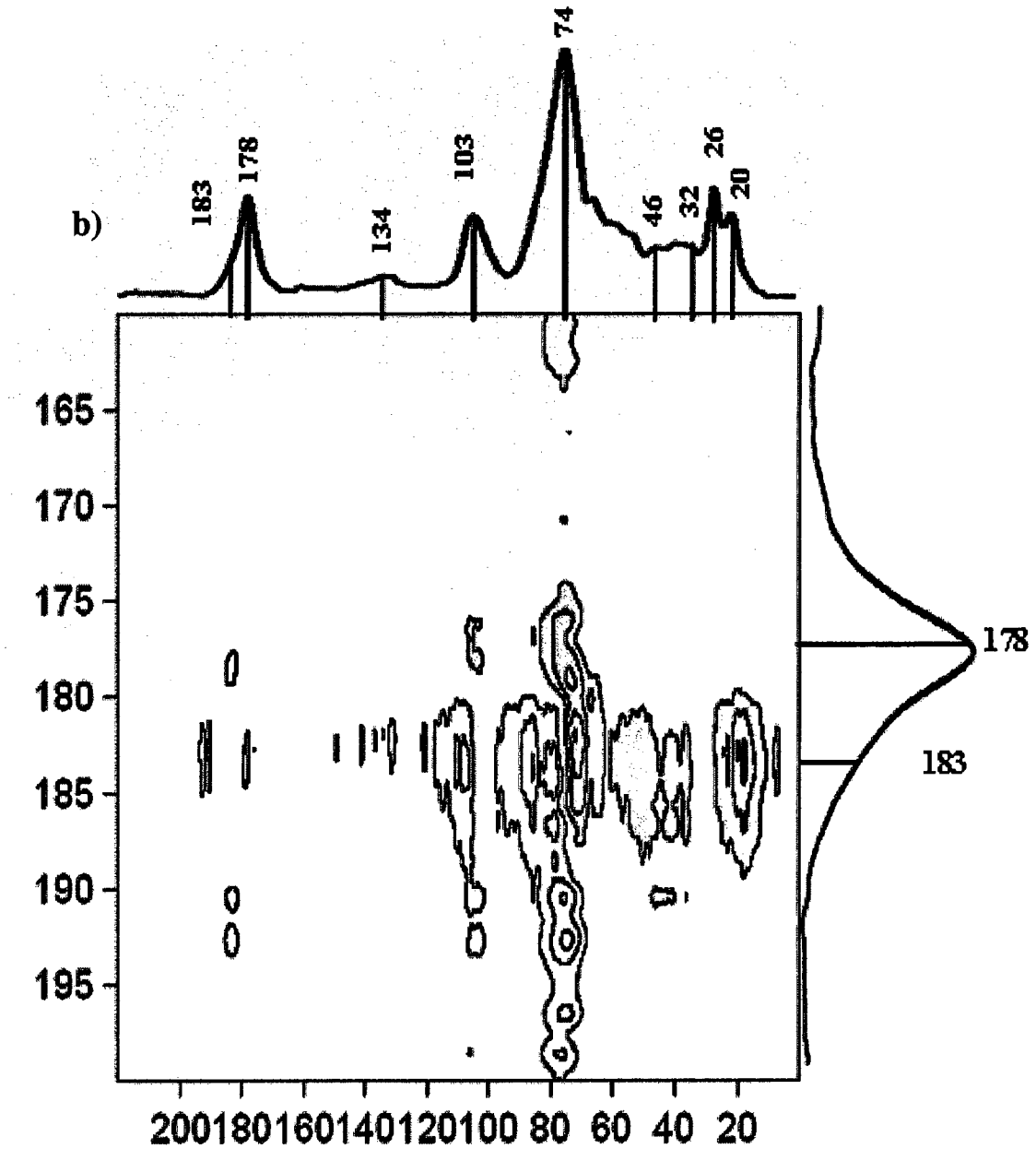

Fig. 3.14. Continued.

Supporting the hypothesis that at least some of the CRC are CRAM, Sleighter and Hatcher (2008) also identify carboxylic-rich compounds from FT-ICR-MS on C_{18} extracts of DOM isolated from the same water collected during November 2006 (1106) from Dismal Swamp to the Offshore site, where they match the proposed structure of the CRAM structures proposed by Hertkorn and co-workers (2006).

3.8. Quantification of the heteropolysaccharide *(HPS), carboxylic rich compound (CRC) and amide/amino sugar (AMS) components using FTIR and ^{13}C-NMR*

From the above discussion of the 2D correlation, I modified the integration of the ^{13}C-NMR used by Dria and co-workers (2002) to an integration that reflects the difference in the biogeochemical reactivity of each of the ^{13}C-NMR regions based on the synchronous maps of the ^{13}C-NMR data. Instead of the traditional integration, I therefore divide the ^{13}C-NMR spectrum into ten regions: $^{1}CH_x$ (0- 29 ppm), $^{2}CH_x$ (29- 40 ppm), $^{1}CH_3$-O (40- 55 ppm), $^{2}CH_3$-O (55- 62 ppm), HC-OH (62- 90 ppm), O-C-O (90- 115 ppm), C=C/ Ar (115- 140 ppm), Ar-O (140-160 ppm), COO/CON (160-190 ppm) and the aldehyde and ketone region (190- 220 ppm). To deconvolute the carboxylic, ester, and amide components of the COO/CON region (160-190 ppm), I couple the ^{13}C-NMR data with the ratio of component area calculated by FTIR as described in my previous work (Section II, this dissertation). In brief, the carbon percentages of the carboxylic acids, amides, and esters are estimated by multiplying the ratio of the area of functional group (as determined by FTIR) by the COO/CON relative area from the ^{13}C-NMR according to the following equation:

$$\%C_{individual} = (A_{individual} / A_{total.}) * \%C_{COO/CON} \qquad Eq.\ (3.4)$$

where $A_{individual}$ is the FTIR total area of either carboxylic acid, amide or ester, A_{total} is the total carbonyl area in FTIR and $\%C_{COO/CON}$ is the relative %C of carboxyl groups from ^{13}C-NMR.

The results of ^{13}C-NMR modified integrations with FTIR coupling are shown in Tables 3.3a-g. In general, I see an increase in the carbohydrate contents in each season as I move toward the marine end member, while the carboxylic carbon percentage decreases. The amide content was significant at estuarine/marine sites along the transect and has an average value of 7.36 ± 0.87 %C; the narrow range of the %C agrees with the small intensity of the autopeak at 178 ppm and 1660 cm^{-1} in the synchronous maps of ^{13}C-NMR and FTIR respectively.

From tables 3.3a-g and the PC-1 loading spectrum (Fig. 3.7), it is clear that, along the transect, there are three major components of the HMW-DOM that have different biogeochemical reactivates. One of them has high carbohydrate content and looks mainly like a suite of heteropolysaccharide (HPS)-rich compounds and its relative composition increases as I move toward the marine end member. The second looks like carboxylic rich compounds (CRC). The third component shows small changes which include the amide functional group (peak around 178 ppm) and part of the CH_3-O/CH_3-N region; I call it the amide/amino sugar component (AMS).

Table 3.3. The relative carbon percentage of HMW-DOM functional groups resulting from modified integration of the ^{13}C-NMR data and the relative carbon percentage of heteropolysaccharides (HPS), carboxyl-rich compounds (CRC) and the amide/amino sugar (AMS) components in the HMW-DOM of the seven seasons. a) November 2005 (1105) b) February 2006 (0206) c) May 2006 (0506) d) August 2006 (0806) e) November 2006 (1106) f) February 2007 (0207) and g) May 2007 (0507).

a) 1105

NMR region	$^1CH_{x1}$	$^2CH_{x1}$	$^1CH_3O$	$^2CH_3O$	HCOH	OCO	C=C/ Ar-C	Ar-O		†COO/CON		C=O	CRC	HPS	AMS
Site	0-29	29-40	40-55	55-62	62-90	90-115	115-140	140-160	Acid	Ester	amide	190-220			
GB	Sample get lost before ^{13}C-NMR analysis														
TP	7.29	7.29	11.37	5.22	27.68	10.35	9.03	5.39	3.54	0.38	9.56	2.91	39.53	45.32	15.15
CBB	8.72	6.22	8.44	4.52	39.22	13.73	4.85	2.06	1.27	0.57	8.40	2.01	24.85	61.67	13.48
OSC	9.74	5.84	7.48	4.53	42.74	13.37	3.10	1.67	0.90	0.55	8.03	2.05	21.03	65.86	13.11

† The carbon percentage of the acid, ester and amide was calculated by coupling FTIR with ^{13}C-NMR (see the text for the details)

Table 3.3. Continued.

b) 0206

NMR region	$^1CH_{x1}$	$^2CH_{x1}$	$^1CH_3O$	$^2CH_3O$	HCOH	OCO	C=O/ Ar-C	Ar-O	Acid	†COO/CON Ester	amide	C=O	CRC	HPS	AMS
Site	0-29	29-40	40-55	55-62	62-90	90-115	115-140	140-160		160-190		190-220			
GB	12.63	8.35	11.35	5.03	28.68	7.70	7.26	3.53	3.93	1.22	7.41	2.91	37.33	49.01	13.66
TP	14.80	7.54	10.57	5.16	29.77	8.54	6.30	3.29	3.26	0.73	8.11	1.93	32.89	53.11	14.00
CBB	10.83	5.18	7.41	5.71	43.87	11.95	2.35	1.60	1.74	0.41	7.20	1.75	20.03	66.65	13.32
OSC	Samples were not collected														

Table 3.3. Continued.

c) 0506

NMR region	$^1CH_{x1}$	$^2CH_{x1}$	$^1CH_3O$	$^2CH_3O$	HCCH	OCO	C=C/ Ar-C	Ar-O	Acid	^{t}COOCON Ester	amide	C=O	CRC	HPS	AMS
Site	0-29	29-40	40-55	55-62	62-90	90-115	115-140	140-160		160-190		190-220			
GB	10.31	7.81	10.32	4.86	32.98	9.70	6.81	3.29	3.27	2.02	7.28	1.36	32.85	52.99	14.15
TP	10.24	6.25	9.01	5.84	40.04	10.55	3.99	2.46	2.33	0.78	7.53	0.97	25.02	60.83	14.15
OBB	10.60	4.11	6.06	5.06	46.03	13.27	2.37	1.42	1.48	0.59	7.54	1.47	16.91	69.90	13.19
OSC	11.05	4.27	6.00	5.87	48.07	12.36	1.20	0.98	0.09	0.38	8.01	1.73	14.27	71.48	14.25

Table 3.3. Continued.

d) 806

NMR region	$^{1}CH_{x1}$	$^{2}CH_{x1}$	$^{1}CH_{3}O$	$^{2}CH_{3}O$	HCCH	OCO	C=C/ Ar-C	Ar-O	†COOH/CON			C=O	CRC	HPS	AMS
Site	0-29	29-40	40-55	55-62	62-90	90-115	115-140	140-160	Acid	Ester	amide	190-220			
GB	11.48	7.88	8.46	5.72	36.24	9.01	5.21	2.5	4.17	1.79	5.57	1.97	30.19	56.73	13.08
TP	12.93	4.70	7.24	5.46	41.88	11.29	3.42	1.53	2.03	0.73	6.13	2.68	21.59	66.10	12.31
OBB	11.84	4.26	6.16	5.68	50.80	12.11	0.39	0.11	0.82	0.57	7.25	0.00	11.75	74.75	13.50
OSC	9.63	4.33	5.04	4.34	50.66	13.72	2.21	0.62	0.43	0.45	7.29	1.25	13.89	74.02	12.09

Table 3.3. Continued.

e) 1106

NMR region	$^1CH_{x1}$	$^2CH_{x1}$	$^1CH_3O$	$^2CH_3O$	HCCH	OCO	C=O/ Ar-C	Ar-O		^{t}COOCON		C=O	CRC	HPS	AMS
Site	0-29	29-40	40-55	55-62	62-90	90-115	115-140	140-160	Acid	Ester	amide	190-220			
GB	9.66	7.18	10.24	5.31	31.35	9.53	6.54	3.79	4.02	1.36	7.29	3.74	35.51	50.54	13.96
TP	8.32	5.41	7.39	4.56	35.73	14.15	8.07	4.58	3.42	0.78	7.15	0.42	29.30	58.21	12.49
OBB	10.55	5.21	7.02	5.41	45.90	12.40	2.77	1.29	1.43	0.90	6.59	0.53	18.26	68.85	12.89
OSC	10.01	5.09	6.21	4.96	50.04	13.51	1.80	0.03	1.05	0.54	6.76	0.00	14.18	73.56	12.27

Table 3.3. Continued.

f) 0207

NMR region	$^1CH_{x1}$	$^2CH_{x1}$	$^1CH_3O$	$^2CH_3O$	HCCH	OCO	C=O/ Ar-C	Ar-O	Acid	†COO/CON Ester	amide	C=O	CRC	HPS	AMS
Site	0-29	29-40	40-55	55-62	62-90	90-115	115-140	140-160		160-190		190-220			
GB	9.16	6.77	9.78	5.29	31.16	11.58	8.90	5.54	3.31	1.15	7.18	0.18	34.48	51.90	13.63
TP	13.65	6.68	8.82	5.13	34.66	10.28	5.75	2.91	2.59	1.05	6.86	1.61	28.36	58.59	13.05
CBB	8.62	4.60	5.22	4.67	44.51	14.95	4.22	2.27	1.67	0.84	6.66	1.77	19.75	68.07	12.17
OSC	Samples were not collected														

Table 3.3. Continued.

g) 0507

NMR region	$^1CH_{x1}$	$^2CH_{x1}$	$^1CH_3O$	$^2CH_3O$	HCOH	OCO	C=O/ Ar-C	Ar-O	Acid	^{t}COO/CON Ester	amide	C=O	ORC	HPS	AMS
Site	0-29	29-40	40-55	55-62	62-90	90-115	115-140	140-160		160-190		190-220			
GB	4.47	5.23	7.53	4.47	26.32	14.57	11.49	7.46	3.65	1.02	8.96	4.83	40.19	45.36	14.45
TP	12.48	6.88	9.28	6.02	38.63	9.78	3.50	1.59	2.59	0.66	8.05	0.54	24.38	60.89	14.72
OBB	9.46	4.58	6.09	5.29	48.20	12.60	1.51	1.74	1.23	1.09	6.38	1.83	16.98	70.26	12.76
OSC	Samples were not collected														

I classify the integration regions into three groups based on their cross peak correlation in the ^{13}C-NMR synchronous map (Fig. 3.9). The first group appears to be mostly heteropolysaccharides (HPS). It includes the following regions: $^{1}CH_x$ (0-29 ppm), HC-OH (62-90 ppm), O-C-O (90-115 ppm).The second group contains the carboxylic-rich compound signature (CRC). I consider it the sum of the integrations of following regions: $^{2}CH_x$ (29-40 ppm), $^{1}CH_3$-O (40-55 ppm), C=C/Ar (115-140 ppm), Ar-O (140-160 ppm), the aldehyde and ketone region (190-220 ppm); the carbon percentage of the carboxylic content is calculated from coupling ^{13}C-NMR and FTIR. The third group contains major functional groups of the amide/amino sugar (AMS) component including the amide and ester carbon percent as estimated from coupling of ^{13}C-NMR and FTIR, in addition to the region of $^{2}CH_3$-O (55-62 ppm).

This classification is an oversimplification, as there will be some overlap in the integration regions. For example, the region $^{1}CH_x$ between 0-29 ppm is assigned to HPS though it is likely to have some contribution from the carbon in the component of the CRC, as shown in the proposed CRAM ^{13}C-NMR by Hertkorn and co-workers (2006). A further indication that this is an oversimplification is that the lower part of the region (0-29 ppm) appears in the negative portion of the PC-1 loading while the upper part shows in positive PC-1. In addition, aromatic compounds like lignin could lead to an overestimation of the CRC contribution. If I account all the integration of the region between the 115-160 ppm to aromatic compounds, it is 28 ± 10% of the total CRC contents; however there are significant contributions of the carbon double bond (C=C) of the unsaturated components of CRC to that region (Hertkorn et al., 2006). In addition, quantifying the amide/amino sugar compound based on the carbon percentage of the

amide functional group and the $^{2}CH_3$-O (55-62 ppm) could underestimate the amount AMS compounds, as these two regions represent only two carbon types of the amide/amino sugar compounds, while the rest of the carbon types could be included in the heteropolysaccharides component (e.g. N-acetyl amino polysaccharides).

In my simplified scheme, the total contribution of the heteropolysaccharides (HPS) in the HMW-DOM (Table 3.3a-g) shows a wide range from 45.32 – 74.75%. The percentages increase as I move toward the marine end member. In general, all sites present their lowest percentages in the winter seasons (0206 and 0207) and their highest during the summer season (0806). Conversely, the carboxylic rich compounds (CRC) shows a range from 11.75 to 40.19% with the highest values during the winter and fall seasons (0206 and 0207) and the lowest percentage in the summer season (0806). This is in agreement with the $\delta^{13}C$ data that show more declined slope in the summer (0806) than winter season (0206, 0207), which indicate probably a higher primary production and photooxidation during the summer season relative to the winter seasons (Harvey and Mannino, 2001; Pennock and Sharp, 1986). In contrast, the amide/amino sugar (AMS) component was within narrow range (12.09 to 15.15%)

When I plot the percentage of heteropolysaccharides (HPS), carboxyl-rich compounds (CRC) and amide/amino sugar (AMS) components from all the sites during the seven seasons against their salinity values (Fig. 3.15) I see that the percentage of the HPS and CRC components are a mirror image of each other. Looking at the HPS and CRC components in Fig. 3.15, I notice a small change below salinity 20 but significant changes after salinity 20 with stabilization after salinity of 25. This change is consistent with the salinity plots of the $\delta^{13}C$ and C/N ratio; all of the evidence indicates that there

are dramatic changes in DOM chemical compositions as I pass the salinity of 20 due most likely to introducing marine autochthonous DOM sources either from onsite primary production or through the complex sub-estuarine systems in the area.

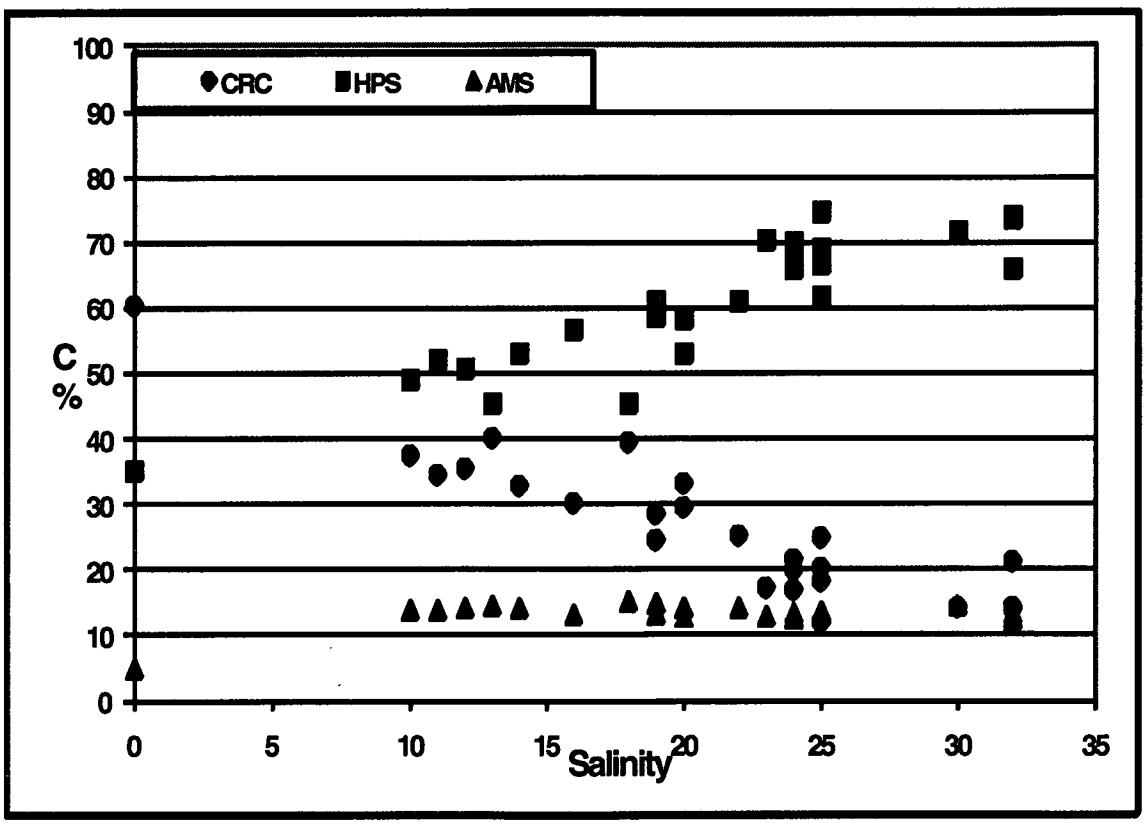

Fig. 3.15. The plot of the carbon percentage of the heteropolysaccharides (HPS)(■), carboxyl-rich compounds (CRC)(●) and amide/amino sugar (AMS) (▲) components in the HMW-DOM as calculated from the modified integration of the ^{13}C-NMR against the salinity of their samples.

The amide/amino sugar (AMS) component, in contrast to the other two components, shows a significant and little changing percentage of HMW-DOC content (average of 13.41 ± 0.84%) along the entire salinity range (from GB to OSC), which could indicate the important role of heterotrophic bacteria in altering the DOM throughout the transect, as they could contribute ~ 50% of the DON to marine environment (Kaiser and Benner, 2008). However, the constant percentage of the AMS amount along the transect from Great Bridge (GB) to Offshore site (OSC) regardless of the season was unexpected and needs further investigation. Are the AMS compounds (or a significant proportion of them) refractory or are their sinks and sources in steady state relative to the HPS and CRC?

When I take a further look into the ratio of NMR signals within HPS components (Tables 3a-g), I notice that the ratio of the carbon percentage of HC-OH (the major functional group in HPS) to the total HPS carbon shows a constant ratio of (1: 2) through all the sites during all the seasons, this confirms that the HPS component consists of compounds that have very similar backbones of carbohydrate-like structures, however the ratio between the aliphatic ($^{1}CH_x$ 0-29 ppm) carbon percentage of the HPS component to the total HPS carbon shows a wide ratio range (1:4 to 1:10), this could highlight the variation between individual compounds within the HPS, where some compounds could have higher aliphatic functional groups than other compounds but both of them have the same backbone carbohydrate structures e.g. glucose versus 3-O-methylglucose, which is in agreement with the previous studies that show availabilities of natural, methyl-and 6-deoxy sugars in the HMW-DOM isolated from open ocean (Panagiotopoulos et al., 2007, Quan and Repeta 2007). This hetero HPS concept is further supported by the combination

of both ^{13}C-NMR synchronous and asynchronous maps, where if HPS consisted of compounds having exactly the same structures, the major functional group of HPS would be exactly in phase with each other (they would increase within the same ratio) and I would not see any correlation in the asynchronous maps. However, the asynchronous map (Fig. 3.10) shows many out-of-phase correlations between the HSP major functional groups, indicating the complexity (multi-compound nature) of this component.

I then applied the same modified integration to the previously reported ^{13}C-NMR spectra of HMW-DOM from the Dismal Swamp isolated on August 2007 (Section II, this thesis), as Dismal Swamp DOM represents one of the major terrestrial DOM sources to my transect. In DS, the carbon percentage of the CRC in the HMW was 60.31% while the HPS was only 34.69%, and the AMS was 5%. When I calculate the ratio of carboxylic acid to the total CRC carbon in the Dismal Swamp it shows a ratio of 1 (carboxylic-carbon): 3 (CRC-carbon) this ratio is in the middle of the reported range of carboxylic –carbon to aliphatic carbon in the CRAM compounds (1:2 to 1:7) proposed by Hertkorn and co-workers (2006). Calculating the carbon-percentage ratio for the carboxylic acid relative to the total CRC of the estuarine and coastal HMW-DOM samples in this study shows a wide ratio range 1:7-1:32. The ratio increases as I move toward the marine end member, which could indicate a faster removal of the carboxylic acid functional group relative to its counter-part functional groups within the CRC component.

My data are consistent with the previous work done by Repeta and co-workers (Aluwihare et al., 2002; Repeta et al., 2002), where they identify two major components of HMW-DOM along the Mid-Atlantic Bight using ^{1}H-NMR. The first component was

the HPS components (which they called acyl polysaccharide APS) which accounts for 50 -80% of the HMW carbon with the highest percentage found in fully marine DOM. The other HMW-DOM component was more abundant in the DOM isolated from estuarine and deep ocean DOM and looks like humic substances. However the work done recently by Hertkorn and co-workers (2006) illustrate that the deep water humic substances are mostly carboxyl-rich compounds. In this work, I show that CRC compounds are also present in estuaries and could potentially come from terrestrial sources. However, unlike Hertkorn and co-workers (2006), I show that carboxylic rich compounds are biogeochemically reactive and not refractory, which raises many questions about the geochemical cycle of carboxylic rich compounds and their sources and sinks.

All this guides me to believe that, although HPS and CRC are present in many aquatic environments at different relative ratios, these components are not each composed of compounds that have the same exact chemical structures from location to location but are instead dynamic mixtures of compounds that share similar backbone structures with significant functional group differences.

4. CONCLUSIONS

From both C/N and $\delta^{13}C$, I notice that the transformation of the HMW-DOM through my transect passes through three regions based on the salinity of the samples: the first is the Dismal Swamp region at salinity of zero, which has a seasonal average C/N ratio of 52.33 and $\delta^{13}C$ seasonal average value of (-27.24‰) which both are typical signals for C3 vascular-plant DOM sources; the second region after salinity of zero until salinity of 20, which has an average values of 20.85 and -26.22‰ for C/N ratio and $\delta^{13}C$

respectively. The third region, from salinity 20 to 32, is characterized by average values of 11.84 and -23.31‰ for the C/N atomic ratio and $\delta^{13}C$, respectively. This indicates a dramatic shift in the relative importance of the processes affecting the HMW-DOM throughout the transect. Flocculation and the effects of heterotrophic bacteria seem to be the major players in the lower salinity region, but at the higher salinity regions the introduction of new carbon sources by primary production seems to be the major process.

The dramatic transformation from heterotrophic to autotrophic sources is further supported by applying principal component analysis (PCA) and two dimensional correlation spectroscopy to the ^{13}C-NMR spectra of the HMW-DOM. Moreover, both PCA and 2D correlation demonstrate that the HMW-DOM in the transect consists of three major components having different biogeochemical reactivity where one component looks like heteropolysaccharides (HPS) and increases as I move to the marine end member, while the second component looks like carboxyl-rich compounds (CRC) and their carbon percentage decreases as I move away from the fresh water end member. The third component shows an almost constant carbon percentage along the salinity transect and it contains major functional groups of amide/amino sugar compounds (AMS).

The 2D-synchronous map from FTIR data also confirms the opposite correlation between the carboxylic and carbohydrate functional groups. Application of 2D hetero-spectral correlation between FTIR and ^{13}C-NMR data verifies my assignments of the carbohydrate and carboxylic bands.

It seems that the HPS and CRC are present in many aquatic environments at different relative ratios. The synchronous and asynchronous 2D correlation maps of both

^{13}C-NMR and FTIR reveals that each of these components is not composed from compounds that have exact chemical structures but from dynamic mixtures of compounds that share similar backbone structures but have significant functional group differences.

The combination of both PCA and 2-D correlation spectroscopy could be used as a powerful biogeochemical tool to track the changes in complex organic matter as a function of space, time, or environmental effects (such as photochemical or microbial degradation).

CHAPTER IV

UNDERSTANDING THE ENHANCED AQUEOUS SOLUBILITY OF STYRENE BY TERRESTRIAL DISSOLVED ORGANIC MATTER USING STABLE ISOTOPE MASS BALANCE AND FTIR

1. INTRODUCTION

Natural dissolved organic matter (DOM) is a quantitatively significant reactive component of the global carbon cycle (Hedges, 1992) whose chemistry and reactivity has been extensively studied. The increased identification of organic pollutants within natural waters has made it even more critical that we understand the interactions between natural DOM and anthropogenic organic compounds and the environmental fate of these compounds.

Many studies have attempted to quantify the chemical interactions between specific small-molecule (generally anthropogenic) compounds and natural organic matter by using simple equilibrium-phase partitioning (Schwarzenbach et al., 2003). However, it is difficult to clearly determine the extent of binding of the sorbate to the natural organic matter. For example, Carter and Suffet (1982) used dialysis to estimate concentrations of radiolabeled p,p'-DDT bound to dissolved humic substances. Using dialysis requires the assumption that sorbate molecules (p,p'-DDT) are bound only to high molecular weight DOM, which cannot cross the dialysis membrane. Dialysis is also limited in scope as it can only be applied to sorbate molecules smaller than the dialysis pore size (Hassett and

Milicic, 1985; Schwarzenbach et al., 2003). Hassett and Milicic (1985) proposed a gas purging technique to differentiate between free and bound analytes; however this technique is only valid for volatile and semi-volatile sorbate molecules. Other techniques, likewise, are restricted in use. Fluorescence quenching (Gauthier et al., 1986) is only applicable to compounds that absorb and fluoresce UV-visible light. Direct solid phase extraction (Landrum et al., 1984) is limited by changing interactions between the solid phase, the sorbent of interest, and the natural organic matter during the extraction procedure. I propose a more sensitive and universally applicable method to measure the extent of binding: the use of isotopically-labeled sorbate molecules and mass balance calculations.

The solubility enhancement approach described by Chiou et al. (1986) assumes a partition-like interaction between the natural DOM and organic analyte. This interaction is defined in Eq. (4.1),

$$S_w^* = S_w + XC_o \qquad \text{Eq. (4.1)}$$

where S_w^* is the apparent analyte solubility in water containing DOM at concentration X (in ppm), S_w is the analyte solubility in pure water, and C_o is the mass of analyte partitioned into DOM per unit mass of DOM. Using variables from Eq. (4.1) the partition coefficient (K) for analyte i between DOM and pure water can be shown as Eq. (4.2).

$$K_{iDOM} = C_o/S_w \qquad \text{Eq. (4.2)}$$

While this method only produces a partition coefficient K_{iDOM} value at saturation, in theory, it could be applicable to many types of compounds (Schwarzenbach et al., 2003).

The ability of DOM to interact with different types of organic compounds is primarily a function of its structural heterogeneity and hydrophobic and hydrophilic properties (Hassett, 2006). Variations in composition, chemical structure, polarity and

size of DOM isolated from different locations, have been related to variations in K_{iDOM} (or K_{iDOC}) (Chin et al., 1997; Chiou et al., 1987; Gauthier et al., 1987; Rutherford et al., 1992; Salloum et al., 2002). For example, an inverse correlation was observed between the polar group content in humic substances (measured by elemental analysis) and the solubility enhancement of such hydrophobic organic compounds as p,p'-DDT, 2,4,5,2',5'-PCB, benzene and carbon tetrachloride (Chiou et al., 1987; Rutherford et al., 1992).

While relationships between DOM structure and its reactivity (e.g., K_{iDOM}) have been identified, the major drawback of current solubility enhancement approaches is their inability to detect small changes in partitioning of organic compounds by DOM. To date, current methods have had limited applicability for: 1) low-DOM-concentration samples such as those found in estuarine and marine DOM (Rutherford et al., 1992) or 2) across spatial (e.g. down-estuary) and temporal (e.g. seasonal) scales as the natural DOM pool shifts in composition in response to mobility, source and sink variations. In addition, current studies have generally been limited to highly hydrophobic compounds that are expected to exhibit high solubility enhancement values. To use solubility enhancement as an effective probe of the reactivity of aquatic DOM, a more precise quantification method is required that can detect both very small partition values and small changes in incorporation values, and be capable of estimating the interactions of different probes with the same DOM.

Because the largest fraction of DOM is as of yet uncharacterizable (Benner, 2002), studying the reaction and interaction of DOM with other organic species is at best an analytical compromise between understanding chemical functionality and specific

chemical structure within DOM. In this work, I proposed to use the solubility enhancement of model organic compounds as a tracer for the chemical reactivity of DOM. I present a new high-precision technique to measure the solubility enhancement of model organic compounds in natural waters by utilizing isotopic mass balance (^{13}C). The isotopic measurements are made by interfacing a standard DOC analyzer with a stable isotope ratio monitoring system (St-Jean, 2003). To test the method, I applied it to address seasonal changes in the reactivity of DOM in sterile-filtered Dismal Swamp water (VA, USA) and its high and low molecular weight fractions (isolated by ultrafiltration), using ^{13}C-labeled styrene as a probe. Styrene was chosen because it is representative of simple aromatic compounds, has less hydrophobicity than organic compounds used in previous solubility enhancement studies, and is commercially readily available with a ^{13}C label. From an environmental prospective, the largest styrene producer in North America (Nova Chemical Corporations) is located locally on the Southern Branch of the Elizabeth River in Chesapeake (VA), for which the Dismal Swamp is the major source of terrestrial dissolved organic matter to the river. Any spill of styrene into the river system poses a significant threat to the local ecosystem and the southern-most Chesapeake Bay.

2. METHODS

2.1. Sampling

Surface water samples were collected using a clean polypropylene bucket in November 2005, February, May, August and November 2006 from Portsmouth Ditch in Great Dismal Swamp, Virginia, USA. The samples were transported to the laboratory in

pre-cleaned, fluorinated polypropylene jerricans. The sample was immediately sterile-filtered using cleaned and conditioned 0.1 μm Whatman Polycap cartridge filters. Two liters of sterile-filtered samples were frozen for a solubility experiment and further analysis.

2.2. Ultrafiltration

An ultrafiltration system equipped with a polysulfone 1KDa cartridge (Separation Engineering, Inc.) was used to separate both high and low molecular weight fractions (hereafter HMW and LMW respectively). The filtration system was cleaned and conditioned after Guo and Santschi (1996). The system was then conditioned with 4-5 L of actual, sterile-filtered (<0.1) natural-water sample, after which 20-40 L of sterile-filtered sample (SF) was concentrated through the system at pressures of approximately 207 kPa (30 psi). Two liters of the pooled filtrate (LMW, low molecular weight) were taken and frozen for solubility experiments and FTIR analysis. Both HMW (high molecular weight) and LMW fractions were sub-sampled for DOC mass balance; the retentate (HMW) was then diafiltrated with 5 L de-ionized water. The system was rinsed twice with 5 L de-ionized water to recover any HMW left in the system. The rinse retentates were added to the diafiltrated retentate, and the combined retentate was frozen and freeze dried. The HMW fraction was then re-dissolved in de-ionized water to its natural concentration as measured by DOC analyses and kept frozen.

2.3. Solubility experiments

The frozen subsamples from the SF, LMW and HMW fractions were allowed to thaw at room temperature in the dark overnight after which an equilibration experiment was conducted according to McAuliffe (1966) with slight modifications. In brief, two replicate subsamples (65 ml each) were placed in 100 ml narrow mouth amber brown glass bottles along with 65 μL of ^{13}C-labeled styrene ($\delta^{13}C_{PDB}$ = 297.2‰) which was prepared by diluting 99 atom % (styrene-2-^{13}C , ISOTEC) with 99.9% certified styrene (Fisher Scientific). The bottles were sealed with Teflon-lined polyethylene caps, placed on a Lab-line Model No. 3587 Multi-wrist shaker (Lab-Line instruments, Inc., Melrose Park, IL), and moderately shaken in the dark for 24 hours. Replicates of DI water samples were prepared in the same manner. After 24 hours, the bottles were removed from the shaker, placed upside down, and left undisturbed for 48 hours to establish the equilibrium. During the total 72 hours of shaking and equilibration, the air temperature was 19.67 ± 0.40 °C, measured every 10 min with HOBO temperature-light loggers (Onset Computer Corp., Bourne, MA). After the equilibration time, the bottles were left carefully in their upside-down position to avoid disturbing the styrene layer. Gently, 35 mL of each sample was withdrawn by a 10 mL hypodermic-needle disposable syringe (BD Medical Systems, Franklin Lakes, NJ) through the silicon septum, and placed in a 40 mL amber borosilicate glass vial with a PTFE resin/silicone septum and a polypropylene closure (I-Chem*, Fisher Scientific). Each vial was closed immediately after filling and samples were analyzed for DOC and $\delta^{13}C$ (see below) the same day.

2.4. DOC and $\delta^{13}C$ analysis

DOC concentrations and $\delta^{13}C$ values of both the natural and the styrene-equilibrated samples were measured using a standard dissolved organic carbon analyzer (Aurora 1030W TOC analyzer, College Station, TX) interfaced with a stable isotope ratio mass spectrometer (Europa, Model Geo 20-20, Cheshire, UK). Interfacing the two instruments merely required connecting the outflow from the near-IR detector on the DCO analyzer to the existing continuous flow inlet on the IRMS via 1/8" tubing. For each sample, duplicate vials were run in triplicate (n=6) using 2.5 ml of sample and 2 ml of 20% sodium persulfate as the wet-chemical oxidant (98%, Fisher Scientific). All stable carbon isotope values are expressed as ‰ (per mil) relative to PDB (Pee Dee Belemnite). Several in-house working standards (asparagine, -24.5‰; sucrose, -10.4‰; urea, -44.1‰) were used for [DOC] calibration and as well as a $\delta^{13}C$ check standards. The concentration of styrene in the equilibrated water sample was determined by using isotopic mass balances according to Eq. (4.3)

$$^{13}F_{TDOC} = {}^{13}F_{DOC} * (1-X_{Sty}) + {}^{13}F_{Sty} * X_{Sty} \qquad \text{Eq.(4.3)}$$

Where $^{13}F_{TDOC}$ is the fractional isotopic abundance of the total DOM in the equilibrated water sample, $^{13}F_{DOC}$ and $^{13}F_{Sty}$ are the fractional isotopic abundances of the initial DOM and of the labeled styrene, and X_{Sty} is the normalized molar abundance of carbon attributed to the styrene. The only unknown is X_{Sty} and all other quantities ($^{13}F_{TDOC}$, $^{13}F_{DOC}$ and $^{13}F_{Sty}$) were explicitly determined. X_{sty} was converted to concentration units by multiplying by the molar carbon concentration of the equilibrated water. The concentration of organic compound partitioned per molar unit of DOC (C_o) was

calculated by rearranging Eq. (4.1), with the appropriate unit conversions to allow [DOC] to replace X as

$$C_o = (S_w^* - S_w) / [DOC] \qquad \text{Eq.(4.4)}$$

2.5. FTIR spectra

Samples were introduced as KBr discs with (1:100) dilution; the KBr was previously dried in an oven for two hours at 105 °C. To make the disks, the sample plus KBr mixture was crushed and homogenized. A subsample was then compressed between two clean, polished iron anvils in a hydraulic press at 20,000 psi to form a KBr window. To minimize wedging effects (Hirschfeld, 1979), the discs were pressed for a second time after they had been rotated 90° before removal from the hydrolic press. FTIR spectra were obtained by collecting 200 scans with a Nicolet 370 FTIR spectrometer (DTGS detector and KBr beam splitter) equipped with Purge Gas Generator unit. Spectra were collected using a resolution of 4 cm^{-1} and Happ-Genzel apodization. To guard against CO_2 contamination from lab air, a 4-min lag-time between closing the analytical chamber and starting the analysis was implemented. The FTIR spectra were converted into absorbance units, and normalized by summed absorbance from 4000-500 cm^{-1} prior to principal component analysis (PCA) using in-house MATLAB code.

3. RESULTS AND DISCUSSION

Over five seasons, the pH of Dismal Swamp water samples ranged from 3.13 to 3.30. The DOC concentration in sterile-filtered water (SF) varied by a factor of two (5,784 to 11,790 μM-C) with the highest concentration in August 2006. The

concentration of DOC within HWM and LMW DOM ranged from 2,556 to 6,120 μM-C and 3,164 to 6,495 μM-C respectively (Table 4.1). The percent recovery of HMW DOC ranged from 44 to 54% with total recovery between 94 to 103% (based upon DOC measurements of SF, HMW and LMW aliquots of the same samples).

Table 4.1. DOC concentrations of the samples used in the solubility experiments: SF, sterile-filtered water; HMW, high molecular weight samples; LMW, low molecular weight samples.

NO.	Sample	SF	HMW		LMW
		DOC μM-C	†DOC μM-C	*Recovery %	DOC μM-C
1	Nov. 2005	8810 ± 380	4150 ± 50	50	4210 ± 40
2	Feb. 2006	7140 ± 230	5150 ± 40	54	3510 ± 100
3	May 2006	5780 ± 240	2560 ± 30	44	3160± 90
4	Aug. 2006	11790 ± 100	6120 ± 70	49	5300 ± 300
5	Nov. 2006	11340 ± 230	3240 ± 120	46	6500 ± 20

† These are the measured DOC concentrations of the re-dissolved, freeze-dried retentate.

*The HMW recovery based on DOC measurements of the retentate recovered from the ultrafiltration system and the initial SF sample, as well as the concentration factor.

3.1. Solubility enhancement

To examine the potential significance of isotope fractionation of styrene during equilibration and phase changes, I performed a solubility experiment for a range of DOC concentrations (3000-7500 μM-C) using the same DOM (HMW-August 2006) and adding the same amount of labeled styrene. The calculated C_o was the same (within the standard deviation) at all DOM concentrations, suggesting that isotope fractionation is not statistically significant (data not shown) and therefore does not interfere with my determinations of solubility enhancement via stable-isotope measurements.

As expected, the $\delta^{13}C$ values of sterile-filtered water samples equilibrated with ^{13}C-labeled styrene showed significant isotopic enrichment compared to natural DOM $\delta^{13}C$ values (Table 4.2). Duplicate, equilibrated water samples (analyzed in triplicate) show low variability with relative standard deviations (RSD) ranging between 1.2 to 2.0%. The equilibrated waters showed significant S_w^* values in the presence of Dismal Swamp DOM, with solubility enhancements of 52 to 118% relative to solubility in the DI (Fig. 4.1). The amount of solubility enhancement varied with season, with November samples showing the highest enhancement (2,517 ± 54 μM-sty for November 2005 and 1,965 ± 23 μM-sty for November 2006) and August 2006 the lowest.

Table 4.2. The $\delta^{13}C$ values (‰, PDB) for sterile filtered (SF), high molecular weight (HMW) and low molecular weight (LMW) DOM fractions from natural water samples and the same fractions from ^{13}C-labeled styrene equilibrated water.

	SF		HMW		LMW	
	Natural ^{13}C	Equilibrated	Natural ^{13}C	Equilibrated	Natural ^{13}C	Equilibrated
Nov. 2005	-28.4 ± 0.1	203 ± 3	-27.5± 0.10	250 ± 8	-29.0 ± 0.4	224 ± 3
Feb. 2006	-27.2 ± 0.3	190 ± 2	-27.4 ± 0.17	213 ± 6	-27.3 ± 0.2	206 ± 6
May-2006	-29.5 ± 0.3	203 ± 3	-27.4 ± 0.26	259 ± 2	-30.9 ± 0.5	187 ± 1
Aug. 2006	-31.8 ± 0.4	147 ± 7	-27.2 ± 0.01	176 ± 3	-32.5 ± 0.1	202 ± 2
Nov.2006	-27.2 ± 0.0	241 ± 1	-27.3 ± 0.12	186 ± 4	-26.8 ± 0.2	221 ± 4

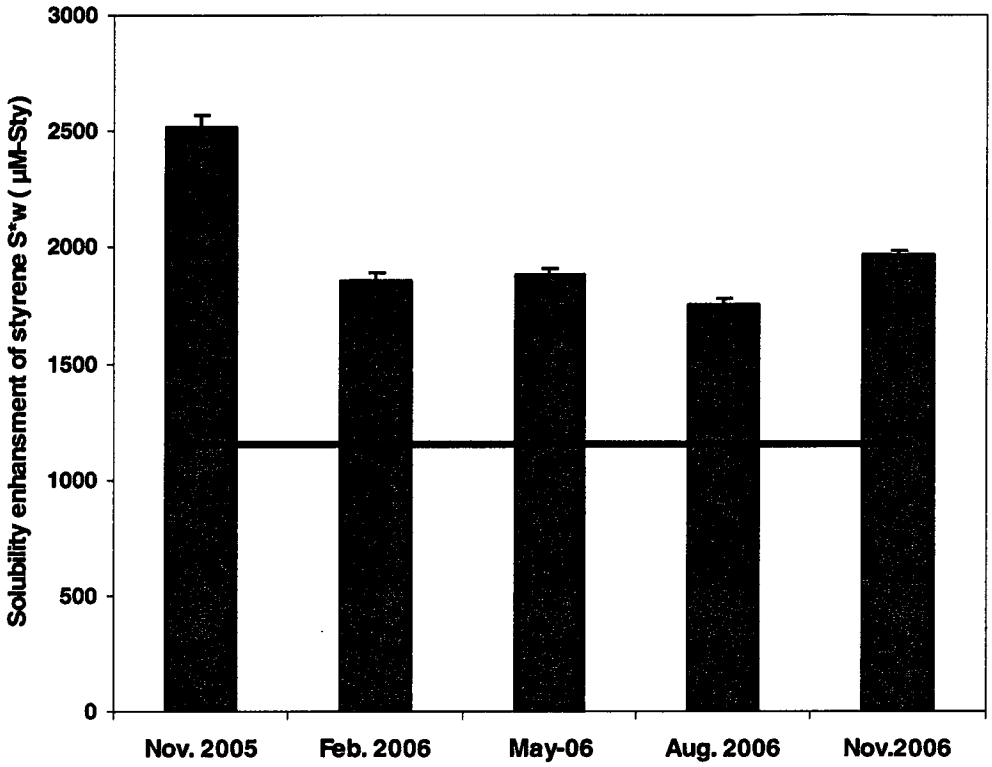

Fig. 4.1. The apparent solubility of styrene (S_w^*) in equilibrated sterile-filtered water (SF) from Dismal Swamp at different seasons as calculated by isotopic mass balance. The solid line represents the solubility of styrene in the de-ionized water (S_w). Error bars are standard deviations from triplicate analyses of duplicate sample vials (n=6).

When solubility enhancement is normalized to DOC concentration by calculating C_o (from Eq. 3), a different seasonal pattern emerges from the SF samples. November 2005 DOM showed the highest reactivity toward styrene with 0.154 ± 0.010 µM-sty/µM-DOC; May 2006 showed the next highest reactivity (0.125 ± 0.010 µM-sty/µM-

DOC), followed by, in order of decreasing reactivity, February 2006, November 2006, and August 2006 (Fig. 4.2).

Inorganic salts in the Dismal Swamp are unlikely to cause these differences in S_w^* and Co. Based on the calculation of major ion concentrations measured at different sites in the Dismal Swamp, the maximum ionic strength is $2.8x10^{-4}$ M (Johannessona et al., 2004). Therefore the "salting-out effect" of this concentration on styrene solubility is negligible (Miller, 2001) .

As with the sterile-filtered samples, high molecular weight DOM fractions enhanced the solubility of styrene, with percentage enhancements of 35 to 85% relative to de-ionized water. The RSD of S_w^* within the same sampling event was 1.3 ± 0.4%, similar to the range seen in the SF samples. The C_o values for the HMW fractions are greater than for corresponding SF samples and show a different order of reactivity among the seasons sampled (Fig. 4.2). In the HMW samples, May 2006 has the highest reactivity toward styrene (0.351 ± 0.020 μM-sty/μM-DOC) and Aug. 2006 has the lowest (0.066 ± 0.008 μM-sty/μM-DOC).

The solubility enhancement of styrene by low-molecular weight DOM ranged from 23 to 75% with RSD values in the range of 1.2 ± 0.4%. With the possible exception of the August 2006 LMW sample, the seasonal changes in C_o (Fig. 4.2) are more similar (in magnitude and relationship among seasonal samples) to the total DOM (SF) samples than to the HMW fractions.

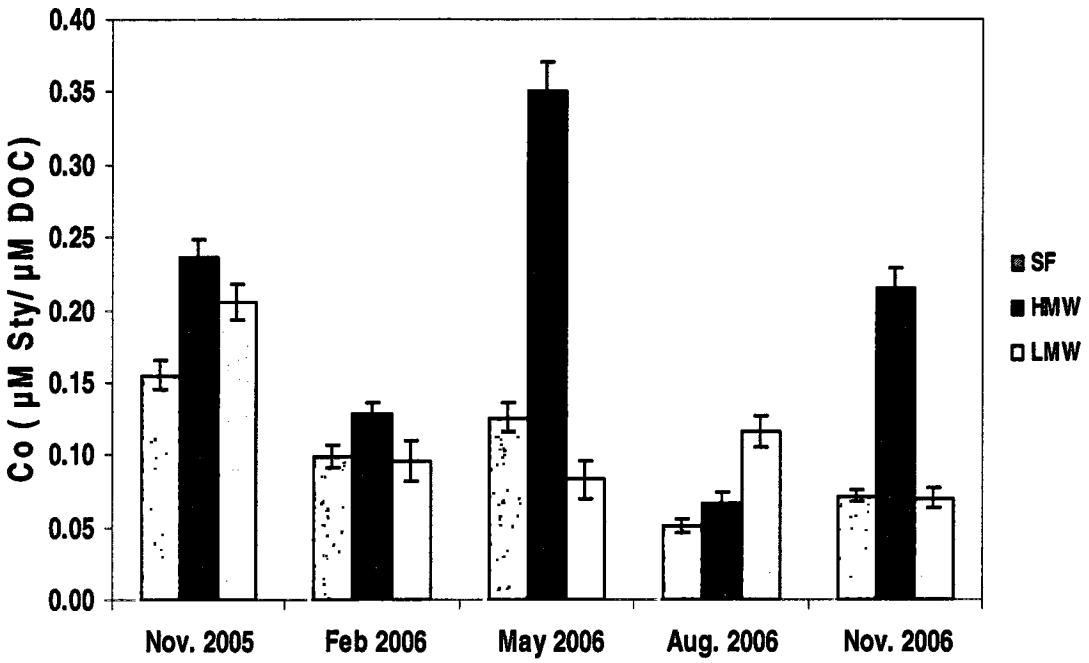

Fig. 4.2. Styrene solubility in sterile filtered water (SF), high molecular weight (HMW) and low molecular weight (LMW) normalized per unit DOC at different seasons as calculated by isotopic mass balance. Error bars represent the standard deviation of triplicate measurements from duplicate vials (n=6).

My isotopic mass balance method provides good precision for investigating the influence of different DOM assemblages on the solubility of individual compounds as shown by the low RSD values ($\leq 2.5\%$) for S_w^*. It is difficult to compare this reproducibility with previous studies as most previous applications of the solubility enhancement model were based upon multiple measurements of single-subsample

incubations where changes in the concentration of humic substances were used to extract the K_{iDOC}. However, Chiou et al (1986) show the variability from duplicate gas chromatography-flame ionization detector (GC-FID) measurements of the same single sample as 8-10% of the concentration of 2,4,5,2',5'-PCB. Chefetz et al. (2000) used triplicate subsamples to determine pyrene solubility enhancement and reported RSDs of up to 15%.

In general, I find that HMW DOM enhances styrene solubility more effectively per unit OC than either sterile-filtered DOM or low-molecular weight DOM, which is consistent with the idea that solute partitioning is primarily responsible for the solubility enhancement. As suggested by Chiou et al. (1986), HMW material should have a larger intermolecular hydrophobic area for interaction with the hydrophobic solute (styrene, in my case). While the relative relationship of C_o among my samples appears reasonable in view of previous studies, my S_w^* values initially appear more perplexing. One would expect that if the apparent styrene solubility (S_w^*) of both high molecular weight and low molecular weight DOM were added together, I would get

$$(S_w^*)_{LMW} + (S_w^*)_{HMW} = 2S_w + (XC_0)_{LMW} + (XC_0)_{HMW} \qquad \text{Eq.(5.5)}$$

Where the subscripts LMW and HMW indicate low molecular weight and high molecular weight DOM. The summation in Eq.5 should be less than 2 times the S_w^* value for SF. However my results show that the addition of S_w^* for the two fractions is 3-5 times higher than the corresponding SF value.

The fact that combining the LMW plus HMW samples yields a larger enhancement of solubility than for the corresponding SF samples suggests that there may be changes in either random coil (Swift, 1999) or supramolecular associations (Sutton

and Sposito, 2005) in the HMW DOM in solution relative to the initial sterile-filtered water. For example, during ultrafiltration and the resulting dilution (in terms of organic carbon and inorganic species) of the HMW solution, a random coil arrangement could shift to a more open configuration that might interact more strongly to bring styrene into solution. It is also possible that the lack of LMW DOM in my HMW DOM solution could alter the equilibrium of hydrophobic and hydrogen-bond interactions stabilizing a supramolecular association (Sutton and Sposito, 2005). It is not clear whether disaggregation would result from a lowering of overall DOC concentration in the HMW solution or if aggregation would occur due to the loss of organic acids in the LMW DOM that would otherwise destabilize larger hydrophobic supramolecular assemblies. Such scenarios could easily explain the excess solubility enhancement for my fractions relative to total sample and should be the subject of further research.

3.2. FTIR analysis

To investigate the potential relationship between seasonal changes in the chemical composition of Dismal Swamp DOM and C_o, I analyzed subsamples of freeze-dried SF, HMW, and LMW samples by FTIR spectroscopy. The spectra of the average normalized SF, HMW, and LMW samples (Fig. 4.3) are in good agreement with published FTIR spectra for humic substances isolated from terrestrial soil (MacCarthy and Rice, 1985; Stevenson, 1994; Stevenson and Goh, 1971). The very wide strong band at 3409 cm^{-1} could be attributed to the O-H stretching of phenol, carbohydrate and carboxylic acid compounds, the broadness of this peak resulting mainly from the intra-molecular and inter-molecular hydrogen bond interactions of carboxylic acids (Pavia et

al., 1996). The area just below 3000 cm^{-1} shows stretching bands for aliphatic C-H bonds. The band at 1720 cm^{-1} is a result of carbonyl stretching ($\upsilon_{C=O}$) of the protonated carboxylic acid functional group and traces of ketone compounds (MacCarthy and Rice, 1985; Stevenson, 1994). The peak at 1630 cm^{-1} is produced by the asymmetric de-protonated carboxyl stretching (υ_{as}), while the symmetric stretching of the de-protonated carboxyl group (υ_s) appears as a broad band at 1408 cm^{-1} (MacCarthy and Rice, 1985; Mayo et al., 2004). The band at 1151 cm^{-1} could come from overlap of the vibrational coupling of C-O stretching of carbohydrate and ester compounds (Mayo et al., 2004; Stevenson and Goh, 1971), the shoulders at lower wavenumber of the C-O stretching could be contributed to the Si-O, S=O, and P=O stretching of silica, sulfate and phosphate respectively (Nakamoto, 1963). The normalized FTIR spectra averaged across the five seasons (Fig. 4.3) show some differences between the SF sample and its corresponding HMW and LMW fractions. The HWM spectrum shows higher absorption of the asymmetric de-protonated carboxyl stretching (υ_{as}) band around 1630 cm^{-1} and much lower absorption in the band around 1151 cm^{-1} relative to the SF sample. The LMW spectrum has higher band absorptions around 1720 cm^{-1} (the C=O stretching of the protonated carboxylic acid) and approximately 1151 cm^{-1} but lower absorption of the υ_{as} stretching than the SF spectrum.

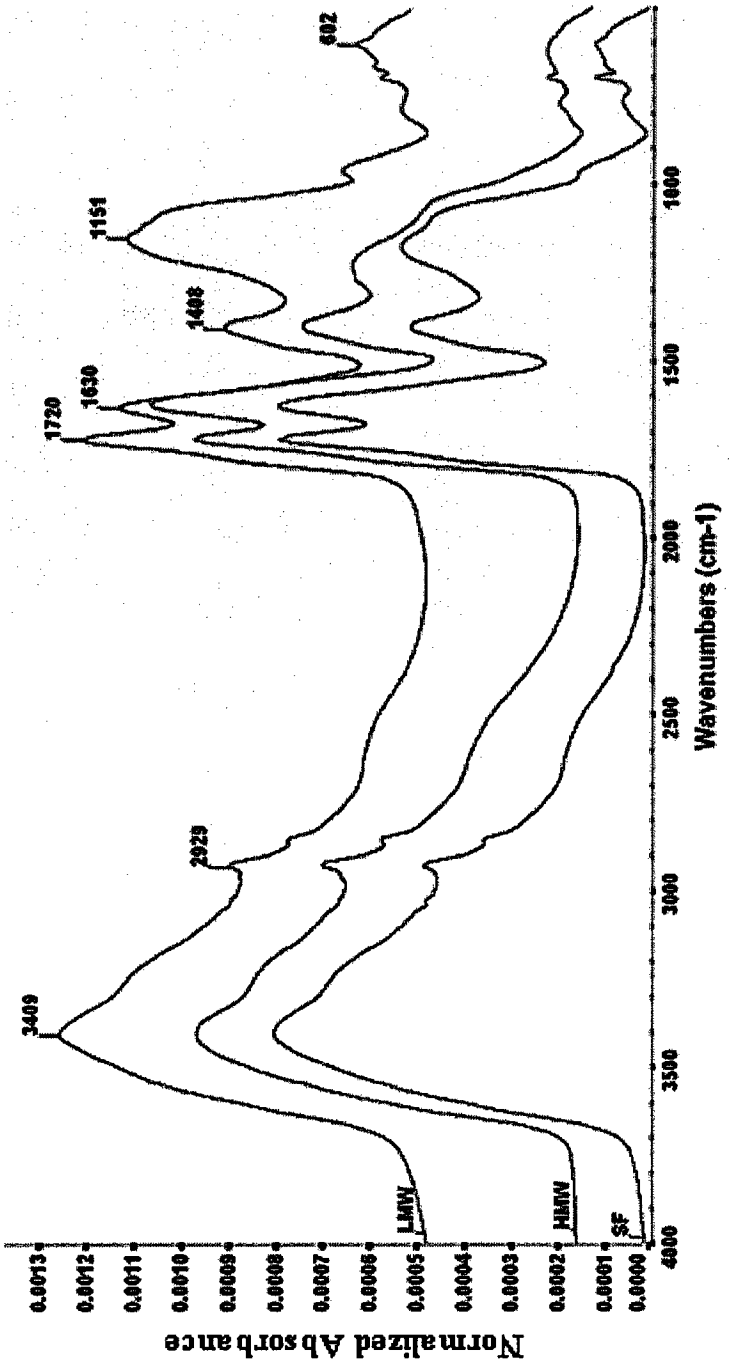

Fig. 4.3. Average (across all 5 seasons) of normalized FTIR spectra of Dismal Swamp sample fractions: SF, sterile-filtered water: HMW, high molecular weight DOM; LMW, and low molecular weight DOM

From the averaged FTIR data, I conclude that the HMW DOM has a higher relative concentration of de-protonated carboxylic groups while the LMW DOM has more protonated carboxylic groups. This is in agreement with the average pH as LMW DOM has a slightly lower pH (3.19 ± 0.07) than HMW DOM (pH 3.35 ± 0.05). The difference in protonation cannot be attributed to differences in ionic strength (e.g. Na^+ concentration) (Stevenson and Goh, 1971) between the two fractions. If ionic strength were involved (for example, through the formation of sodium adducts), the LMW fraction, which is not diafiltered like the HMW fractions, should have a higher percentage of de-protonated carboxylic groups. The presence of a shoulder around 980 cm^{-1} (stretching of Si-O, S=O, and P=O) in LMW and its absence from the HMW fraction is additional evidence of higher salt content in LMW relative to HMW DOM. To clarify the possible effects of diafiltration on the asymmetric stretching (υ_{as}) of the HMW fraction, I performed FTIR on the HMW fraction from November 2006 before and after diafiltration (data not shown); no significant difference in υ_{as} was observed.

The other main difference between the average FTIR spectra of HMW DOM and LMW DOM is a shift in the asymmetric de-protonated carboxyl stretching (υ_{as}) band of the average HMW DOM to a wavenumber 10 cm^{-1} lower than in the LMW fraction. Knowing that the υ_{as} is very sensitive to any change in the chemical structure of carboxylic compounds (Hay and Myneni, 2007), the shift could possibly attributed to differences in the chemical structures of the carboxylic compounds of the HMW relative to LMW fractions (Hay and Myneni, 2007) or, perhaps, to an increase in bidentate chelation of the carboxylic groups by metal in the HMW fraction relative to LMW DOM. (Deacon and Phillips, 1980).

Principal component analysis (PCA) of the FTIR spectra shows that the first two principal components (PC) account for 92% of the variability among the FTIR spectra (Fig. 4.4). The PC-1 scores (along the x-axis in Fig. 4.4) clearly separate the HMW and LMW fractions, indicating their differences in chemical composition, while the sterile-filtered samples, as might be expected, appear intermediate in composition between the HMW and LMW fractions. Plotting the PC-1 loadings spectra (Fig. 4.5) illustrates the differences in the chemical composition of the Dismal Swamp between the different fractions of DOM and, to a smaller extent, between seasons. The loadings spectra show that the HMW samples (and a subset of the SF samples) have a greater contribution from de-protonated carboxyl groups as indicated by υ_{as} at 1630 cm^{-1} and υ_{s} at 1405 cm^{-1} (MacCarthy and Rice, 1985; Mayo et al., 2004). The negative y-axis of PC-1 shows that the LMW samples and SF-3 are distinguished by higher C-O stretching at 1151 cm^{-1} and could be higher in silicate and sulfate concentration based upon symmetric S-O stretching at 980 cm^{-1} and Si-O bending at 620 cm^{-1} (Nakamoto, 1963). From PCA, therefore, the HMW fraction appears to have higher carboxylic contents than the LMW fraction, while the LMW fraction has higher carbohydrate contents than the HMW DOM. Chemically, the sterile-filtered (SF) material is intermediate between its two fractions.

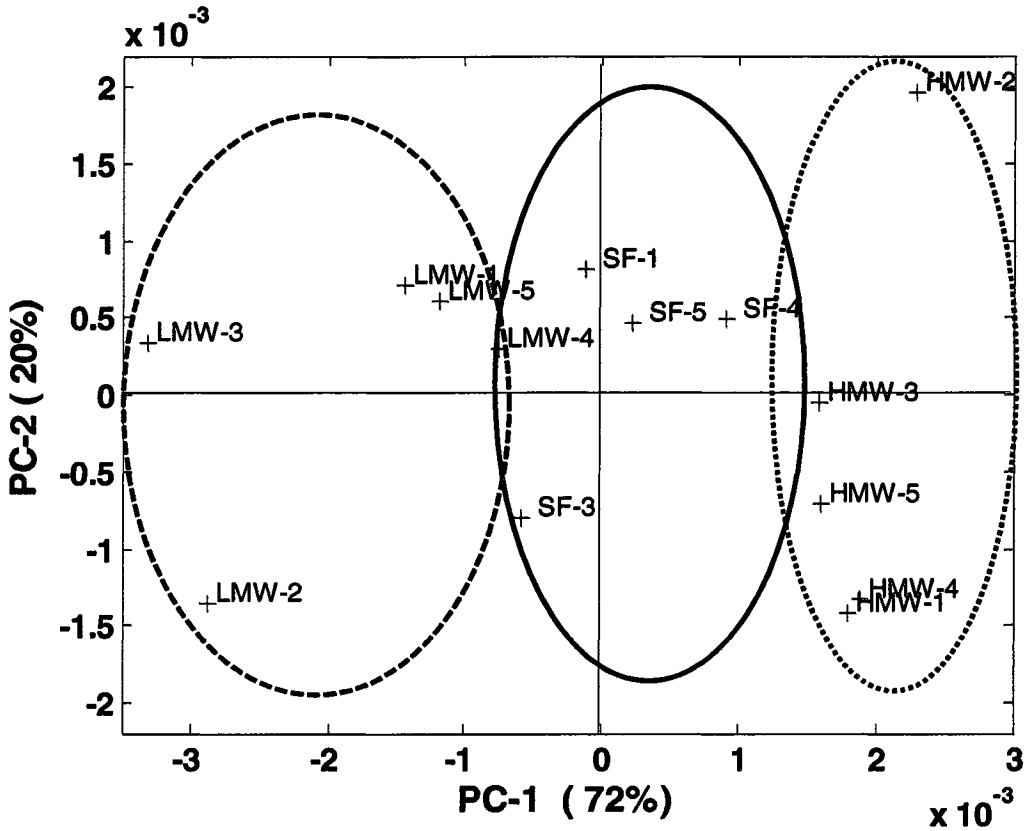

Fig. 4.4. Principal component analysis for FTIR spectra normalized to the total area of absorbance. Symbols are: SF = sterile-filtered sample, HMW = ultrafiltered high molecular weight DOM and LMW = ultrafiltered low molecular weight DOM and numbers indicate sampling season as shown in Table 4.1 (-1 = Nov. 05; -2 = Feb. 06; -3 = May. 06; -4 = Aug. 06; -5 = Nov. 06). Ovals are qualitative and indicating groupings of sample types; they are not part of statistical analysis.

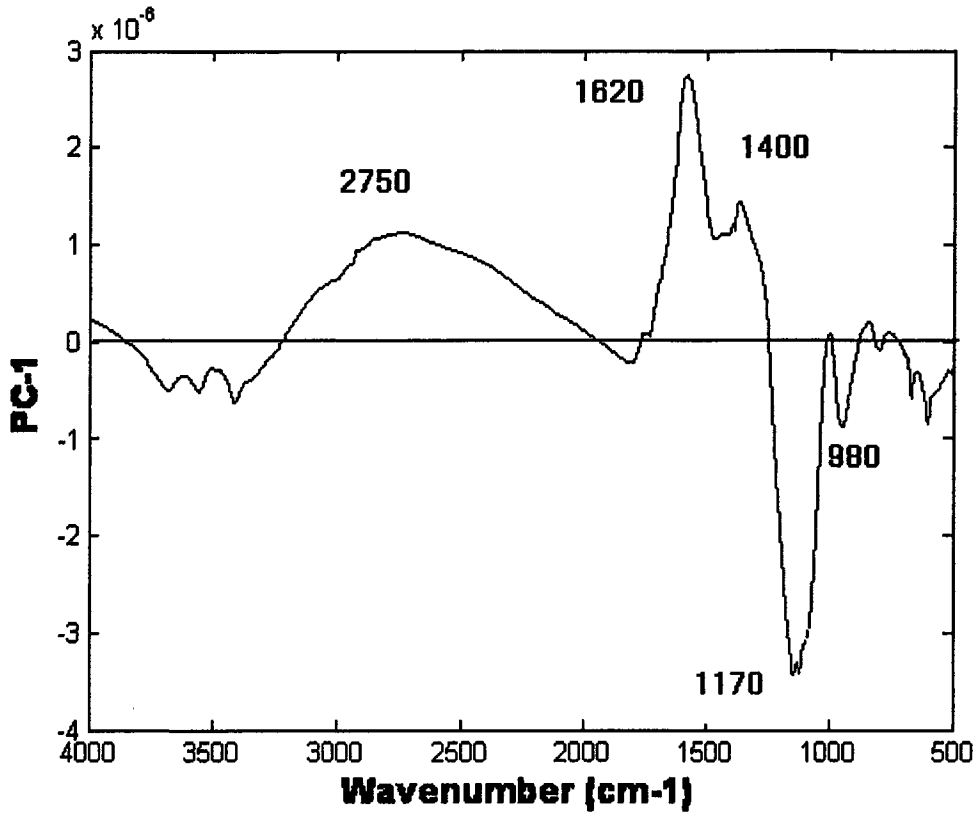

Fig. 4.5. Loading of the FTIR wavenumber along the principal component PC-1.

As carboxylic content appeared to be a major component in the structural variations among my Dismal Swamp DOM samples, I decided to further investigate its relationship with styrene solubility. To do so I integrated the area from 1860 cm^{-1} to 1500 cm^{-1} within the normalized FTIR spectra by using the perpendicular drop method with baseline correction. The resulting area should account for most of carboxylic content because it contains the bands at 1720 cm^{-1} and 1630 cm^{-1} that represent protonated and

de-protonated carboxylic groups, respectively. Previously, Celi et al (1997) showed a good correlation in the total absorbance of carboxyl groups in that region of the FTIR spectra and carboxyl content determined by wet chemical methods. A plot of carboxylic carbon area relative to C_o (Fig. 4.6) reveals a significant positive correlation (based upon t-testing using a significance level α of 5%) between the carboxyl area and the amounts of styrene per mole of DOC ($r^2 = 0.80$) when all the sample fractions were analyzed together. The r^2 of the correlation for SF samples alone was 0.58, not significant at an α of 5%, while the HMW samples and LMW samples both showed significant correlations, with r^2 values of 0.87 and 0.94 respectively.

4. CONCLUSIONS

The ^{13}C-label method presented here for determining the enhanced aqueous solubility of organic compounds by natural aqueous DOM is a promising new tool for investigating the reactivity of DOM. Relative to existing approaches, this method offers the advantage of great sensitivity and flexibility and can be tuned to provide maximum isotopic difference for a given range of model compound solubilities and initial natural DOC functionalities. My use of this method coupled with FTIR analysis provides insights into the relationship between aqueous DOM reactivity (in this case, enhancement of styrene solubility) and structure across seasons in a terrestrially-dominated swamp system. My FTIR and solubility enhancement results are consistent with those of Chiou et al. (1986) in showing that higher molecular weight fractions of natural organic matter are more effective in enhancing the solubility of hydrophobic compounds but highlight the importance that the organic composition of the DOM plays. The change in the

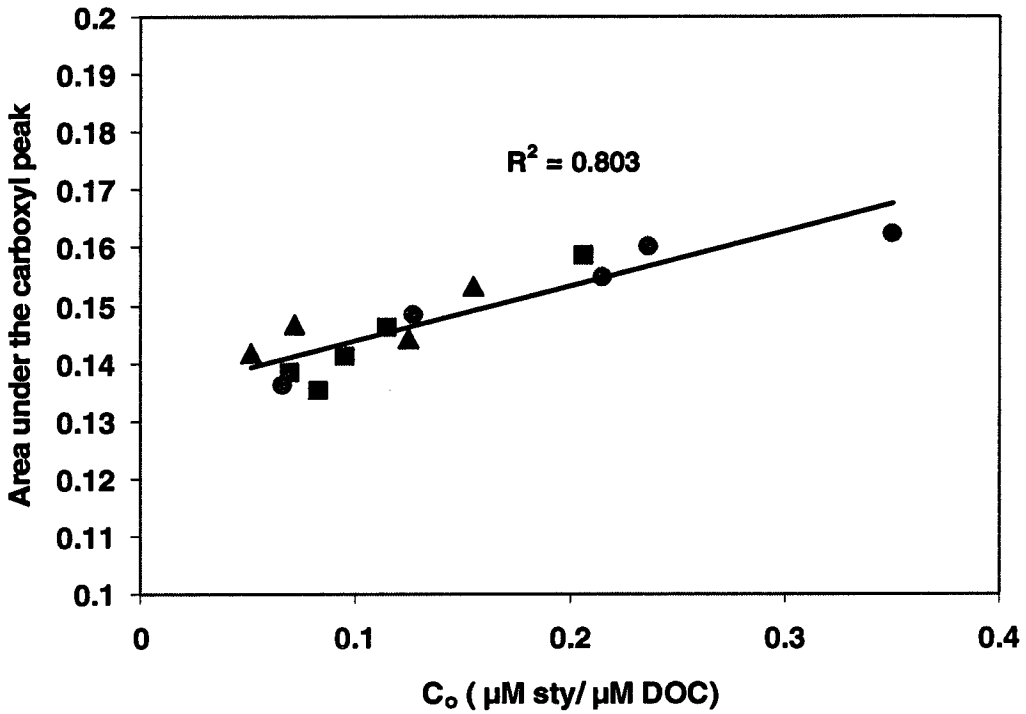

Fig. 4.6. The correlation between the area under the carboxyl peak of the normalized FTIR spectra and the amounts of styrene partitioned into unit mole of DOC (C_o). Sterile-filter SF (▲), high molecular weight, HMW (●) and low molecular weight LMW (■) of Dismal Swamp for the five seasons.

carboxyl contents between the seasons and DOM fractions is significantly correlated with the observed amounts of styrene partitioned into unit mole of DOC (C_o). That carboxylic acids can interact with styrene in aqueous solutions has been well demonstrated in the

polymer field, where the interactions have been exploited in surfactant-free styrene co-polymerization (Ceska, 1974).

My solubility enhancement results and FTIR spectra also indicate, as concluded by Assemi and co-workers (2004) as well, that ultrafiltration is not merely a pure physical separation but involves a chemical separation as well. How much the chemical separation is due to actual size differences of the DOM components and how much is due to chemical interactions with the ultrafiltration membrane is a matter of current research interest and should be further studied. By continuing these solubility studies with more model compounds of varying functionality with DOM samples from different aquatic environments (e.g., terrestrial and marine), I hope to come to a more complete understanding of DOM chemistry and the role it plays in fate of discrete organic molecules.

CHAPTER V

CONCLUSIONS AND FUTURE WORK

1. CONCLUSIONS

1.1. Chemical characterization of HMW-DOM

Coupling FTIR and ^{13}C-NMR analyses is a powerful way to investigate the qualitative changes of major compound classes in complex organic matter mixtures such as those seen in estuarine DOM. It appears especially useful in investigating carboxylic acid, amide and ester compositions. Although DOC measurements reveal a net loss in the DOC along my transect, the quantitative measurements of individual functional groups showed a more detailed picture concerning the changes in chemical composition and greater insight into DOM's possible sources and reactivity. For example, carbohydrate, and amide carbon percentages showed a net source in the middle of the transect which could indicate autochthonous DOM inputs, either directly or from the confluence of the Elizabeth River branches and the James River. Conversely, carboxylic acids and aromatic compounds showed a net loss through the estuary most likely due to a combination of flocculation and photoxidation processes. Interestingly, iron complexed to carboxylic acids appears to be lost between the Dismal Swamp and the low-salinity GB site.

Applying the 2nd derivative to FTIR spectra resolved many overlapped peaks and gave more details about the chemical structures of the DOM functional groups. One of the interesting points that results is the availability of three different pools of de-protonated carboxylic acids in Dismal Swamp: one of them is complexed with iron and

disappears between the DS and GB sites; the second pool appears biogeochemically reactive and its signal decreases down-estuary, while the third pool seems to be refractory and has the potential to be exported to and accumulate within the open ocean. The ester compounds show different chemical structures between my two transect end members; a five member ring ester (γ-lactone) was the dominant ester in the Dismal Swamp, while the highly aliphatic ester and acetate ester functional groups are the major ester in the other estuary/marine sites.

From both C/N and $\delta^{13}C$, I notice that the transformation of the HMW-DOM through the transect varies in three salinity regions. The first is the Dismal Swamp region (salinity of zero), which has a seasonal average C/N ratio of 52.33 and a $\delta^{13}C$ seasonal average value of (-27.24‰) which both are typical signals for C3 vascular-plant DOM sources. The second region, after salinity of zero until salinity of 20, has average values of 20.85 and -26.22‰ for the C/N ratio and $\delta^{13}C$ respectively. The third region, with salinity ranging from > 20 to 32, is characterized by average values of 11.84 and -23.31‰ for the C/N atomic ratio and $\delta^{13}C$ respectively. These regions indicate a dramatic shift in the relative importance of the processes that affect HMW-DOM along the transect from fresh water to the marine end member, where flocculation and the effects of heterotrophic bacteria seem to be the major players in the lower salinity region, but at the higher salinity regions the introduction of new carbon sources by primary production seems to be the major process.

The dramatic transformation from heterotrophic reworking to the effects of autotrophic sources is further supported by applying principal component analysis (PCA) and two dimensional correlation spectroscopy to the ^{13}C-NMR spectra of the HMW-

DOM. Moreover, both PCA and 2D correlation demonstrate that the HMW-DOM in the transect consists of three major components have different biogeochemical reactivity. One component looks like heteropolysaccharides (HPS) and is increasing as I move to the marine end member. A second component looks like carboxyl-rich compounds (CRC); the carbon percentage of the CRC like component decreases as I move away from the fresh water end member. The third component contains the major functional groups of amide/amino sugar compounds (AMS) and its carbon percentage stays almost constant regardless of the spatial and seasonal differences along the salinity transect.

The 2D-synchronous map of the FTIR also confirmed the opposite correlation between carboxylic and carbohydrate functional groups and the 2D hetero-spectra correlation between FTIR and ^{13}C-NMR verifies my assignments of the carbohydrate and carboxylic bands.

It seems that the HPS and CRC are present in many aquatic environments at different relative ratios, nevertheless, the synchronous and asynchronous 2D correlation map of both ^{13}C-NMR and FTIR revealed that each of these components is not composed from compounds that have exact chemical structures but from compounds that share similar backbone structures but have significant functional group differences.

1.4. Probing the reactivity of DOM

The ^{13}C-label method presented here for determining the enhanced aqueous solubility of organic compounds by natural aqueous DOM is a promising new tool for investigating the reactivity of DOM. Relative to existing approaches, this method offers the advantage of great sensitivity and flexibility and can be tuned to provide maximum

isotopic difference for a given range of model compound solubilities and initial natural DOC functionalities. My use of this method coupled with FTIR analysis provides insights into the relationship between aqueous DOM reactivity (in this case, enhancement of styrene solubility) and structure across seasons in a terrestrially-dominated swamp system.

My FTIR and solubility enhancement results are consistent with those of Chiou et al. (1986) in showing that higher molecular weight fractions of natural organic matter are more effective in enhancing the solubility of hydrophobic compounds but highlight the importance that the organic composition of the DOM plays. The change in the carboxyl contents between the seasons and DOM fractions is significantly correlated with the observed amounts of styrene partitioned into unit mole of DOC (C_o). That carboxylic acids can interact with styrene in aqueous solutions has been well demonstrated in the polymer field, where the interactions have been exploited in surfactant-free styrene co-polymerization (Ceska, 1974).

My solubility enhancement results and FTIR spectra also indicate, as concluded by Assemi and co-workers (2004) as well, that ultrafiltration is not merely a pure physical separation but involves a chemical separation as well. How much the chemical separation is due to actual size differences of the DOM components and how much is due to chemical interactions with the ultrafiltration membrane is a matter of current research interest and should be further studied. By continuing these solubility studies with more model compounds of varying functionality with DOM samples from different aquatic environments (e.g., terrestrial and marine), I hope to come to a more complete

understanding of DOM chemistry and the role it plays in fate of discrete organic molecules.

2. FUTURE WORK

This dissertation supports the presence of two major components in the HMW-DOM that have different biogeochemical reactivity, however, using the 2D-correlation of both ^{13}C-NMR and FTIR highlights significant variation within each component as I move along the estuary transect. I think there is a need to understand the chemical variation within each of these components, in order to understand their sources and sinks, which ultimately will help me to have better grasp of the ecological and environmental roles of DOM.

2.1. Carboxylic rich compounds (CRC)

My view regarding the reactivity of the carboxylic rich compounds (CRC): They start as compounds (from terrestrial sources) that are rich in carboxylic groups; however as they move through the estuaries the carboxylic groups are cleaved while the rest of the compound remains within the HMW-DOM fraction. With further loses of the carboxylic groups, the compounds (the aliphatic backbone) is removed from the HMW-DOM pool to either the LMW-DOM pool, adsorbtion into the particulate phase or utilization by heterotrophic bacteria. To prove that, I need to analyse the FT-ICR-MS data I have from the HMW-DOM to search for compounds that are similar to CRC model compounds but exhibiting losses of CO_2 molecular weight. And also I need to run some of the HMW-DOM by HMQC-NMR to prove the presence of the CRC compounds and determine

whether they may have a large CRAM component.

The distribution of CRC compounds in the environment still raise several questions: How they form? What was their original chemical structure? Is the CRC found in the deep ocean coming from land through the estuaries or is it produced in the deep ocean?. By answering these questions will able to estimate the recycle rate of these components, and their ecological and environmental roles.

2.2. Heteropolysaccharides (HPS) and amides/amino sugars (AMS)

One of the unresolved questions rising from this dissertation is the reactivity of the amide functional group in estuarine HMW-DOM. Why does it show a relatively constant carbon percentage throughout the estuary and how is it related to the heteropolysaccharides component (HPS). I believe the combination of spectroscopic techniques (^{13}C-NMR, ^{1}H-NMR, ^{15}N-NMR, FTIR) with wet chemical methods of characterization of amino acids and carbohydrate could give me better picture of these changes.

2.3. Two–dimensional correlation spectroscopy.

This dissertation demonstrates the power of 2D-correlation in exploring the reactivity and changes in the chemical structure of aquatic DOM. I highly believe that it could open the door to better understanding the effect of different perturbations (temperature, photoxidation, bacterial utilization, pressure, pH, salinity) in the structure of the DOM by using wide varieties of spectroscopic techniques (e.g. NMR, FTIR, mass spectroscopy, UV-visible). Applying 2-D correlation under controlled experimental

conditions (unlike in situ in an estuary) will enable me to get the maximum advantages of the asynchronous spectrum, where I can look at the coincident order of changes of specific functional groups relative to each other.

2.4. Probing the reactivity of DOM

The ^{13}C-label method presented here for determining the enhanced aqueous solubility of organic compounds by natural aqueous DOM is a promising new tool for investigating the reactivity of DOM. Relative to existing approaches, this method offers the advantage of great sensitivity and flexibility and can be tuned to provide maximum isotopic difference for a given range of model compound solubilities and initial natural DOC functionalities. In addition, it could be used as unified method to estimate the interactions of different probes with the same DOM, to be able to combine the results to give me a better understanding of the reactivity and chemical structure of DOM.

My primary results from the interaction of the three dissolved organic matter fractions (Sterile-filter, HMW and LMW) of the Dismal Swamp with other model compounds (dodecanol and decanoic acid) show different reactivities than what I observed with styrene (see Fig. 5.1 and Fig. 5.2).That shows that using different model compounds that have different chemical functional groups will allow me to investigate different DOM functionality characteristics, which will produce better comprehensive understanding of DOM chemical structures and reactivity. In addition, the great sensitivity and flexibility of this method give it the capability to investigate the reactivity of low-DOM-concentration samples such as those found in estuarine and marine DOM.

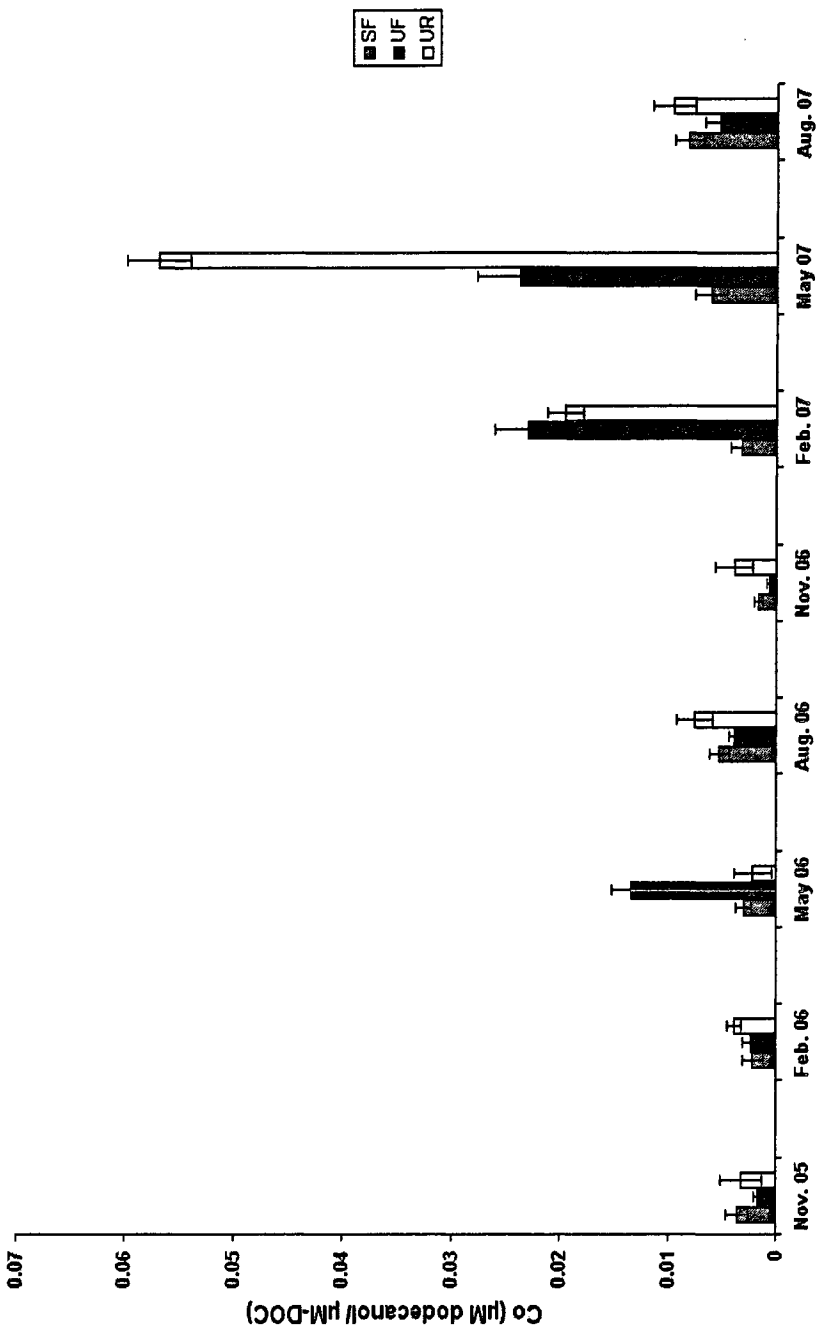

Fig. 5.1. Dodecanol solubility in sterile filtered water (SF), high molecular weight (HMW) and low molecular weight (LMW) normalized per unit DOC at different seasons as calculated by isotopic mass balance. Error bars represent the standard deviation of triplicate measurements from duplicate vials (n=6).

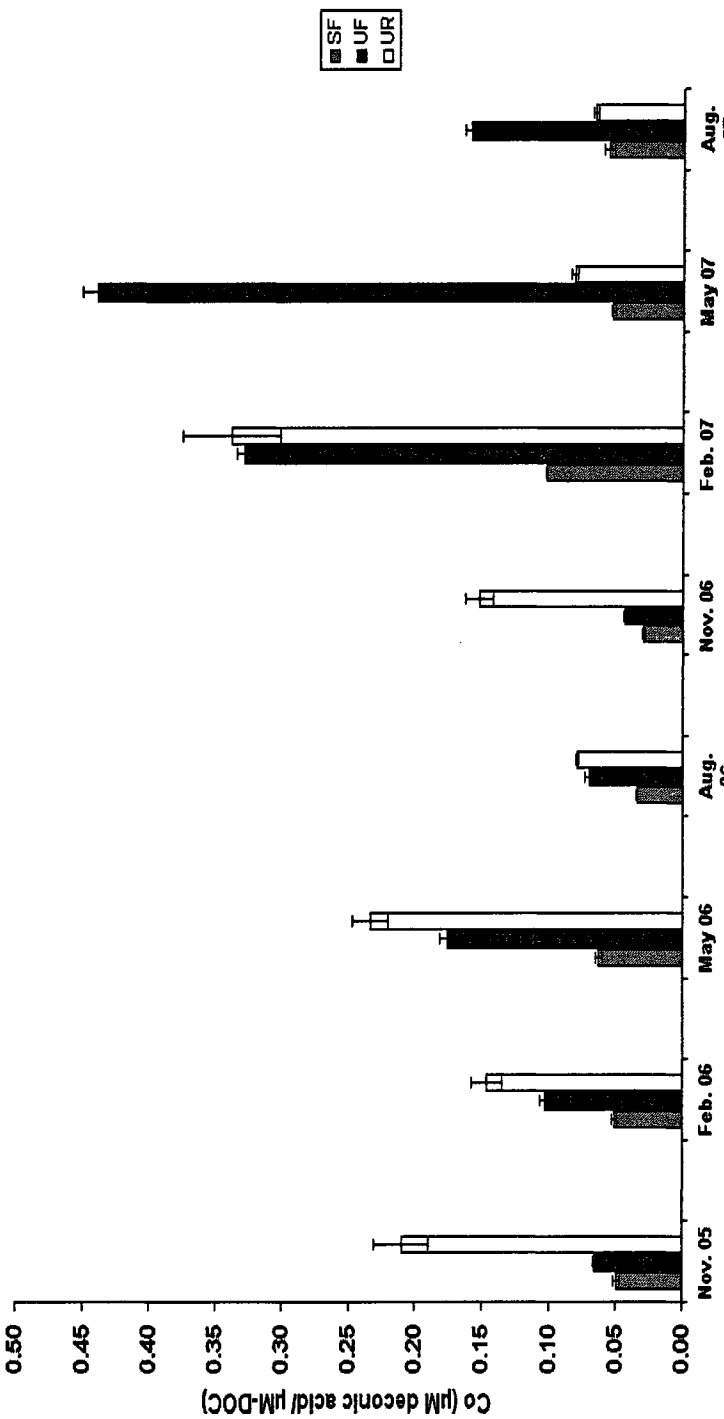

Fig. 5.2. Decanoic acid solubility in sterile filtered water (SF), high molecular weight (HMW) and low molecular weight (LMW) normalized per unit DOC at different seasons as calculated by isotopic mass balance. Error bars represent the standard deviation of triplicate measurements from duplicate vials (n=6).

LITERATURE CITED

Aluwihare, L. I., Repeta, D. J., Chen, R. F., 1997. A major biopolymeric component to dissolved organic carbon in surface sea water. Nature 387, 166-169.

Aluwihare, L. I., Repeta, D. J., Chen, R. F., 2002. Chemical composition and cycling of dissolved organic matter in the Mid-Atlantic Bight. Deep-Sea Research 49, 4421-4437.

Aluwihare, L. I., Repeta, D. J., Pantoja, S., Johnson, C. G., 2005. Two chemically distinct pools of organic nitrogen accumulate in the ocean. Science 308, 1007-1010.

Amon, R. M. W., Benner, R., 1994. Rapid cycling of high-molecular-weight dissolved organic matter in the ocean. Nature 369, 549-552.

Amon, R. M. W., Benner, R., 1996. Bacterial utilization of different size classes of dissolved organic matter. Limnology and Oceanography 41, 41-51.

Arnarson, T. S., Keil, R. G., 2001. Organic-mineral interactions in marine sediments studied using density fractionation and X-ray photoelectron spectroscopy. Organic Geochemistry 32, 1401-1415.

Assemi, S., Newcombe, G., Hepplewhite, C., Beckett, R., 2004. Characterization of natural organic matter fractions separated by ultrafiltration using flow field-flow fractionation. Water Research 38, 1467-1476.

Awichi, A., Tee, E. M., Srikanthan, G., Zhao, W., 2002. Identification of overlapped near-infrared bands of glucose anomers using two-dimensional near-infrared and middle-infrared correlation spectroscopy. Applied Spectroscopy 56, 897-901.

Azam, F., 1998. Microbial control of oceanic carbon flux: The plot thickens. Science 280, 694-696.

Azam, F., Fenchel, T., Field, J. G., Gray, J. S., Meyer-Reil, L. A., Thingstad, F., 1983. The ecological role of water-column microbes in the sea. Marine Ecology Progress Series 10, 257-263.

Barton, F. E., Himmelsbach, D. S., Duckworth, J. H., Smith, M. J., 1992. Two-dimensional vibration spectroscopy: correlation of mid-and near-infrared regions. Applied Spectroscopy 46, 420-429.

Benner, R., 2002. Chemical composition and reactivity. In: Hansell, D. A., Carter, C. W. (Eds.), Biogeochemistry of Marine Dissolved Organic Matter. Academic Press, London, UK., pp. 59-90.

Benner, R., Biddanda, B., Black, B., McCarthy, M., 1997. Abundance, size distribution, and stable carbon and nitrogen isotopic compositions of marine organic matter isolated by tangential-flow ultrafiltration. Marine Chemistry 57, 243-263.

Benner, R., Louchouarn, P., Amon, R., 2005. Terrigenous dissolved organic matter in the Arctic Ocean and its transport to surface and deep waters of the North Atlantic. Global Biogeochemical Cycles 19, GB2025.

Benner, R., Opsahl, S., 2001. Molecular indicators of the sources and transformations of dissolved organic matter in the Mississippi river plume. Organic Geochemistry 32, 597-611.

Benner, R., Pakulski, J., McCarthy, M., Hedges, J. I., Hatcher, P. G., 1992. Bulk chemical characteristics of dissolved organic matter in the ocean. Science 255, 1561-1564.

Benoit, G., Oktay-Marshall, S., Cantu, A., Hood, E., Coleman, C., Corapcioglu, M., Santschi, P., 1994. Partitioning of Cu, Pb, Ag, Zn, Fe, Al, and Mn between filter-retained particles, colloids, and solution in six Texas estuaries. Marine Chemistry 45, 307-336.

Bernhardt, P., Mulholland, M., Gobler, C., Morse, R., Procise, L., Filippino, K. C., Boneillo, G., 2008. Ecosystem impacts of a *Cochlodinium polykrikoides* bloom in a mid-Atlatic estuaries. Ocean Science Meeting, Orlando, FL. March 2-7 2008.

Bertilsson, S., Stepanauskas, R., Cuadros-Hansson, R., Graneli, W., Wikner, J., Tranvik, L., 1999. Photochemically induced changes in bioavailable carbon and nitrogen pools in a boreal watershed. Aquatic Microbial Ecology 19, 47-56.

Bianchi, T. S., 2007. Biogeochemistry of Estuaries. Oxford University Press, New York, USA.

Bianchi, T. S., Filley, T., Dria, K., Hatcher, P. G., 2004. Temporal variability in sources of dissolved organic carbon in the lower Mississippi River. Geochimica et Cosmochimica Acta 68, 959-967.

Boon, J. J., Klap, V. A., Eglinton, T. I., 1998. Molecular characterization of microgram amounts of oceanic colloidal organic matter by direct temperature-resolved ammonia chemical ionization mass spectrometry. Organic Geochemistry 29, 1051-1061.

Boyle, E. A., Edmond, J. M., Sholkovitz, E. R., 1977. The mechanism of iron removal in estuaries. Geochimica et Cosmochimca Acta 41, 1313–1324.

Brandenburg, K., Seydel, U., 1996. Fourier transform infrared spectroscopy of cell surface polysaccharides. In: Mantsch, H. H., Chapman, D. (Eds.), Infrared Spectroscopy of Biomolecules. Wiley-Liss, Inc., New York, pp. 203-278.

Brandenburg, K., Seydel, U., 2002. Vibrational spectroscopy of carbohydrates and glycoconjugates. In: Chalmers, J. M. and Griffiths, P. R. (Eds.), Handbook of Vibrational Spectroscopy, Applications in Life, Pharmaceutical and Natural Sciences. John Wiley and Sons, LTD., Chichester, UK.

Bronk, D. A., 2002. Dynamics of DON. In: Hansell, D., Carter, C. (Eds.), Biogeochemistry of Marine Dissolved Organic Matter. Academic Press, London, UK., pp. 153- 231.

Buesseler, K., 1996. Introduction to "Use of cross-flow filtration (CFF) for the isolation of marine colloids". Marine Chemistry 55, vii-viii.

Buesseler, K., Bauer, J., Chen, R., Eglinton, T., Gustafsson, O., Landing, W., Mopper, K., Moran, S., Santschi, P. H., Vernonclark, R., Wells, M. L., 1996. An intercomparison of cross-flow filtration techniques used for sampling marine colloids: Overview and organic carbon results. Marine Chemistry 55, 1-31.

Buffeteau, T., Pezolet, M., 1998. Photoinduced orientation in azopolymers studied by infrared spectroscopy: Cooperative and biaxial orientation in semicrystalline polymers. Macromolecules 31, 2631-2635.

Byler, D. M., Gerasimowicz, W. V., Susi, H., Schnitzer, M., 1987. FT-IR spectra of soil constituents: fulvic acid and fulvic acid complex with ferric ions. Applied Spectroscopy 41, 1428-1430.

Cabaniss, S. E., 1991. Carboxylic acid content of a fulvic acid determined by potentiometry and aqueous Fourier transform infrared spectrometry. Analytica Chimica Acta 255, 23-30.

Carter, C. W., Suffet, I. H., 1982. Binding of DDT to dissolved humic materials. Environmental Science and Technology 16, 735-740.

Celi, L., Schnitzer, M., Negre, M., 1997. Analysis of carboxyl groups in soil humic acids by a wet chemical method, Fourier transform infrared spectrophotometry, and solution-state carbon-13 nuclear magnetic resonance. A comparative study. Soil Science 162, 189-197.

Ceska, G. W., 1974. The effect of carboxylic monomers on surfactant-free emulsion copolymerization. Journal of Applied Polymer Science 18, 427-437.

Chefetz, B., Deshmukh, A. P., Hatcher, P. G., Guthrie, E. A., 2000. Pyrene sorption by natural organic matter. Environmental Science and Technology 34, 2925-2930.

Chin, Y. P., Aiken, G. R., Danielsen, K. M., 1997. Binding of pyrene to aquatic and commercial humic substances: The role of molecular weight and aromaticity. Environmental Science and Technology 31, 1630–1635.

Chiou, C. T., Kile, D. E., Brinton, T. I., Malcolm, R. L., Leenheer, J. A., MacCarthy, P., 1987. A comparison of water solubility enhancements of organic solutes by aquatic humic materials and commercial humic acids. Environmental Science and Technology 21, 1231-1234.

Chiou, C. T., Malcolm, R. L., Brinton, T. I., Kile, D. E., 1986. Water solubility enhancement of some organic pollutants and pesticides by dissolved humic and fulvic acids. Environmental Science and Technology 20, 502-508.

Cloern, J. E., Alpine, A. E., Cole, B. E., Wong, R. L. J., Arthur, J. F., Ball, M. D., 1983. River discharge controls phytoplankton dynamics in the northern San Francisco Bay estuary. Estuarine, Coastal and Shelf Science 16, 415-429.

Czarnecki, M. A., Wu, P., Siesler, H. W., 1998. 2D FT-NIR and FT-IR correlation analysis of temperature-induced changes of nylon12. Chemical Physics Letters 283, 326-332.

Dagg, M., Benner, R., Lohrenz, S., Lawrence, D., 2004. Transformation of dissolved and particulate materials on continental shelves influenced by large rivers: Plume processes. Continental Shelf Research 24, 833-858.

Dalzell, B. J., Minor, E. C., Beaudet, A., Bowlds, R., 2007. Salinity effects on recovery and characterization of terrestrially-derived dissolved organic matter. American Chemical Society 234 National Meeting and Expo, August 19-23, 2007, Boston, MA.

Dalzell, B. J., Minor, E. C., Mopper, K. M., 2009. Photodegradation of estuarine dissolved organic matter: a multi-method assessment of DOM transformation. Organic Geochemistry 40, 243-257.

Davis, J., Benner, R., 2007. Quantitative estimates of labile and semi-labile dissolved organic carbon in the western Arctic Ocean: A molecular approach. Limnology and Oceanography 52, 2434-2444.

Deacon, G. B., Phillips, R. J., 1980. Relationships between the carbon-oxygen stretching frequencies of carboxylato complexes and the type of carboxylate coordination. Coordination Chemical Review 33, 227-250.

Del Vecchio, R., Blough, N. V., 2004. Spatial and seasonal distribution of chromophoric dissolved organic matter and dissolved organic carbon in the Middle Atlantic Bight. Marine Chemistry 89, 169-187.

Denoyer, L. K., Dodd, J. G., 2002. Smoothing and derivatives in spectroscopy. In: Chalmers, J. M., Griffiths, P. R. (Eds.), Handbook of Vibrational Spectroscopy: Sample Characterization and Spectral Data Processing. John Wiley and Sons, LTD., Chichester, UK., pp. 2173-2184.

Dria, K. J., Sachleben, J. R., Hatcher, P. G., 2002. Solid-state carbon-13 nuclear magnetic resonance of humic acids at high magnetic field strengths. Journal of Environmental Quality 31, 393-401.

Ebihara, K., Takahashi, H., Noda, I., 1993. Nanosecond two-dimensional resonance Raman correlation spectroscopy of benzil radical anion. Applied Spectroscopy 47, 1343-1344.

Edmond, J. M., Spivack, A., Grant, B. C., Hu, M. H., Chen, Z., Chen, S., Zeng, X., 1985. Chemical dynamics of the Changjiang estuary. Continental Shelf Research 4, 17-36.

Eglinton, G., Hamilton, R. J., 1963. The Distribution of Alkanes. In: Swain, T. (Ed.), Chemical Plant Taxonomy. Academic Press, New York, pp. 187-217.

Eglinton, T. I., Benitez-Nelson, B. C., Pearson, A., Mcnichol, A. P., Bauer, J. E., Druffel, E. R. M., 1997. Variability in radiocarbon ages of individual organic compounds from marine sediments. Science 277, 796-799.

Eglinton, T. I., Repeta, D. J., 2003. Organic matter in the contemporary ocean. In: Holland, H. D., Turekian, K. K. (Eds.), Treatise on Geochemistry. Elsevier, Oxford, UK., pp. 145-180.

Ekgasit, S., Ishida, H., 1995. Quantitative two-dimensional infrared (2D IR) spectroscopy: Theoretical development for general and specific cases. Applied Spectroscopy 49, 1243-1253.

Faust, B. C., Zepp, R. G., 1993. Photochemistry of aqueous iron (III)-polycarboxylate complexes: roles in the chemistry of atmospheric and surface waters. Environmental Science and Technology 27, 2517-2522.

Filardo, M. J., Dunstan, W. M., 1985. Hydrodynamic control of phytoplankton in low salinity waters of the James River estuary, Virginia, U. S. A. Estuarine, Coastal and Shelf Science 21, 653-667.

Finmen, R. L., Cory, R. M., Chin, Y. P., Trouts, T. D., McKnight, D. M., 2007. Probing the oxidation–reduction properties of terrestrially and microbially derived dissolved organic matter. Geochimica et Cosmochimica Acta 71, 3003-3015.

Fisher, T. R., Harding, L., Stanley, D. W., Ward, L. G., 1988. Phytoplankton, nutrients, and turbidity in the Chesapeake, Delaware, and Hudson Estuaries. Estuarine, Coastal and Shelf Science. 27, 61-93.

Gardner, W. S., Cotner, J. B., Eadie, B. J., Cavaletto, J. F., Benner, R., Chin-Leo, G., 1994. Mineralization of organic material and bacterial dynamics in Mississippi River plume water. Estuaries and Coasts 17, 816-828.

Gattuso, J. P., Frankignoulle, M., Wollast, R., 1998. Carbon and carbonate metabolism in coastal aquatic ecosystems. Annual Reviews in Ecology and Systematics 29, 405-434.

Gauthier, T. D., Seitz, W. R., Grant, C. L., 1987. Effects of structural and compositional variations of dissolved humic materials on pyrene Koc values. Environmental Science and Technology 21, 243-248.

Gauthier, T. D., Shane, E. C., Guerin, W. F., Seitz, W. R., Grant, C. L., 1986. Fluorescence quenching method for determining equilibrium constants for polycyclic aromatic hydrocarbons binding to dissolved humic materials. Environmental Science and Technology 20, 1162-1166.

Gordon, E. S. Goñi, M. A., 2003. Sources and distribution of terrigenous organic matter delivered by the Atchafalaya River to sediments in the northern Gulf of Mexico. Geochimica et Cosmochimica Acta 67, 2359-2375.

Griffiths, P. R., De Haseth, J. A., 2007. Fourier Transform Infrared Spectroscopy. Wiley-Interscience, New Jersey.

Günzler, H., Gremlich, H. U., 2002. IR Spectroscopy: An Introduction. Wiley-VCH, Weinheim, Germany.

Guo, L., Santschi, P. H., 1996. A critical evaluation of the cross-flow ultrafiltration technique for sampling colloidal organic carbon in seawater. Marine Chemistry 55, 113-127.

Guo, L., Santschi, P. H., 1997. Isotopic and elemental characterization of colloidal organic matter from the Chesapeake Bay and Galveston Bay. Marine Chemistry 59, 1-15.

Guo, L., Wen, L.-S., Tang, D., Santschi, P. H., 2000. Re-examination of cross-flow ultrafiltration for sampling aquatic colloids: Evidence from molecular probes. Marine Chemistry 69, 75-90.

Hansell, D. A., Carlson, C. A., 2001. Marine dissolved organic matter and the carbon cycle. Oceanography 14, 41–49.

Harvey, H. R., Mannino, A., 2001. The chemical composition and cycling of particulate and macromolecular dissolved organic matter in temperate estuaries as revealed by molecular organic tracers. Organic Geochemistry 32, 527-542.

Hassett, J. P., 2006. Dissolved natural organic matter as a microreactor. Science 311, 1723-1724.

Hassett, J. P., Milicic, E., 1985. Determination of equilibrium and rate constants for binding of a polychlorinated biphenyl congener by dissolved humic substances. Environmental Science and Technology 19, 638-643.

Hay, M. B., Myneni, S. C. B., 2007. Structural environments of carboxyl groups in natural organic molecules from terrestrial systems. Part 1: Infrared spectroscopy. Geochimica et Cosmochimica Acta 71, 3518-3532.

Hayes, J. M., Freeman, K. H., Popp, B. N., Hoham, C. H., 1990. Compound-specific isotopic analyses: A novel tool for reconstruction of ancient biogeochemical processes. Organic Geochemistry 16, 1115-1128.

He, Y., Wang, G., Cox, J., Geng, L., 2001. Two-dimensional fluorescence correlation spectroscopy with modulated excitation. Analytical Chemistry 73, 2302-2309.

Hedges, J. I., 1992. Global biogeochemical cycles: Progress and problems. Marine Chemistry 39, 67-93.

Hedges, J. I., 2002. Why dissolved organics matter?. In: Hansell, D. A. and Carlson, C. A. (Eds.), Biogeochemistry of Marine Dissolved Organic Matter. Academic Press, London, UK., pp. 1-34.

Hedges, J. I., Blanchette, R. A., Weliky, K., Devol, A. H., 1988. Effects of fungal degradation on the CuO oxidation products of lignin: A controlled laboratory study. Geochimica et Cosmochimica Acta 52, 2717-2726.

Hedges, J. I., Hatcher, P. G., Ertel, J. R., Meyers-Schulte, K. J., 1992. A comparison of dissolved humic substances from seawater with Amazon River counterparts by ^{13}C-NMR spectroscopy. Geochimica et Cosmochimica Acta 56, 1753-1757.

Hedges, J. I., Keil, R. G., Benner, R., 1997. What happens to terrestrial organic matter in the ocean?. Organic Geochemistry 27, 195-212.

Heissenberger, A., Herndl, G. J., 1994. Formation of high molecular weight material by free-living marine bacteria. Marine Ecology Progress Series 111, 129-135.

Hergert, H. T., 1960. Infrared spectra of lignin and related compounds. II. Conifer lignin and model compounds. Journal of Organic Chemistry 25, 405-413.

Hernes, P. J., Benner, R., 2003. Photochemical and microbial degradation of dissolved lignin phenols: Implications for the fate of terrigenous dissolved organic matter in marine environments. Journal of Geophysical Research.C. Oceans 108, 3291.

Hertkorn, N., Benner, R., Frommberger, M., Schmitt-Kopplin, P., Witt, M., Kaiser, K., Kettrup, A., Hedges, J. I., 2006. Characterization of a major refractory component of marine dissolved organic matter. Geochimica et Cosmochimica Acta 70, 2990-3010.

Hirschfeld, T., 1979. Diagnosis and correction of wedging errors in absorbance subtract Fourier transform infrared spectrometry. Analytical Chemistry 51, 495-499.

Hoch, M. P., Kirchman, D. L., 1993. Seasonal and inter-annual variability in bacterial production and biomass in a temperate estuary. Marine Ecology Progress Series 98, 283-295.

Holligan, P. M., 1992. Do marine phytoplankton influence global climate? In: Falkowski, P. G., Woodhead, A. D. (Eds.), Primary Productivity and Biogeochemical Cycles in the Sea. Springer, New York, pp. 487-504.

Hopmans, E. C., Weijers, J. W. H., Schefuss, E., Herfort, L., Damste, J. S. S., Schouten, S., 2004. A novel proxy for terrestrial organic matter in sediments based on branched and isoprenoid tetraether lipids. Earth and Planetary Science Letters 224, 107-116.

Hu, B. W., Zhou, P., Noda, I., Ruan, Q. X., 2006. Generalized two-dimensional correlation analysis of NMR and Raman spectra for structural evolution characterizations of silk fibroin. Journal of Physical Chemistry B-Condensed Phase 110, 18046-18051.

Huang, W., Peng, P., Yu, Z., Fu, J., 2003. Effects of organic matter heterogeneity on sorption and desorption of organic contaminants by soils and sediments. Applied Geochemistry 18, 955-972.

Hunter, K. A., Liss, P. S., 1982. Organic matter and the surface charge of suspended particles in estuarine waters. Limnology and Oceanography 27, 322-335.

Izawa, K., Ogasawara, T., Masuda, H., Okabayashi, H., Noda, I., 2002a. Two-dimensional correlation gel permeation chromatography study of octyltriethoxysilane sol-gel polymerization process. Macromolecules 35, 92-96.

Izawa, K., Ogasawara, T., Masuda, H., Okabayashi, H., O'Connor, C. J., Noda, I., 2002b. Two-dimensional correlation gel permeation chromatography (2D GPC) study of 1H, 1H, 2H, 2H-perfluorooctyltriethoxysilane sol-gel polymerization process. Journal of Physical Chemistry B 106, 2867-2874.

Jacobsen, N. E., 2007. NMR spectroscopy explained: simplified theory, applications and examples for organic chemistry and structural biology. Wiley-Interscience, New Jersey.

Jaffe, R., Boyer, J. N., Lu, X., Maie, N., Yang, C., Scully, N. M., Mock, S., 2004. Source characterization of dissolved organic matter in a subtropical mangrove-dominated estuary by fluorescence analysis. Marine Chemistry 84, 195-210.

Johannesson, K. H., Tang, J., Daniels, J. M., Bounds, W. J., Burdige, D. J., 2004. Rare earth element concentrations and speciation in organic-rich black waters of the Great Dismal Swamp, Virginia, USA. Chemical Geology 209, 271-294.

Johnston, C. T., Davis, W. M., Erickson, C., Delfino, J. J., Cooper, W. T., 1994. Characterization of humic substances using Fourier transform infrared spectroscopy. In: Senesi, N., Miano, T. M. (Eds.), Humic Substances in the Global Environment and Implications on Human Health. Elsevier, Amsterdam, pp. 145-152.

Jung, Y. M., Shin, H. S., Kim, S. B., Noda, I., 2002. New approach to generalized two-dimensional correlation spectroscopy. 1: Combination of principal component analysis and two-dimensional correlation spectroscopy. Applied Spectroscopy 56, 1562-1567.

Kaiser, K., Benner, R., 2008. Major bacterial contribution to the ocean reservoir of detrital organic carbon and nitrogen. Limnology and Oceanography 53, 99-112.

Karlsson, T., Elgh-Dalgren, K., Björn, E., Skyllberg, U., 2007. Complexation of cadmium to sulfur and oxygen functional groups in an organic soil. Geochimica et Cosmochimica Acta 71, 604-614.

Kattner, G., Lobbes, J. M., Fitznar, H. P., Engbrodt, R., Nöthig, E. M., Lara, R. J., 1999. Tracing dissolved organic substances and nutrients from the Lena River through Laptev Sea (Arctic). Marine Chemistry 65, 25-39.

Kawasaki, N., Benner, R., 2006. Bacterial release of dissolved organic matter during cell growth and decline: Molecular origin and composition. Limnology and Oceanography 51, 2170-2180.

Kester, D. R., Duedall, I. W., Connors, D. N., Pytkowicz, R. M., 1967. Preparation of artificial seawater. Limnology and Oceanography 12, 176-179.

Kim, D., Oda, T., Muramatsu, T., Matsuyama, Y., Honjo, T., 2002. Possible factors responsible for the toxicity of *Cochlodinium polykrikoides*, a red tide phytoplankton. Comparative Biochemistry and Physiology Part C 132, 415-423.

Kitis, M., Karanfil, T., Wigton, A., Kilduff, J. E., 2002. Probing reactivity of dissolved organic matter for disinfection by-product formation using XAD-8 resin adsorption and ultrafiltration fractionation. Water Research 36, 3834-48.

Knicker, H., Hatcher, P. G., 1997. Survival of protein in an organic-rich sediment: Possible protection by encapsulation in organic matter. Naturwissenschaften 84, 231-234.

Knicker, H., Lüdemann, H. D., 1995. N-15 and C-13 CPMAS and solution NMR studies of N-15 enriched plant material during 600 days of microbial degradation. Organic Geochemistry 23, 329-341.

Kubelka, J., Pancoska, P., Keiderling, T. A., 1999. Novel use of a static modification of two-dimensional correlation analysis. Part II: Hetero-spectral correlations of protein Raman, FT-IR, and circular dichroism spectra. Applied Spectroscopy 53, 666-671.

Lam, B., Baer, A., Alaee, M., Lefebvre, B., Moser, A., Williams, A., Simpson, A. J., 2007. Major structural components in freshwater dissolved organic matter. Environmental Science and Technology 41, 8240-8247.

Landrum, P. F., Nihart, S. R., Eadie, B. J., Gardner, W. S., 1984. Reverse-phase separation method for determining pollutant binding to Aldrich humic acid and dissolved organic carbon of natural waters. Environmental Science and Technology 18, 187-192.

Latch, D. E., Mcneill, K., 2006. Microheterogeneity of singlet oxygen distributions in irradiated humic acid solutions. Science 311, 1743-1747.

Leenheer, J. A., Nanny, M. A., Mcintyre, C., 2003. Terpenoids as major precursors of dissolved organic matter in landfill leachates, surface water, and groundwater. Environmental Science and Technology 37, 2323-2331.

Leenheer, J. A., Wershaw, R. L., Reddy, M. M., 1995. Strong-acid, carboxyl-group structures in fulvic acid from the Suwannee River, Georgia. 1. Minor structures. Environmental Science and Technology 29, 393-398.

Liu, Y., Chen, Y. R., Ozaki, Y., 2000. Two-dimensional visible/near-infrared correlation spectroscopy study of thermal treatment of chicken meats. Journal of Agricultural and Food Chemistry 48, 901-908.

Liu, Y., Ozaki, Y., Noda, I., 1996. Two-dimensional Fourier transform near-infrared correlation spectroscopy study of dissociation of hydrogen-bonded N-methylacetamide in the pure liquid state. Journal of Physical Chemistry 100, 7326-7332.

Loder, T. C., Reichard, R. P., 1981. The dynamics of conservative mixing in estuaries. Estuaries and Coasts 4, 64-69.

Lu, X. Q., Hanna, J. V., Johnson, W. D., 2000. Source indicators of humic substances: An elemental composition, solid state ^{13}C CP/MAS NMR and Py-GC/MS Study. Applied Geochemistry 15, 1019-1033.

MacCarthy, P., Rice, J. A., 1985. Spectroscopic methods (other than NMR) for determining functionality in humic substances. In: Aiken, G., McKnight, D., Wershaw, R., MacCarthy, P. (Eds.), Humic Substances in Soil, Sediment, and Water: Geochemistry, Isolation, and Characterization. John Wiley and Sons, New York , pp. 527-559.

Madyastha, K. M., Bhattacharyya, P. K., Vaidyanathan, C. S., 1977. Metabolism of a monoterpene alcohol, linalool, by a soil pseudomonad. Canadian Journal of Microbiology 23, 230-239.

Mannino, A., Harvey, H. R., 2000. Biochemical composition of particles and dissolved organic matter along an estuarine gradient: sources and implications for DOM reactivity. Limnology and Oceanography 45, 775-788.

Mascarenhas, M., Dighton, J., Arbuckle, G. A., 2000. Characterization of plant carbohydrates and changes in leaf carbohydrate chemistry due to chemical and enzymatic degradation measured by microscopic ATR FT-IR spectroscopy. Applied Spectroscopy 54, 681-686.

Matsushita, A., Ren, Y., Matsukawa, K., Inoue, H., Minami, Y., Noda, I., Ozaki, Y., 2000. Two-dimensional Fourier transform Raman and near-infrared correlation spectroscopy studies of poly (methyl methacrylate) blends 1. Immiscible blends of poly (methyl methacrylate) and atactic polystyrene. Vibrational Spectroscopy 24, 171-180.

Mayo, D. W., Miller, F. A., Hannah, R. W., 2004. Course Notes on the Interpretation of Infrared and Raman Spectra. Wiley-Interscience, New Jersey.

McAuliffe, C., 1966. Solubility in water of paraffin, cycloparaffin, olefin, acetylene, cycloolefin, and aromatic hydrocarbons. The Journal of Physical Chemistry 70, 1267-1275.

McCallister, S. L., Bauer, J. E., Canuel, E. A., 2006. Bioreactivity of estuarine dissolved organic matter: A combined geochemical and microbiological approach. Limnology and Oceanography 51, 94-100.

McCarthy, M., Hedges, J., Benner, R., 1996. Major biochemical composition of dissolved high molecular weight organic matter in seawater. Marine Chemistry 55, 281-297.

McCarthy, M., Pratum, T., Hedges, J., Benner, R., 1997. Chemical composition of dissolved organic nitrogen in the ocean. Nature 390, 150-154.

Mecozzi, M., Pietrantonio, E., 2006. Carbohydrates proteins and lipids in fulvic and humic acids of sediments and its relationships with mucilaginous aggregates in the Italian Seas. Marine Chemistry 101, 27-39.

Meyers-Schulte, K. J., Hedges, J. I., 1986. Molecular evidence for a terrestrial component of organic matter dissolved in ocean water. Nature 321, 61-63.

Michalska, D. F., Back, D. M., Polavarapu, P. L., 1984. Identification of the characteristic, anomeric bands in the infrared spectrum of lyxose in aqueous solution. Carbohydrate Research 131, 29-38.

Miller, A. E. J., 1999. Seasonal investigations of dissolved organic carbon dynamics in the Tamar Estuary, UK. Estuarine, Coastal and Shelf Science 49, 891-908.

Miller, E. J., 2001. Seawater effects on the aqueous solubility and polymerization of Styrene monomer., Master thesis, Christopher Newport University.

Miller, W. L., Zepp, R. G., 1995. Photochemical production of dissolved inorganic carbon from terrestrial organic matter: Significance to the oceanic organic carbon cycle. Geophysical Research Letters 22, 417-417.

Minor, E. C., Boon, J. J., Harvey, H. R., Mannino, A., 2001. Estuarine organic matter composition as probed by direct temperature-resolved mass spectrometry and traditional geochemical techniques. Geochimica et Cosmochimica Acta 65, 2819-2834.

Minor, E. C., Dalzell, B. J., Stubbins, A., Mopper, K., 2007. Evaluating the photoalteration of estuarine dissolved organic matter using direct temperature-resolved mass spectrometry and UV-visible spectroscopy. Aquatic Sciences-Research Across Boundaries 69, 440-455.

Minor, E. C., Pothen, J., Dalzell, B. J., Abdulla, H., Mopper, K., 2006. Effects of salinity changes on the photodegradation and ultraviolet–visible absorbance of terrestrial dissolved organic matter. Limnology and Oceanography 51, 2181-2186.

Minor, E. C., Simjouw, J. P., Boon, J. J., Kerkhoff, A. E., Van Der Horst, J., 2002. Estuarine/marine UDOM as characterized by size-exclusion chromatography and organic mass spectrometry. Marine Chemistry 78, 75-102.

Mitra, S., Bianchi, T. S., Guo, L., Santschi, P. H., 2000. Terrestrially derived dissolved organic matter in the Chesapeake Bay and the Middle Atlantic Bight. Geochimica et Cosmochimica Acta 64, 3547-3557.

Mopper, K., Kieber, D. J., 2000. Marine photochemistry and its impact on carbon cycling the effects of UV radiation in the marine environment. In: de Mora,S., Demers, S., Vernet, M. (Eds.), The Effect of UV Radiation in the Marine Environment. Cambridge University Press, Cambridge, UK., pp. 101-129.

Mopper, K., Kieber, D. J., 2002. Photochemistry and the cycling of carbon, sulfur, nitrogen and phosphorus. In: Hansell, D. A., Carlson, C. A. (Eds.), Biogeochemistry of Marine Dissolved Organic Matter. Academic Press, London, UK., pp. 456-508.

Moran, M. A., Zepp, R. G., 1997. Role of photoreactions in the formation of biologically labile compounds from dissolved organic matter. Limnology and Oceanography 42, 1307-1316.

Mulholland, M. R., Floge, S., Carpenter, E. J., Capone, D. G., 2002. Phosphorus dynamics in cultures and natural populations of *Trichodesmium* spp. Marine Ecology Progress Series 239, 45-55.

Nakamoto, K., 1963. Infrared Spectra of Inorganic and Coordination Compounds.Wiley New York.

Nakashima, K., Yashuda, S., Ozaki, Y., Nodas, I., 2000. Two-dimensional fluorescence correlation spectroscopy. I. Analysis of polynuclear aromatic hydrocarbons in cyclohexane solutions. Journal of Physical Chemistry A 104, 9113-9120.

Naumann, D., Schultz, C. P., Helm, D., 1996. What can infrared spectroscopy tell us about the structure and composition of intact bacterial cells?. In: Mantsch, H. H. and Chapman, D. (Eds.), Infrared Spectroscopy of Biomolecules. Wiley-LISS, New York, pp. 279-310.

Nguyen, R. T., Harvey, H. R., Zang, X., Van Heemst, J. D. H., Hetényi, M., Hatcher, P. G., 2003. Preservation of algaenan and proteinaceous material during the oxic decay of *Botryococcus braunii* as revealed by pyrolysis-gas chromatography/mass spectrometry and ^{13}C NMR spectroscopy. Organic Geochemistry 34, 483-497.

Ning, X., Vaulot, D., Liu, Z., 1988. Standing stock and production of phytoplankton in the estuary of the Changjiang (Yangtse River) and the adjacent East China Sea. Marine Ecology Progress Series 49, 141-150.

Noda, I., 1993. Generalized two-dimensional correlation method applicable to infrared, Raman, and other types of spectroscopy. Applied Spectroscopy 47, 1329-1336.

Noda, I., Ozaki, Y., 2004. Two-Dimensional Correlation Spectroscopy: Applications in Vibrational and Optical Spectroscopy. John Wiley and Sons, LTD, West Sussex, England.

Obernosterer, I., Benner, R., 2004. Competition between biological and photochemical processes in the mineralization of dissolved organic carbon. Limnology and Oceanography 49, 117-124.

Ogawa, H., Amagai, Y., Koike, I., Kaiser, K., Benner, R., 2001. Production of refractory dissolved organic matter by bacteria. Science 292, 917-920.

Opsahl, S., Benner, R., 1997. Distribution and cycling of terrigenous dissolved organic matter in the ocean. Nature 386, 480-482.

Opsahl, S., Benner, R., Amon, R. M. W., 1999. Major flux of terrigenous dissolved organic matter through the Arctic Ocean. Limnology and Oceanography 44, 2017-2023.

Ozaki, Y., 2002. Two-dimensional correlation spectroscopy in vibrational spectroscopy. In: Chalmers, J. M., Griffiths, P. R. (Eds.), Handbook of Vibrational Spectroscopy, Sample Characterization and Spectra Data Processing. John Wiley and Sons, LTD., Chichester, UK.

Pavia, D. L., Lampman, G. M., Kriz, G. S., 1996. Introduction to Spectroscopy: A Guide for Students of Organic Chemistry. Saunders College Pub., Orlando, FL.

Pakulski, J. D., Benner, R., Amon, R., Eadie, B., Whitledge, T., 1995. Community metabolism and nutrient cycling in the Mississippi River plume: Evidence for intense nitrification at intermediate salinities. Marine Ecology Progress Series 117, 207-218.

Pakulski, J. D., Benner, R., Whitledge, T., Amon, R., Eadie, B., Cifuentes, L., Ammerman, J., Stockwell, D., 2000. Microbial metabolism and nutrient cycling in the Mississippi and Atchafalaya River plumes. Estuarine, Coastal and Shelf Science 50, 173-184.

Panagiotopoulos, C., Repeta, D. J., Johnson, C. G., 2007. Characterization of methyl sugars, 3-deoxysugars and methyl deoxysugars in marine high molecular weight dissolved organic matter. Organic Geochemistry 38, 884-896.

Pandey, K. K., 1999. A study of chemical structure of soft and hardwood and wood polymers by FTIR spectroscopy. Journal of Applied Polymer Science 71, 1969-1975.

Pennock, J. R., Sharp, J. H., 1986. Phytoplankton production in the Delaware Estuary: temporal and spatial variability. Marine Ecology Progress Series 34, 143-155.

Piccolo, A., Stevenson, F. J., 1994. Infrared spectroscopy evidence of thermal decarboxylation in potassium salts of humic substances. In: Senesi, N., Miano, T. M. (Eds.), Humic Substances in the Global Environment and Implications on Human Health. Elsevier. Amsterdam, pp. 329-334.

Quan, T. M., Repeta, D. J., 2007. Periodate oxidation of marine high molecular weight dissolved organic matter: Evidence for a major contribution from 6-deoxy-and methyl sugars. Marine Chemistry 105, 183-193.

Raymond, P. A., Bauer, J. E., 2001. Use of ^{14}C and ^{13}C natural abundances for evaluating riverine, estuarine, and coastal DOC and POC sources and cycling: A review and synthesis. Organic Geochemistry 32, 469-485.

Repeta, D. J., Quan, T. M., Aluwihare, L. I., Accardi, A., 2002. Chemical characterization of high molecular weight dissolved organic matter in fresh and marine waters. Geochimica et Cosmochimica Acta 66, 955-962.

Rochelle-Newall, E. J., Fisher, T. R., 2002. Chromophoric dissolved organic matter and dissolved organic carbon in Chesapeake Bay. Marine Chemistry 77, 23-41.

Rutherford, D. W., Chiou, C. T., Kile, D. E., 1992. Influence of soil organic matter composition on the partition of organic compounds. Environmental Science and Technology 26, 336-340.

Salloum, M. J., Chefetz, B., Hatcher, P. G., 2002. Phenanthrene sorption by aliphatic-rich natural organic matter. Environmental Science and Technology 36, 1953-1958.

Sannigrahi, P., Ingall, E. D., Benner, R., 2005. Cycling of dissolved and particulate organic matter at station Aloha: Insights from ^{13}C NMR spectroscopy coupled with elemental, isotopic and molecular analyses. Deep Sea Research Part I: Oceanographic Research Papers 52, 1429-1444.

Santschi, P. H., Lenhart, J. J., Honeyman, B. D., 1997. Heterogeneous processes affecting trace contaminant distribution in estuaries: The role of natural organic matter. Marine Chemistry 58, 99-125.

Sasic, S., Muszynski, A., Ozaki, Y., 2000. A new possibility of the generalized two-dimensional correlation spectroscopy. 1. Sample-sample correlation spectroscopy. Journal of Physical Chemistry A 104, 6380-6387.

Sasic, S., Ozaki, Y., 2001. Statistical two-dimensional correlation spectroscopy: Its theory and applications to sets of vibrational spectra. Analytical Chemistry 73, 2294-2301.

Schnitzer, M., Ghosh, K., 1982. Characteristics of water-soluble fulvic acid-copper and fulvic acid-iron complexes. Soil Science 134, 354-363.

Schnitzer, M., Skinner, S. I. M., 1963. Organo-metallic interactions in soils: 1. Reactions between a number of metal ions and the organic matter of a Podzol Bh Horizon. Soil Science 96, 86-93.

Schwarzenbach, R. P., Gschwend, P. M., Imboden, D. M., 2003. Environmental Organic Chemistry. John Wiley and Sons, New York.

Sessions, A. L., Burgoyne, T. W., Schimmelmann, A., Hayes, J. M., 1999. Fractionation of hydrogen isotopes in lipid biosynthesis. Organic Geochemistry 30, 1193-1200.

Shiller, A. M., Duan, S., Van Erp, P., Bianchi, T. S., 2006. Photo-oxidation of dissolved organic matter in river water and its effect on trace element speciation. Limnology and Oceanography 51, 1716-1728.

Sholkovitz, E. R., 1976. Flocculation of dissolved organic and inorganic matter during the mixing of river water and seawater. Geochimica et Cosmochimica Acta 40, 831-845.

Sholkovitz, E. R., Boyle, E. A., Price, N. B., 1978. The removal of dissolved humic acids and iron during estuarine mixing. Earth and Planetary Science Letters 40, 130-136.

Shurell, H. F., 2002. Spectra-structure correlations in the mid-and far-infrared. In: Chalmers, J.M., Griffiths, P.R. (Eds.), Handbook of Vibrational Spectroscopy, Sample Characterization and Spectra Data Processing. John Wiley and Sons, LTD., Chichester, UK., pp.1783-1816.

Sleighter, R. L., Hatcher, P. G., 2008. Molecular characterization of dissolved organic matter (DOM) along a river to ocean transect of the lower Chesapeake Bay by ultrahigh resolution electrospray ionization Fourier transform ion. Marine Chemistry 110, 140-152.

Sleighter, R. L., Liu, Z., Abdulla, H., Dias, R. F., Hatcher, P. G., 2008. Evidence of lignin sources for previously uncharacterized components of Dissolved organic matter (DOM) in Marine waters. Ocean Science Meeting, Orlando, FL. March 2-7 2008.

Smith, B. C., 1996. Fundamentals of Fourier transform infrared spectroscopy. CRC Press, Boca Raton, Florida.

Smith, B. C., 1999. Infrared spectral interpretation: A systematic approach. CRC Press, Boca Raton, Florida.

St-Jean, G., 2003. Automated quantitative and isotopic (^{13}C) analysis of dissolved inorganic carbon and dissolved organic carbon in continuous-flow using a total

organic carbon analyzer. Rapid Communications in Mass Spectrometry 17, 419-428.

Steele, D., 2002. Infrared spectroscopy: Theory. In: Chalmers, J. M., Griffiths, P. R. (Eds.), Handbook of Vibrational Spectroscopy: Theory and Instrumentation. John Wiley and Sons, LTD, New York, pp. 44-70.

Stevenson, F. J., 1994. Humus chemistry: Genesis, Composition, and Reactions. John Wiley and Sons, New York.

Stevenson, F. J., Goh, K. M., 1971. Infrared spectra of humic acids and related substances. Geochimica et Cosmochimica Acta 35, 471-483.

Strathmann, T. J., Myneni, S. C. B., 2004. Speciation of aqueous Ni (II)-carboxylate and Ni (II)-fulvic acid solutions: Combined ATR-FTIR and XAFS analysis. Geochimica et Cosmochimica Acta 68, 3441-3458.

Stumm, W., 1990. Aquatic Chemical Kinetics: Reaction Rates of Processes in Natural Waters. Wiley/Interscience, New York.

Sutton, R., Sposito, G., 2005. Molecular structure in soil humic substances: The new view. Environmental Science and Technology 39, 9009-9015.

Swift, R. S., 1999. Macromolecular properties of soil humic substances: Fact, fiction, and opinion. Soil Science 164, 790-802.

Tranvik, L. J., 1992. Allochthonous dissolved organic matter as an energy source for pelagic bacteria and the concept of the microbial loop. Hydrobiologia 229, 107-114.

Turner, R. E., Rabalais, N. N., Zhang, Z. N., 1990. Phytoplankton biomass, production and growth limitations on the Huanghe (Yellow River) continental shelf. Continental Shelf Research 10, 545-571.

Vonach, R., Lendl, B., Kellner, R., 1997. Hyphenation of ion exchange high-performance liquid chromatography with Fourier transform infrared detection for the determination of sugars in nonalcoholic beverages. Analytical Chemistry 69, 4286-4290.

Waidner, L. A., Kirchman, D. L., 2008. Diversity and distribution of ecotypes of the aerobic anoxygenic phototrophy gene pufM in the Delaware Estuary. Applied and Environmental Microbiology 74, 4012-4021.

Wakeham, S. G., Hedges, J. I., Lee, C., Peterson, M. L., Hernes, P. J., 1997. Compositions and transport of lipid biomarkers through the water column and

surficial sediments of the equatorial Pacific Ocean. Deep Sea Research Part II: Topical Studies in Oceanography 44, 2131-2162.

Wang, H., Palmer, R. A., 1999. Further insights on 2D-correlation theory. In: Ozaki, Y., Noda, I. (Eds.), Two- Dimensional Correlation Spectroscopy. American Institute of Physics. AIP Conference Proceedings No. 53, Kobe-Sanda, Japan, pp. 41-54.

Wang, X. C., Altabet, M. A., Callahan, J., Chen, R. F., 2004. Stable carbon and nitrogen isotopic compositions of high molecular weight dissolved organic matter from four US estuaries. Geochimica et Cosmochimica Acta 68, 2681- 2691.

Watanabe, S., Noda, I., Ozaki, Y., 2008. Thermally induced conformational changes in polyethylene studied by two-dimensional near-infrared–infrared hetero-spectral correlation spectroscopy. Journal of Molecular Structure 883, 173-180.

Wellington, B. I., Driscoll, C. T., 2004. The episodic acidification of a stream with elevated concentrations of dissolved organic carbon. Hydrological Processes 18, 2663-2680.

Williams, P. M., Druffel, E. R. M., 1987. Radiocarbon in dissolved organic matter in the central North Pacific Ocean. Nature 330, 246-248.

Wilson, M. A., 1987. N.M.R. Techniques and Applications in Geochemistry and Soil Chemistry. Pergamon Press, Oxford.

Xie, H., Zafiriou, O. C., Cai, W. J., Zepp, R. G., Wang, Y., 2004. Photooxidation and its effects on the carboxyl content of dissolved organic matter in two coastal rivers in the southeastern United States. Environmental Science and Technology 38, 4113-4119.

Zhao, W., Song, C., Zheng, B., Liu, J., Viswanathan, T., 2002. Thermal recovery behavior of fluorinated single-walled carbon nanotubes. Journal of Physical Chemistry B-Condensed Phase 106, 293-296.

Zuo, L., Wang, X. C., 2004. Bacterial roles in the formation of high-molecular-weight dissolved organic matter in estuarine and coastal waters: Evidence from lipids and the compound-specific isotopic ratios. Limnology and Oceanography 49, 297-302.

APPENDIX A :

DOC CONCETRATION TABLES

Appendix Table A.1. Dissolved organic carbon (DOC) concentration, mass balance and HMW recovery percentage of the November 2005 season (1105).

	Filtered		LMW		HMW-Vol.		Recovery		Massbalance		HMW- from the cell		Recovery from cell	
	uM-C	STD	uM-C	STD	uM-C	STD	%	STD	%	STD	uM-C	STD	%	STD
DS-1105	8813	382	4214	43	4583	105	52	3	100	5	4583	105	52	3
GB-1105	1015	7	556	5	515	26	51	3	106	3	485	21	48	2
TP-1105	519	12	342	24	166	16	36	3	102	6	171	11	33	2
CBB-1105	231	25	134	8	78	4	34	4	92	11	72	2	31	3
OSC-1105	150	4	107	5	50	7	33	5	105	6	45	4	30	3

Appendix Table A.2. Dissolved organic carbon (DOC) concentration, mass balance and HMW recovery percentage of the February 2006 season (0206).

	Filtered		LMW		HMW-Vol.		Recovery		Massbalance		HMW- from the cell		Recovery from cell	
	uM-C	STD	uM-C	STD	uM-C	STD	%	STD	%	STD	uM-C	STD	%	STD
DS-0206	7138	228	3510	104	3887	215	54	3	104	5	3887	215	54	3
GB-0206	940	14	520	25	387	19	41	2	96	4	363	38	39	4
TP-0206	581	49	364	11	194	8	33	3	96	8	183	9	31	3
CBB-0206	391	19	315	34	105	6	27	2	107	10	93	15	24	4

Appendix Table A.3. Dissolved organic carbon (DOC) concentration, mass balance and HMW recovery percentage of the May 2006 season (0506).

	Filtered		LMW		HMW-Vol.		Recovery		Massbalance		HMW- from the cell		Recovery from cell	
	uM-C	STD	uM-C	STD	uM-C	STD	%	STD	%	STD	uM-C	STD	%	STD
DS-0506	5780	237	3165	87	3085	79	53	3	108	5	3085	79	53	3
GB-0506	695	16	456	4	257	8	37	1	103	3	231	19	33	3
TP-0506	281	14	218	26	67	9	24	3	101	11	54	10	19	4
CBB-0506	185	7	151	3	32	7	17	4	99	6	22	6	12	3
OSC-0506	131	5	107	7	20	6	15	5	97	8	15	3	11	2

Appendix Table A.4. Dissolved organic carbon (DOC) concentration, mass balance and HMW recovery percentage of the August 2006 season (0806).

	Filtered		LMW		HMW-Vol.		Recovery		Massbalance		HMW- from the cell		Recovery from cell	
	uM-C	STD	uM-C	STD	uM-C	STD	%	STD	%	STD	uM-C	STD	%	STD
DS-0806	11788	97	5299	295	6248	183	53	2	98	3	6248	183	53	2
GB-0806	648	12	326	13	247	17	38	3	88	4	238	28	37	4
TP-0806	260	12	174	17	77	14	30	6	97	10	65	8	25	3
CBB-0806	168	14	101	3	47	9	28	6	88	9	42	6	25	4
OSC-0806	109	6	74	5	21	7	19	7	87	9	19	4	17	4

Appendix Table A.5. Dissolved organic carbon (DOC) concentration, mass balance and HMW recovery percentage of the November 2006 season (1106).

	Filtered		LMW		HMW-Vol.		Recovery		Massbalance		HMW- from the cell		Recovery from cell	
	uM-C	STD	uM-C	STD	uM-C	STD	%	STD	%	STD	uM-C	STD	%	STD
DS-1106	11340	233	6492	124	5441	158	48	2	105	3	5441	158	48	2
GB-1106	856	16	426	23	411	32	48	4	98	5	369	45	43	5
TP-1106	438	1	194	17	186	13	42	3	87	5	166	18	38	4
CBB-1106	281	14	165	13	92	7	33	3	91	7	84	5	30	2
OSC-1106	189	5	124	6	60	5	32	3	97	5	53	9	28	5

Appendix Table A.6. Dissolved organic carbon (DOC) concentration, mass balance and HMW recovery percentage of the February 2007 season (0207).

	Filtered		LMW		HMW-Vol.		Recovery		Massbalance		HMW- from the cell		Recovery from cell	
	uM-C	STD	uM-C	STD	uM-C	STD	%	STD	%	STD	uM-C	STD	%	STD
DS-0207	3720	6	1338	23	1928	195	52	5	88	5	1928	195	52	5
GB-0207	754	25	489	27	317	8	42	2	107	5	302	32	40	4
TP-0207	578	36	357	19	187	13	32	3	94	7	181	11	31	3
CBB-0207	425	22	261	4	105	8	25	2	86	5	95	15	22	4

Appendix Table A.7. Dissolved organic carbon (DOC) concentration, mass balance and HMW recovery percentage of the May 2007 season (0507).

	Filtered		LMW		HMW-Vol.		Recovery		Massbalance		HMW- from the cell		Recovery from cell	
	uM-C	STD	uM-C	STD	uM-C	STD	%	STD	%	STD	uM-C	STD	%	STD
DS-0507	6539	145	1213	15	4489	194	69	3	87	4	4489	194	69	3
GB-0507	731	24	376	35	259	23	35	3	87	6	242	39	33	5
TP-0507	362	15	274	12	97	5	27	2	102	6	91	14	25	4
CBB-0507	190	2	129	5	46	8	24	4	92	5	40	4	21	2

APPENDIX B:

PEAK FITTING FOR THE CARBONYL AREA OF THE FTIR SPECTRUM

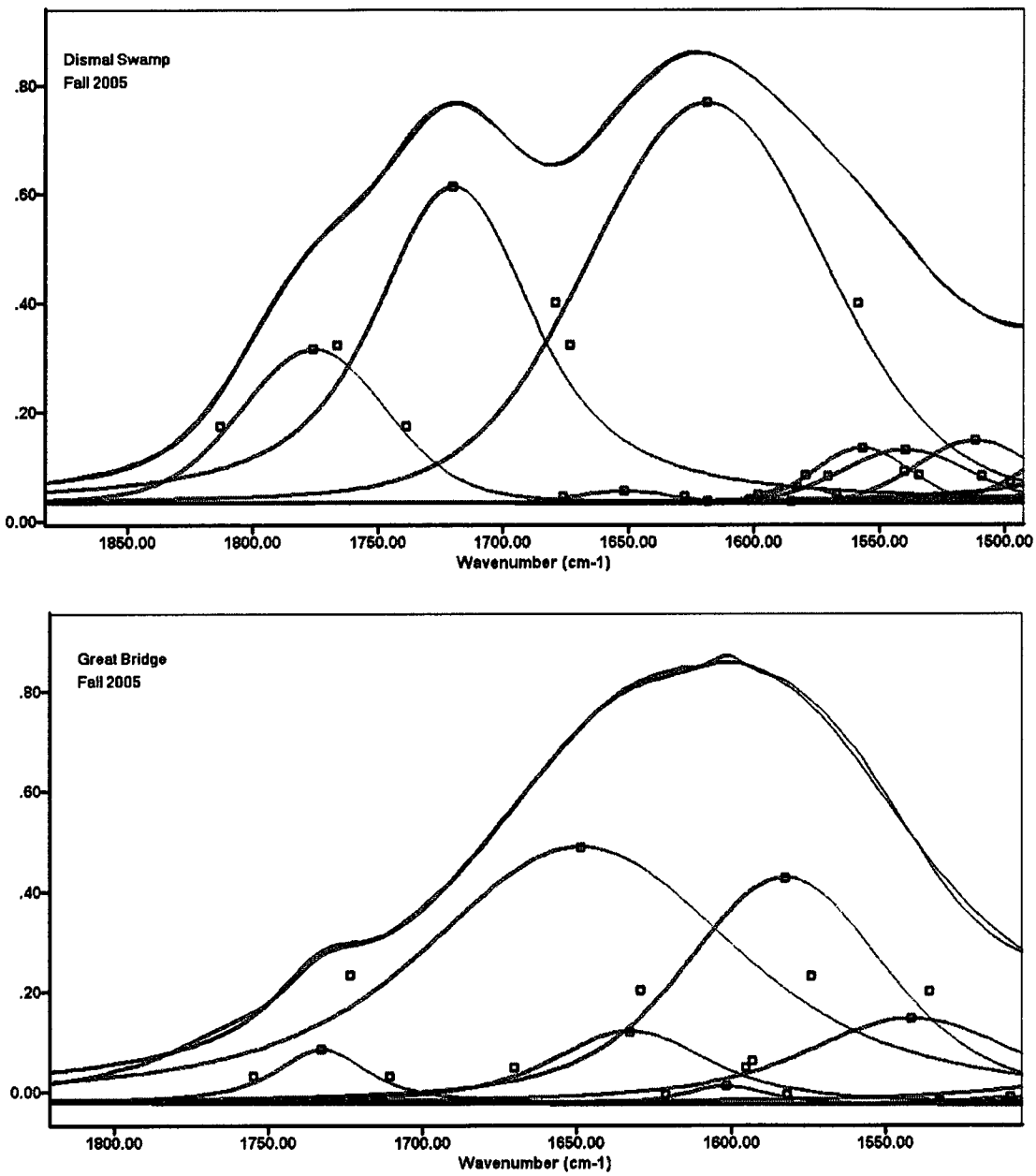

Appendix B. Fig 1 Peak fitting results for the carbonyl area of the FTIR of DS, GB, TP, CBB, OSC from the November 2005 to May 2007 (seven seasons). The red line is the original spectrum, blue line the fitted spectrum, and green line the individual peaks.

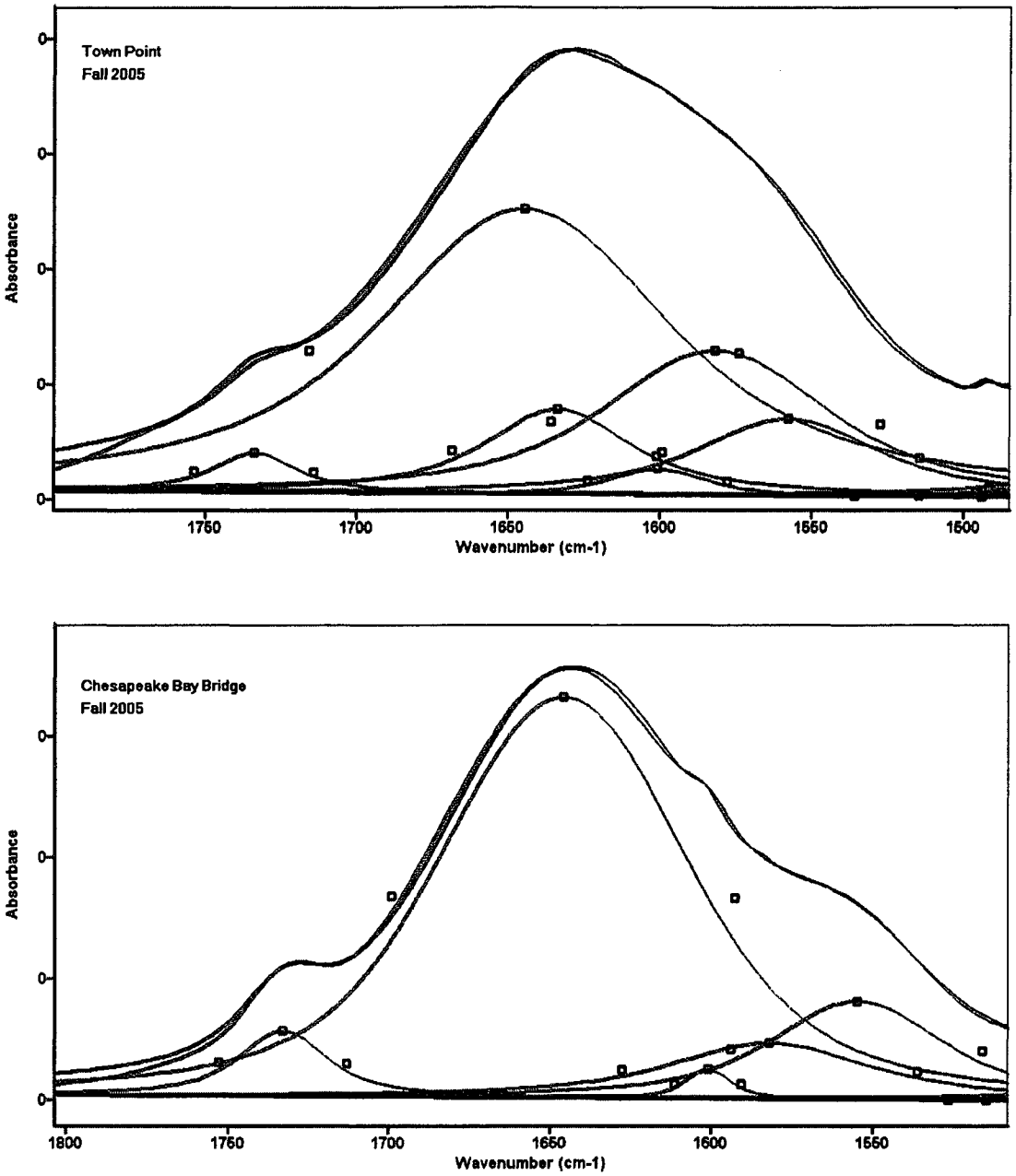

Appendix B. Fig. 1. Continued.

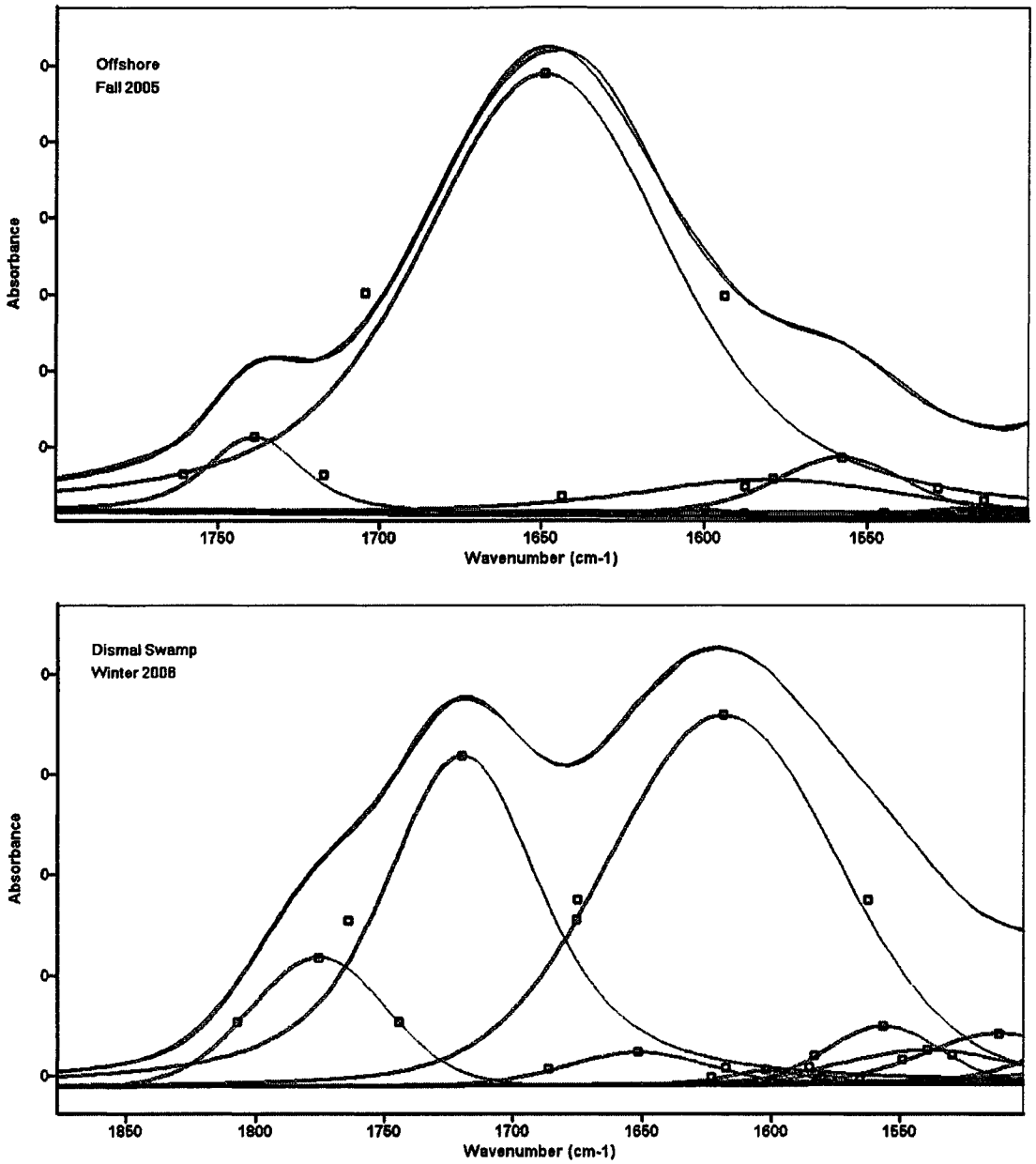

Appendix B. Fig. 1. Continued.

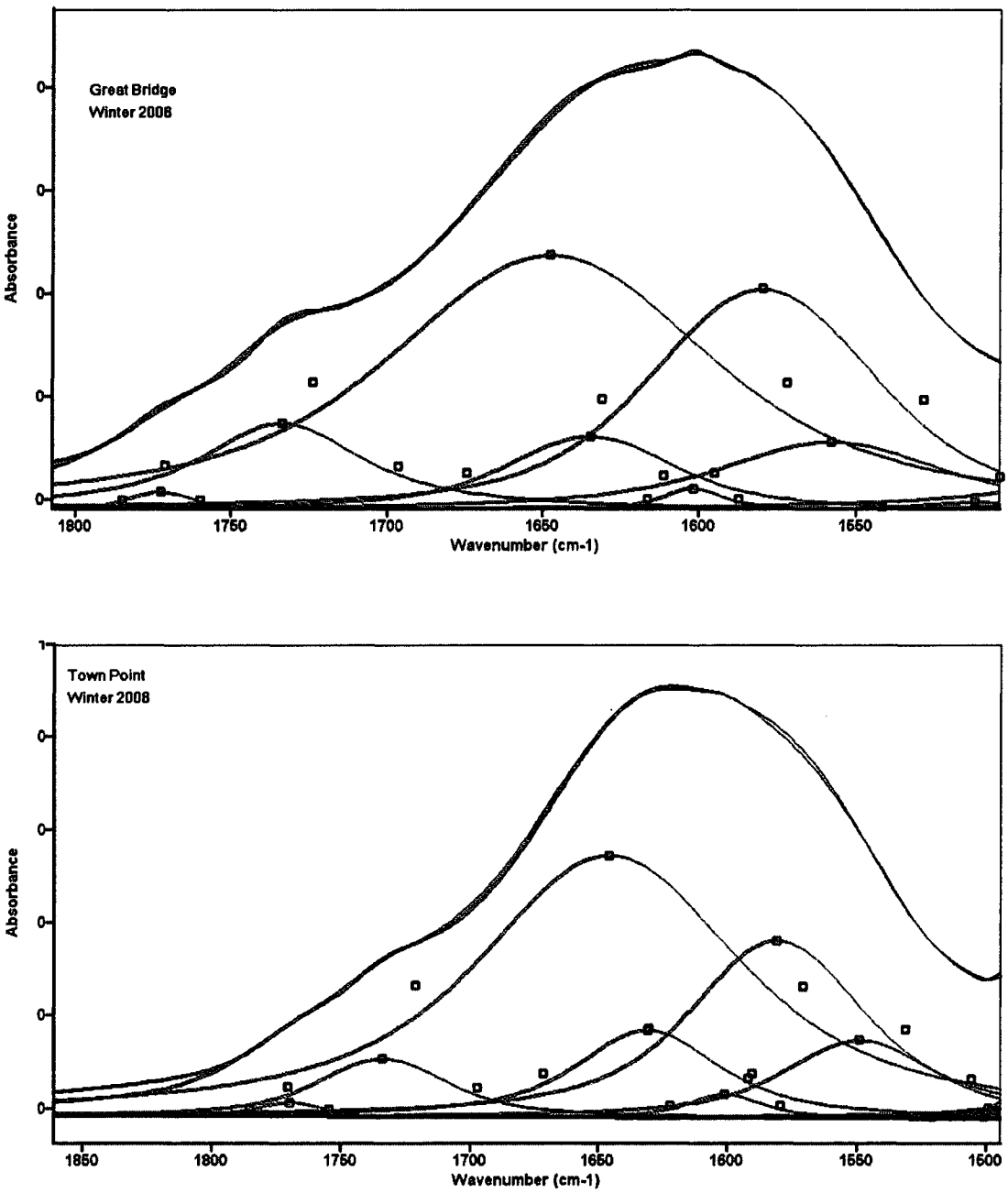

Appendix B. Fig. 1. Continued.

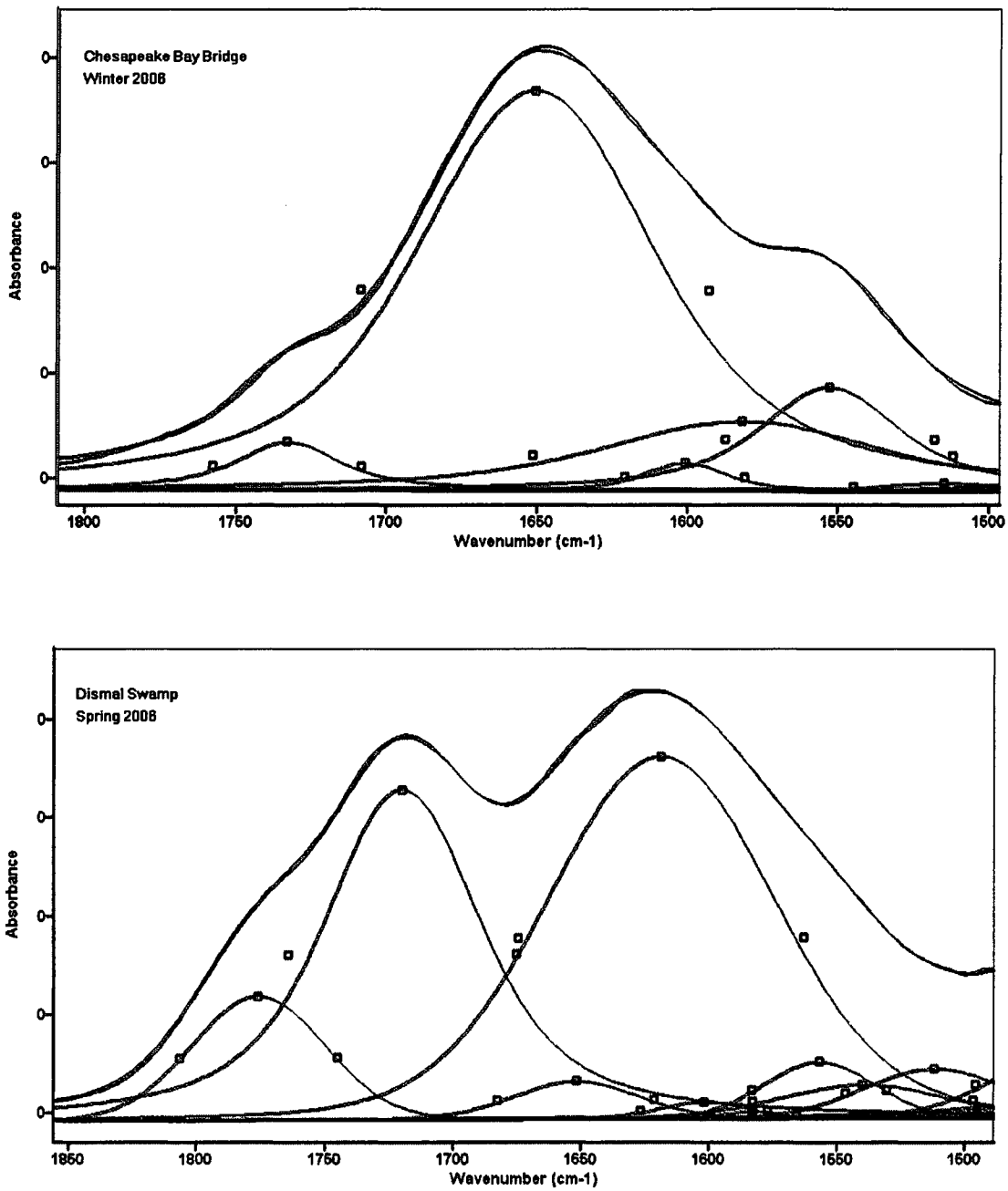

Appendix B. Fig. 1. Continued.

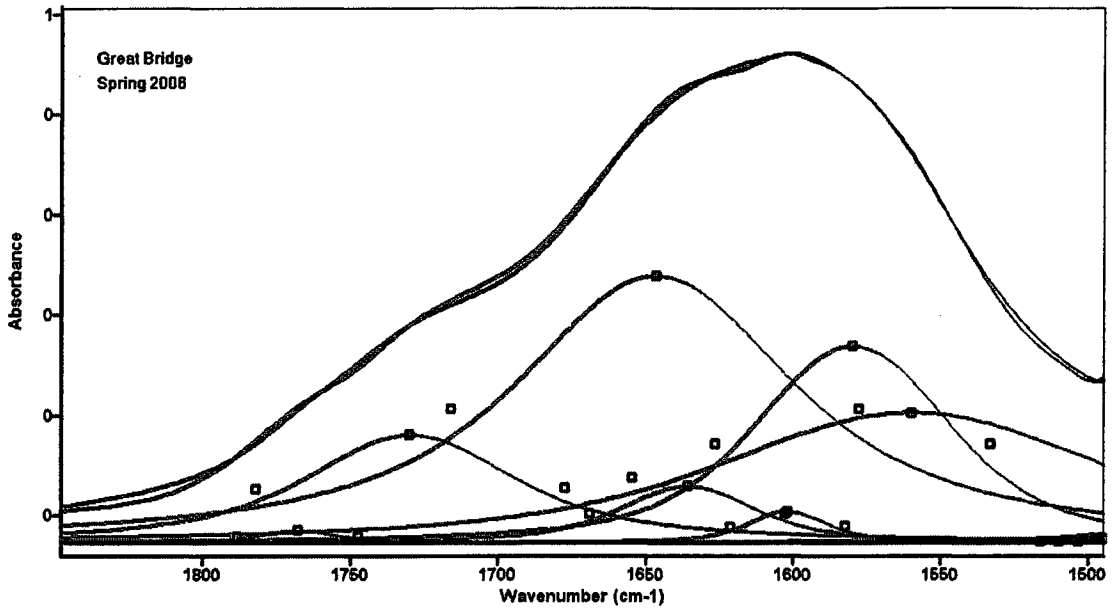

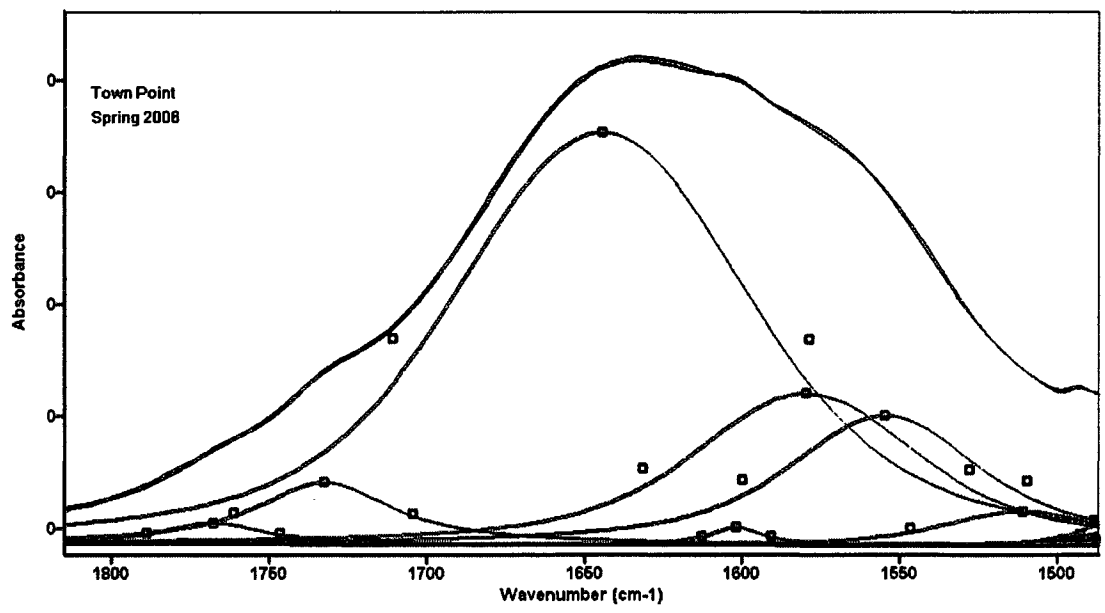

Appendix B. Fig. 1. Continued.

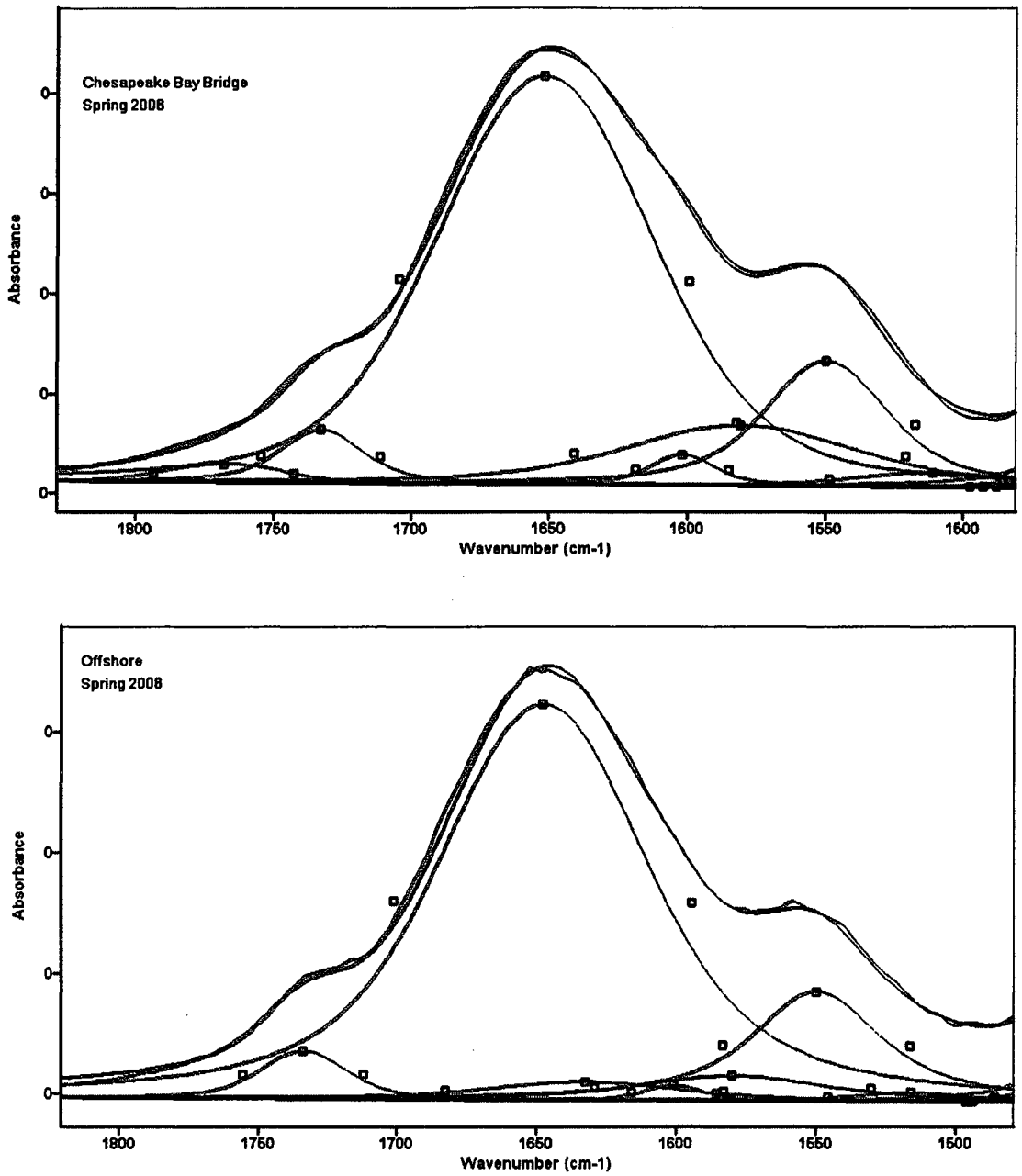

Appendix B. Fig. 1. Continued .

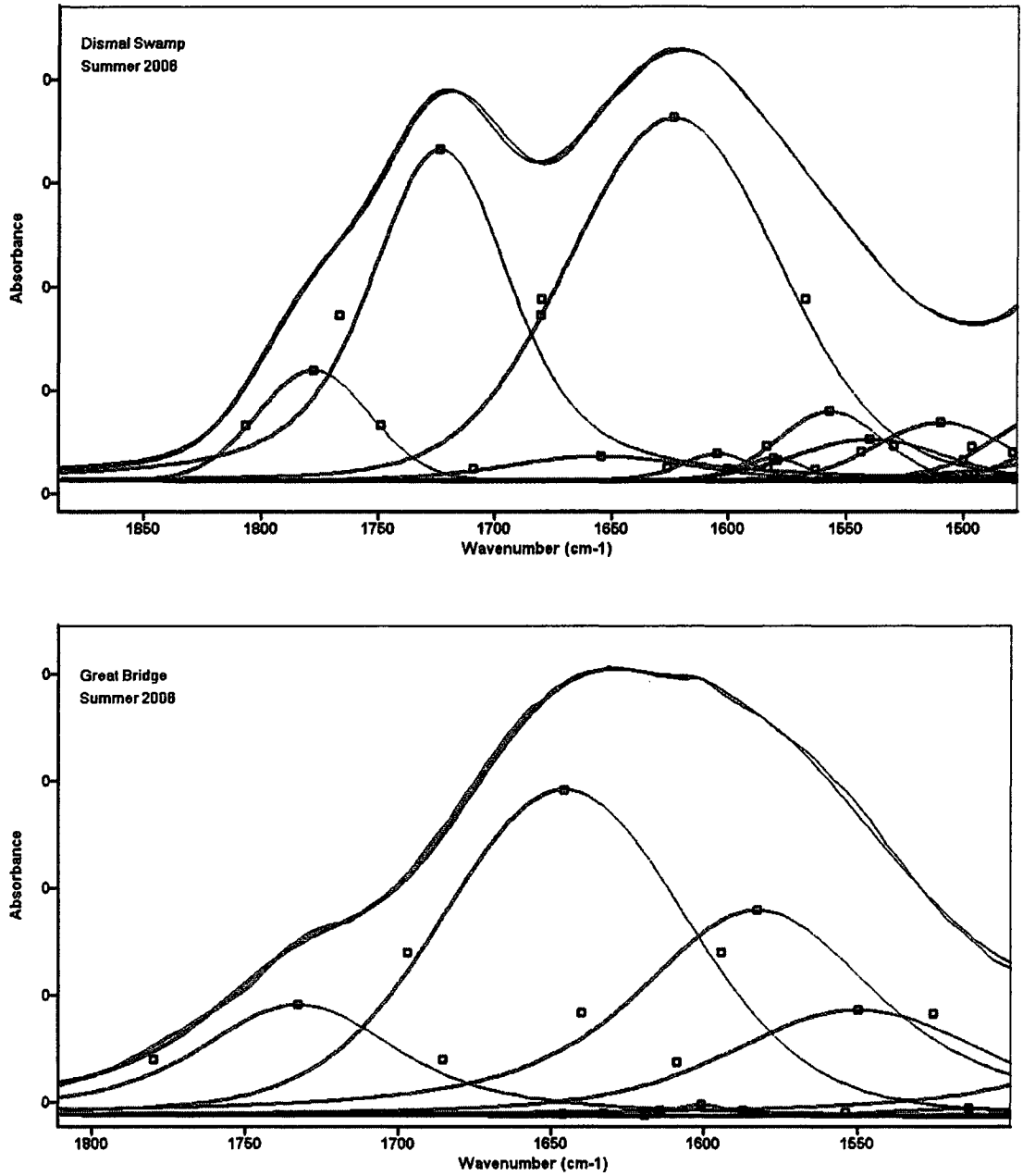

Appendix B. Fig. 1. Continued.

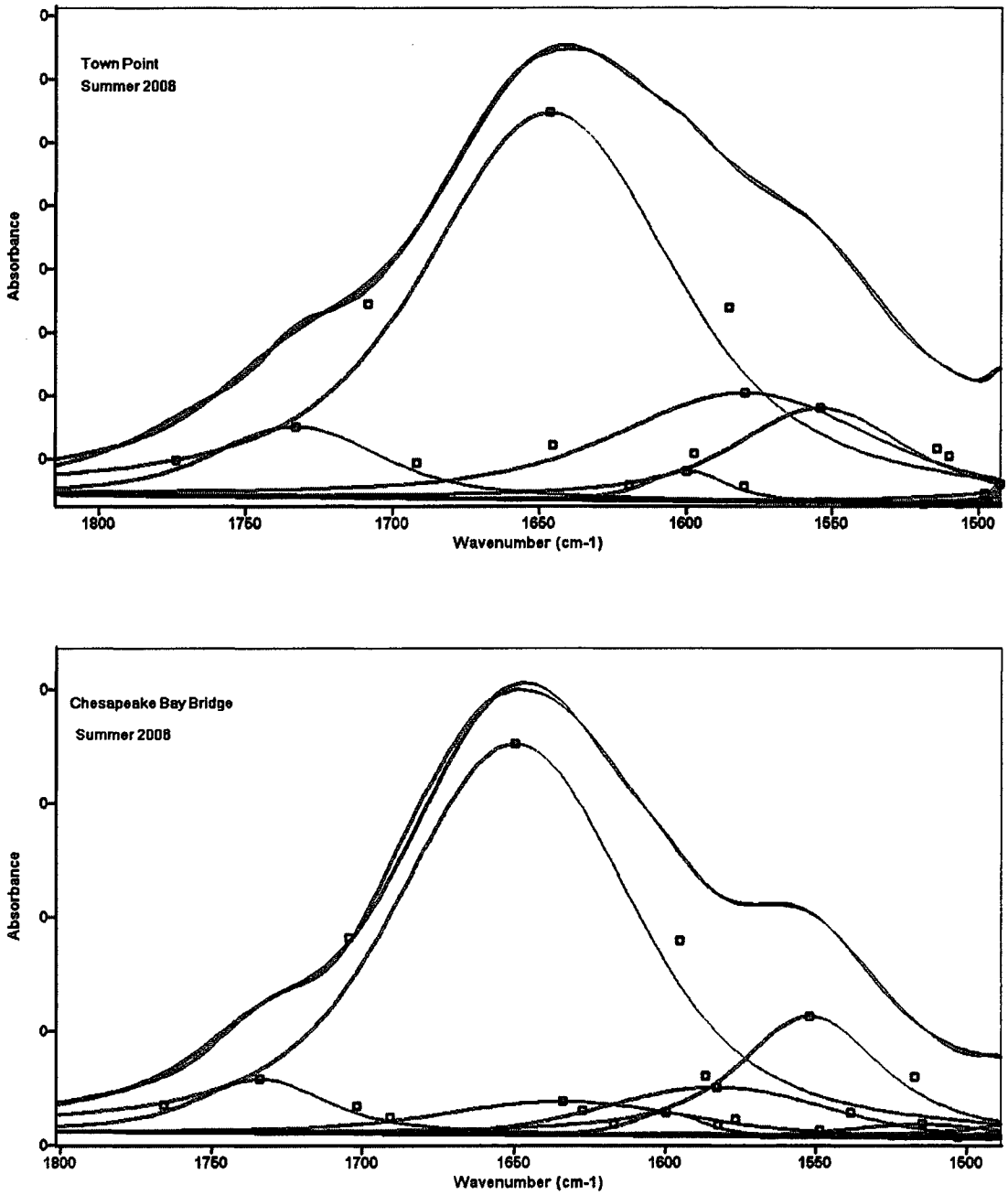

Appendix B. Fig. 1. Continued.

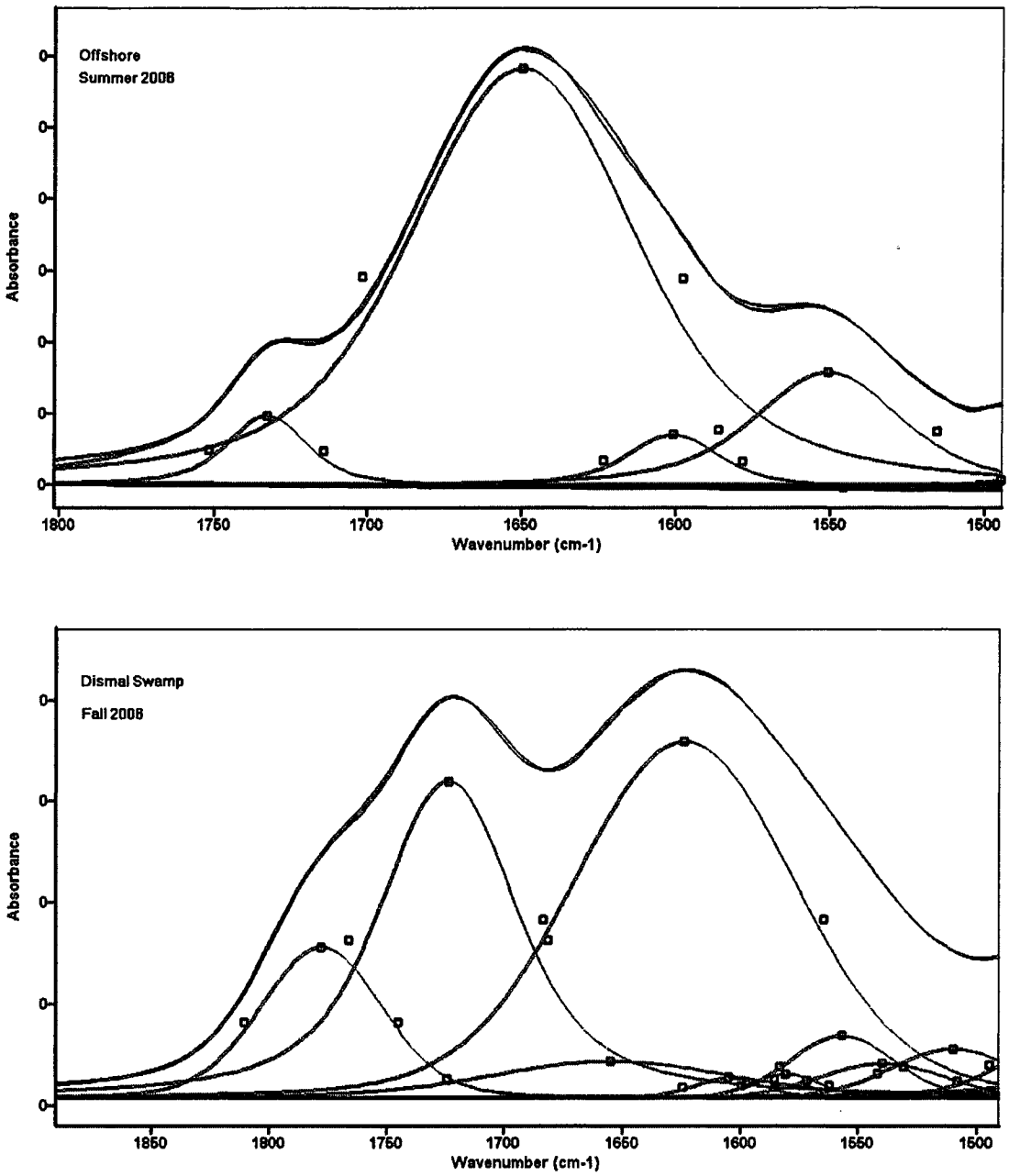

Appendix B. Fig. 1. Continued.

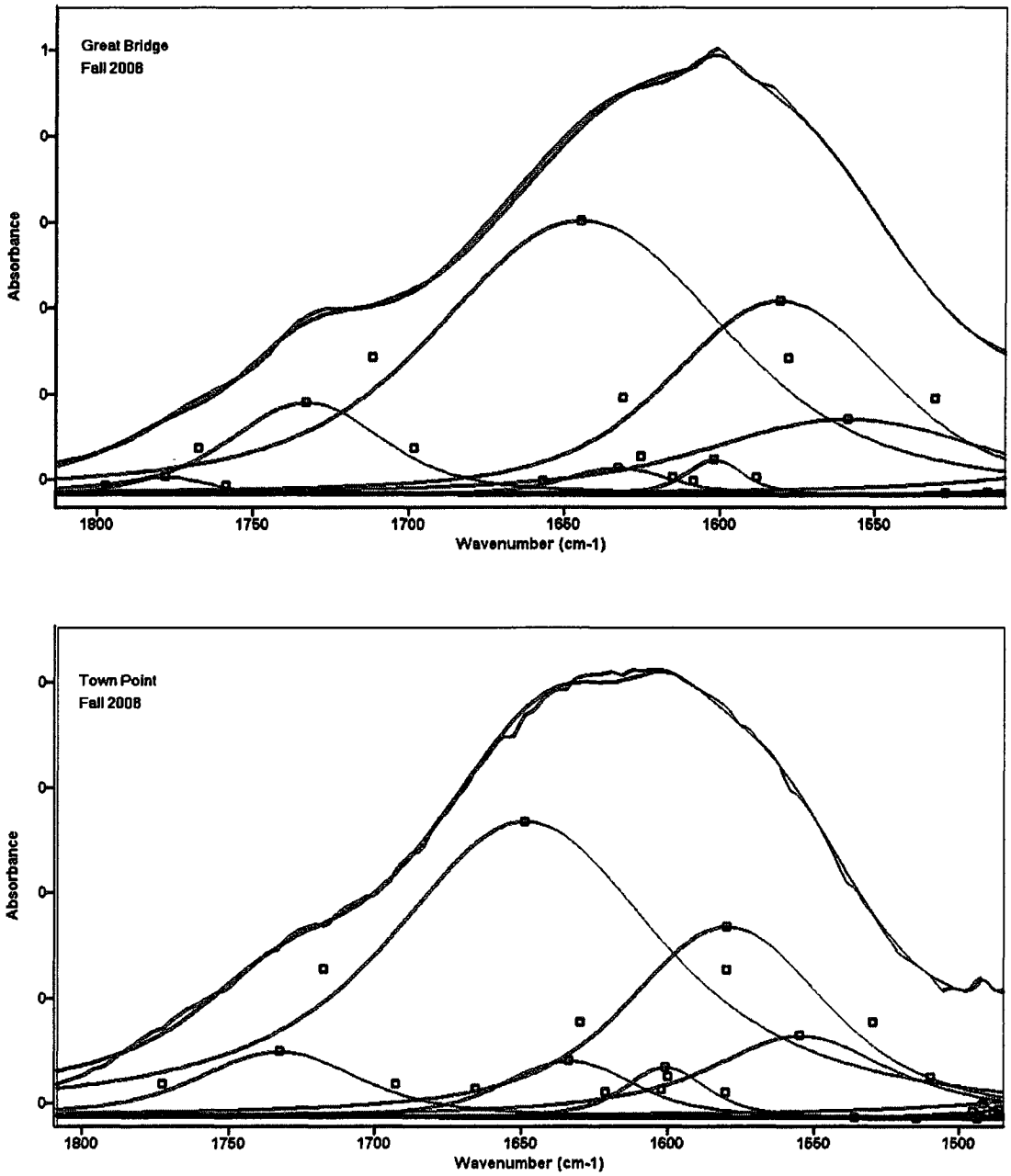

Appendix B. Fig. 1. Continued.

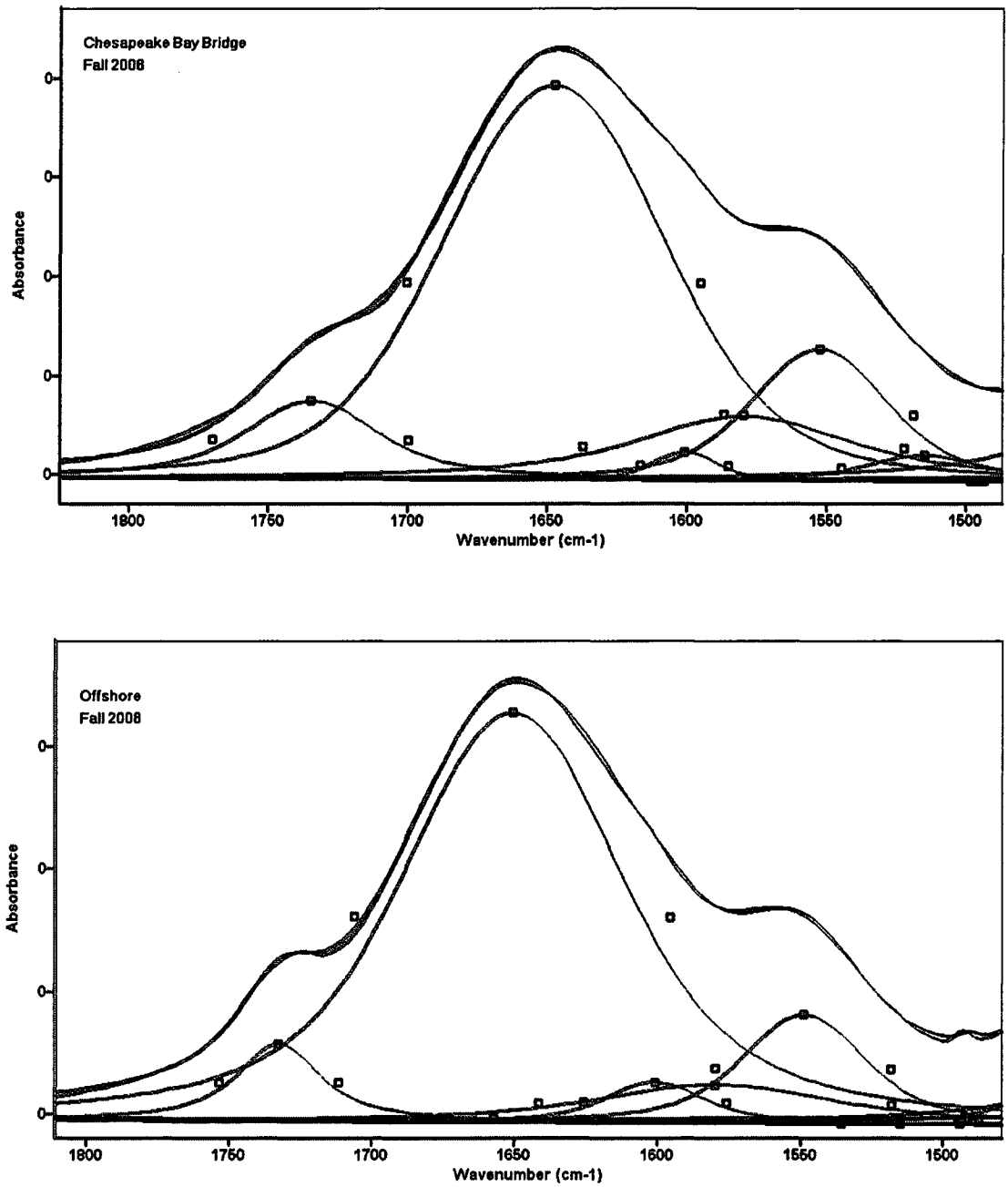

Appendix B. Fig. 1. Continued.

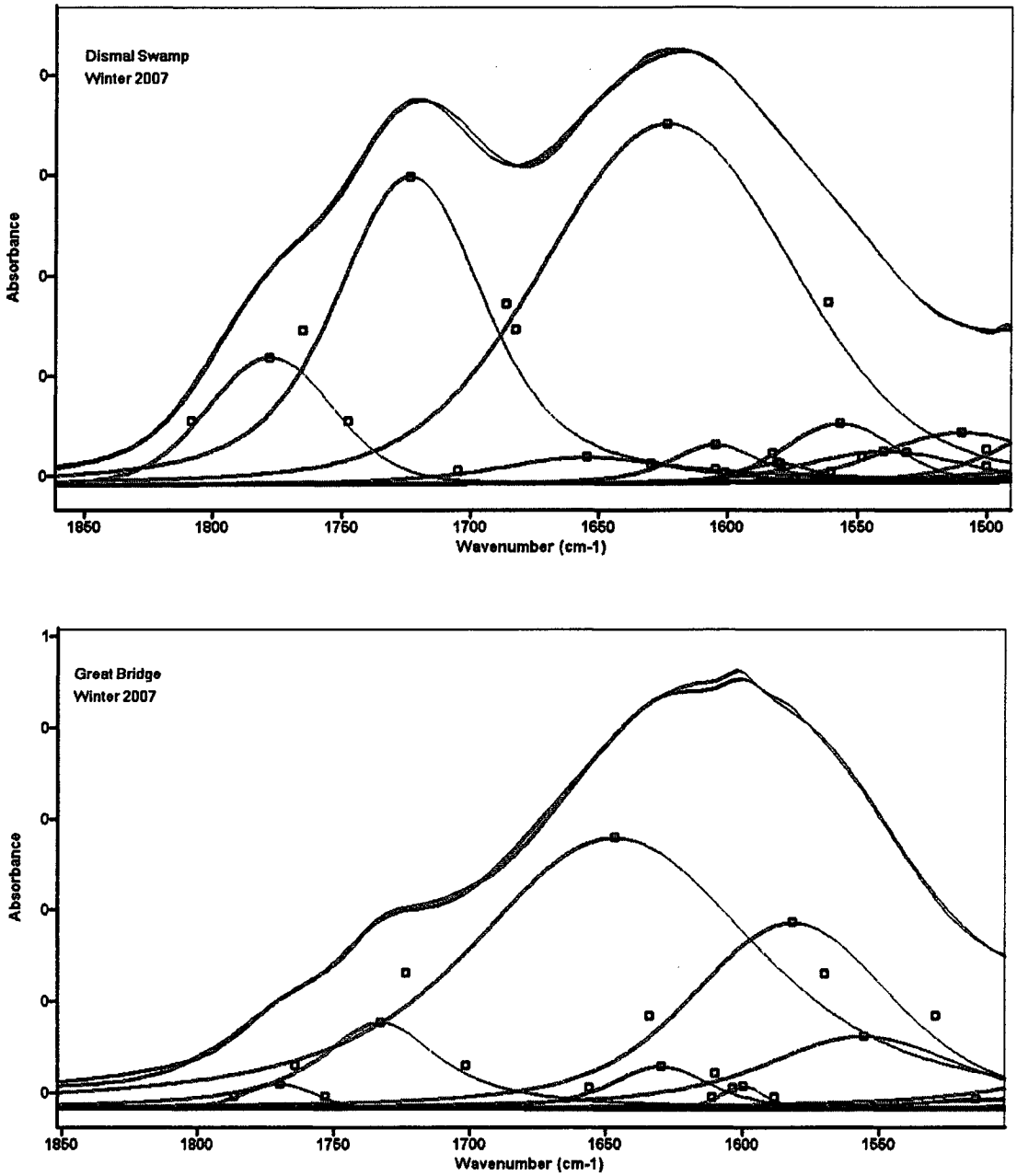

Appendix B. Fig. 1. Continued.

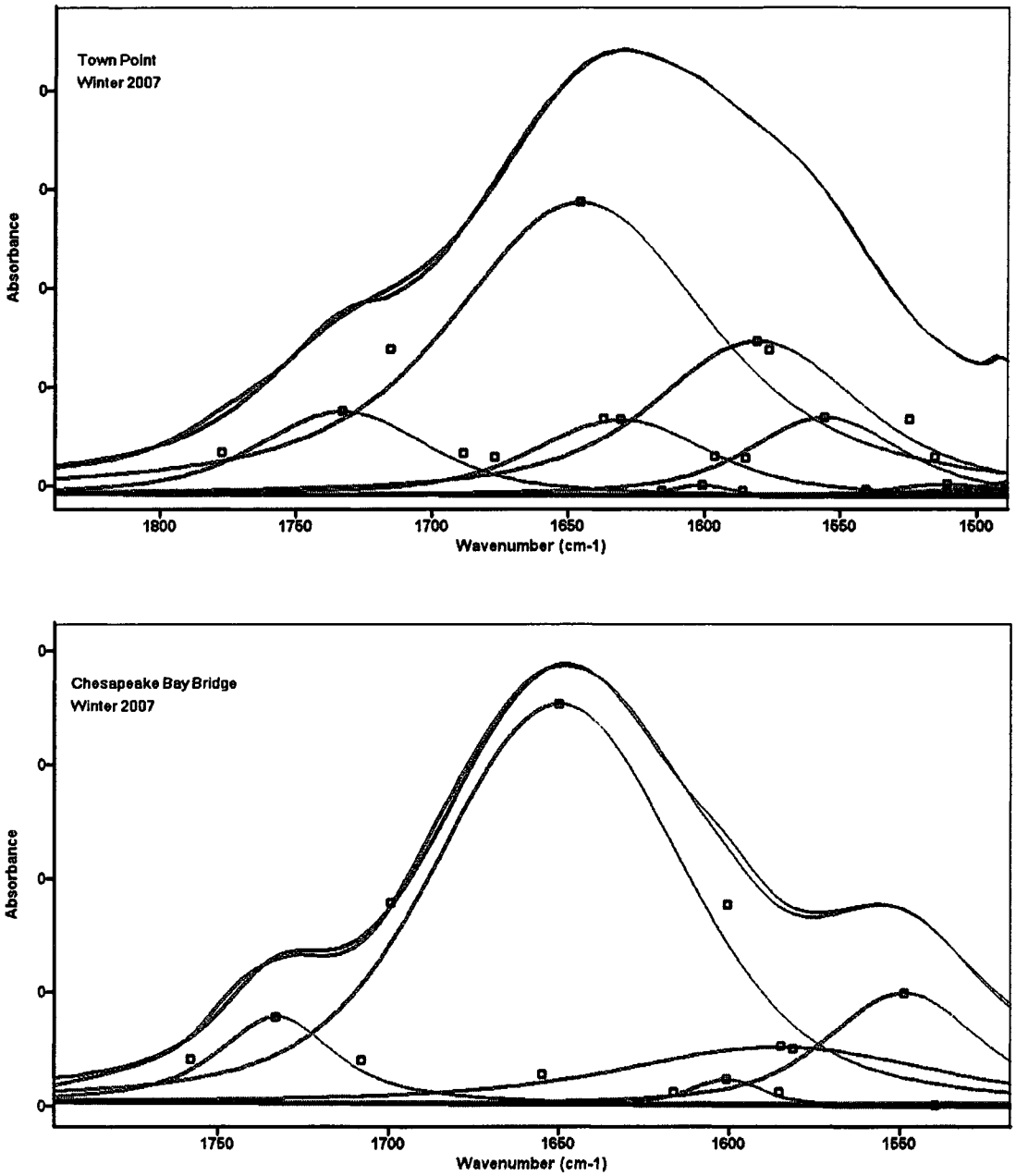

Appendix B. Fig .1. Continued.

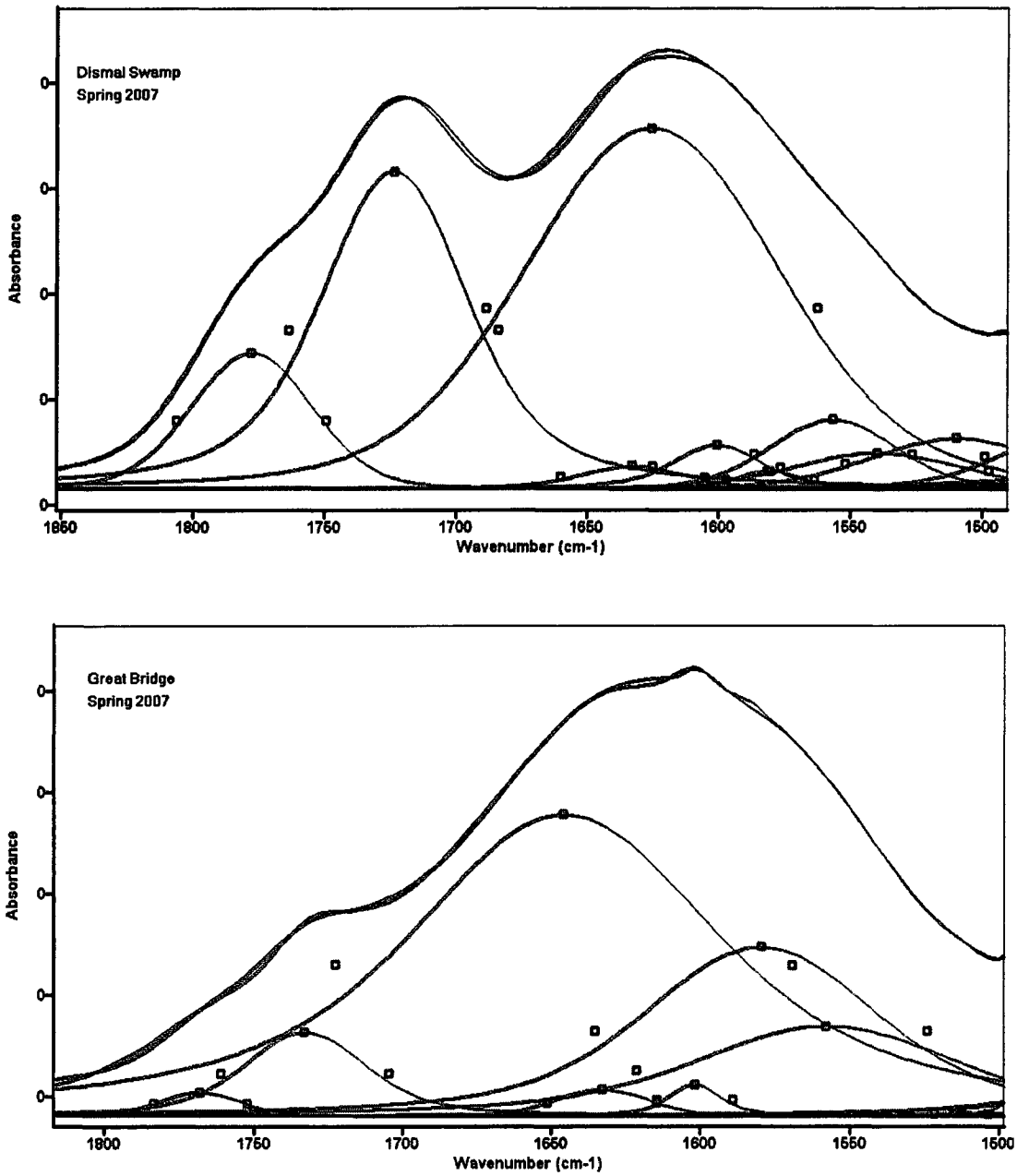

Appendix B. Fig. 1. Continued.

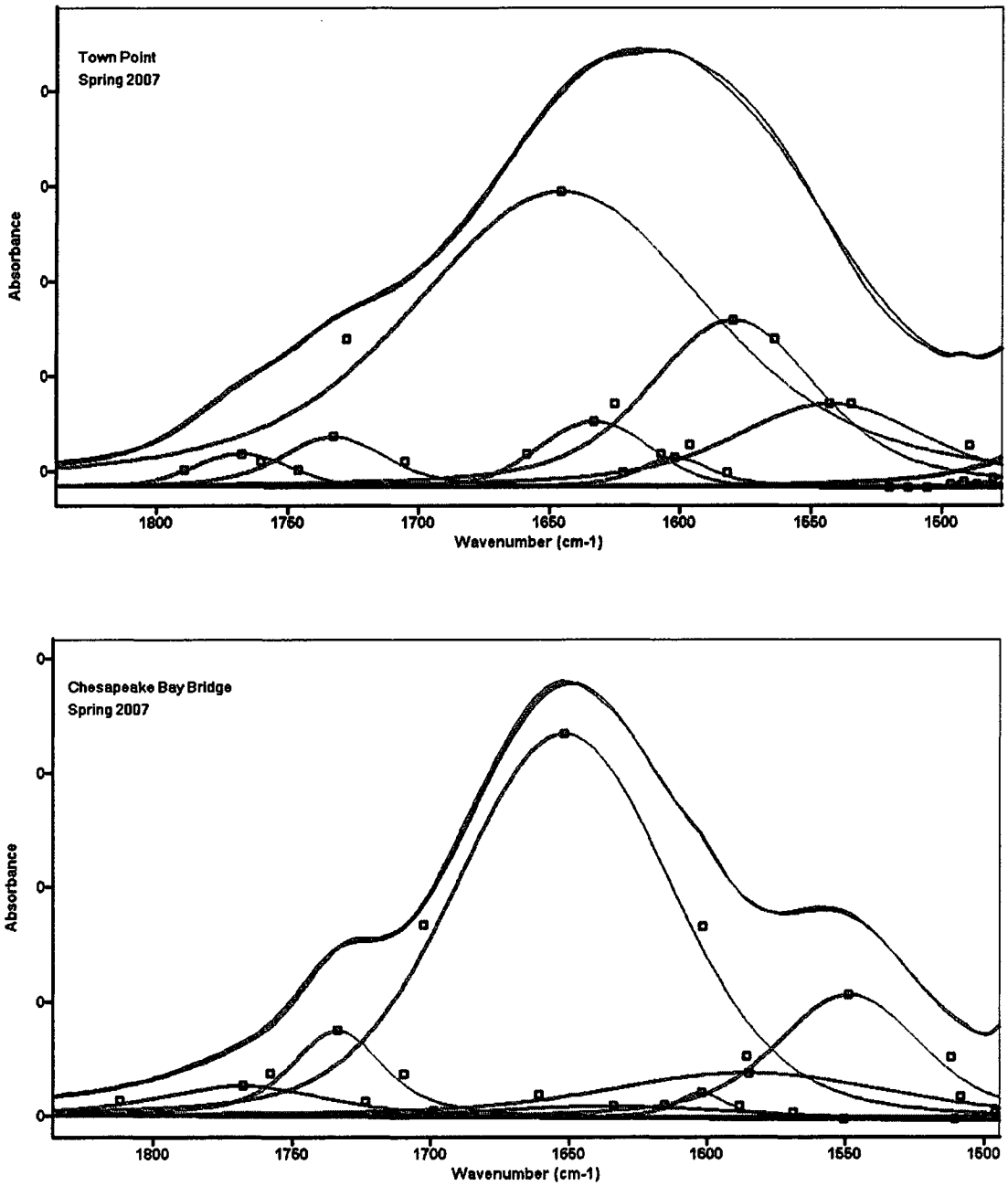

Appendix B. Fig. 1. Continued.

VITA

Hussain A. Nabi Ali Abdulla

EDUCATION:

2009	Ph.D	Oceanography - Old Dominion University -United States of America
2005	M.S.	Oceanography - Old Dominion University - United States of America
1998	B.S. (with Honor)	Chemistry - Bahrain University - Bahrain

REVIEWED PUPLICATIONS:

Ali-Mohamed, A.Y., **Ali, H.A.N.**, 2000. Estimation of atmospheric inorganic water-soluble particulate matter in Muharraq Island, Bahrain, (Arabian Gulf), by ion chromatography. Atmospheric Environment 35, 761-768.

Hassan, A.M., Mandeel, Q.A., **A.Nabi, H.**, 2003. Evaluation of some metals in commonly consumed spices in Bahrain. Arab Gulf Journal of Scientific Research 21, 79-85.

Minor, E.C., Pothen, J., Dalzell, B., **Abdulla, H.**, Mopper, K., 2006. Effects of salinity changes on the photodegradation and UV-visible absorbance of terrestrial dissolved organic matter. Limnology and Oceanography 51, 2181- 2186.

Abdulla, H.A.N., Dias, R.F., Minor, E.C., 2009. Understanding the enhanced aqueous solubility of styrene by terrestrial dissolved organic matter using stable isotope mass balance and FTIR. Organic Geochemistry 40, 547- 552.

Abdulla, H.A.N., Minor, E.C., Dias, R.F., Hatcher, P.G., (*In Preparation for Geochimica et Cosmochimica Acta.*). Changes in the compound classes of dissolved organic matter along an estuarine transect: A study using FTIR and ^{13}C-NMR.

Abdulla, H.A.N., Minor, E.C., Dias, R.F., Hatcher, P.G., (*In preparation for Liminology and Oceanography).* Seasonal and spatial changes in the chemical compositions of dissolved organic matter along an estuarine transect: A study using isotope ratio mass spectrometry and ^{13}C-NMR.

Abdulla, H.A.N., Minor, E.C., Dias, R.F., Hatcher, P.G., (*In preparation for Environmental Science and Technology).* Changes in the chemical structures of estuarine dissolved organic matter using two dimensional correlation ^{13}C-NMR and of FTIR.

Abdulla H.A.N., Minor, E.C., Sleighter, R., Hatcher, P.G., (*In preparation for Marine Chemistry*), Seasonal variability of DOM in a sub-estuary: Implications for terrestrial carbon Cycling, view from a FT-ICR-MS and spectroscopy techniques.

AWARDS:

2006-2007	Dorothy Brown Smith Scholarship – Ocean, Earth and Atmospheric Sciences Department, Old Dominion University – United States of America.
2003- 2005	Fulbright student scholarship to study M.S. in Oceanography.
1996	The prize of His Highness Sheikh Hamad bin Isa Al Khalifa, King of Bahrain, to eminent students – Bahrain University – Kingdom of Bahrain.
1992- 1998	Ministry of Education scholarship to study B.S. in Chemistry – Bahrain University - Kingdom of Bahrain.